A COMPUTATIONALLY EFFICIENT METHOD FOR NONLINEAR MULTIHULL SEAKEEPING

by

William F. Belknap

A dissertation submitted in partial fulfillment
of the requirements for the degree of
Doctor of Philosophy
(Naval Architecture and Marine Engineering)
in The University of Michigan
2008

Doctoral Committee:

Professor Robert F. Beck, Chair
Professor Bogdan I. Epureanu
Professor Michael G. Parsons
Professor Armin W. Troesch

Acknowledgments

I would like to thank the Naval Surface Warfare Center Carderock Division, and in particular, Mr. Terrence Applebee, Dr. In-Young Koh, and Dr. Arthur Reed for supporting my advanced studies. I am also very appreciative of the many beneficial discussions with my colleagues, Dr. Michael Hughes, Mr. John Telste, and Mr. Bradley Campbell.

Special thanks are owed to my committee chair, Professor Beck. Without his encouragement, I may never have begun down this long road. Without his patience, I would not have finished. I am also grateful to Professors Epureanu, Parsons, and Troesch for their thoughtful participation on my committee and their accommodation of last-minute committee meetings.

For their help in running LAMP and providing basis input files for the Delft catamaran, I thank Mr. Kenneth Weems and Dr. Sheguang Zhang of SAIC. Dr. Kevin Maki and Prof. Larry Doctors are also deserving of recognition for providing geometry and model data for the HSSL trimaran.

Finally, I offer sincere thanks to my wife, Kelly, and daughter, Lucienne. I could not have completed this dissertation without their support, encouragement, and patience.

Table of Contents

Chapters

List of Figures

List of Tables

List of Appendices

Appendix

Nomenclature

a	Ambient wave amplitude
A_{jk}	Total 3D added mass coefficient
A_{jk}^{∞}	Total 3D added mass coefficient at infinite frequency
$\underline{A}_{jk}$	3D added mass coefficient due to independent demi-hull calculation
$\tilde{A}_{jk}$	3D added mass coefficient due to radiation interactions
A_n	Amplitude of n^{th} frequency component of a wave spectrum
B_{jk}	Total 3D damping coefficient
B_{jk}^{∞}	Total 3D damping coefficient at infinite frequency
$\underline{B}_{jk}$	3D damping coefficient due to independent demi-hull calculation
$\tilde{B}_{jk}$	3D damping coefficient due to radiation interactions
β	Wave heading angle
C_{jk}	Hydrostatic stiffness coefficients
ε	A small parameter
ε_n	Phase angle of n^{th} frequency component of a wave spectrum
D_{sweep}	Distance radiated wave is swept downstream before impact
F	A general force
$F^{D}_{j}(t)$	Time-domain diffraction force in direction, j
$F^{HSFK}_{j}(t)$	Time-domain hydrostatic and Froude-Krylov force in direction, j
$F^{R}_{j}(t)$	Time-domain radiation force in direction, j

F_n	Froude number, = $U/\sqrt{g \cdot L}$
ϕ	Euler angle representing roll
ϕ_0	Ambient wave velocity potential
ϕ_k	Radiation velocity potential in mode of motion, k
$\tilde{\phi}^I_k$	Radiated far-field incident wave velocity potential
$\tilde{\phi}^D_k$	Diffraction velocity potential due to far-field radiated wave
ϕ_7	Diffraction velocity potential due to ambient wave
ϕ_s	Steady forward speed potential
Φ	Total velocity potential
g	Gravitational constant
$G_{l,m}$	Green Function
$G^{FF}_{l,m}$	Far-field Green function
η	Wave elevation
k or ν	Wavenumber, = $2\pi/\lambda$
L	Ship length
λ	Wavelength
$\hat{n}$	Inward pointing (out of fluid) unit normal
p	A general pressure
p^{FK}	Froude-Krylov pressure
p^{HS}	Hydrostatic pressure
$Q_{m,k}$	Source strength of panel, m, in mode of motion, k
θ	Euler angle representing pitch
ρ	Fluid mass density

t	time
U_o	Ship speed
V_g	Wave group velocity (m/s)
ω_o	Ambient wave circular frequency (rad/s)
ω_e	Frequency of encounter (rad/s)
x	Longitudinal coordinate in inertial (moving with speed U) frame
$\bar{x}$	Longitudinal coordinate in ship's axis system
X	X-coordinate in world axis system
x^*	Longitudinal coordinate of radiating source in inertial axis system
x_i	Longitudinal coordinate of station that feels radiated wave from section at x*
y	Transverse coordinate in inertial (moving with speed U) frame
$\bar{y}$	Transverse coordinate in ship's axis system
Y	Y-coordinate in world axis system
ψ	Euler angle representing yaw
ψ_k	2D radiation potential for mode, k
$\psi^{\sim I}_k$	2D incident far-field radiated wave potential for mode, k
z	Vertical coordinate in inertial (moving with speed U) frame
$\bar{z}$	Vertical coordinate in ship's axis system
Z	Z-coordinate in world axis system

Abbreviations

BBC	Bottom boundary condition
Body BC	Body boundary condition
DFSBC	Dynamic free surface boundary condition
KFSBC	Kinematic free surface boundary condition
MARIN	Maritime Research Institute Netherlands
ONR	Office of Naval Research
TCB	Transverse Center of Buoyancy

Abstract

A method for predicting the large amplitude motions of multihull vessels in a computationally efficient and robust manner has been developed and demonstrated. The present theory utilizes frequency domain hydrodynamic coefficients that include hull interactions in the radiation problem and a body-exact solution of the time-varying hydrostatic and Froude-Krylov forces in the time-domain. The theory and computational tool have been developed with a stated objective of supporting multihull design optimization, which requires extremely fast and stable computations that can accurately assess the seakeeping measure of merit in a relative sense. Higher fidelity tools can be used subsequent to a converged design to obtain a more accurate assessment of seakeeping performance.

The contribution of this work to the general body of knowledge is in the development of a theory that captures hull interaction effects at lower ship speeds, where interaction effects are likely, while retaining the numerical efficiency of strip theory. A far-field approximation is invoked, whereby the radiated waves from one demi-hull appear as incident waves to another demi-hull. Comparisons of the present theory to model test data and 3D computations have shown fairly good agreement for some ship designs and, while capturing correct trends, relatively poor agreement for other ship designs. Agreement is generally better for multihulls that are long and slender with demi-hull separation greater than two times the demi-hull beam.

Chapter 1

Introduction

1.1 Background

High-speed ships have always been of interest to the commercial and naval communities, but have recently been the source of renewed focus by the high-speed ferry industry and the militaries of the world. The US Navy is currently challenging concept designers to develop high-speed sealift ships, troop transports, and "street fighters". One common theme in requirements for these high speed ships is access to shallow water ports. Increasingly, the designer's solution to meeting these requirements is a multi-hulled vessel. An example of a modern catamaran design is the US Navy's Sea Fighter, shown in Figure 1.1.

The longer and slender hulls of a catamaran or trimaran are designed to give very low wave resistance in calm water, with the multihull arrangement providing a stable platform with shallow draft and increased mission space. However, little thought is given to the ship's performance in waves, particularly at the concept-level design stage, which can lead to unexpected severe motions later. One reason is that there are very few tools available to the early-stage designer to assess seakeeping performance of multihulls.

Perhaps the largest difficulty in developing a seakeeping prediction tool for high-speed multi-hulls is that there is such a wide array of pertinent hydrodynamic aspects. Faltinsen et al. (2003) highlight the various issues associated with modeling multi-hull seakeeping and loads:

- At low speeds, where strip theory is accurate, there will be interactions between the hulls' radiated waves that may need to be taken into account.

- At high speeds, where strip theory is not accurate, radiated waves from one hull will not reach the other hull, but the interactions between the steady and unsteady potentials may be important.
- Slamming, particularly on the wet-deck (the underside of cross-structure), can be frequent and result in very large impact pressures.

Figure 1.1 US Navy's Littoral Surface Craft-Experimental "Sea Fighter" (FSF-1)[1]

As noted by Journée (1992), traditional prediction tools have served the design community well for years generally by simplifying the complete problem into a series of tractable 2D problems allowable through hull slenderness assumptions. However, in the case of a multi-hulled vessel, the presence of one or more additional hulls complicates the problem. In the limit of zero forward speed and infinitely long demi-hulls, 2D simplifications may be adequate. In practice though, forward speed and finite length hulls mean that the multihull seakeeping problem is truly a 3D problem. Perhaps the

[1] Photo from **www.navy.mil**

most prominent "3D" feature of the multihull seakeeping problem is the fact that the radiated waves from one demi-hull will interact with the other demi-hull(s) downstream. It follows then that the tools most capable of properly accounting for the physics of a multihull with forward speed are 3D codes, but these are not as useful at the preliminary design stage because of their relatively costly computation time and the necessary expertise to use the tool.

Having recognized the need to give concept-level designers new tools for designing multihulls, the Office of Naval Research (ONR) has supported the development of a multihull design optimization program, including the tools for assessing resistance and seakeeping performance. Because the optimization tool will automatically generate and analyze hundreds or thousands of hull forms, it is imperative that the analysis tools are computationally efficient. Yet at the same time, in order to incorporate meaningful optimization logic, the tools must be accurate up to the operational requirement levels. Because the operational requirements may set seakeeping performance criteria up to Sea State 5 or higher, it becomes necessary to use a nonlinear seakeeping assessment tool capable of predicting large amplitude motion.

The object of the research presented in this dissertation is to develop the nonlinear seakeeping analysis tool to be incorporated into the ONR design optimization program. The prime requirement is that it must be very efficient and very robust, given the fact that the program will be executed blindly hundreds or thousands of times, yet rationally account for the hull interaction physics.

1.2 Prior Work

The problem of predicting the seakeeping performance of multi-hulled ships is not new. As general seakeeping theory has expanded over recent decades, so too have efforts to apply the techniques to multihulls. While there are many approaches that can be taken for solving the hydrodynamic forces of a ship undergoing motion in waves (see Beck and Reed (2001) for a comprehensive taxonomy of methods), the majority employ the assumptions of inviscid, irrotational, and incompressible flow. This leads to the use of a velocity potential in formulating the boundary value problem (BVP). This trend has held true for predicting the motions of multihulls.

1.2.1 Early Attempts

As recognized by Journée (1992), 2D strip theory, as developed by Salvesen et al. (1970), fits a practical need for assessing ship motions at the early design stage. Traditional strip theory reduces the 3D nonlinear problem into a series of linear 2D problems solved at transverse cuts of the hull. The assumption is that for a long and slender hull, the changes in the x direction will be of higher order. The first attempts at solving the multihull seakeeping problem, however, resorted to strip theory not because it was more efficient, but rather because it was the only practical theory available.

One early attempt at predicting motions of a catamaran was by Wahab and Hubble (1972). They used strip theory and neglected interactions between the hulls to calculate heave and pitch in head seas and roll in beam seas, treating roll as the alternate heaving of two hulls. They concluded that neglecting interaction effects gives reasonable results for roll in beam seas, but heave and pitch predictions were poor for predictions up to Fn=0.38. Additionally, they note that catamaran motions can be much different than monohulls. Jones (1972) also attempted to use strip theory for catamaran motions, but this time included both hulls in the boundary value problem. He identified the problem of critical frequencies where there is a standing wave trapped between the hulls. Jones also notes that there is decreasing accuracy with increasing speed.

As the popularity of the SWATH concept took hold with the US Navy, more effort was contributed to the multihull prediction problem. Lee (1976) attempted to use a six degree-of-freedom (6-DOF) linear strip theory for multiple headings. Similar to Jones (1972), Lee included both hulls in the boundary value problem. He also noted the singular solution corresponding to the trapped wave as well as the importance of viscous damping and modeling the stabilizing fins for a SWATH hull form.

Later, Lee (1978) attempted to model the hull interactions by solving the single demi-hull boundary value problem and adding the solution of the phase-shifted opposite hull wave at the far field ($y \rightarrow \infty$). In terms of the far field wave amplitude, he determined B_{ij} and then obtains A_{ij} by the "Kramers-Kronig" relations. Lee concluded that this method gives satisfactory results within the frequency range of interest, but that it does not capture the "abrupt discontinuities" of the hydrodynamic coefficients.

Sun (1982) describes a different far field approach for modeling the interactions between hulls of a catamaran. He proposes a linear frequency-domain strip theory to predict arbitrary heading, constant speed catamaran motions, noting that the method can be extended to multiple hulls. Interaction effects are included by assuming demi-hulls are in each other's far-field and the radiation potential exists as a progressive wave in the far-field. The progressive wave potential travels perpendicular to the demi-hull center-plane and appears as a deepwater incident wave to the opposite hull downstream. The progressive wave potential is given in terms of a section's velocity, an amplitude coefficient, and phase (a single phase for vertical and lateral motions, respectively). Sun writes that this wave will reflect off the hull with the same magnitude but opposite direction. Through an iterative process, interaction coefficients are obtained. While the overall concept described by Sun sounds promising, the theory does not appear to address forward speed effects properly in some potentials. No comparisons to model data are provided.

Breit and Sclavounos (1986) wrote of another approximation for the wave interaction between parallel slender bodies. In this theory, they solve the zero forward speed problem for a single body via strip theory, assuming the separation distance is on the order of the demi-hull length. The interaction occurs from a solution of the infinite series of reflection and transmission of waves between the bodies. They also cite work from Simon (1982) who treats the force on a section solely due to its own radiation potential, an incident wave from the opposite body's motion, and the diffraction from that incident wave. Breit and Sclavounos claim that this method is not adequate for 3D dissipation of the wave energy.

Watanabe (1992) presented his own method of modeling the interactions between hulls. In this method, he uses thin ship theory to develop symmetric and anti-symmetric potentials for each demi-hull, where the symmetric is due to single body motion and anti-symmetric is due to "distortion of flow and radiating waves by one of" the demi-hulls that "induces on the other demi-hull anti-symmetric flow about its centerplane."

1.2.2 Recent Research

While the early designers and Navy experts did not have much choice other than to use strip theory for the prediction of multihull motions, 2D calculations continue to be developed for this use, simply because they are so much more efficient than the 3D codes. Additionally, because the typical multihull demi-hull is extremely long and slender it would be perfectly suited for strip theory if interactions were neglected and it was applied at low forward speed. In fact, Zhao and Aarsnes (1995) claim that, while 2D strip theories are not appropriate for use at high Froude number (> ~0.5), linear 3D methods have not done much better. Min et al. (1993) come to the same conclusion regarding strip theory and a linear 3D panel method at Fn=0.8.

Of course, much progress has been made in the development of 3D codes for use with multihull problems. Kring and Sclavounos (1991) presented their results for a 3D linear Rankine Panel method applied to a Wigley catamaran, noting the improvement when the basis flow was based upon a double-body linearization. They also note the importance of applying a Morino-Kutta condition for a wake model at the stern, because of interaction effects. More recently, Bailey et al. (1999) presented their work on a 3D linear potential flow method for head seas. In this method, they try to account for arbitrary forward speed by using a translating, pulsating source distribution on the wetted surface. Bailey et al. claim that a 3D code is needed for multihulls and, like Faltinsen et al. (2003), cite the need to consider the interaction between steady and unsteady waves.

The largest effort in recent research has been devoted to solving the high-speed aspect of the multihull seakeeping problem. In order to solve this problem, researchers have acknowledged that the inherent three-dimensionality of the problem must be taken into account. In order to accomplish this, yet still maintain a certain degree of computational efficiency, the 2½-D (or 2D+t) approach has been adopted as the most popular choice.

The fundamental idea of the 2½-D method is to solve a series of 2D problems, but use the 3D free surface boundary conditions. The solution is started at the bow and stepped toward the stern section-by-section. The assumption that the solution can be stepped downstream requires that waves do not travel forward. For this to be true, the

Froude number must have a lower limit, typically taken to be about 0.4. Another consequence of the 2½ approach is that only the diverging waves are captured, but this is reasonable for high speed, where the diverging waves are dominant.

Faltinsen and Zhao (1991) applied this method to solving the high-speed ship motion problem for a monohull, but assumed a strong link between the steady and unsteady potentials. The method of Faltinsen and Zhao is a linear frequency-domain method that attempts to capture the influence of the steady potential on the unsteady potential by expanding the free-surface boundary conditions about the steady wave surface.

Zhao and Faltinsen (1992) later extended their method to a linear time domain, which was followed by the extension to nonlinear time domain by Zhao and Aarsnes (1995) (explained more completely by Zhao, 1997). Zhao and Aarsnes solve the nonlinear motions of a catamaran by employing the time domain 2½-D method, with the linearized free surface boundary conditions applied on the total wave surface (steady + incident waves) and using the instantaneous wetted surface to calculate the hydrostatic and Froude-Krylov forces. However, they do not include hydrodynamic interaction between the hulls. Zhao (2003) later used this method as the basis for calculating relative motions to be used in solving the impact problem as a post-processor.

Ohkusu and Wen (1993) and Hermundstat et al. (1999) are two more examples of the application of the 2½-D method to solving the high speed catamaran problem. While Hermundstat et al. decouple the steady potential from the unsteady potential (they use Neumann-Kelvin linearization), they claim that they account for hull interactions by "utilizing the vessel's port-starboard symmetry." They do this by splitting the incident wave potential into an odd and an even part to get a so-called symmetric and anti-symmetric diffraction potential. While allowing only weak interaction with the steady potential, they recognize its importance at high speed. They conclude though that their method for hull interaction does not lead to significant improvement for correlation with model data.

The important question that needs to be answered is for how low of a Froude number is the 2½-D method valid. Tønnessen et al. (1993) attempt to answer this

question by comparing the results of a 2½-D code to a 3D panel code. For a monohull, they show that the 2½-D code gives similar solutions to the 3D code at Fn=0.3. They also examine the demi-hull separation of a catamaran to see when interaction effects are important. Their conclusion is when the separation is less than approximately 0.2L.

Holloway (1998), Holloway et al. (2003), and Davis and Holloway (2003) also employ a high-speed strip theory, but unlike other 2½-D methods, develop a time-domain solution on strips fixed in space with a different (downstream) strip of the hull intersecting the plane at each time step. Their method is able to capture hull interactions, the effect of which they not surprisingly conclude to be somewhat weak at higher speeds.

With all the attention being paid to high-speed-specific codes, Kashiwagi (1993) presents a linear frequency-domain method using Newman's unified slender-ship theory and an interaction model using a far field approach. He compares predictions against model data (Lewis form demi-hulls) at Fn=0.15 and 0.3, concluding that the theory agrees well with the experiments, except for pitch at higher Froude number and low frequencies. Ronæss (2002) recently extended this approach to independent bodies with similar success.

For the purposes of exercising ordinary 2D strip theory on a trimaran hullform, Doctors and Scrace (2004) compared predictions of roll in oblique seas using no interactions (independent demi-hull solutions, see Figure 1.2) and strip theory with a full transverse cut of the hull (see Figure 1.3). They conclude that the no-interactions case more closely matches model test data in general, suggesting that interaction effects are small. However, the particular trimaran design that was examined had outer hulls with fairly small displacement in comparison to the primary hull.

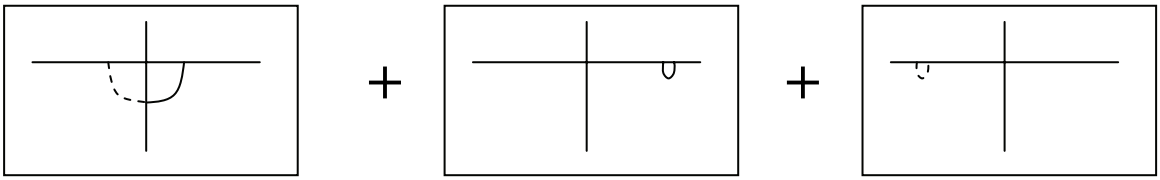

Figure 1.2 Representation of trimaran case with demi-hulls treated independently

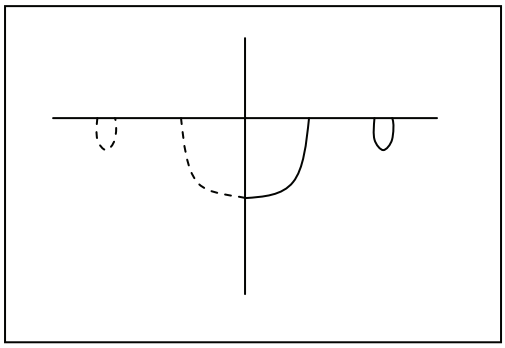

Figure 1.3 Representation of trimaran case using full transverse cut

1.2.3 Conclusions Based on Prior Work

The past several decades of research on the prediction of multihull vessel motion have revealed many of the relevant physics and approaches to capturing them.

Given modern computer capabilities and the development of 3D seakeeping codes, using a high fidelity 3D panel code would seem to be the preferred choice for predicting multihull seakeeping performance. One primary advantage is the fact that hull interactions are automatically included. However, computations are orders of magnitude slower than traditional strip theories and a high level of expertise is required to run these codes in order to ensure numerical stability and physical correctness of the solution. These disadvantages preclude their use at this point in time as an early-stage design optimization tool.

The early research that focused on the use of strip theory revealed that the solution of a 2D transverse cut is not appropriate, because it leads to "wave trapping" and can result in the so-called "piston mode resonance" (see Faltinsen, 2005). The interaction of the demi-hulls is consequently forced into being 2D, when in reality, 3D dissipation is required. This is especially true when the vessel has forward speed, because the radiated waves are swept downstream (in a ship-fixed frame of reference). Some researchers have concluded that it is better to evaluate the demi-hulls individually, thereby assuming that there is no interaction. This would be correct for the cases when the radiated waves are swept completely downstream. Given the long and slender demi-hulls of most multihull designs, 2D strip theory would then appear to be a rational choice. However, depending

on ship speed, hull spacing, and frequency of encounter, there is likely to be some interaction with the other demi-hull(s). Furthermore, ordinary strip theory is not valid for high forward speed, with the upper limit considered to be Fn=0.3-0.4.

Much of the recent research appears to be focused on solving the high-speed aspect of the multihull seakeeping problem. With the development of the 2½-D methods, researchers have shown relatively good success in predicting the motion of both monohulls and multihulls at high forward speed. They have concluded that the interaction of the steady potential and the unsteady potential is important. The 2½-D methods also take advantage of the fact that the hull interactions, at least in the case of radiated waves, are likely to be small or non-existent at high speed. The disadvantage, however, is that these methods can only be used at high ship speeds (the lower limit typically taken to be Fn=0.3-0.4).

Perhaps the best alternative of past multihull research is Kashiwagi's development of a slender body unified theory for multihulls. His successful use of a far-field approximation allows the rational solution of hull interaction effects that is valid for low ship speed. With respect to its application to multihull design optimization, it has the disadvantage of being more computationally intense than strip theory, but certainly less so than 3D codes.

1.3 Present Approach

The motivation for the present theory is producing a very fast method that can be utilized in a hull-form optimization scheme for multihulls, where the seakeeping measure of merit may include a time-domain assessment of motions in large waves. To satisfy these requirements, the present approach is based on a frequency-domain strip theory with quasi-3D radiation interaction forces that is extended to a nonlinear time-domain solution for predicting motions in large waves.

Given the conclusion that hull interaction effects are important, at least up through moderate forward speed, it is essential that the present theory capture this physics in a rational manner. However, in order to attain the computational efficiency required, a 2D strip theory with interactions will be developed for the frequency-domain solution in

a manner similar to Sun rather than following the unified slender body theory for multihulls developed by Kashiwagi.

The present theory assumes that the demi-hulls exist in each other's far-field and subsequently solves the 2D (zero-speed) frequency-domain problem on the independent demi-hulls. For the radiation problem, this avoids the problem of piston mode resonance, but by itself would not capture any hull interactions. Therefore, following the solution of the source strengths, the far-field Green function is used to determine the far-field radiation potential for the corresponding mode of motion. This far-field radiation potential takes the form of a progressive wave, with amplitude and phase captured automatically by the far-field Green function. Radiation interaction forces are then determined by treating the far-field radiation potential as a wave that is incident upon the other demi-hull at a point downstream. No reflections of this radiated wave will be modeled though, following the assumption that only long wavelengths are likely to reflect and "re-impact" on the originating hull before being swept downstream. The longer the radiated wavelength, the less likely there will be an appreciable reflection.

A key feature of this method is that the 2D radiation potential calculations, which are independent of incident wave and ship speed, can be pre-calculated over a range of basis frequencies and stored. For any number of speed, wavelength, and wave heading combinations, the demi-hull radiation potentials on each 2D panel and the far-field radiation potential of each section is simply interpolated. The determination of the far-field radiated potential on a panel of a section downstream (necessary for determining a force) is accomplished analytically given the progressive wave form of the potential. Such a formulation means that the motions can be calculated almost instantaneously.

Once the frequency-domain hydrodynamic coefficients have been calculated, a time-domain simulation can be executed. Because geometric nonlinearities can be significant on multi-hulled vessels, particularly when considering the wet-deck, it is necessary to capture the dominant forces due to the changing wetted geometry when the ship is undergoing large amplitude motion. In the present approach, a "blended method" is used, whereby the hydrostatic and Froude-Krylov pressures are calculated on the instantaneous wetted portion of the ship.

The theory developed in the present approach has been implemented in a code named “NSHIPMO_multihull”. Comparisons are made with catamaran and trimaran model data for validation purposes.

Chapter 2

Multihull Frequency-Domain Ship Motion Problem

The foundation of the present multihull seakeeping prediction tool is the linear frequency-domain solution. The linear frequency domain solution can provide an overall characterization of the ship's motions across all speeds, headings, and sea states, as well provide the hydrodynamic coefficients to be used in the nonlinear (blended-method) time-domain simulation. With the stated objective of the present work being computationally efficient predictions, emphasis has been placed on developing theory that satisfies the objective of speed while attempting to capture the relevant physics of multi-hulled bodies.

2.1 Problem Statement

The solution of the dynamics of the multihull vessel requires the solution of the fluid forces acting upon it. These forces are considered to be hydrostatic and hydrodynamic.

Potential flow is used in developing the hydrodynamic forces, where the hydrodynamic forces can be separated as those due to steady flow and those due to time-varying flow. The time-varying flow consists of the radiation and ambient wave excitation potentials.

The fundamental assumption of the present multihull seakeeping theory is that interaction effects only occur in the 3D radiation problem. This assumption is made by assuming the demi-hulls are in each other's far field. The mechanism for interaction is the generated far-field radiated waves from each demi-hull appearing as an incident wave on the other demi-hull(s).

The radiation portion of the multihull seakeeping problem is assumed to be linear. Strip theory is utilized as the foundation of the present frequency-domain solution following Salvesen, Tuck and Faltinsen (1970). The steady potential is assumed to be zero, acknowledging this will not be adequate for high-speed, as shown by the 2½-D methods. By this assumption, the wetted geometry is defined by the mean calm waterline at zero speed.

2.1.1 Far-Field Assumption

In adopting a strip theory approach, the hydrodynamic forces are determined independently for each section of each demi-hull with hull interaction forces included for the radiation problem by formally assuming that the demi-hulls are in each other's far-field. That is to say that the solution of the radiation potential on a given "strip" is not influenced by the presence of another demi-hull and that the interaction force can be treated additively. To satisfy this condition, all spatially decaying components of the radiated wave (i.e. the stationary wave) must go to zero in the distance separating the demi-hulls. The only interaction effect will therefore come from the remaining progressive wave.

Strip theory assumes that the beam and draft of a hull is much less than the length. Similarly, the separation distance between hulls must be much greater than the beam in order for the far-field assumption to hold. It is noted then that the separation distance between hulls must be $O(\mathrm{L})$.

When there is forward speed, a progressive wave radiated from one demi-hull cannot reflect back upstream and be incident upon the original radiating demi-hull, so the far-field assumption would appear to be very good. For there not to be any influence though, it must be shown that the frequency-independent portion of the radiation potential, which is satisfied instantaneously, dies out significantly over the separation distance of the demi-hulls.

In the special case of zero-speed, there exists the possibility that the radiated wave would have a measurable reflection off of the opposite demi-hull and be incident upon the original radiating section. While it would appear that this violates the condition that

the presence of the other demi-hull not influence the solution of the radiation potential, the reflected wave can be considered an additive potential of a progressive wave form, provided the amplitude and phase were determinable. In the present theory, reflections are not considered (though the force due to the first reflection is), because the solution of the diffraction potential on the opposite demi-hull would be required, which would add considerable computational expense. However, it is noted that this is an area for future improvement of the theory. The "no reflections" assumption is poorest in the zero-speed case though and should become less noticeable with increasing forward ship speed. That is because only the lowest frequency radiated waves are likely to travel quickly enough to be able to reflect off of the opposite demi-hull and re-impact the original radiating hull, yet the lowest frequency waves (longest wavelengths) should have the lowest coefficient of reflection.

2.1.2 Other Assumptions

Consistent with linear theory, it is assumed that the amplitudes of motion are small and that the individual potentials can be superimposed in order to find the total potential. Additionally, all strip theory assumptions hold on the solution of a demi-hull. This primarily means that derivatives in the x-direction are much smaller than the derivatives in the y- and z-directions and that the x-component of the unit normal, n_1, is much smaller than the y- and z-components of the unit normal, n_2 and n_3.

In order to provide faster computations and to simplify the program, the implemented code assumes port-starboard symmetry of the ship, though no such restriction is set on the geometry of individual demi-hulls, unless the demi-hull is the center-hull of a trimaran. Furthermore, the theory has only been implemented for catamarans and trimarans.

2.1.3 Total Hydrodynamic Potential

Following the principal of linear superposition, the total velocity potential, Φ, is decomposed into a steady potential, ϕ_S, and a time-varying potential, ϕ_T, that oscillates with $e^{i\omega_e t}$ time dependence.

$$\Phi(x,y,z,t) = -U_0 x + \phi_s(x,y,z) + \phi_T(x,y,z)e^{i\omega_e t} \quad \textbf{(2.1)}$$

In the current approach, ϕ_s is assumed to be zero. The time-varying potential consists of the incident wave potential, ϕ_0, six demi-hull radiation potentials, ϕ_k, six incident far-field radiated wave potentials, $\phi^{\sim I}_k$, six diffracted far-field radiated wave potentials, $\phi^{\sim D}_k$, and the ambient incident wave diffraction potential, ϕ_7.

$$\phi_T = \phi_0 + \sum_{k=1}^{6} \phi_k \zeta_k + \sum_{k=1}^{6} \phi_k^{\sim I} \zeta_k + \sum_{k=1}^{6} \phi_k^{\sim D} \zeta_k + \phi_7 \quad \textbf{(2.2)}$$

where ζ_k is the amplitude of body motion in k-th mode. The six incident far-field radiated wave potentials and six diffracted far-field radiated wave potentials correspond to each of the six demi-hull radiated wave potentials. The ambient incident wave potential, ϕ_0, is known a priori and is, in the inertial frame, given by equation 2.3.

$$\phi_0 = \frac{iga}{\omega_o} e^{kz} e^{-ik(x\cos\beta + y\sin\beta)} \quad \textbf{(2.3)}$$

where a is the wave amplitude, ω_o is the wave circular frequency (as opposed to encounter frequency), k is the wavenumber, and β is the wave heading angle.

2.1.4 Demi-Hull Radiation Boundary Value Problem

The boundary value problem solved on the independent demi-hull follows the strip theory developed by Salvesen, Tuck, and Faltinsen (1970). Because the solution of the radiation potentials on the radiating demi-hulls is necessary for the determination of the interaction potentials, the implemented strip theory is reviewed here.

The demi-hull radiation boundary value problem is developed in an inertial frame that moves with constant velocity, U_o, equal to the ship mean velocity. The inertial reference frame, given by the right-handed axes (x, y, z), has its origin at the intersection of the mean free surface, ship centerplane, and midship plane. The positive x-axis extends out the ship bow. The positive y-axis extends out the port side of the ship. The positive z-axis extends up from the mean free surface.

The volumetric domain travelling in the inertial frame is bounded by the sea bottom, vertical control surfaces at infinity, the free surface and the wetted ship body. The statement of conservation of mass leads to the continuity equation,

$$\nabla \cdot \vec{V} = 0 \tag{2.4}$$

which, when put in terms of the total velocity potential, Φ, leads to the Laplace equation:

$$\nabla^2 \Phi = 0 \tag{2.5}$$

The Laplace equation holds true throughout the fluid domain.

The general (3D) boundary value problem contains boundary conditions on the body, the free-surface, the sea floor (in the case of finite depth), and at infinity in the (x,y) direction. The fully nonlinear and 3D boundary value problem has been simplified to a series of linearized boundary value problems solved on strips (transverse cuts) of the independent demi-hulls. To differentiate between the solution to the three-dimensional radiation potentials and the two-dimensional radiation potential, the variable ψ_k is introduced and defined by equation 2.6.

$$\phi_k(x,y,z) \approx \psi_k(y,z;x) \tag{2.6}$$

2.1.4.1 Boundary Conditions

The 2D boundary value problem that must be solved is illustrated in Figure 2.1. The boundary value problem is solved for the oscillatory motion of a single demi-hull, without any influence from or need to satisfy boundary conditions on any other demi-hull (represented by the dashed lines). The only boundary conditions that exist are the radiation condition, the free surface boundary conditions, the bottom boundary condition, and the body boundary condition.

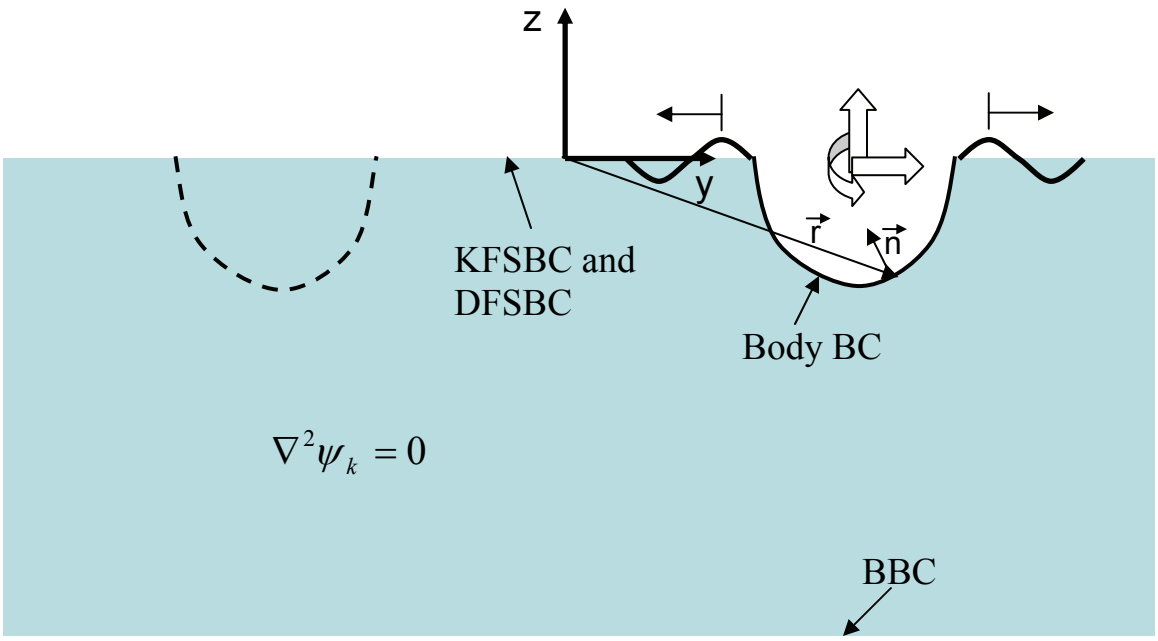

Figure 2.1 2D boundary value problem domain and boundary conditions

The radiation condition simply states that the radiated waves must exit the domain. There are two free surface boundary conditions: the kinematic and dynamic. Derived from the definition of a free-surface, the condition is set that there is no flow through the free-surface, η(x,y,t). In other words, a particle on the free surface stays on the free surface. This condition is known as the kinematic free surface boundary condition (KFSBC), which when linearized and applied at the mean free surface gives:

$$\frac{\partial \eta}{\partial t} = \frac{\partial \psi_k}{\partial z} \qquad \text{on } z = 0 \qquad \textbf{(2.7)}$$

The dynamic free-surface boundary condition (DFSBC) states that the pressure at the free-surface is atmospheric, which when linearized and applied at the mean free surface leads to:

$$\frac{\partial \psi_k}{\partial t} = -g\eta \qquad \text{on } z = 0 \qquad \textbf{(2.8)}$$

There is no flow through the bottom boundary, leading to the finite-depth bottom boundary condition (BBC):

$$\frac{\partial \psi_k}{\partial n} = 0 \qquad \text{on } z = -h(y) \qquad \textbf{(2.9)}$$

where h is the depth. Alternatively, in the case of infinite depth, the disturbance velocity must go to zero as z goes to minus infinity:

$$\nabla \psi_k = 0 \qquad \text{as } z \rightarrow -\infty \tag{2.10}$$

The final condition states that there is no flow through the ship's hulls, giving the body boundary condition (Body BC). While the other boundary conditions are independent of ship speed, due to the linearization and assumption of ϕ_s=0, the body boundary condition does include ship speed. The pitch and yaw modes of motion lead to an "angle of attack" effect that can not be neglected. In terms of the general radiation potential, ϕ_k, the Timman-Newman body boundary condition can be derived as (see Timman and Newman, 1962):

$$\frac{\partial \phi_k}{\partial n} e^{i\omega_e t} = \left[\dot{\vec{\alpha}} + \nabla \times \left(\vec{\alpha} \times \vec{W}\right)\right] \cdot \hat{n} \qquad \text{on the mean wetted surface, } S_o \tag{2.11}$$

where $\vec{\alpha}$ is the displacement vector on the body, $\vec{n} = (n_1, n_2, n_3)$ is the unit normal into the body, and $\vec{W}$ is the total steady velocity. In this case, because ϕ_s=0,

$$\vec{W} \approx -U_o \hat{i} \tag{2.12}$$

Alternatively stated, equation 2.11 is written as the well known body boundary condition:

$$\frac{\partial \phi_k}{\partial n} = i\omega_e n_k + U_o m_k \qquad \text{on } S_o \tag{2.13}$$

where $n_k = \vec{r} \times \hat{n} = (yn_3 - zn_2, -xn_3, xn_2)$ for k=4, 5, 6 (having assumed $n_1 \ll n_2, n_3$) and the "m-terms" are defined as:

$$\vec{m} = -(\vec{n} \cdot \nabla) \cdot \frac{1}{U_o} \vec{W} \qquad \text{for k=1, 2, 3} \tag{2.14}$$

and

$$\vec{m} = -(\vec{n} \cdot \nabla) \cdot \frac{1}{U_o} (\vec{r} \times \vec{W}) \qquad \text{for k=4, 5, 6} \tag{2.15}$$

Following equation 2.12, the m-terms are simply:

$$m_k = (0,0,0,0,n_3,-n_2) \tag{2.16}$$

At this point, it is convenient to separate the general radiation potential into speed-independent and speed-proportional parts in the manner of equation 2.17.

$$\phi_k = \phi_k^0 + \frac{U_o}{i\omega_e}\phi_k^U \tag{2.17}$$

Taking the partial derivative of equation 2.17 with respect to the body normal leads to:

$$\frac{\partial \phi_k}{\partial n} = \frac{\partial \phi_k^0}{\partial n} + \frac{U_0}{i\omega_e}\frac{\partial \phi_k^U}{\partial n} \tag{2.18}$$

Matching terms with equation 2.13, the body boundary condition can now be stated separately in terms of ϕ_k^0 and ϕ_k^U:

$$\frac{\partial \phi_k^0}{\partial n} = i\omega_e n_k \tag{2.19}$$

$$\frac{\partial \phi_k^U}{\partial n} = i\omega_e m_k \tag{2.20}$$

The m-terms, as given in equation 2.16, can be substituted into equations 2.20 and 2.18 to show that the forward-speed potentials for surge, sway, heave, and roll are equal to zero, while forward-speed potentials for pitch and yaw are equal to ϕ_3^0 and $-\phi_2^0$, respectively. In terms of the zero-speed potentials only, equation 2.17 can be simplified to:

$$\phi_k = \phi_k^0 \qquad \text{k=1, 2, 3, 4} \tag{2.21}$$

$$\phi_5 = \phi_5^0 + \frac{U_o}{i\omega_e}\phi_3^0 \qquad \text{k=5}$$

$$\phi_6 = \phi_6^0 - \frac{U_o}{i\omega_e}\phi_2^0 \qquad \text{k=6}$$

Furthermore, taking advantage of the strip theory assumption that the n_1 normal vector is much smaller than n_2 and n_3, the n_5 and n_6 normal vectors reduce to $-xn_3$ and xn_2, respectively. From equation 2.19, it is found that

$$\phi_5^0 = -x\phi_3^0 \tag{2.22}$$

and $\phi_6^0 = x\phi_2^0$

The general radiation potential, ϕ_k, can now be determined from the solution of the 2D radiation boundary value problem in terms of ψ_k (k=1, 2, 3, 4). The zero-speed and forward-speed components of ϕ_k in terms of ψ_k are summarized in Table 2.1.

Table 2.1 Zero and forward speed radiation potentials in terms of 2D potential

k	ϕ^0_k	ϕ^U_k
1	ψ_1	0
2	ψ_2	0
3	ψ_3	0
4	ψ_4	0
5	$-x\ \psi_3$	ψ_3
6	$+x\ \psi_2$	$-\psi_2$

2.1.5 Hydrodynamic Force Calculation

The potential flow hydrodynamic force is determined from integration of the dynamic pressure, p_d, over the mean wetted body. The dynamic pressure is determined from the Bernoulli equation, which appears without simplification and in terms of the total hydrodynamic potential (see equation 2.1) as:

$$p_d = -\rho\left(\frac{\partial\Phi}{\partial t} + \frac{1}{2}(\nabla\Phi)^2 - \frac{1}{2}U_o^2\right) \qquad \textbf{(2.23)}$$

Having assumed that ϕ_s is 0, and utilizing the vector form, $\vec{W}$, of the steady fluid velocity from equation 2.12,

$$\nabla\Phi = \vec{W} + \nabla\left(\phi_T e^{i\omega_e t}\right) \qquad \textbf{(2.24)}$$

and $$(\nabla\Phi)^2 = \vec{W}^2 + 2\vec{W}\cdot\nabla\left(\phi_T e^{i\omega_e t}\right) + \left(\nabla\left(\phi_T e^{i\omega_e t}\right)\right)^2$$

Dropping higher order terms, the hydrodynamic pressure from Bernoulli reduces to:

$$\begin{aligned} p_d &= -\rho\left(i\omega_e\phi_T e^{i\omega_e t} + \vec{W}\cdot\nabla\phi_T e^{i\omega_e t}\right) \qquad \textbf{(2.25)} \\ &= -\rho\left(i\omega_e + \vec{W}\cdot\nabla\right)\phi_T e^{i\omega_e t} \end{aligned}$$

Substituting equation 2.12 yields:

$$p_d = -\rho\left(i\omega_e - U_0\frac{\partial}{\partial x}\right)\phi_T e^{i\omega_e t} \tag{2.26}$$

Therefore, the total (3D) hydrodynamic force in the j[th] direction is:

$$F_{HD,j} = \iint_{S_0} p_d n_j ds \tag{2.27}$$

$$= -\rho\iint_{S_0} n_j\left(i\omega_e - U_0\frac{\partial}{\partial x}\right)\phi_T e^{i\omega_e t} ds$$

The linear superposition assumption allows the force contribution from each of the various components of the time-varying potential to be calculated separately and summed. Furthermore, the strip theory assumption allows for the longitudinal integration of the strip-wise sectional force to obtain the total ship force.

2.1.6 Numerical Solution of 2D Boundary Value Problem

The numerical solution of the 2D demi-hull radiation problem follows the method developed by Frank (1967), which is commonly referred to as a close-fit method. A section is discretized into 2D "panels" that have a constant source density applied across the length of the panel. The body boundary condition is satisfied at the midpoint of each panel and the 2D Green function developed by Wehausen and Laitone (1960) for a pulsating source below the free surface is used to satisfy the free surface boundary conditions. The simultaneous solution of the complex source strengths leads to the solution of the complex potential.

As a demonstration of the present interaction theory, only the infinite depth solution (as developed by Frank) has been examined. It should be noted that there is no reason why the present theory cannot be applied to the finite depth case, because the solution of the demi-hull radiation problem is independent of the interaction theory. However, it should be noted that the validity of the far-field assumption must be evaluated with respect to the rate of spatial decay inherent to the finite depth problem.

Frank defines the 2D radiation problem in complex coordinates where

z' = x'+ iy' is a field point and $\zeta = \xi + i\eta$ is a source point. Unlike the present problem statement, Frank defines the unit normal on the body as pointing into the fluid and defines an $e^{-i\omega_e t}$ time dependence. Figure 2.2 shows a sample catamaran demi-hull section in Frank's coordinate system. As had been done in the SHIPMO.BM computer program (see Beck and Troesch, 1989), in which the present theory has been implemented, Frank's notation and time-dependence will be retained for clarity. The significance of having a $-\omega_e t$ time-dependence versus a $+\omega_e t$ time-dependence is that the conjugate of the complex influence coefficients must be taken in order to ensure proper phase consistency.

The infinite-depth Green function from which Frank's work is based is:

$$G(z,\zeta) = \Re\left\{\frac{1}{2\pi}\left[\ln(z-\zeta) - \ln(z-\overline{\zeta}) + 2\cdot P.V.\int_0^\infty \frac{e^{-ik(z-\overline{\zeta})}}{\nu - k}\,dk\right]\right\} - i\cdot\Re\left\{e^{-i\nu(z-\overline{\zeta})}\right\} \qquad \textbf{(2.28)}$$

where $\overline{\zeta}$ is the complex conjugate of ζ and represents the source's image about the free surface.

It should be noted that the source points would not be imaged about the x'=0 plane (in Frank's coordinates) when solving for the source strengths, because the influence of the opposite demi-hull is not considered in the solution due to the far-field assumption.

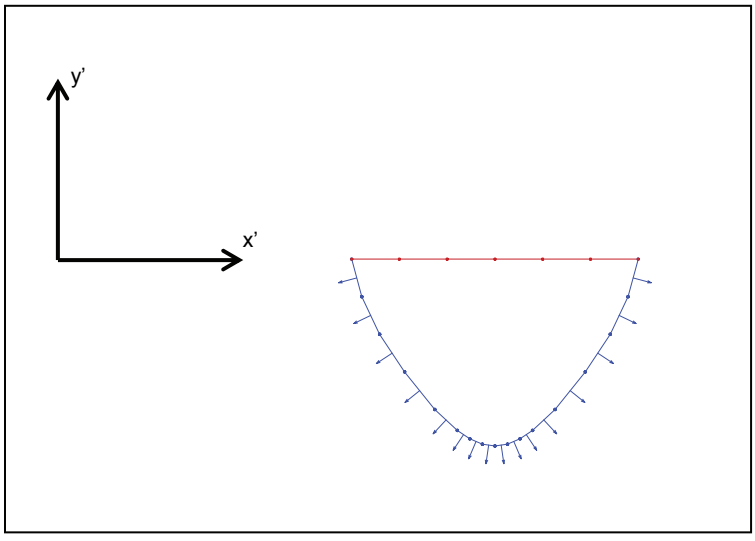

Figure 2.2 Sample paneled 2D section in Frank's coordinate system showing inward (into fluid) pointing unit normals

The Green function given in equation 2.28 can provide insight into the form of the radiated wave and subsequently the validity of the far-field assumption. The first two complex log terms are independent of wave frequency and therefore would immediately show an influence on the opposite demi-hull. This "wave-free" portion is the difference of the complex log of the distance between the field point and the source and the complex log of the distance between the field point and the source's image about the free surface. For the far-field assumption to be valid, the difference of the complex logs must vanish at the separation distance of the demi-hulls. A sample plot of the spatial decay is presented in Figure 2.3 for the case of a source point just below the free surface. For this case, a panel length is taken to be $O(1)$, the demi-hull beam $O(10)$, and the demi-hull length $O(100)$. The magnitude of the difference between the complex logs has been normalized by the magnitude of the wave-free term at a distance of 1. In this case, the influence at a distance of the demi-hull beam is about 10% of the influence at a point one panel length away. At a distance equal to the demi-hull length, the influence is about 1%. Therefore, the assumption that a demi-hull separation distance must be on the order of the ship length in order for the far-field condition to hold seems to be valid for the wave-free influence. In fact, a separation distance on the order of the demi-hull beam could prove to be sufficient.

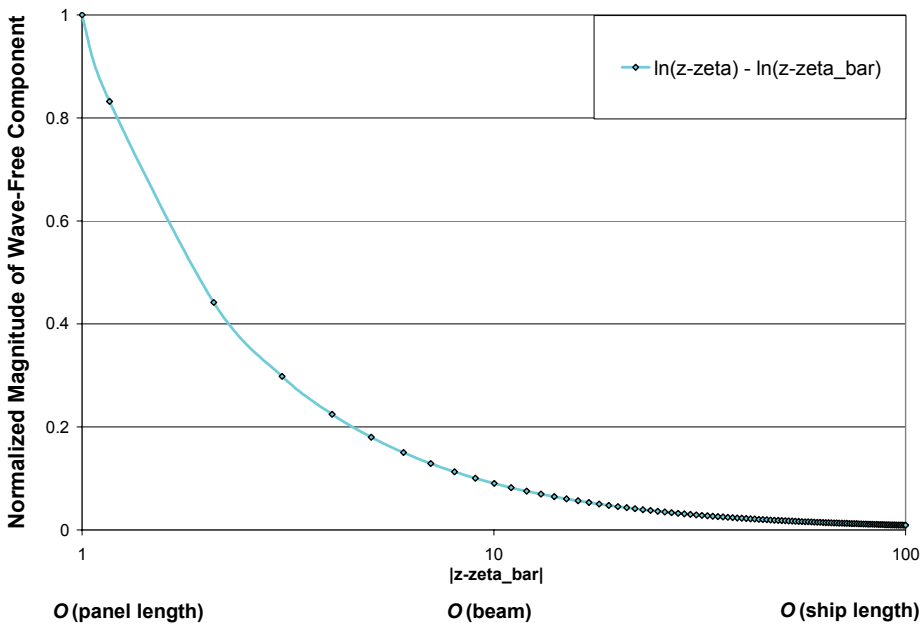

Figure 2.3 Normalized example of wave-free term spatial decay

The third term in the Green function is a principal value integral that has a non-obvious effect by inspection. The evaluation of the integral can be solved numerically when it is re-written as shown in equation 2.29, where E_1 is the complex exponential integral given in equation 2.30.

$$P.V.\int_0^\infty \frac{e^{-ik\left(z-\bar{\zeta}\right)}}{\nu-k}dk = e^{-i\nu\left(z-\bar{\zeta}\right)}\left[i\pi - E_1\left(-i\nu\left(z-\bar{\zeta}\right)\right)\right] \tag{2.29}$$

$$E_1\left(-i\nu\left(z-\bar{\zeta}\right)\right) = P.V.\int_{-i\nu\left(z-\bar{\zeta}\right)}^\infty \frac{e^{-t}}{t}dt \tag{2.30}$$

The $e^{-i\nu\left(z-\bar{\zeta}\right)}$ term on the right-hand-side of equation 2.29 represents the equation for a progressive wave. It is multiplied by iπ, a constant, and the complex exponential integral (E_1). The first term will not decay and therefore will exist in the far-field. The complex exponential integral, however, will decay spatially with increasing separation distance. Unlike the complex log terms in the Green function, the complex exponential term is dependent on wavenumber. To demonstrate the rate of decay, the E_1 function has been plotted in Figure 2.4 for three wavelengths as a function of the separation distance from a source just below the free surface. As has been done in Figure 2.3, the values of the functions have been normalized by their value at a separation distance equal to a panel length. The solid line represents the E_1 decay for a wavelength on the order of a panel length. Its decay rate is nearly identical to the wave-free term's decay rate, which is plotted for reference. The short-dashed line represents E_1 spatial decay for a radiated wavelength on the order of the demi-hull beam. Like the wave-free term, it too experiences significant decay at a separation distance on the order of the beam. The E_1 decay for a wavelength on the order of the ship length, as shown by the long-dashed line, is not nearly as rapid. On the order of a beam separation distance, the function remains at more than 30% of its magnitude at a distance equal to a panel length. Furthermore, when plotted without normalization, as seen in Figure 2.5, it is clear that the magnitude of the term is much larger for longer radiated wavelengths. Still, the requirement of a separation distance on the order of the ship length in order for the far-field assumption to hold appears to be sufficient. A separation distance any less than the ship length, however, may prove to violate the far-field assumption.

The final term in the Green function is a pure progressive wave, so there will be no spatial decay and, therefore, this wave will appear in the far field.

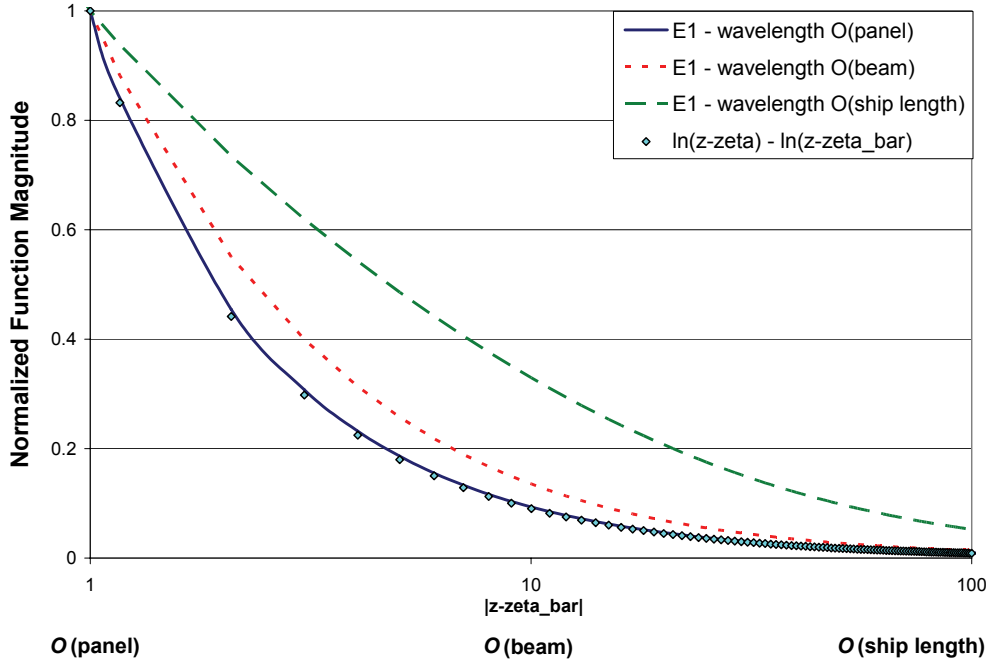

Figure 2.4 Normalized examples of complex exponential integral spatial decay

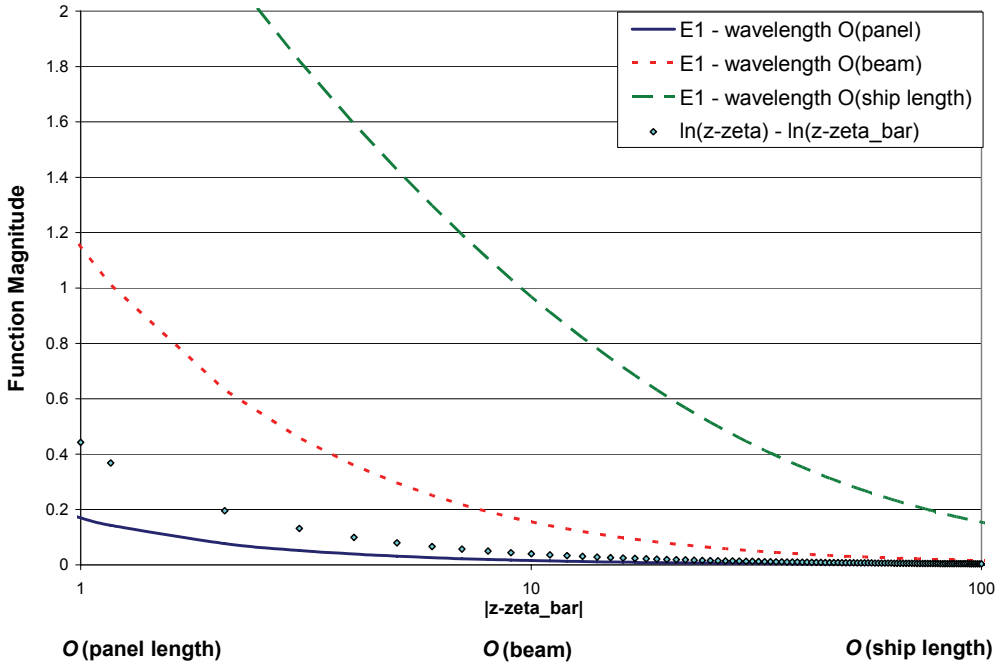

Figure 2.5 Complex exponential integral spatial decay, non-normalized

2.2 Radiation Interaction Force

The radiation interaction force is obtained by determining the incident wave forces on a demi-hull section, where the incident wave is the far-field radiated wave from a section on another demi-hull. Because the far-field radiated wave is a progressive wave and because the "receiving" section has had no influence on the creation of the incident radiated wave, the force is equivalent to a Froude-Krylov force and a diffraction force that would be experienced from an incident ambient wave. That is, there is a force due to the undisturbed incident radiated wave potential and a force due to the diffracted radiated wave potential. In the case of the radiation interaction forces, though, there is a unique radiated wave for each of the six modes of motion. For this reason, it is necessary to define twelve radiation interaction potentials (six incident and six diffraction) in the problem statement, as shown in equation 2.2.

2.2.1 Interaction Section

The interaction potentials at a given demi-hull section of interest are a function of the radiating section. For that reason, the first step in determining the radiation interaction force is to determine the point on the ship that is radiating a wave upon the section.

It is known that the radiating section will be upstream from the receiving section, or directly opposite the receiving section in the limit of zero ship speed. This is because the assumption is made that the radiated waves travel directly out the transverse axis of a 2D section. The radiated wave can be considered a packet of energy that takes time to reach the other demi-hull, traveling at the wave group velocity, V_g, where

$$V_g = \frac{1}{2} \cdot \frac{g}{\omega_e} \quad \text{in deep water} \tag{2.31}$$

It is important to note that the radiated wave has frequency equal to the ambient wave encounter frequency and therefore the radiated wavelength, λ, (and its wavenumber, k) is not the same as the ambient incident wavelength. The relationship between ω_e and the ambient incident wave frequency, ω_o, is given in equation 2.32.

$$\omega_e = \omega_o - \frac{U_o \omega_o^2}{g} \cos\beta \tag{2.32}$$

The relationship between ω_e and the radiated wavelength is given by the linear deep water dispersion relation given in equation 2.33.

$$\omega_e^2 = gk = g \cdot \frac{2\pi}{\lambda} \tag{2.33}$$

Even though a wave crest travels with the phase speed and the waves are incident upon the receiving section at the encounter frequency, the "wave front" travels at the group velocity; a point made by Sun (1982), Ronæss (2002), and Faltinsen (2005). If the ship has forward speed, then the receiving demi-hull will have moved forward in the time it takes for the radiated wave to arrive. In a ship-fixed reference frame, the radiated wave essentially takes on a vector defined by its velocities in the longitudinal ($-U_o$) and transverse (V_g) directions. This vector has been demonstrated in Figure 2.6, which shows the free surface elevation contours, as predicted by the LAMP 3D panel code (see Lin, et al., 1999), of a catamaran at forward speed oscillating in pure heave. The bottom contour plot shows the radiated waves for oscillation at a frequency twice that in the top contour plot. The ($-U_o$, V_g) vector has been drawn on both contour plots to illustrate the validity of this assertion.

From equation 2.32, it is seen that a higher encounter frequency will radiate waves with a smaller group velocity, which means the waves from a radiating section will impact the opposite demi-hull at a point farther downstream than if the encounter frequency were higher. If the ship is moving fast enough or the radiated wave is slow enough, the radiated wave may not impact any point on the opposite demi-hull at all. Of the two cases depicted in Figure 2.6, only the low-frequency case appears to have the radiated wave impacting a portion of the opposite demi-hull. The high-frequency case radiates waves that travel slower, so given the forward speed of the ship and the group velocity of the waves, even the forward-most edge of the radiated waves (represented by the drawn vectors) on the inboard side of the demi-hulls will not reach the opposite demi-hull within the time it takes the ship to travel a distance equal to the ship length, L. In the present theory, such a case would have zero interaction force.

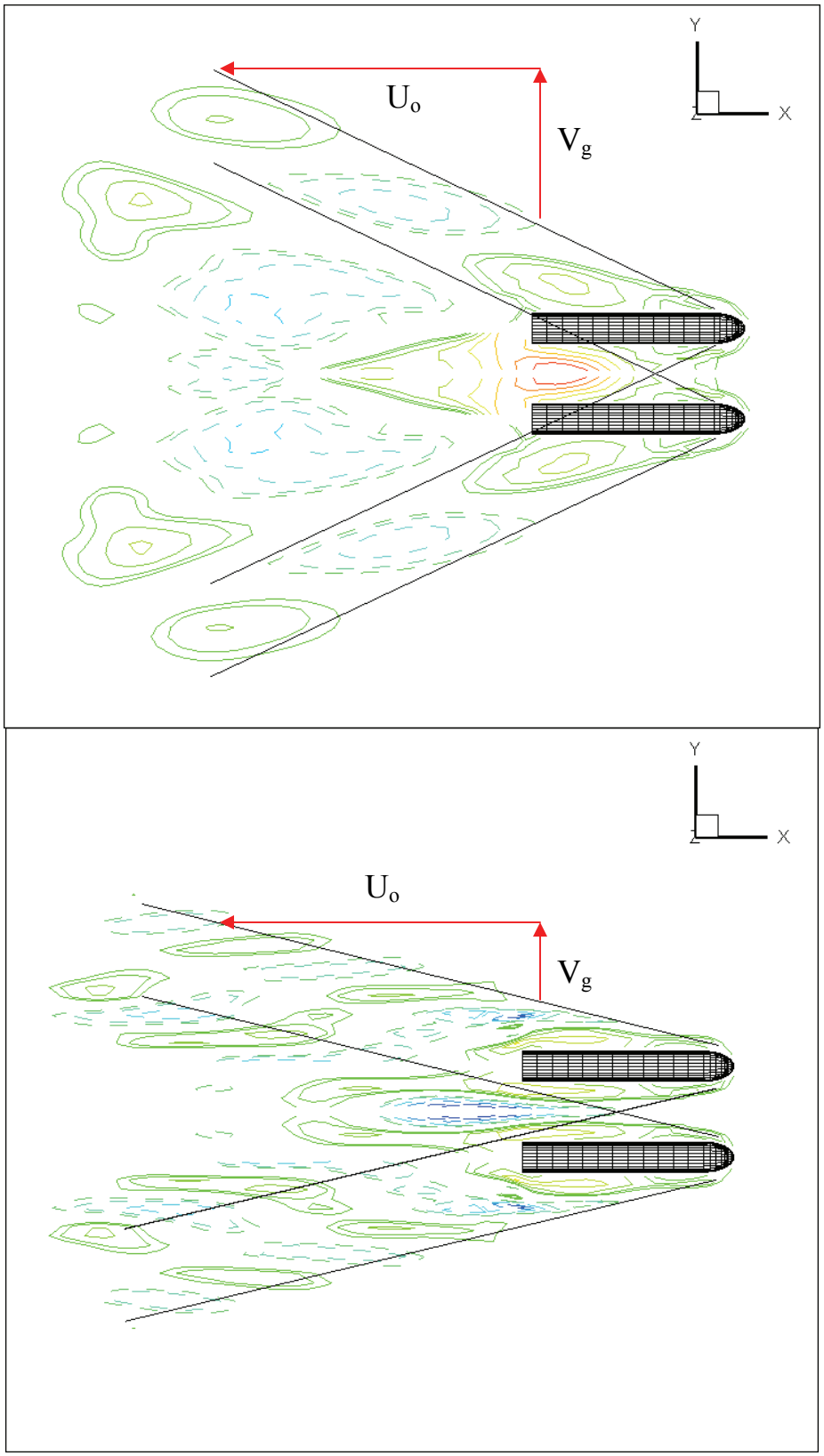

Figure 2.6 Free surface contours for low (top) and high (bottom) frequency heave oscillations with forward speed

To determine the x-coordinate, x^*, of the radiating demi-hull where the radiating section lies, it is necessary to define a representative transverse distance between the radiating section and the receiving section. This separation distance over which the radiated wave will travel is needed to determine how far longitudinally the ship will travel in the same amount of time for the radiated wave to cover the transverse distance. The longitudinal distance, D_{sweep} or sweep-down distance, defines which section on the opposite demi-hull is interacting with the section of interest. Because all points on the radiating section have an influence on the far-field radiated wave, the representative y-coordinate of the radiating section is taken to be its transverse center of buoyancy (TCB). Likewise, the representative y-coordinate of the receiving section is also taken to be its TCB. While there is no restriction that sectional TCB remains a constant, strip theory assumptions restrict any change in TCB as a function of x to be small. However, because TCB can change, the solution of D_{sweep} then becomes dependent on speed, encounter frequency, and TCB(x). The equation for D_{sweep} can then be defined as:

$$D_{sweep} = \frac{U_{ship}}{V_g} \cdot \left| TCB_i - TCB_r \right| \tag{2.34}$$

where TCB_i is the TCB of the receiving section's TCB, which is known, and TCB_r is the radiating section's TCB, which is unknown. D_{sweep} is always positive, because the ship speed is greater than or equal to zero. The solution of x^* is then given as:

$$x^* = x_i + D_{sweep} \tag{2.35}$$

where x_i is the x-coordinate of the receiving station of interest.

Figure 2.7 illustrates the radiated wave vectors in an example catamaran case. The demi-hulls of the catamaran are represented by their traces of sectional TCB. While the radiated wave vectors are parallel, D_{sweep} is not necessarily constant, due to variable TCB. It is also noted that the radiating source points are likely not to coincide with a defined section cut, which means $TCB_r(x)$ must be inferred. In the present theory, because change in TCB is assumed to be small, it is deemed sufficient to assume a linear variation of TCB between known values at defined sections.

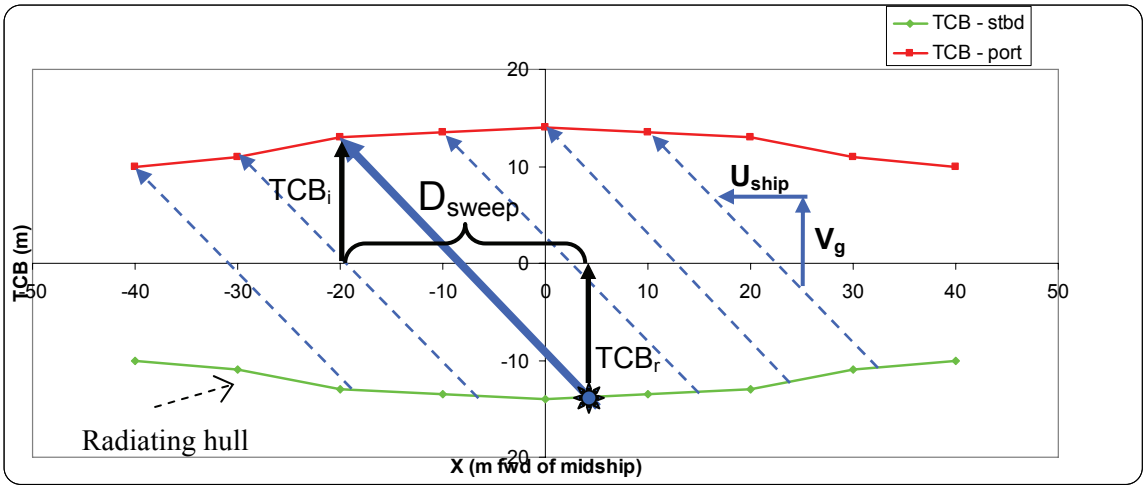

Figure 2.7 Representation of radiated wave vectors relating source points to receiving points

The solution of the radiating section location, x^*, is obtained by solving the reverse problem of finding D_{sweep} for the radiated waves from a defined section. That is, using the known transverse distance TCB_i of the receiving section of interest, the sweep-down distance of candidate radiating sections can be calculated using their known TCB_r. As shown in Figure 2.8, the value of x^* can be bracketed once successive candidate sections are shown to produce radiated waves that impact the opposite demi-hull at points forward and aft of the receiving section of interest. A linearly varying expression for $TCB_r(x)$ can be generated over this interval and x* subsequently determined algebraically using the expression for TCB_r and equations 2.34 and 2.35.

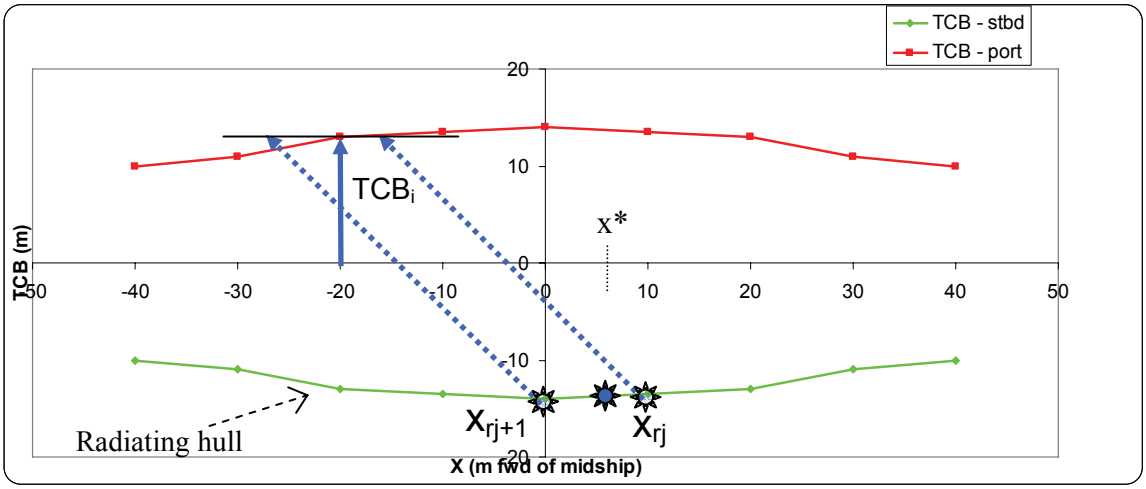

Figure 2.8 Radiated wave impact locations from defined sections

2.2.1.1 Trimaran Special Case

The determination of the radiating source location for a catamaran is fairly straight forward. Having assumed no reflections, a given demi-hull can only interact with the opposite, identical demi-hull. In the case of a trimaran, it is necessary to define the possible scenarios and the assumptions used in determining the interacting sections.

A trimaran's main-hull will radiate waves outward that can only interact with the outer-, or sub-hulls. This is illustrated in Figure 2.9. However, the sub-hulls' radiated waves can impact either the main-hull or the opposite sub-hull. In the present theory, the assumption is made that there is only one possible solution. That is, if the radiated wave vector from a sub-hull crosses the centerline at a point where the main-hull has wetted sectional area, then the radiated wave will impact only that section and not continue on with the possibility of impacting the opposite sub-hull. The possible impact scenarios for waves radiated from the sub-hulls is given in Figure 2.10.

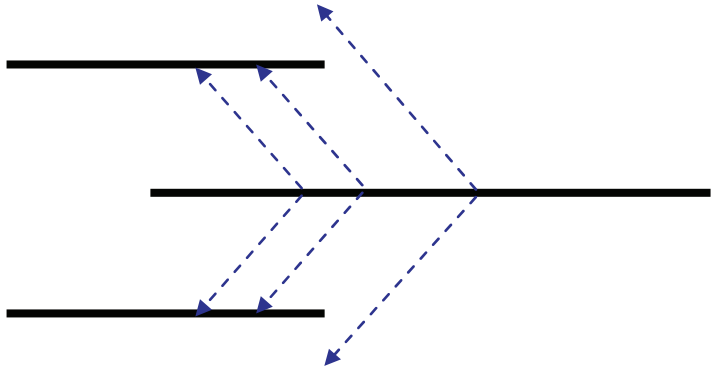

Figure 2.9 Possible impact scenarios for trimaran main-hull's radiated waves

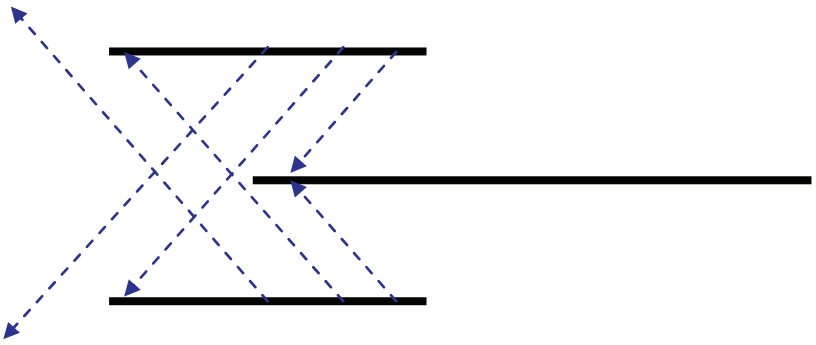

Figure 2.10 Possible impact scenarios for trimaran sub-hulls' radiated waves

2.2.2 Solution of Interaction Potentials and Forces

The solution of the interaction potentials and forces depends on the solution of the far-field radiated waves produced by each demi-hull due to oscillation in all 6 degrees of freedom in calm water. Therefore, the properties of the radiated wave and then the radiation interaction force can be solved only once the demi-hull radiation potential has been determined at each section of all demi-hulls and the radiating source section locations have been identified as described in the previous section. Solution of the incident far-field radiation potential at each panel of the receiving section leads to both the incident far-field interaction force and the diffraction force due to the incident radiated wave.

2.2.2.1 Incident Far-Field Radiated Wave Potentials and Forces

There are three options in determining the incident far-field radiated wave potentials on the receiving section's panels due to each mode of motion of the radiating section:

1. Damping coefficients of radiating source section
2. Direct integration of far-field Green function at receiving section's panels
3. Analytical determination based on direct integration of far-field Green function at reference point – Present approach

The first method, using damping coefficients of the radiating source section, recognizes that the amplitude of the far-field radiated wave can be related to the damping coefficient of an oscillating body (see Newman, 1977, or Faltinsen, 1990) through an energy flux analysis. The relationship is found to be

$$a_k = \sqrt{b_{kk} \frac{\omega^3}{\rho g^2}} \tag{2.36}$$

where a_k is the amplitude of the radiated wave and b_{kk} is the damping coefficient for the k-th mode of motion. Noting that the radiating source section at x^* does not necessarily coincide with a defined section for which the radiation potentials have been solved, such a method would be attractive because the amplitude of the far-field wave could be determined by interpolating the sectional damping coefficients. However, this approach was ultimately deemed unsuitable because it does not capture phase information.

The second method directly integrates the influence of the radiating section's panels' source strengths at each of the panels on the receiving section. The influence is determined by the far-field Green function, G^{FF}, which is found by retaining only the progressive wave terms of the Green function given in equation 2.28. This solution is expressed continuously and for the discretized problem by:

$$\psi_k^{\sim I}(z) = \int_{c_x(radiating\_section)} Q_k(\zeta) \cdot G^{FF}(z;\zeta) dl \qquad \textbf{(2.37)}$$

$$\psi_{l,k}^{\sim I} = \sum_{m=1,npts(rad\_station)} Q_{m,k} \cdot G_{l,m}^{FF} \qquad \textbf{(2.38)}$$

where $\psi_{l,k}^{\sim I}$ is the 2D incident far-field radiated wave potential at panel l due to motion in the k-th mode, $Q_{m,k}$ is the source strength density on panel m of the radiating section due to motion in the k-th mode and $G^{FF}_{l,m}$ gives the influence of panel m on panel l of the receiving section. Evaluating 2.38 essentially means that radiating sections are paired with receiving sections as shown in Figure 2.11, Figure 2.12, and Figure 2.13. In these figures, the receiving section's positive-y side is shown, because the potentials and forces only need to be obtained on this side due to port-starboard symmetry. It should be noted, however, that the radiating sections on the negative-y must multiply by -1 the source strengths, $Q_{m,k}$, for lateral plane modes, because they will have been developed in the demi-hull radiation problem for the positive-y demi-hull.

The simple examples presented in these figures show only a few panels per radiating section. To obtain a converged solution, many more panels are likely to be required. Following equation 2.38, it can be seen that a detriment of this approach is that the solution of the far-field incident radiated wave potential, $\psi_{l,k}^{\sim I}$, on each panel requires as many multiplications as there are panels on the radiating section, which in a typical application is on the order of 15-20. This can lead to a more computationally expensive operation than desired. Additionally, because the panelized definition of the section geometry and the source strengths are available only at the defined sections cuts, this calculation would have to be done twice – once for the section forward of x^* and once for the section aft of x^* – and the answer interpolated from the two solutions.

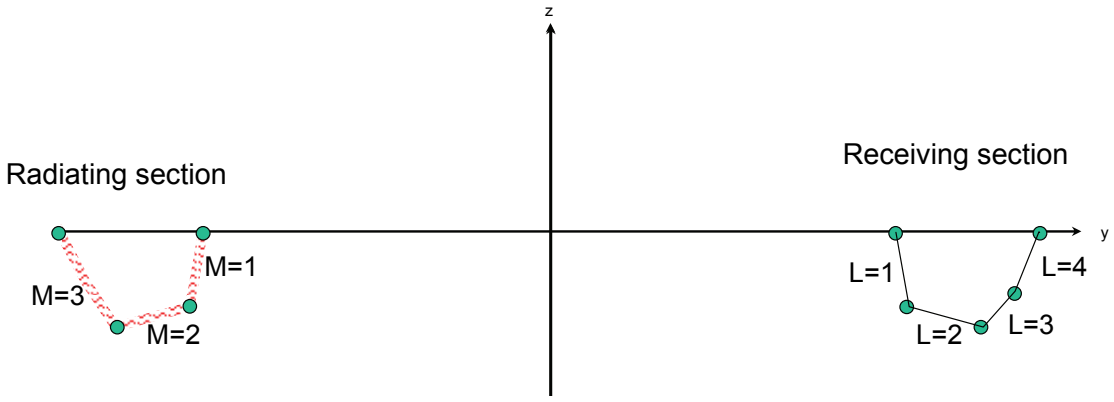

Figure 2.11 Example arrangement of radiating and receiving section panels

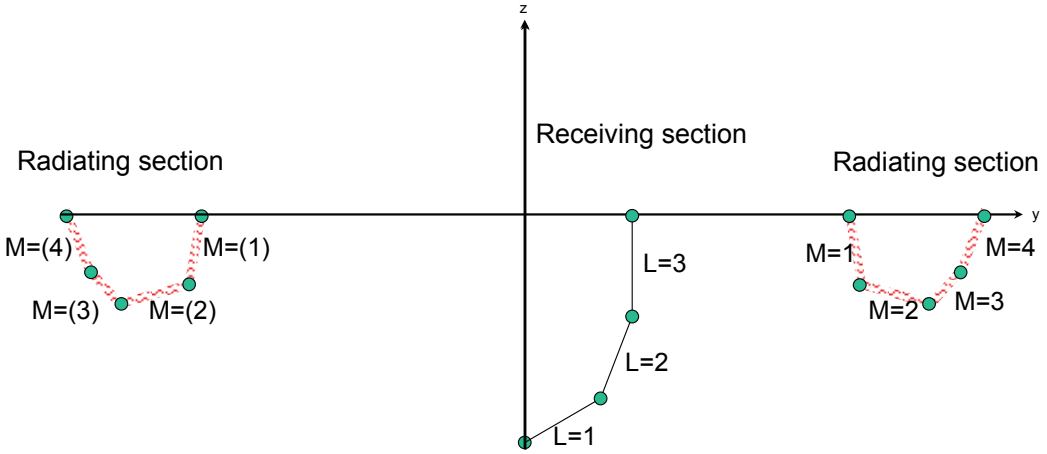

Figure 2.12 Example arrangement for trimaran sub-hulls radiating waves onto the main-hull

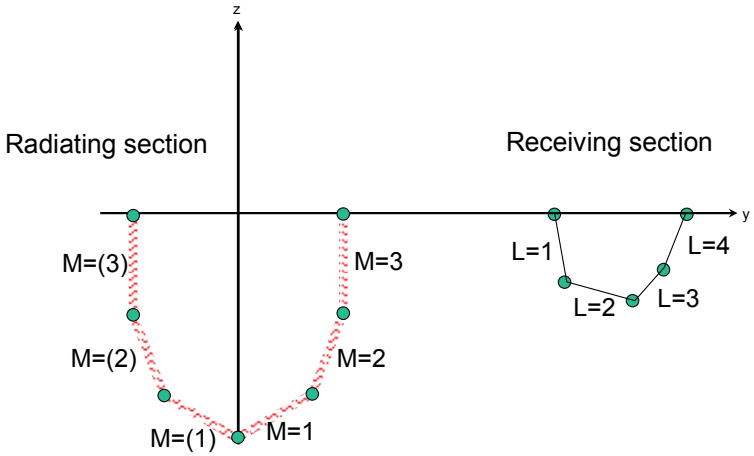

Figure 2.13 Example arrangement for trimaran main-hull radiating waves onto the outer-hull

The third approach, which has been applied for the present theory, takes advantage of the known form of a progressive wave potential to analytically define the far-field potential at all points in the y-z plane of the receiving section. Similar to the second approach, the far-field Green function is used to integrate the effect of all panels on the radiating section. Rather than evaluate this influence at each panel on the receiving section, a reference point is chosen for a single evaluation.

In order to present the full details behind this approach, it is first helpful to develop the form of the incident far-field radiation potential for all modes of motion, k. Because the source strengths, $Q_{m,k}$, in equation 2.38 satisfy the demi-hull radiation boundary conditions on the radiating section, the far-field potentials generated using the source strengths will take the form of the demi-hull radiation potentials as given in Table 2.1. That is, the far-field incident radiation potentials can be described in terms of the 2D zero-speed potentials and the radiating section's x-coordinate, x^*, in the following manner:

$$\phi_k^{\sim I}(x,y,z) = \psi_k^{\sim I}(y,z;x,x*) \qquad \text{k=1,2,3,4} \qquad \textbf{(2.39)}$$

$$\phi_5^{\sim I} = -x* \cdot \psi_3^{\sim I} + \frac{U_o}{i\omega_e}\psi_3^{\sim I} \qquad \text{k=5}$$

$$= -(x + D_{sweep})\psi_3^{\sim I} + \frac{U_o}{i\omega_e}\psi_3^{\sim I}$$

$$\phi_6^{\sim I} = x* \cdot \psi_2^{\sim I} - \frac{U_o}{i\omega_e}\psi_2^{\sim I} \qquad \text{k=6}$$

$$= (x + D_{sweep})\psi_2^{\sim I} - \frac{U_o}{i\omega_e}\psi_2^{\sim I}$$

The key difference in the far field potentials from the radiation potentials is that the pitch and yaw modes use x^* as a multiplier, not the x-value of the section where the potential is being evaluated. This is because the far-field radiated waves incident upon the receiving section have been generated by the motion of the radiating section. In the case of angular motion, the further from the ship's origin, the larger the amplitude of the motion and subsequent radiated waves will be. The resulting radiated wave pattern is demonstrated by Figure 2.14, which compares the free surface contours of a catamaran

oscillating in pitch with forward speed and the same condition for the catamaran oscillating in heave.

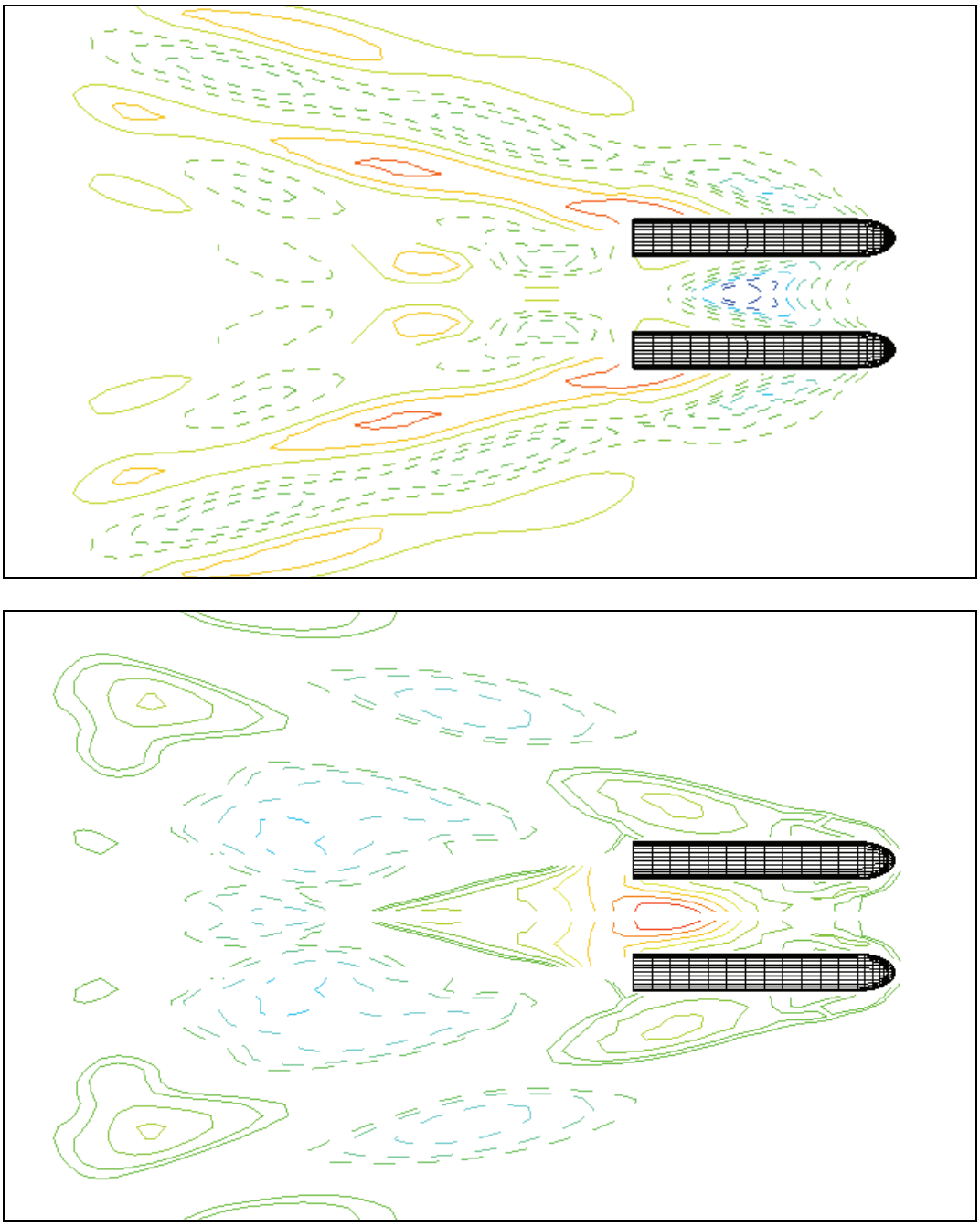

Figure 2.14 Free Surface contours for catamaran oscillating in pitch (top) and heave (bottom) at identical frequency and forward speed

The solution of the 2D incident wave interaction potential then follows from equation 2.38 using the source strengths that were determined in the demi-hull radiation potential solution. The far-field Green function, G^{FF}, is obtained by retaining the terms in the Green function shown in equation 2.28 that do not decay spatially, as described in section 2.1.6. Following Frank's notation, $G^{FF}_{l,m}$ can be given as:

$$G^{FF}_{l,m} = I^{FF}_{l,m} + iJ_{l,m} \tag{2.40}$$

The conjugate has been taken of the Green function to align the influence coefficients in equation 2.40 with the $e^{+i\omega t}$ time dependence. As noted in section 2.1.6, $J_{l,m}$ is entirely a progressive wave term that does not decay, so there is no difference between $J_{l,m}$ in equation 2.40 and the imaginary term in equation 2.28. The real term in equation 2.40, $I_{l,m}$, is derived from the portion of the principal value integral term in equation 2.28. When stated as given in equation 2.29, the progressive wave portion of the principal value term is readily apparent. However, care must be taken that the proper sign is carried on the wave terms to ensure that the radiation condition (outgoing waves) is satisfied.

The complete $I^{FF}_{l,m}$ and $J_{l,m}$ terms are given for the discretized problem as:

$$I^{FF}_{l,m} = \mathrm{Re}\left\{\left(\frac{-i}{\upsilon}\right)\cdot e^{i\alpha_m}\left[i\,\mathrm{sgn}\left(x_l-\xi_{m+1}\right)\cdot e^{-i\upsilon\left(z_l-\overline{\zeta_{m+1}}\right)} - i\,\mathrm{sgn}\left(x_l-\xi_m\right)\cdot e^{-i\upsilon\left(z_l-\overline{\zeta_m}\right)}\right]\right\} \tag{2.41}$$

$$\pm\,\mathrm{Re}\left\{\left(\frac{-i}{\upsilon}\right)\cdot e^{-i\alpha_m}\left[i\,\mathrm{sgn}\left(x_l+\xi_{m+1}\right)\cdot e^{-i\upsilon\left(z_l+\zeta_{m+1}\right)} - i\,\mathrm{sgn}\left(x_l+\xi_m\right)\cdot e^{-i\upsilon\left(z_l+\zeta_m\right)}\right]\right\}$$

$$J_{l,m} = \mathrm{Re}\left\{\left(\frac{-i}{\upsilon}\right)\cdot e^{i\alpha_m}\left[e^{-i\upsilon\left(z_l-\overline{\zeta_{m+1}}\right)} - e^{-i\upsilon\left(z_l-\overline{\zeta_m}\right)}\right]\right\} \tag{2.42}$$

$$\pm\,\mathrm{Re}\left\{\left(\frac{-i}{\upsilon}\right)\cdot e^{-i\alpha_m}\left[e^{-i\upsilon\left(z_l+\zeta_{m+1}\right)} - e^{-i\upsilon\left(z_l+\zeta_m\right)}\right]\right\}$$

Because the numerical solution utilizes the symmetry of the ship, the demi-hull radiation source strengths have been solved on only the positive-y portion of the ship (i.e., the port catamaran demi-hull, the port side of a trimaran's main-hull or the port trimaran sub-hull). The "imaged" panels of the radiating section provide the influence of the starboard side of the ship and are included in equations 2.41 and 2.42 by the second quantities in

each equation (led by the +/- sign). The + sign is taken for lateral modes of motion (k=2,4), while the - sign is used for the vertical modes of motion (k=1,3). This is due to the direction of the panels being reversed on the imaged side and the fact that the source strengths for lateral modes are 180 degrees out of phase with the positive-y panels on which the source strengths are known.

With the aim being to develop the far-field incident radiated wave potentials on the positive-y side of the ship where all other hydrodynamic forces are being determined, the radiating sections will be generating waves from the starboard (negative-y) demi-hull or sub-hull. As such, it is the influence of the imaged panels that is needed. In the case of a trimaran's main-hull as the radiating section, the influence of the positive-y panels must also be included. However, even when the trimaran main-hull is the receiving section, the influence of the starboard sub-hull only is included so that the wave potential is well-defined. The force is eventually multiplied by 2 due to the symmetry of the problem.

The far-field Green function retains only progressive wave terms, which means that the far-field potentials obtained by equation 2.38 will take the form of a progressive wave. Having limited the radiating sections to those generating waves out the positive-y axis, the far-field incident radiation potential can be expressed as:

$$\psi_k^{\sim I}(y,z;x,x^*) = \underline{\psi_k^{\sim I}}(x^*)e^{kz}e^{-iky} \qquad \textbf{(2.43)}$$

where $\underline{\psi_k^{\sim I}}$ is a complex constant for k=1,2,3,4. By evaluating the influence of a radiating section's panels at a single reference point, such as (0,0), $\underline{\psi_k^{\sim I}}$ can be determined. Expressing the potential in this manner then allows the potential to be determined at an arbitrary point without having to resort to integrating the panels' influence at that point. Additionally, $\underline{\psi_k^{\sim I}}$ can be pre-calculated and stored with the radiating section, because it is independent of the receiving section. If the radiation problem is pre-computed for a set of basis encounter frequencies, intermediate values can be obtained simply by interpolation, which allows for rapid generation of hydrodynamic coefficients for arbitrary speed-heading and ambient incident wave combinations. Perhaps more importantly, this value can be interpolated for the exact radiating source section at x^*

from the defined sections forward and aft of x*. Once the interpolated value of $\underline{\psi_k^{\sim I}}$ has been obtained for the x* relevant to the receiving section of interest, the values of $\psi_k^{\sim I}$ at the midpoints of each of the section's panels can be calculated from equation 2.43.

With the potentials determined at the panel midpoints on the receiving section, the forces due to the incident far-field radiated wave potentials can be found via equations 2.44 and 2.45.

$$F_{j,k}^{\sim I} = \iint_{S_0} n_j \cdot p_k^{\sim I} ds \tag{2.44}$$

$$p_k^{\sim I} = -\rho\left(i\omega_e - U_0 \frac{\partial}{\partial x}\right)\phi_k^{\sim I} e^{i\omega_e t} \tag{2.45}$$

Though the partial derivatives with respect to x are considered small in strip theory, they can be approximated by using Tuck's theorem, which is given from the demi-hull radiation problem as:

$$\iint_{S_0} n_j \left(\vec{W} \cdot \nabla\right)\phi_k ds = -U_0 \iint_{S_0} m_j \phi_k ds + \int_c (neglected) \tag{2.46}$$

where $\vec{W} \cdot \nabla = -U_0 \frac{\partial}{\partial x}$ and m_j=(0, 0, 0, 0, n_3, -n_2) in the present problem. Substituting $\phi_k^{\sim I}$ for ϕ_k, the incident interaction force can be written as:

$$F_{j,k}^{\sim I} = -\rho i\omega_e \iint_{S_0}\left(n_j - \frac{U_0}{i\omega_e} m_j\right)\phi_k^{\sim I} ds \tag{2.47}$$

Combining equations 2.39 and 2.47, the total (3D) ship forces become:

$$F_{j,k}^{\sim I} = -\rho i\omega_e \iint_{S_0} n_j \psi_k^{\sim I} ds \qquad \text{j=1,2,3,4, k=1,2,3,4} \tag{2.48}$$

$$F_{j,5}^{\sim I} = -\rho i\omega_e \iint_{S_0} n_j \left(-x^* + \frac{U_o}{i\omega_e}\right)\psi_3^{\sim I} ds \qquad \text{j=1,2,3,4, k=5}$$

$$F_{j,6}^{\sim I} = -\rho i\omega_e \iint_{S_0} n_j \left(x^* - \frac{U_o}{i\omega_e}\right)\psi_2^{\sim I} ds \qquad \text{j=1,2,3,4, k=6}$$

$$F_{5,k}^{\sim I} = -\rho i\omega_e \iint_{S_0} n_3 \left(-x - \frac{U_0}{i\omega_e}\right)\psi_k^{\sim I} ds \qquad \text{j=5, k=1,2,3,4}$$

$$F_{6,k}^{\sim I} = -\rho i\omega_e \iint_{S_0} n_2 \left(x + \frac{U_0}{i\omega_e} \right) \psi_k^{\sim I} ds \qquad \text{j=6, k=1,2,3,4}$$

$$F_{5,5}^{\sim I} = -\rho i\omega_e \iint_{S_0} n_3 \left(x + \frac{U_0}{i\omega_e} \right) \left(x^* - \frac{U_0}{i\omega_e} \right) \psi_3^{\sim I} ds \qquad \text{j=5, k=5}$$

$$F_{6,6}^{\sim I} = -\rho i\omega_e \iint_{S_0} n_2 \left(x + \frac{U_0}{i\omega_e} \right) \left(x^* - \frac{U_0}{i\omega_e} \right) \psi_2^{\sim I} ds \qquad \text{j=6, k=6}$$

In the present approach, sectional incident radiated wave force are defined as:

$$f_{jk}^{\sim I}(x) = -\rho i\omega_e \int_{c_x} n_j \psi_k^{\sim I} dl \qquad \text{k=1,2,3,4} \qquad \textbf{(2.49)}$$

$$f_{j5}^{\sim I}(x) = -\left(x^* - \frac{U_0}{i\omega_e} \right) f_{j3}^{\sim I} \qquad \text{k=5}$$

$$f_{j6}^{\sim I}(x) = \left(x^* - \frac{U_0}{i\omega_e} \right) f_{j2}^{\sim I} \qquad \text{k=6}$$

which leads to a total ship force in the j direction due to motion in the k-th mode of:

$$F_{jk}^{\sim I} = \int_L f_{jk}^{\sim I}(x) dx \qquad \text{j=1,2,3,4, k=1,2,3,4,} \qquad \textbf{(2.50)}$$

$$F_{5k}^{\sim I} = -\int_L \left(x + \frac{U_0}{i\omega_e} \right) f_{3k}^{\sim I}(x) dx \qquad \text{j=5, k=1,2,3,4}$$

$$F_{6k}^{\sim I} = \int_L \left(x + \frac{U_0}{i\omega_e} \right) f_{2k}^{\sim I}(x) dx \qquad \text{j=6, k=1,2,3,4}$$

$$F_{55}^{\sim I} = \int_L \left(x + \frac{U_0}{i\omega_e} \right) \left(x^* - \frac{U_0}{i\omega_e} \right) f_{33}^{\sim I}(x) dx \qquad \text{j=5, k=5}$$

$$F_{66}^{\sim I} = \int_L \left(x + \frac{U_0}{i\omega_e} \right) \left(x^* - \frac{U_0}{i\omega_e} \right) f_{22}^{\sim I}(x) dx \qquad \text{j=6, k=6}$$

2.2.2.2 Diffracted Far-Field Radiated Wave Forces

The second half of the radiation interaction problem is determining the forces due to the diffraction of the incident radiated wave. Rather than solving for the diffracted far-field radiated wave potential, $\phi_k^{\sim D}$, which would be computationally expensive, the Haskind relation will be used to develop a sectional force.

To develop the total ship forces due to the diffraction of the incident radiated wave, the force via pressure integration is given by the following equations for force in the j-th direction due to motion in the k-th mode:

$$F_{j,k}^{\sim D} = \iint_{S_0} n_j \cdot p_k^{\sim D} ds \tag{2.51}$$

$$p_k^{\sim D} = -\rho\left(i\omega_e - U_0 \frac{\partial}{\partial x} \right)\phi_k^{\sim D} \tag{2.52}$$

$$F_{jk}^{\sim D} = -\rho \iint_{S_0} n_j \left(i\omega_e - U_0 \frac{\partial}{\partial x} \right)\phi_k^{\sim D} ds \tag{2.53}$$

Using Tuck's theorem, as given in equation 2.46, the integrated force can be rewritten as:

$$F_{jk}^{\sim D} = -\rho \iint_{S_0} \left(n_j i\omega_e - U_0 m_j \right)\phi_k^{\sim D} ds \tag{2.54}$$

From the demi-hull radiation problem, the quantity $\left(n_j i\omega_e - U_0 m_j \right)$ is recognized as the body boundary condition from equation 2.13, which is repeated here (for motion in mode k) as:

$$\frac{\partial \phi_k}{\partial n} = i\omega_e n_k + U_0 m_k$$

Having defined zero- and forward-speed portions of the radiation potential and their boundary conditions in equations 2.17 through 2.20 as:

$$\phi_k = \phi_k^0 + \frac{U_0}{i\omega_e}\phi_k^U$$

with $\frac{\partial \phi_k^0}{\partial n} = i\omega_e n_k$, $\frac{\partial \phi_k^U}{\partial n} = i\omega_e m_k$, and $\frac{\partial \phi_k}{\partial n} = \frac{\partial \phi_k^0}{\partial n} + \frac{U_0}{i\omega_e}\frac{\partial \phi_k^U}{\partial n}$,

it follows from equation 2.54 that

$$F_{jk}^{\sim D} = -\rho \iint_{S_0} \left(\frac{\partial \phi_j^0}{\partial n} - \frac{U_0}{i\omega_e}\frac{\partial \phi_j^U}{\partial n} \right)\phi_k^{\sim D} ds \tag{2.55}$$

Using Green's theorem to change what $\frac{\partial}{\partial n}$ acts on, equation 2.55 becomes:

$$F_{jk}^{\sim D} = -\rho \iint_{S_0} \left(\phi_j^0 - \frac{U_0}{i\omega_e}\phi_j^U \right)\frac{\partial \phi_k^{\sim D}}{\partial n} ds \tag{2.56}$$

The body boundary condition for the diffracted radiated wave potential is:

$$\frac{\partial \phi_k^{\sim D}}{\partial n} = -\frac{\partial \phi_k^{\sim I}}{\partial n} \tag{2.57}$$

This equation allows the force equation to be given in terms of only the radiation potentials at the receiving section and the incident far-field radiated wave potentials, as given by:

$$F_{jk}^{\sim D} = +\rho \iint_{S_0} \left(\phi_j^0 - \frac{U_0}{i\omega_e} \phi_j^U \right) \frac{\partial \phi_k^{\sim I}}{\partial n} ds \tag{2.58}$$

where $\frac{\partial \phi_k^{\sim I}}{\partial n} = \hat{n} \cdot \nabla \phi_k^{\sim I} = n_1 \frac{\partial \phi_k^{\sim I}}{\partial x} + n_2 \frac{\partial \phi_k^{\sim I}}{\partial y} + n_3 \frac{\partial \phi_k^{\sim I}}{\partial z}$.

It is noted that both n_1 and $\frac{\partial \phi_k^{\sim I}}{\partial x}$ are small quantities according to the present strip theory, except for when k=5 and 6, so their product will be neglected when k=1, 2, 3, and 4. If D_{sweep} is assumed to be approximately constant (i.e., TCB(x) is constant + ε*x), then $\frac{\partial \phi_k^{\sim I}}{\partial x}$ for k=5 and 6 follows from 2.39 and 2.43 to be:

$$\frac{\partial \phi_5^{\sim I}}{\partial x} = -\psi_3^{\sim I} \qquad \text{k=5} \tag{2.59}$$

$$\frac{\partial \phi_6^{\sim I}}{\partial x} = \psi_2^{\sim I} \qquad \text{k=6}$$

Equation 2.43 also yields:

$$\frac{\partial \phi_k^{\sim I}}{\partial y} = -ik \cdot \psi_k^{\sim I} \qquad \text{k=1,2,3,4,5,6} \tag{2.60}$$

$$\frac{\partial \phi_k^{\sim I}}{\partial z} = k \cdot \psi_k^{\sim I} \qquad \text{k=1,2,3,4,5,6} \tag{2.61}$$

Therefore, $\frac{\partial \phi_k^{\sim I}}{\partial n}$ can be summarized as:

$$\frac{\partial \phi_k^{\sim I}}{\partial n} = \left(-ikn_2 + kn_3 \right) \psi_k^{\sim I} \qquad \text{k=1,2,3,4} \tag{2.62}$$

$$\frac{\partial \phi_5^{\sim I}}{\partial n} = \left[-n_1 + \left(-ikn_2 + kn_3 \right) \cdot \left(-x^* + \frac{U_o}{i\omega_e} \right) \right] \psi_3^{\sim I} \qquad \text{k=5}$$

$$\frac{\partial \phi_6^{\sim I}}{\partial n} = \left[n_1 + \left(-ikn_2 + kn_3 \right) \cdot \left(x^* - \frac{U_o}{i\omega_e} \right) \right] \psi_2^{\sim I} \qquad \text{k=6}$$

Substitution of equation 2.62 into 2.58 leads to:

$$F_{jk}^{\sim D} = +\rho \iint_{S_0} \left(\phi_j^0 - \frac{U_0}{i\omega_e} \phi_j^U \right) \left[-ikn_2 + kn_3 \right] \psi_k^{\sim I} ds \qquad \text{k=1,2,3,4} \qquad \textbf{(2.63)}$$

$$F_{j5}^{\sim D} = +\rho \iint_{S_0} \left(\phi_j^0 - \frac{U_0}{i\omega_e} \phi_j^U \right) \left[-n_1 - \left(x^* - \frac{U_o}{i\omega_e} \right) \left(-ikn_2 + kn_3 \right) \right] \psi_3^{\sim I} ds \qquad \text{k=5}$$

$$F_{j6}^{\sim D} = +\rho \iint_{S_0} \left(\phi_j^0 - \frac{U_0}{i\omega_e} \phi_j^U \right) \left[n_1 + \left(x^* - \frac{U_o}{i\omega_e} \right) \left(-ikn_2 + kn_3 \right) \right] \psi_2^{\sim I} ds \qquad \text{k=6}$$

From the demi-hull radiation problem, Table 2.1 provides the values for ϕ^0_j and ϕ^U_j in terms of the zero speed sectional radiation potentials, ψ_j. Following the assumption that the total ship force is approximately equal to the lengthwise integration of the sectional forces, the sectional forces reduce to:

$$f_{jk}^{\sim D}(x) = +\rho k \int_{c_x} \left(n_3 - in_2 \right) \psi_k^{\sim I} \psi_j \, dl \qquad \text{j=1,2,3,4 and k=1,2,3,4} \qquad \textbf{(2.64)}$$

$$f_{j5}^{\sim D}(x) = -\rho \int_{c_x} n_1 \psi_3^{\sim I} \psi_j \, dl - \left(x^* - \frac{U_o}{i\omega_e} \right) \cdot f_{j3}^{\sim D}(x) \qquad \text{j=1,2,3,4 and k=5}$$

$$f_{j6}^{\sim D}(x) = +\rho \int_{c_x} n_1 \psi_2^{\sim I} \psi_j \, dl + \left(x^* - \frac{U_o}{i\omega_e} \right) \cdot f_{j2}^{\sim D}(x) \qquad \text{j=1,2,3,4 and k=6}$$

The total ship forces due to the diffraction of the incident radiated wave can then be obtained by integrating the sectional forces over the length of the ship, as given by:

$$F_{jk}^{\sim D} = \int_L f_{jk}^{\sim D}(x) dx \qquad \text{j=1,2,3,4 and k=1,2,3,4,5,6} \qquad \textbf{(2.65)}$$

$$F_{5k}^{\sim D} = -\int_L \left(x + \frac{U_0}{i\omega_e} \right) f_{3k}^{\sim D}(x) dx \qquad \text{j=5 and k=1,2,3,4,5,6}$$

$$F_{6k}^{\sim D} = \int_L \left(x + \frac{U_0}{i\omega_e} \right) f_{2k}^{\sim D}(x) dx \qquad \text{j=6 and k=1,2,3,4,5,6}$$

2.3 "3D" Added Mass and Damping Coefficients with Forward Speed

The total 3D added mass and damping coefficients can be determined once the radiation forces and the radiation interaction forces have been calculated. The conventional Salvesen, Tuck and Faltinsen (Salvesen et al., 1970) forward speed corrections are applied to the independent demi-hull radiation added mass and damping coefficients to obtain $\underline{A}_{jk}$ and $\underline{B}_{jk}$. The integrated added mass and damping coefficients from the interaction forces are obtained via equations 2.66 and 2.67.

$$\tilde{A}_{j,k} = \Re\left(\tilde{F}^{I}_{j,k} + \tilde{F}^{D}_{j,k}\right)/\omega_e^2 \tag{2.66}$$

$$\tilde{B}_{j,k} = \Im\left(\tilde{F}^{I}_{j,k} + \tilde{F}^{D}_{j,k}\right)/\left(-\omega_e\right) \tag{2.67}$$

The independent demi-hull and interaction added mass and damping coefficients are subsequently combined as given by equations 2.68 and 2.69 to create the final 3D coefficients to be used in the equations of motion.

$$A_{j,k} = \underline{A}_{j,k} + \tilde{A}_{j,k} \tag{2.68}$$

$$B_{j,k} = \underline{B}_{j,k} + \tilde{B}_{j,k} \tag{2.69}$$

2.4 Other Forces and Equations of Motion

To complete the frequency-domain solution of the multihull ship motion problem, the wave excitation hydrodynamic forces, fluid hydrostatic forces, and viscous forces must be determined.

2.4.1 Ambient Wave Exciting Forces

The ambient wave excitation forces are the forces due to ϕ_0 (Froude-Krylov forces) and ϕ_7 (diffraction forces). By definition, there are no interaction effects in the Froude-Krylov force. It is assumed that the interaction effects for the incident wave diffraction forces are also near zero and can be neglected. Consequently, the wave excitation forces can be calculated on the individual independent demi-hulls following traditional linear strip theory methods.

2.4.1.1 Froude-Krylov Forces

Applying the incident wave potential given in equation 2.3 to equation 2.27, the sectional and total ship Froude-Krylov forces are:

$$f_{j0}(x) = \rho g a \int_{c_x} n_j e^{kz} e^{-iky\sin\beta} dl \qquad \text{j=1,2,3,4} \qquad \textbf{(2.70)}$$

$$F_{j0} = \int_L e^{-ikx\cos\beta} f_{j0}(x) dx \qquad \text{j=1,2,3,4}$$

$$F_{5,0} = -\int_L x \cdot e^{-ikx\cos\beta} f_{3,0}(x) dx \qquad \text{j=5}$$

$$F_{6,0} = \int_L x \cdot e^{-ikx\cos\beta} f_{2,0}(x) dx \qquad \text{j=6}$$

2.4.1.2 Diffraction Forces

As was done for the diffraction force due to the incident far-field radiated wave, the diffraction force due to the ambient incident wave is found by using the Haskind relation. The sectional and total ship forces are derived similar to $F^{\sim D}_{jk}$, except the incident wave potential is given by equation 2.3. The sectional diffraction force, $h_j(x)$, and the total ship diffraction forces are:

$$h_j(x) = \rho k \int_{c_x} (n_3 - i(n_1\cos\beta + n_2\sin\beta)) e^{kz} e^{-iky\sin\beta} \psi_j dl \qquad \text{j=1,2,3,4} \qquad \textbf{(2.71)}$$

$$F_{j,7} = \int_L e^{-ikx\cos\beta} h_j(x) dx \qquad \text{j=1,2,3,4}$$

$$F_{5,7} = -\int_L e^{-ikx\cos\beta} \left(x - \frac{U_o}{i\omega_e} \right) h_3(x) dx \qquad \text{j=5}$$

$$F_{6,7} = \int_L e^{-ikx\cos\beta} \left(x - \frac{U_o}{i\omega_e} \right) h_2(x) dx \qquad \text{j=6}$$

2.4.2 Hydrostatic Forces

Consistent with linear theory, the hydrostatic forces are linear, which means they can be expressed as stiffness coefficients developed from waterplane properties. Because the mean wetted portion of the ship is considered to be invariant with ship speed, the stiffness coefficients, C_{jk}, are also invariant with speed.

2.4.3 Viscous forces

In the present approach, there has been no attempt to develop a viscous force model specific to multihull ships. An assumption is made that viscous roll damping models, such as the model employed in this method, are still appropriate for multihulls. Furthermore, it is noted that the increased wavemaking damping in roll due to the nearly vertical motion of outboard demi-hulls will be automatically captured by the radiation force model.

2.4.4 Equations of Motion

Once the exciting forces and the hydrostatic and hydrodynamic coefficients have been determined, the equation of motion can be solved. In the present approach, the origin is taken at midship, so the mass matrix becomes

$$\left[M_{jk}\right]=\begin{bmatrix} M & 0 & 0 & 0 & \bar{z}_g M & 0 \\ 0 & M & 0 & -\bar{z}_g M & 0 & \bar{x}_g M \\ 0 & 0 & M & 0 & -\bar{x}_g M & 0 \\ 0 & -\bar{z}_g M & 0 & I_{44} & 0 & -I_{64} \\ \bar{z}_g M & 0 & -\bar{x}_g M & 0 & I_{55} & 0 \\ 0 & \bar{x}_g M & 0 & -I_{64} & 0 & I_{66} \end{bmatrix}$$

and the equation of motion is given by:

$$\{-\omega_e^2[M+A] + i\omega_e[B] + [C]\ \}\ \{\zeta\} = \{F\} \qquad \textbf{(2.72)}$$

Noting that the ship is symmetric about the centerplane, the vertical and lateral plane forces and motions will remain de-coupled. Therefore, equation 2.72 will be solved independently for the vertical and lateral plane motions to obtain the complex motions, ζ.

Chapter 3

Nonlinear Time-Domain Solution

When a ship is operating in large amplitude waves, the hydrodynamic forces and subsequent motions of the ship can no longer be considered to be in the linear regime. Therefore, in order to provide more accurate predictions of a multihull's motion in large waves, the significant nonlinear forces must be captured. Because the problem is not linear, the motions must be calculated in the time domain.

3.1 General Formulation

Beck and Reed (2001) note that a common approach for solving the nonlinear time-domain problem is to employ a "blended method" that attempts to capture the most significant nonlinear forces. A blended method treats the large nonlinear forces more exactly while the other forces remain linear. The principal nonlinearity in the hydrodynamic forces derives from the time-varying wetted geometry, which affects the evaluation of all hydrodynamic forces. However, it has been argued (see, for example, de Kat, 1994) that the most important nonlinear forces to capture are the hydrostatic and Froude-Krylov forces on the time-varying wetted geometry. This approach of "body-exact" hydrostatic and Froude-Krylov forces is taken in the present theory, with all other fluid forces considered linear.

The problem to be solved is the large amplitude seakeeping problem, as opposed to the maneuvering-in-waves problem, which means that large lateral motion (such as lateral drift or heading change) and change of speed are not considered. Such an analysis would require a maneuvering model and propulsion model, as well as an effective heading control system. However, to provide generality, the environment is defined in

the world axis system, which can be linked to the inertial axis system used in the frequency-domain solution by:

$$X = x + U_o t \tag{3.1}$$

$$Y = y$$

$$Z = z$$

3.2 Wave Environment

The wave environment is considered linear and can be described by the incident wave velocity potential for regular seas or the superposition of the incident wave velocity potentials for each frequency component of the wave spectrum in an irregular sea.

The total wave elevation, η_{total}, at a point in the world coordinate system is then given by:

$$\eta_{total} = \Re\left\{ \sum_{n=1}^{Nwaves} A_n \cdot e^{-ik_n\left(X\cos\beta + Y\sin\beta\right)} \cdot e^{i\omega_{o,n}t} \cdot e^{i\varepsilon_n} \right\} \tag{3.2}$$

where A_n is the amplitude and ε_n is the phase of the n-th wave component. In this coordinate system, the circular frequency of the wave component is used, not the encounter frequency.

The wave pressure equation utilizes Wheeler stretching (Wheeler, 1969) when determining the pressure at a given point. This "pressure stretching" method attempts to provide a more accurate representation of the dynamic pressure near the free-surface by ensuring that the total fluid pressure is 0.0 on the undisturbed free-surface. The hydrostatic pressure, p^{HS}, and dynamic, or Froude-Krylov, pressure, p^{FK}, are:

$$p^{HS} = -\rho g Z \tag{3.3}$$

$$p^{FK} = \rho g \cdot \sum_{n=1}^{Nwaves} A_n \cdot \Re\left\{ e^{k_n\left(Z-\eta_{tot}\right)} e^{i\left(\omega_{o,n}t - k_n\left(X\cos\beta + Y\sin\beta\right) + \varepsilon_n\right)} \right\} \tag{3.4}$$

3.3 Forces

In the present blended method theory, the hydrostatic and Froude-Krylov forces are nonlinear while all other hydrodynamic forces are considered to be linear. The linear forces have been calculated in the frequency domain as described in the previous chapter.

3.3.1 Radiation Force

In the time-domain, there exists a memory effect in the radiation force due to the waves the ship has produced in the past. For a multihull ship, the memory effect at a given section is not only due to the waves that the section produced, but also the waves that were produced by a section upstream. For this reason, attempting to capture the nonlinear aspect of emerging multihull sections would be extremely difficult, given the interactions. For a monohull ship, if memory effects were to be ignored (i.e. use a single frequency's coefficients), the nonlinear body-exact radiation force could be approximated by integrating 3D added mass and damping coefficients from scaled sectional coefficients, where the scaling is based on the change in draft of a section. One may argue that the equivalent approach for multihulls with interaction would be to scale a section's demi-hull added mass and damping coefficients by its draft at time, t, then add scaled sectional interaction added mass and damping coefficients based on the draft of the source section at time = t-(x^*-x)/U. Such an approach could be investigated in the future, but has not been considered in the present theory.

The radiation forces are considered linear in the present blended method approach. To properly account for the memory effect in the linear radiation force in the time domain, the use of a convolution integral would be required. The expression for the radiation force in the j-th direction would then be given as:

$$F_j^R(t) = \sum_{k=1}^{6}\left(- A_{jk}^{\infty} \cdot \ddot{x}_k(t) - B_{jk}^{\infty} \cdot \dot{x}_k(t) - \int_{-\infty}^{t} K_{jk}(t-\tau) \cdot \dot{x}_k(\tau) d\tau \right) \qquad \textbf{(3.5)}$$

where the kernel function, K_{jk} is…

$$K_{jk}(t) = \frac{2}{\pi}\int_0^{\infty}\left[B_{jk}(\omega) - B_{jk}(\infty)\right]\cos(\omega t)d\omega \;=\; \frac{2\omega}{\pi}\int_0^{\infty}\left[A_{jk}(\omega) - A_{jk}(\infty)\right]\sin(\omega t)d\omega$$

and the ship's velocities, $\dot{x}_k$, and accelerations, $\ddot{x}_k$, are relative to the inertial (seakeeping) frame.

In practice, the memory effects need only be considered for a finite length of time in the past, beyond which the influence of a wave that has travelled away from the hull will be negligible. It should be noted that a sufficient window length for a monohull may not be sufficient for a multihull, due to the interaction effects. For a multihull, the

window must be long enough such that it covers the time for the highest frequency radiated waves (that produce a measurable interaction force) to reach the receiving demi-hull.

In the present approach, because the code serves for demonstration purposes, a limiting assumption has been made to simplify the implementation of the radiation force. This assumption states that $A_{jk}(\omega) = A_{jk}(\infty) = A_{jk}$ and, likewise, $B_{jk}(\omega) = B_{jk}(\infty) = B_{jk}$. The ramification of this assumption is that the kernel function, $K_{jk}(t)$, becomes zero and there are no memory effects to be calculated. By assuming that the added mass and damping coefficients are frequency-independent, the forces are valid only in the case of single-harmonic ship response, provided that the selected frequency for the coefficients matches the frequency of the ship motion. For the demonstration code, such an assumption is reasonable for regular waves, and perhaps in the case of a narrow-banded irregular wave spectrum, when the regular wave or spectrum peak encounter frequencies are used in selecting the added mass and damping coefficients.

3.3.2 Diffraction Force

The diffraction force in the present time-domain theory is assumed to be linear. As with the radiation force, the diffraction force could be obtained through the use of a convolution integral. However, using the assumption that there are no significant memory effects in the diffraction problem, the total diffraction force is obtained as a linear superposition of the force due to each frequency component of the defined ambient wave environment. An assumption of nominally constant speed and heading is made, thereby allowing a constant ω_e to be defined for a given frequency component. The time-domain diffraction force in the j-th direction is then obtained by:

$$F_j^D(t) = \sum_{n=1}^{Nwaves} A_n \cdot \Re\left\{e^{i\omega_{n,e}t} e^{i\varepsilon_n} \cdot F_j^7(\omega_{n,e})\right\} \qquad \textbf{(3.6)}$$

where $F_j^7(\omega_{n,e})$ is the frequency-domain diffraction force coefficient (force per unit wave amplitude) for the total ship.

3.3.3 Hydrostatic and Froude-Krylov Force

The combined hydrostatic and Froude-Krylov force is assumed to provide the most significant nonlinear contribution to the multihull large amplitude ship motion problem. In the present time-domain theory, the hydrostatic and Froude-Krylov pressures are evaluated on the exact wetted surface geometry, as determined by the intersection of the undisturbed incident wave and the instantaneous position of the ship. Given the breadth of typical multihull designs, even a small roll angle can lead to large displacement of the outer-hulls, resulting in potentially large changes to the wetted surface geometry. Figure 3.1 shows a cross-section from an example trimaran design at even keel with a large amplitude wave overlaid. Figure 3.2 demonstrates how, in the same wave-field as Figure 3.1, even small body motion can lead to significant changes in wetted geometry. In this case, just 7 degrees of roll and small heave has a noticeable effect.

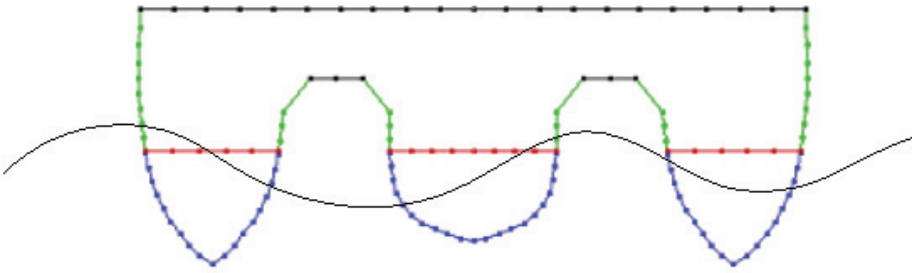

Figure 3.1 Example trimaran cross-section (even-keel) in large waves

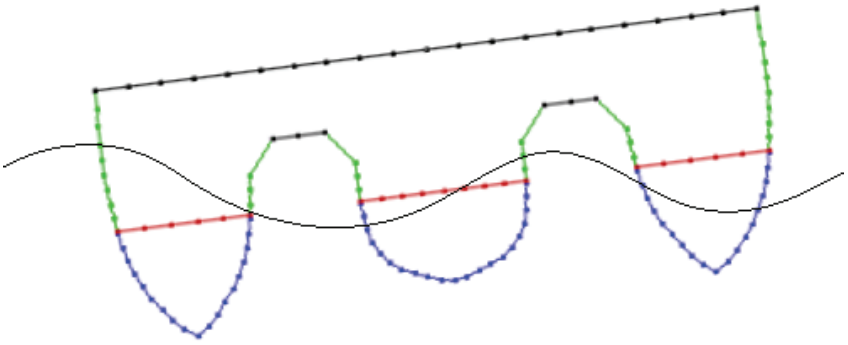

Figure 3.2 Example trimaran cross-section (with motion) in large waves

The body-exact hydrostatic and Froude-Krylov force is obtained on a sectional basis by integrating the pressures as given by equations 3.3 and 3.4 over the time-varying wetted geometry and then integrated over the length of the ship to find the total ship force.

$$f_j^{HSFK}(t;x) = \int_{c_x(t)} \left(p^{HS} + p^{FK}\right) n_j \, dl \qquad \text{j=1,2,3,4} \qquad \textbf{(3.7)}$$

$$F_j^{HSFK}(t) = \int_L f_j^{HSFK}(t;x) dx \qquad \text{j=1,2,3,4}$$

$$F_5^{HSFK}(t) = -\int_L x \cdot f_3^{HSFK}(t;x) dx \qquad \text{j=5}$$

$$F_6^{HSFK}(t) = \int_L x \cdot f_2^{HSFK}(t;x) dx \qquad \text{j=6}$$

In the solution of the sectional forces, the wave elevation is evaluated per equation 3.2 at the (X,Y) position of each vertex of a two dimensional panel on a given section and compared to the Z position of each vertex to determine if the panel is wetted. At each time step, it is necessary to determine the position of each 2D panel in world coordinates so that the free surface elevation can be evaluated and compared to the panel's Z-value at that (X,Y) location. To do so, the following transformation is used:

$$\begin{pmatrix} X \\ Y \\ Z \end{pmatrix} = [T_W] \cdot \begin{pmatrix} x \\ y \\ z \end{pmatrix} + \begin{pmatrix} \eta_1 \\ \eta_2 \\ \eta_3 \end{pmatrix} \qquad \textbf{(3.8)}$$

where

$$T_W = \begin{bmatrix} \cos\theta\cos\psi & \sin\phi\sin\theta\cos\psi - \cos\phi\sin\psi & \cos\phi\sin\theta\cos\psi + \sin\phi\sin\psi \\ \cos\theta\sin\psi & \sin\phi\sin\theta\sin\psi + \cos\phi\cos\psi & \cos\phi\sin\theta\sin\psi - \sin\phi\cos\psi \\ -\sin\theta & \sin\phi\cos\theta & \cos\phi\cos\theta \end{bmatrix}$$

and ϕ, θ, and ψ are the Euler angles for roll, pitch, and yaw, respectively and η_1, η_2, and η_3 are the surge, sway, and heave displacements.

3.4 Equations of Motion

Although the total hydrodynamic forces in the time-domain theory are nonlinear, the implemented equations of motion are linear. While the focus of this work is on seakeeping, where pitch and yaw can be considered small angles, roll could potentially be

large. A further improvement would be to extend the time-domain solution to use the fully nonlinear Euler equations of motion.

In the present implementation, the equations of motion remain separated between vertical and lateral plane motions. That is, the vertical and lateral planes are still considered to be de-coupled. Such an approximation is not reasonable in general, but sufficient for demonstration purposes and for examining pure head or following seas. The 3x3 matrix equation to be solved separately for the vertical and lateral plane accelerations is simply:

$$\left[M_{jk}\right]\{\ddot{\eta}_k\} = F_j^{total} \qquad \textbf{(3.9)}$$

where $F_j^{total} = F_j^R + F_j^D + F_j^{HSFK} + G_j$

and

$G_j = 0$ j=1,2,6

$G_j = -M \cdot g$ j=3

$G_j = -M \cdot g \cdot z_g \cdot \sin\eta_4$ j=4

$G_j = M \cdot g\left(x_g + z_g \sin\eta_5\right)$ j=5

Following the solution of the accelerations, the accelerations and velocities are integrated in time for the velocity and position, respectively, at the next time step using a fourth-order Runge-Kutta integration scheme.

Chapter 4

Verification and Validation

The presently developed theory and its implementation in a code, referred to as NSHIPMO_multihull, has undergone verification and validation to assess its capabilities. Verification ensures that the theory has been implemented correctly in the computer code. Validation ascertains the ability of the theory to correctly model the real-world physics. Verification was performed first to ensure that any validation conclusions could be attributed to the theory, rather than improper implementation of the theory.

4.1 Verification

The computer code was developed through substantial modification of the SHIPMO code. The definition of section geometry was changed to be done by 2D panels versus successive points, to ensure that gaps (due to a bulb or main-hull to sub-hull separation on a trimaran) are properly modeled. The first part of the verification process examined simple monohull and "2D image" catamaran (full transverse cut of ship) cases to ensure that the new code matched the old code's results. Verification then focused on ensuring that the radiation interaction forces were properly implemented.

4.1.1 Geometry Parsing

The change in geometry definition led to a need to verify that the program correctly interprets and processes the input for the demi-hull(s). The sectional geometry definition is shown in Figure 4.1, where panels 1 through 7 are defined by their endpoints (A_nodeY, A_nodeZ) and (B_nodeY, B_nodeZ). The waterline slicing subroutine determines which panels are wetted in the linear sense (below the calm waterline) and cuts the panels intersecting the free surface. If desired, the program also creates lid

panels to be used in the 2D frequency-domain radiation calculation to help suppress irregular frequencies. Wet-deck and main-deck panels can also be created for use in the body-exact hydrostatic and Froude-Krylov calculation in the time-domain simulation.

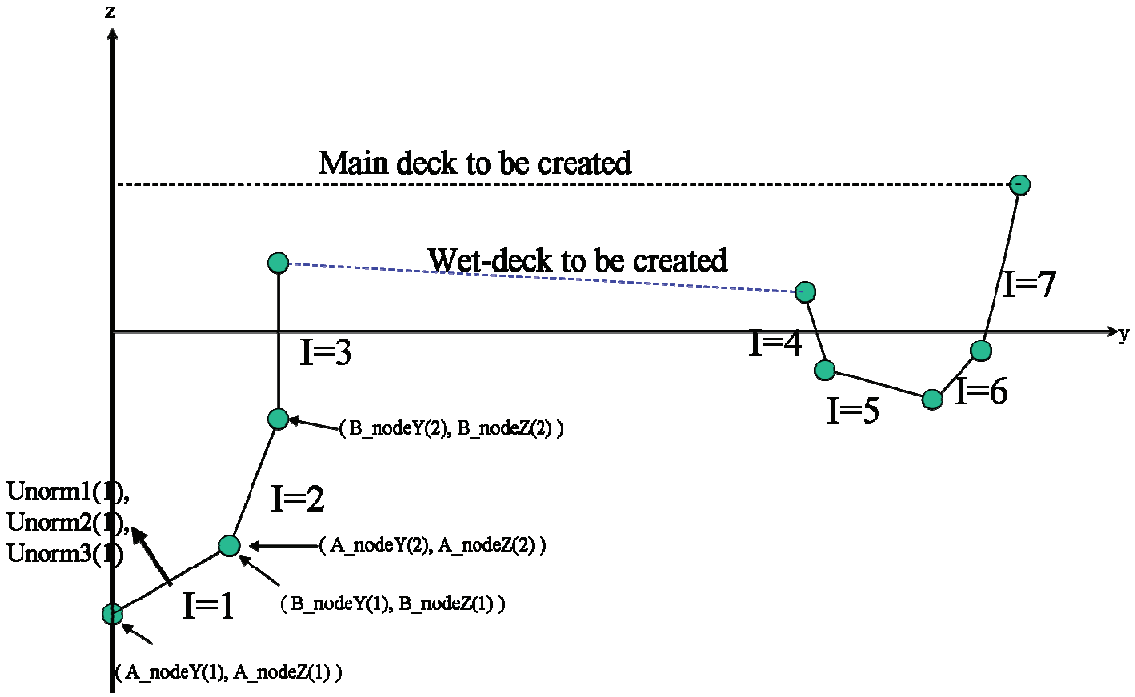

Figure 4.1 Geometry input example for a trimaran section

Figure 4.2 shows the processed geometry of an example trimaran section. The raw input panels are shown in green, along with the usual outward-pointing (out of the fluid) unit normals placed at the midpoint of the panels. The mean-wetted panels are shown in blue, along with the inward-pointing (into fluid) normals used in setting the body boundary condition in the Frank subroutine. The automatically created lid panels are shown in red and the automatically generated wet-deck and main deck panels are shown in black.

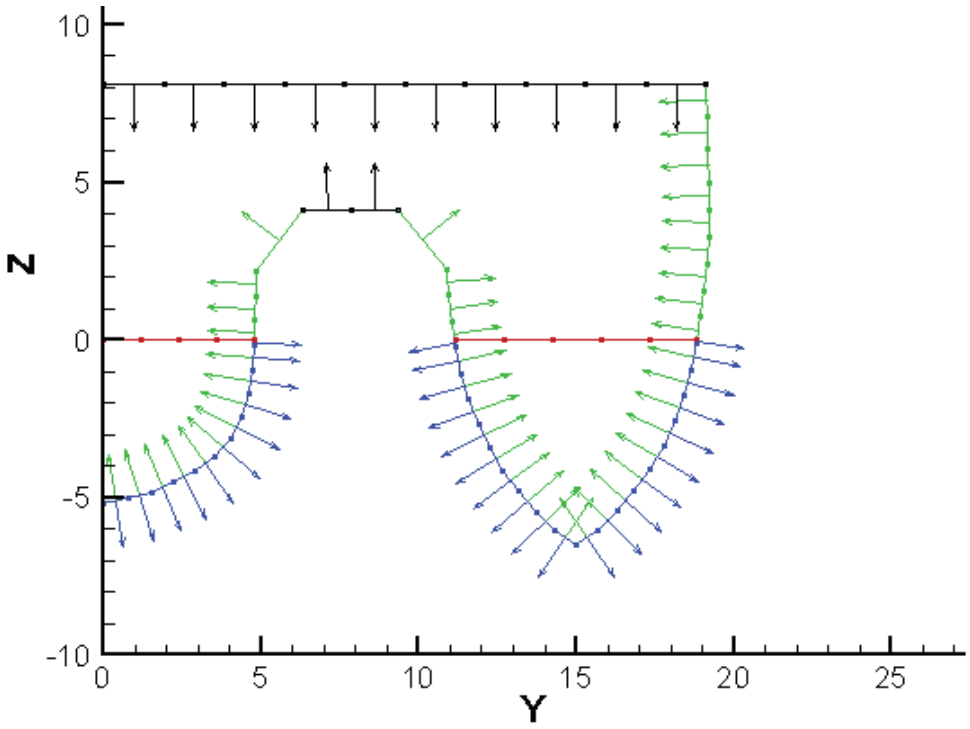

Figure 4.2 Parsed geometry of example trimaran section

4.1.2 Independent Demi-Hull Radiation Forces

The next verification task examined the 2D boundary value problem solution and its capability to calculate the radiation potentials on an independent demi-hull (no assumption is made of demi-hull port-starboard symmetry). The first step compared the present program's calculations to the original SHIPMO. That is, the cases examined were monohull calculations as well as catamaran calculations that use the full 2D transverse cut (i.e. uses the centerplane image of the demi-hull) in the calculation of the radiation. To verify that the independent demi-hull calculations (centerplane image of catamaran demi-hull not included in calculation) are done correctly in the present code, a catamaran with demi-hulls identical to the monohull is compared to the monohull calculation. Illustrations of the difference between the full transverse cut calculation and independent demi-hull calculation are given in Figure 4.3 and Figure 4.4 for a catamaran and trimaran, respectively.

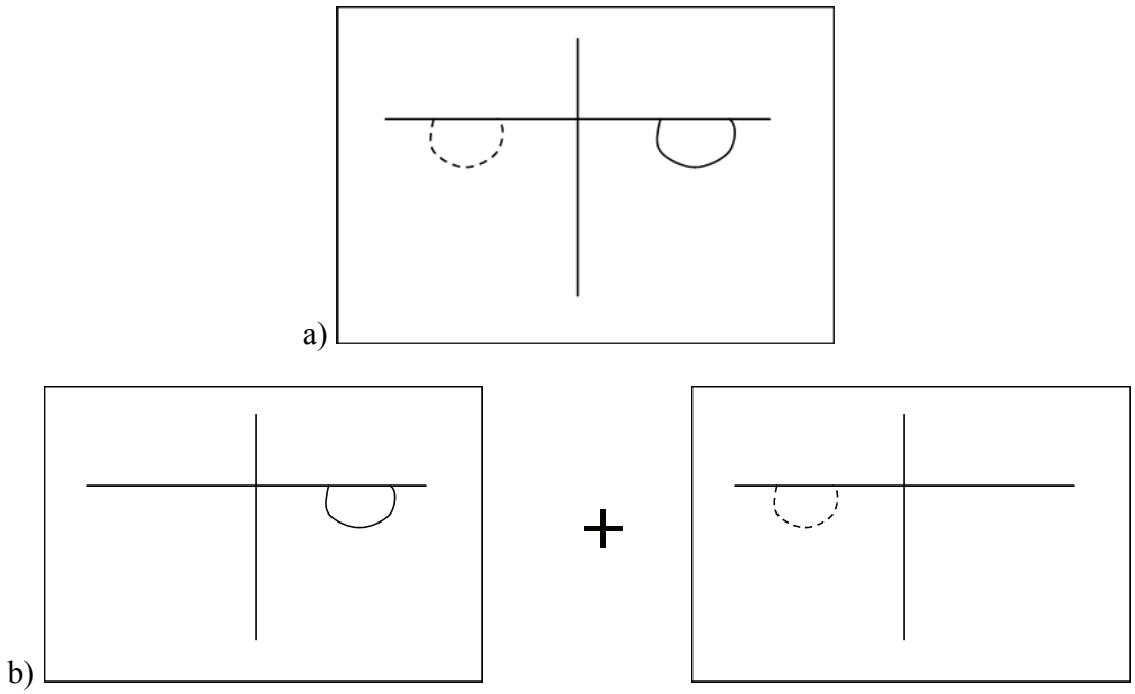

Figure 4.3 Illustration of catamaran boundary value problem for cases a) Full transverse cut, and b) Independent demi-hulls

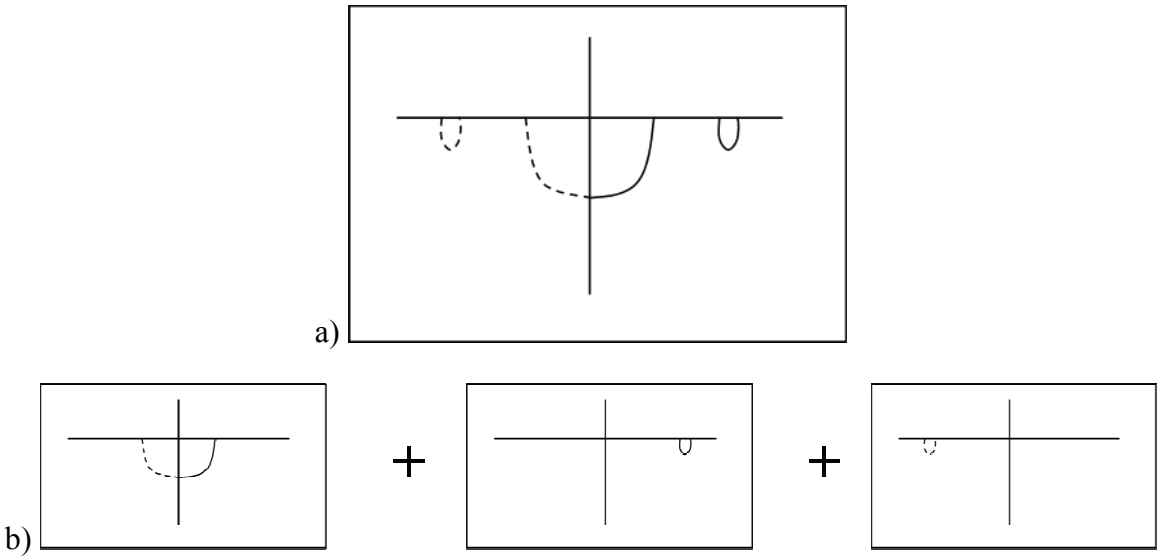

Figure 4.4 Illustration of trimaran boundary value problem for cases a) Full transverse cut, and b) Independent demi-hulls

4.1.2.1 Original SHIPMO vs. Present Code

The calculation of the radiation potentials has been verified by comparing the 2D added mass and damping coefficients of a monohull section and a catamaran demi-hull section. The present code provides the option for including the images about the centerplane (in the case of a catamaran or trimaran sub-hull), which for this verification task, was set to include the images (original SHIPMO automatically includes the images).

The geometry for the monohull section is shown in Figure 4.5. The sectional added mass and damping coefficients were found to match the original SHIPMO exactly. Two examples are provided in Figure 4.6 and Figure 4.7. Similarly, the full-2D-cut radiation potential calculation was verified for the catamaran section, shown in Figure 4.8. Examples of the comparison of the present code's results to the original SHIPMO for the full-2D-cut catamaran are given in Figure 4.9 and Figure 4.10.

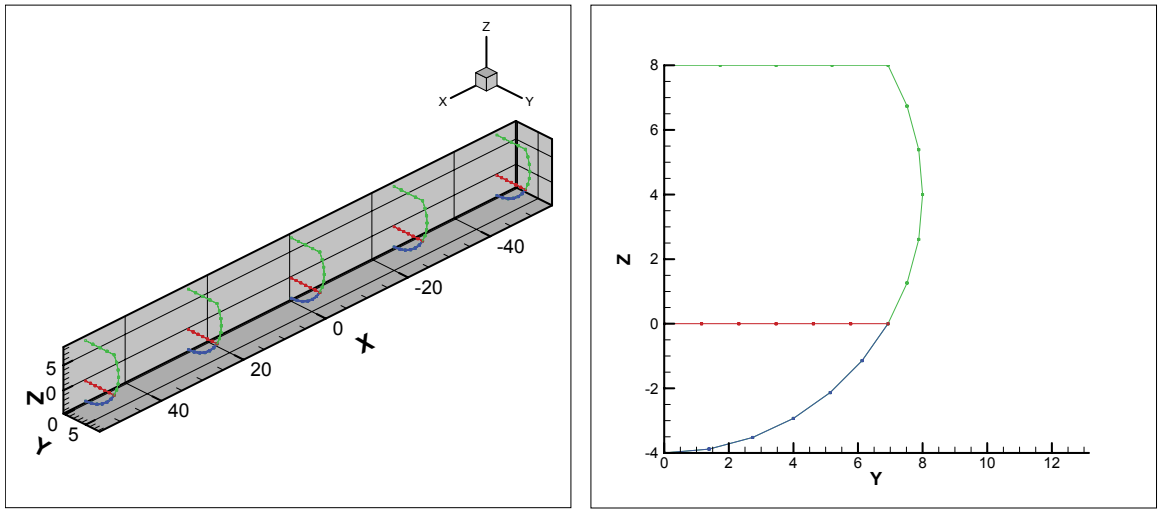

Figure 4.5 Monohull 2D sections for verification runs (isometric and body-plan views)

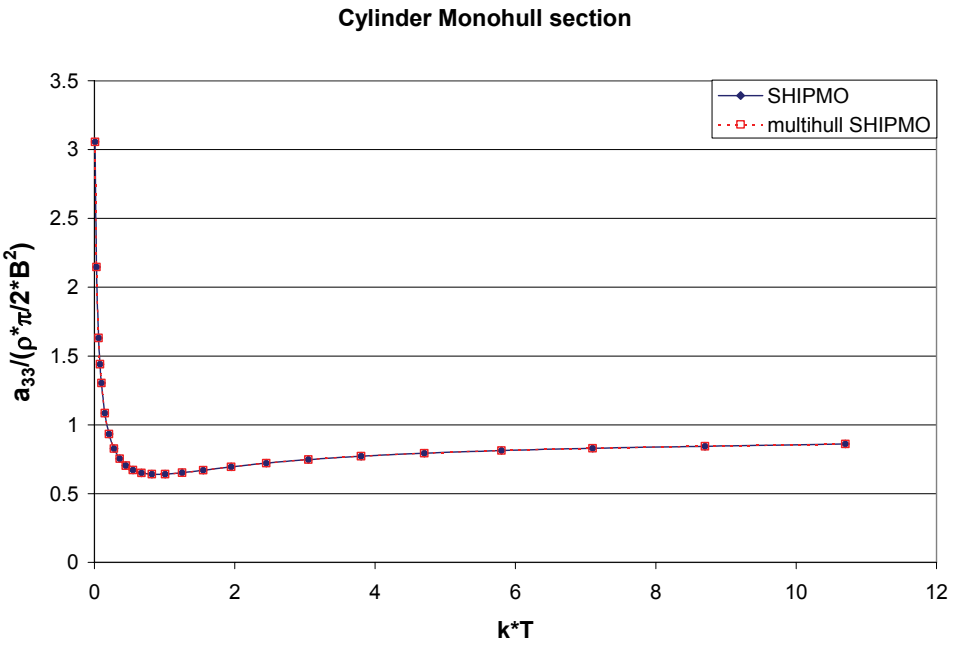

Figure 4.6 Monohull section heave added mass (a_{33}) comparison for original SHIPMO and present code

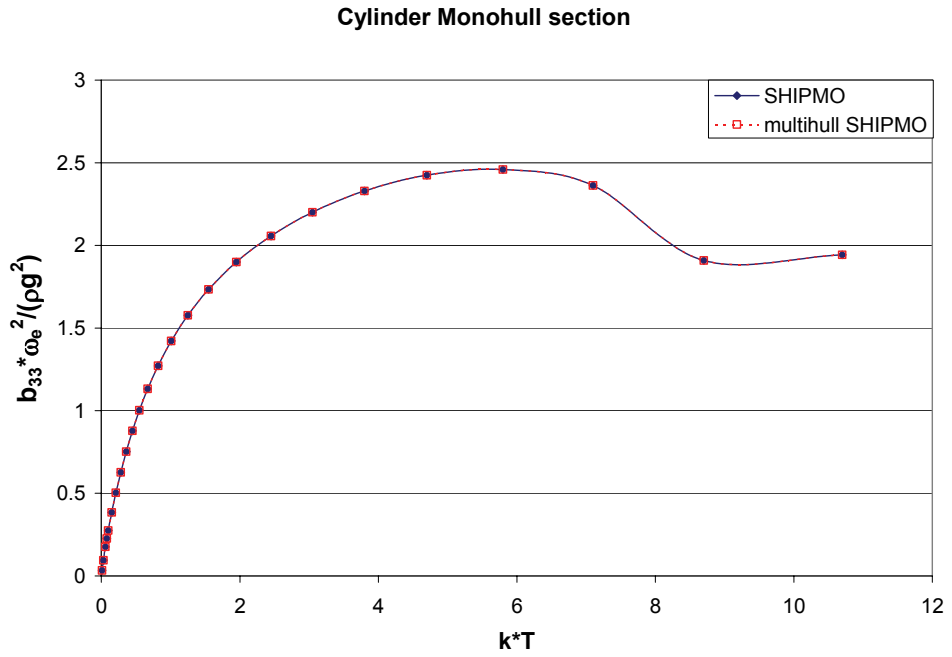

Figure 4.7 Monohull section heave damping (b_{33}) comparison for original SHIPMO and present code

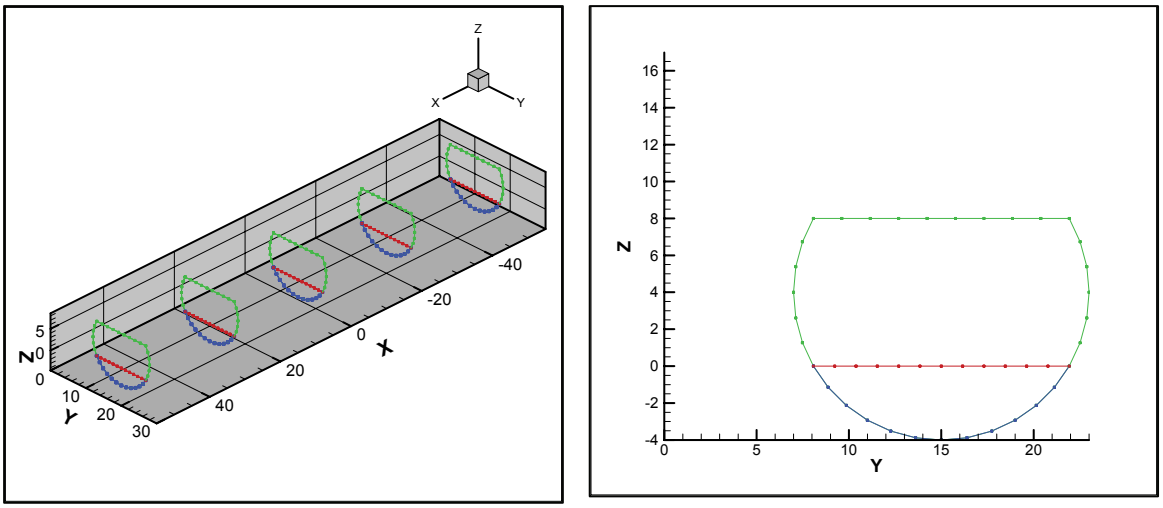

Figure 4.8 Catamaran 2D sections for verification runs (isometric and body-plan views)

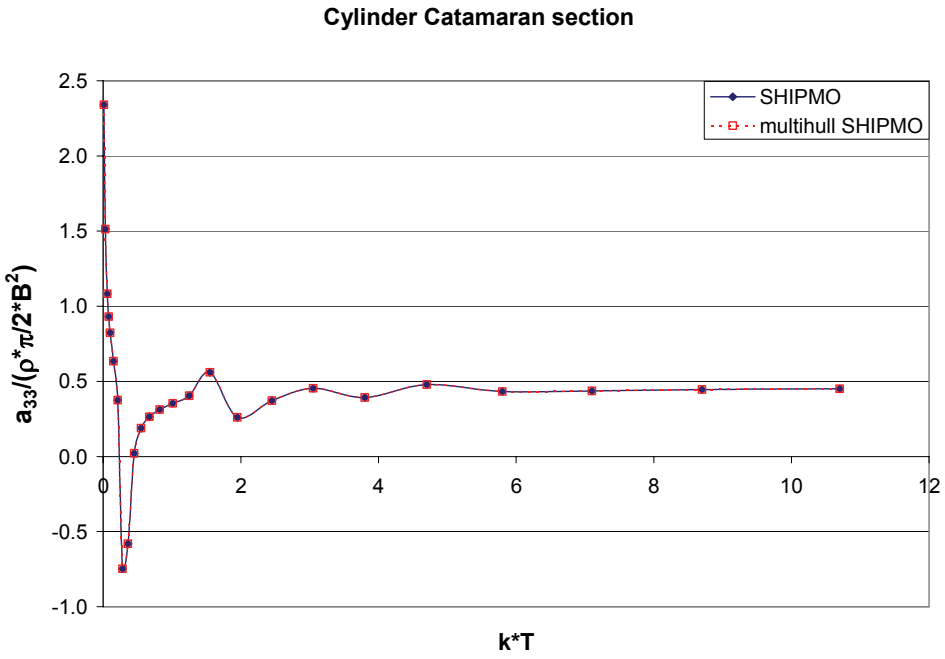

Figure 4.9 Catamaran section heave added mass (a_{33}) comparison for original SHIPMO and present code

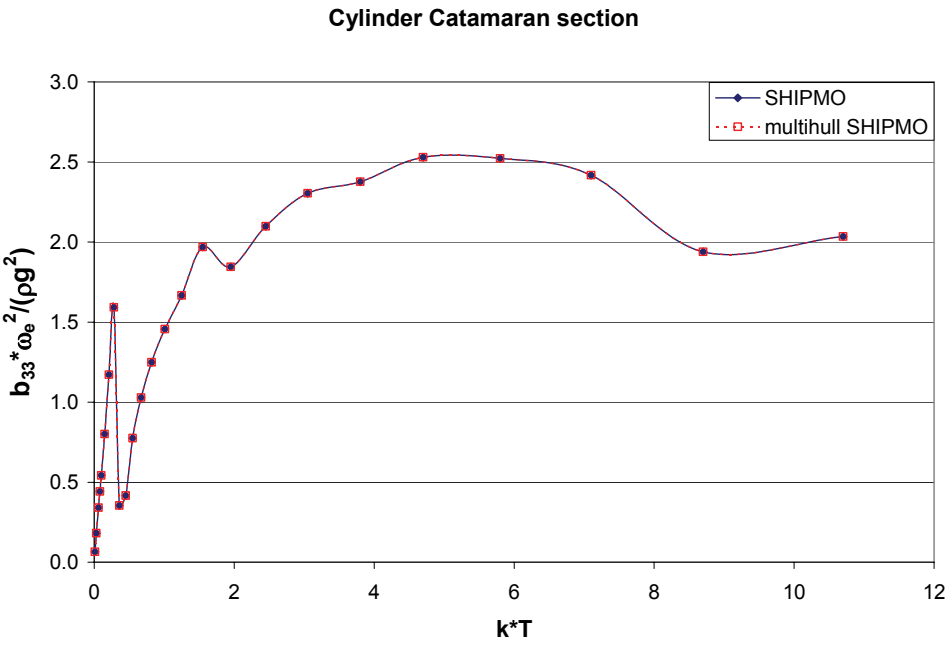

Figure 4.10 Catamaran section heave damping (b_{33}) comparison for original SHIPMO and present code

4.1.2.2 Independent Demi-Hull Comparison

Having shown that the calculation is being performed correctly in the case where the full transverse cut is included, it was then necessary to confirm that the independent demi-hull calculation (i.e. no centerplane images included) is being done correctly. This was done by comparing the added mass and damping coefficients, non-dimensionalized by sectional area, of the catamaran demi-hulls to the monohull. Example plots are presented in Figure 4.11 to Figure 4.16. For comparison purposes, the "imaged" demi-hull calculation is included.

For sway (k=2) and heave (k=3) modes of motion, the non-dimensionalized coefficients for the independent demi-hull calculation should match the monohull calculation exactly. This has been confirmed in the plots. For roll, the unit normal provides that the motion is almost entirely vertical, though not completely. For that reason, the independent demi-hull results do not collapse to the monohull results.

The inclusion of the full-2D-cut (imaged) solution in the plots demonstrates two of the theoretical ramifications for choosing to model the demi-hulls as independent. First, as shown in Figure 4.13, the low-frequency limit of a_{44} is singular. This is due to the strength of n_3 in the n_4 unit normal and the lack of a compensating panel with the opposite n_4 normal on the negative-y side. Second, as demonstrated in the plots of sectional damping, the independent demi-hull allows all of its radiated waves to reach the far-field. This leads to generally higher damping coefficients than the calculation that includes images, which traps a certain amount of energy between the hulls that cannot escape to the far-field.

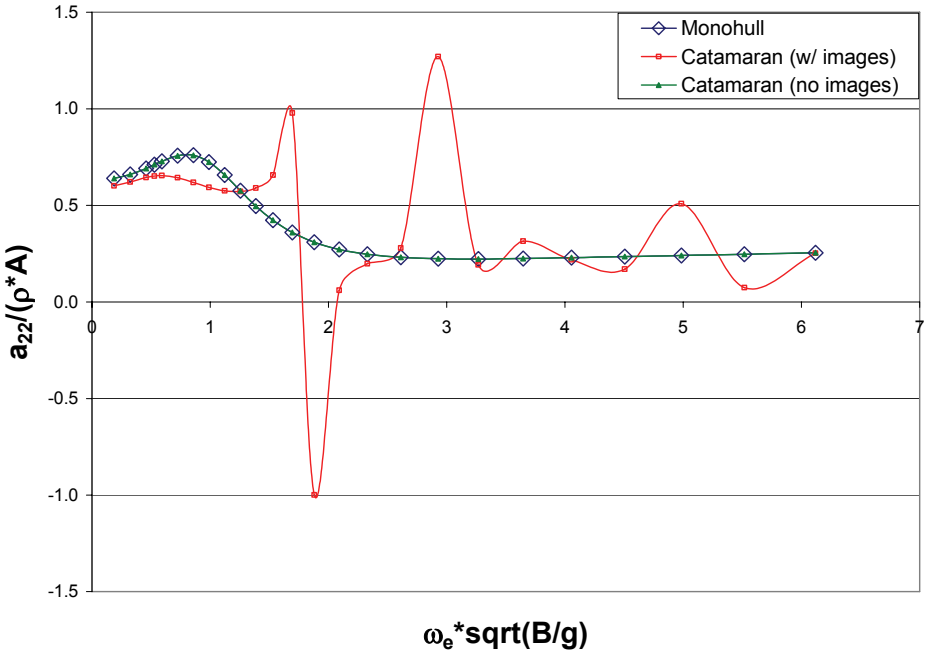

Figure 4.11 Non-dimensional a_{22} for monohull and catamaran imaged and independent demi-hulls

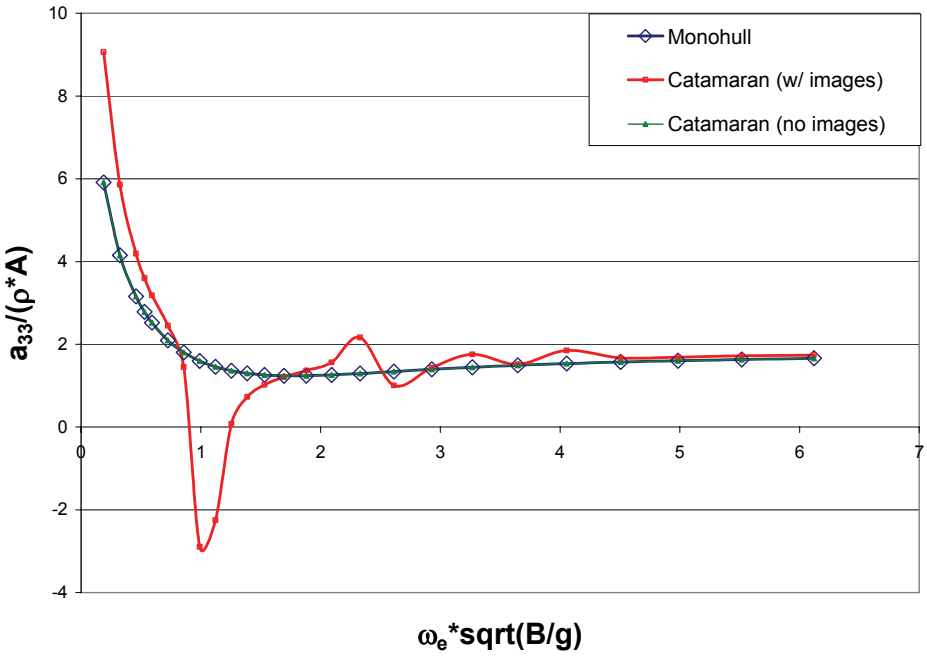

Figure 4.12 Non-dimensional a_{33} for monohull and catamaran imaged and independent demi-hulls

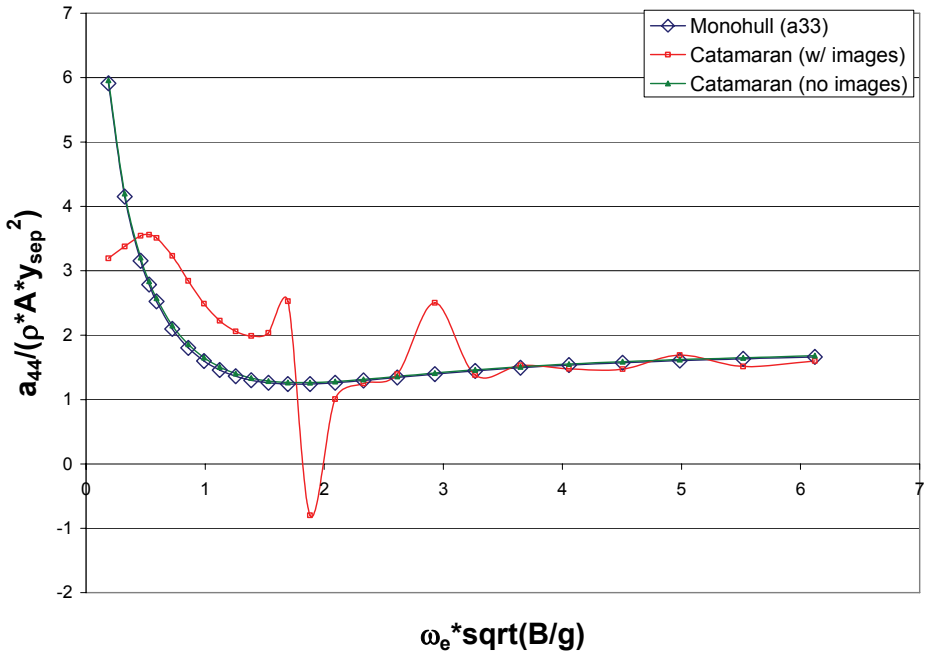

Figure 4.13 Non-dimensional a_{44} for catamaran imaged and independent demi-hulls compared to monohull a_{33}

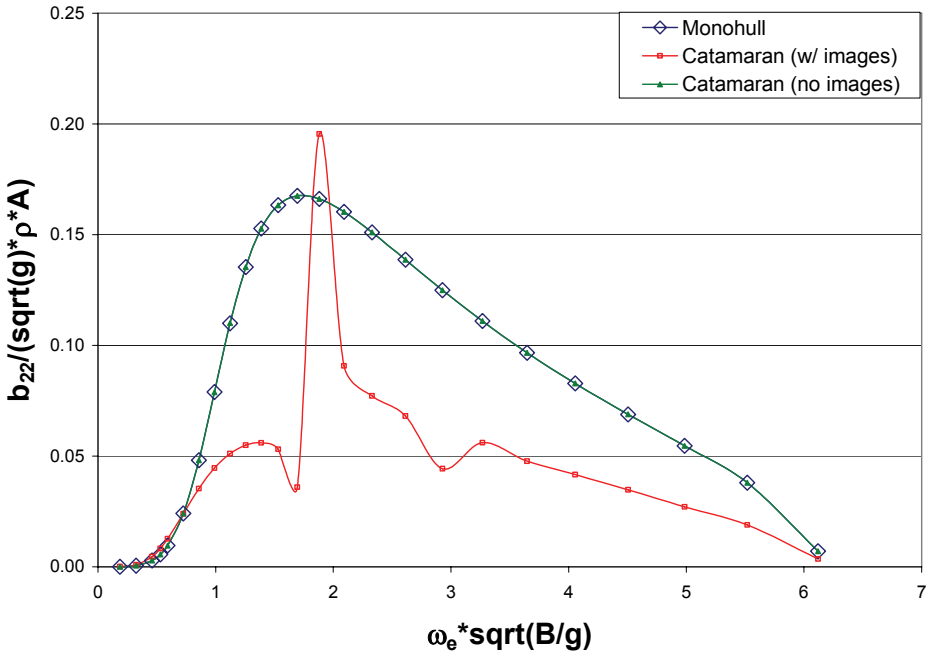

Figure 4.14 Non-dimensional b_{22} for monohull and catamaran imaged and independent demi-hulls

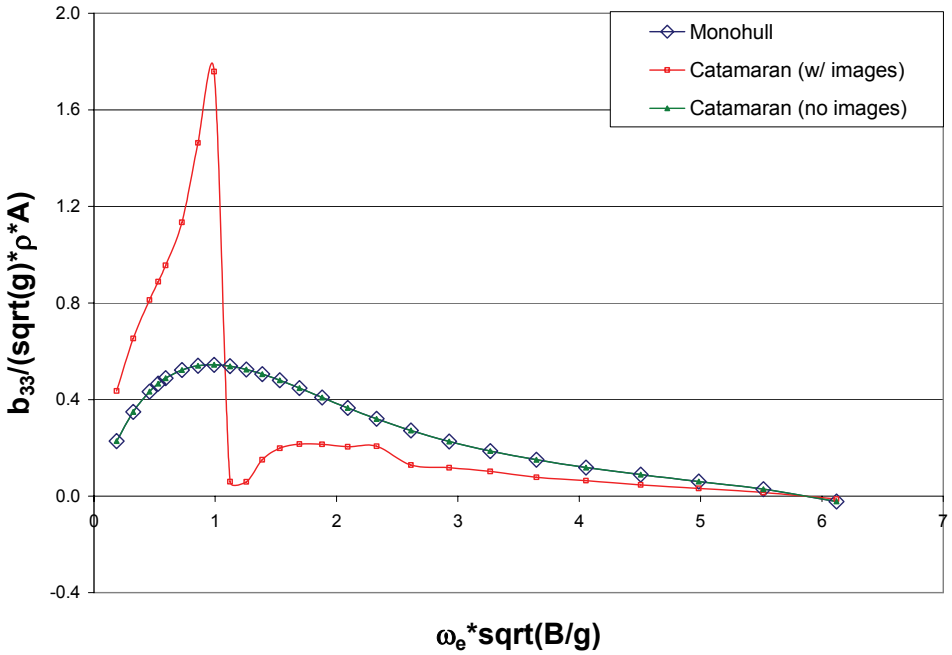

Figure 4.15 Non-dimensional b_{33} for monohull and catamaran imaged and independent demi-hulls

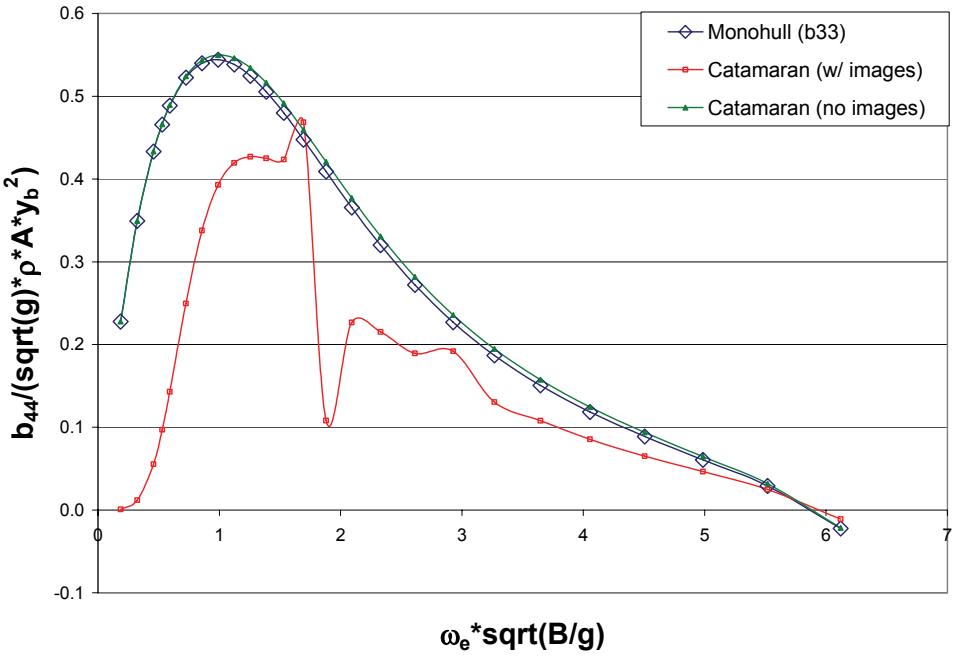

Figure 4.16 Non-dimensional b_{44} for catamaran imaged and independent demi-hulls compared to monohull b_{33}

4.1.3 Radiated Wave Phasing

Critical to the calculation of the interaction forces is the proper calculation of the radiated wave phase. This is due to the radiated wavelengths generally being longer than the beam of the demi-hull. An incorrect determination of wave phase leads to an incorrect determination of interaction force.

In the present theory, the wave phase is automatically captured by the use of the far-field Green function. The incident far-field radiated wave potential, as described in section 2.2.2.1, provides the definition of the radiated wave elevation. To verify that the phase of the potential has been determined correctly, the radiated wave elevation in space was compared to the radiated wave as generated by the 3D panel code, LAMP. The radiated wave pattern predicted by LAMP of a demi-hull oscillating in heave at zero-forward speed is shown in Figure 4.17. A midship slice of the 3D wave pattern is compared in Figure 4.18 to the 2D wave pattern given by the far-field incident radiated

wave potential in the present theory. This figure confirms that the phase has been properly captured.

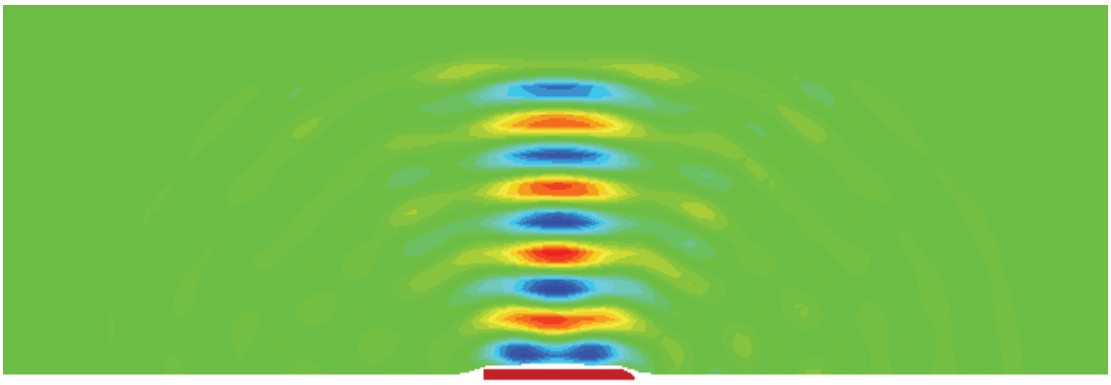

Figure 4.17 3D radiated wave from demi-hull, using LAMP

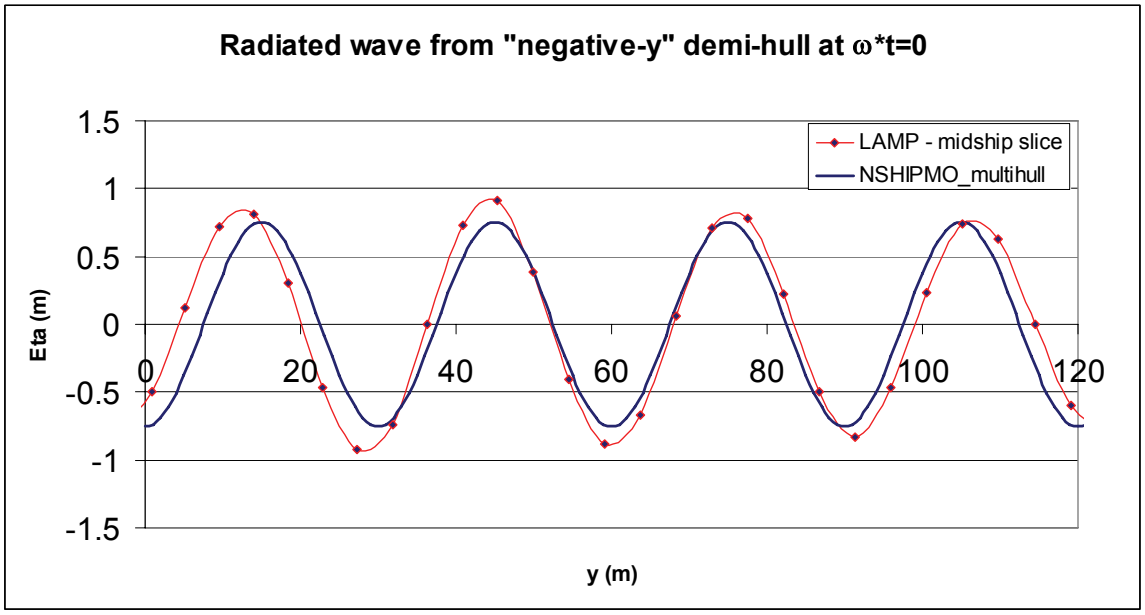

Figure 4.18 Midship slice of radiated wave from LAMP and present theory

4.1.4 Interaction forces

The final step in the verification process is to verify that the interaction forces are correctly calculated. After verifying (through active monitoring of variables in debug mode) that x^* is correctly determined for a given ship speed and encounter frequency, the incident radiated wave force, $F^{\sim I}$, and diffracted radiated wave force, $F^{\sim D}$, were checked. This was done by comparing the respective forces to ambient wave Froude-Krylov and diffraction forces on a demi-hull (by using a monohull equivalent), where the ambient wave has the same amplitude and frequency as the radiated wave. In this exercise, the amplitude of the ambient wave is determined from the far-field incident radiation potential for the example mode of motion. Figure 4.19 shows that the forces, presented in the complex plane, match as expected.

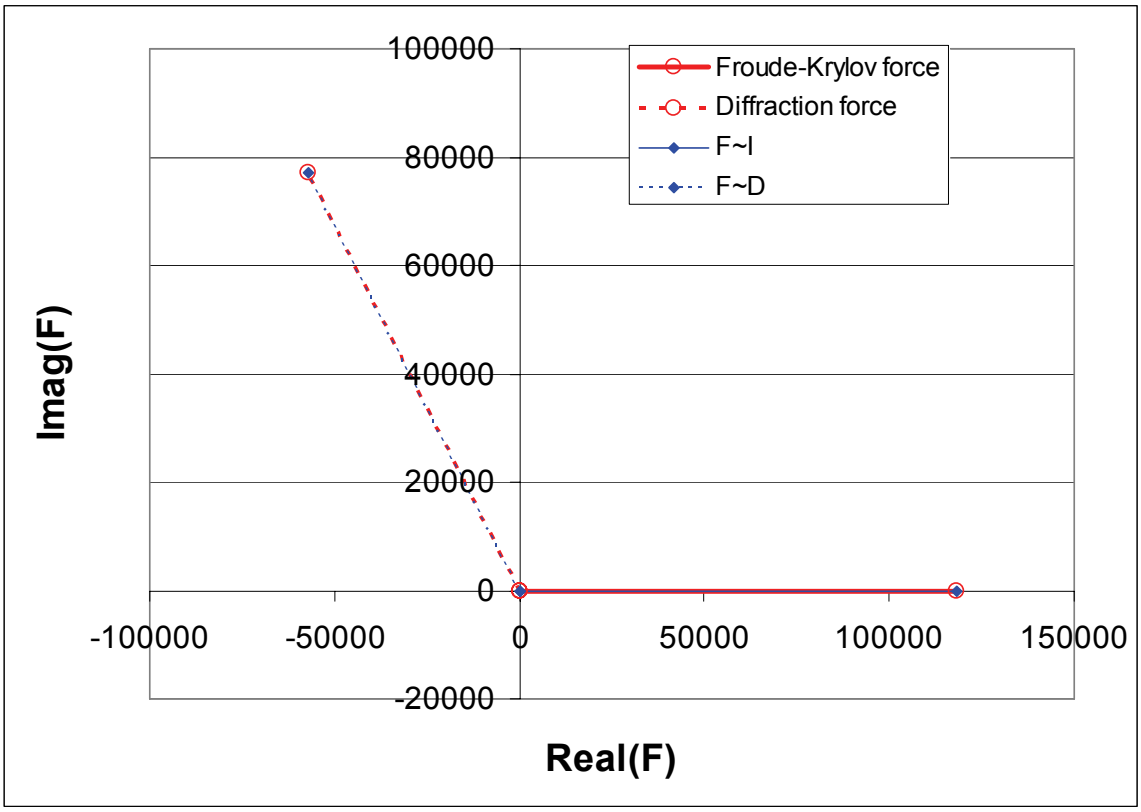

Figure 4.19 Comparison of interaction forces to Froude-Krylov and diffraction forces for wave of same amplitude, frequency, and phase

4.2 Frequency-Domain Validation

To validate the multihull frequency-domain interaction theory, comparisons were made to model test data and higher fidelity computational tools for:

- added mass and damping coefficients as a function of frequency and ship speed
- motion transfer functions
- wave excitation, where available

Table 4.1 presents a list of the hull forms used in the frequency-domain validation tasking. With the exception of the Cylinder Catamaran, validation data is provided by scale-model experiments. The Cylinder Catamaran is a fictional design that has been run in the LAMP program for comparison. The data sets comprise a mix of L/B ratios and separation distances, with perhaps only the Cylinder Catamaran and Delft Catamaran appearing well-suited for the application of the present theory. Given real-world design variations of multihulls, testing over a range of parameters helps determine the practical utility of the present theory.

Table 4.1 Characteristics of Validation Cases

Ship	Demi-hull L/B	(TCB-to-TCB Separation)/B	(Inboard Waterline Separation)/B
Cylinder Catamaran	7	3	2
Delft Catamaran	12.5	2.9	1.9
Kashiwagi Catamaran	6	2	1
HSSL Trimaran	16.8	1.5 (main-hull to sub-hull)	0.5 (main-hull to sub-hull)
		3 (sub-hull to sub-hull)	2 (sub-hull to sub-hull)

Throughout the validation cases, the present theory is presented in plots as a blue solid line. Traditional strip theory results have also been included for comparison, with a red dotted line representing the calculation with the full 2D cut of the ship (includes centerplane images) and a green dashed line showing the independent demi-hull calculation (no interaction in any form). Model data points are given as dark blue circles.

4.2.1 Cylinder Catamaran

The Cylinder catamaran is a design created specifically for verification and validation of the present theory. The demi-hull consists of semi-circle sections that are of constant area for 6/7 of the length of the demi-hull. Isometric and body views of the design are given below.

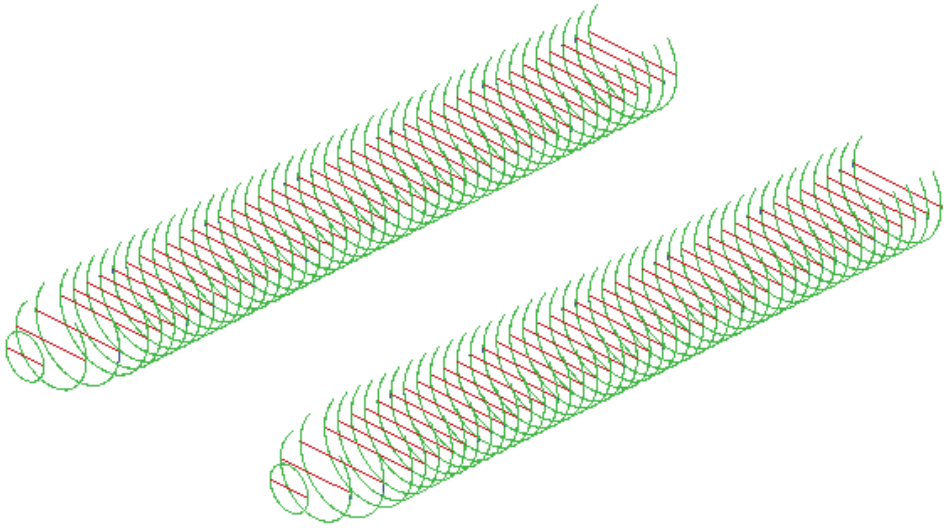

Figure 4.20 Cylinder Catamaran isometric view of sections

Figure 4.21 Cylinder Catamaran parallel midbody section panels

In the absence of model data, frequency-domain comparisons have been made against LAMP for added mass and damping coefficients and motion transfer functions. LAMP is a time-domain 3D panel code that can be run in a body-linear mode (LAMP-1) or body-exact mode (for more details, see Lin et al., 1999). The added mass and damping coefficients were obtained from the impulse response function capability in LAMP, whereas the transfer function points were obtained by a harmonic analysis of time-domain simulations using LAMP-1 and the linear pressure option.

4.2.1.1 Added Mass and Damping Coefficients

The Cylinder Catamaran geometry provides an opportunity to validate the notion that the interaction forces dissipate with increasing forward speed as the radiated waves are swept downstream. Figure 4.22 through Figure 4.24 show A_{33} versus encounter frequency for increasing ship speed. At Fn=0.0, the full-2D-cut strip theory matches the LAMP solution very closely, while the present theory follows the trend less precisely. For example, there is a small bump in the zero-speed A_{33} curve at a non-dimensional frequency of approximately 4.7 that is not predicted by the present theory. At this frequency, the radiated wave length is twice the demi-hull beam, which, per Table 4.1, is also the separation distance at the waterline. It is likely then that this small bump is due to a reflection, which is not modeled by the present theory. As forward speed increases, the present theory tends toward the LAMP solution fairly well, with both approaching the independent demi-hull solution. This appears to validate the foundation of the present theory. The small bump that had existed at zero speed disappears for the LAMP prediction, while it remains for the full-2D-cut strip theory as a consequence of having no speed dependence.

Figure 4.25 through Figure 4.28 show example coefficients due to pitch motion. In the first two plots, the present theory follows the LAMP trend fairly well, but with a noticeable offset in B_{35} example. Figure 4.27 and Figure 4.28 are examples of where the present theory does not match very well. Appendix A provides the entire set of added mass and damping coefficient comparisons. There are many examples of both good correlation and poor correlation for the present theory.

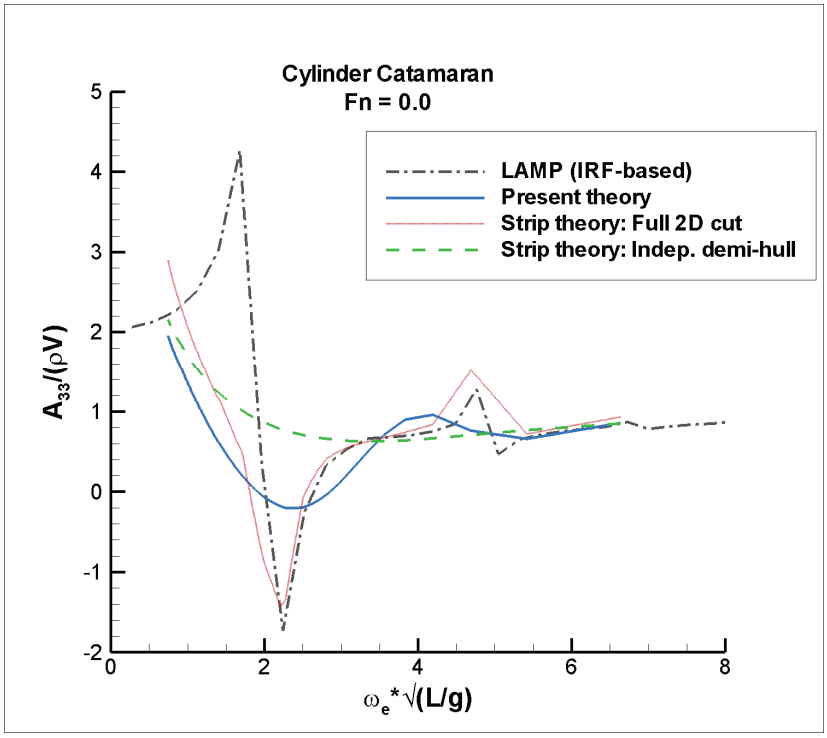

Figure 4.22 Cylinder Catamaran A_{33} at Fn=0.0

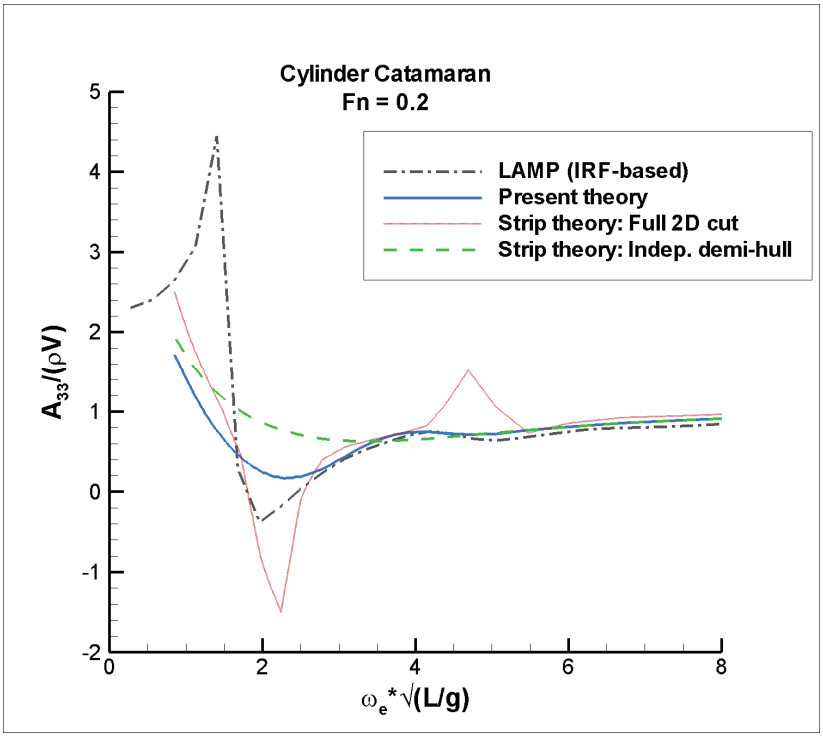

Figure 4.23 Cylinder Catamaran A_{33} at Fn=0.2

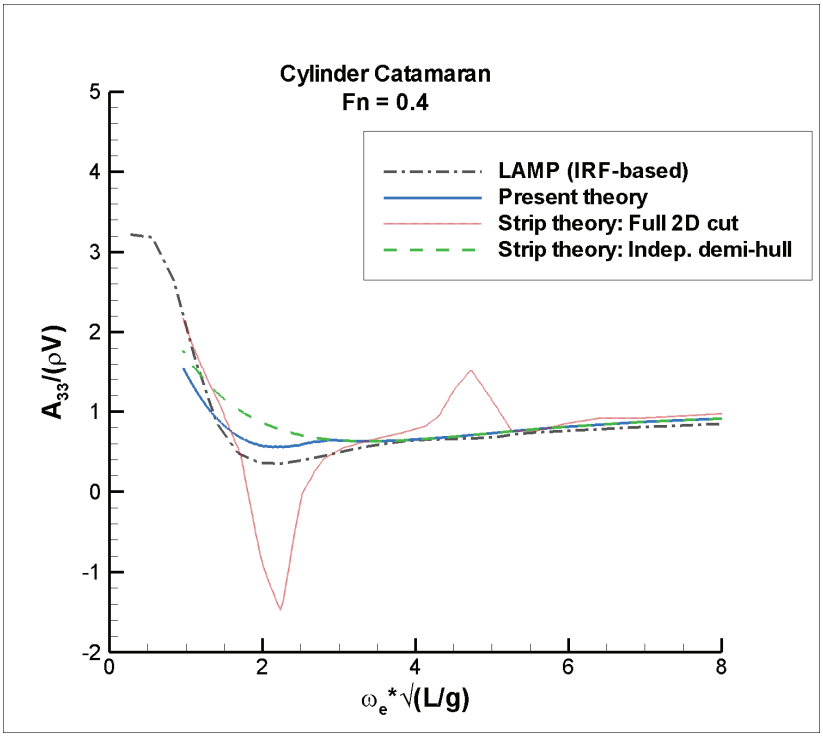

Figure 4.24 Cylinder Catamaran A_{33} at Fn=0.4

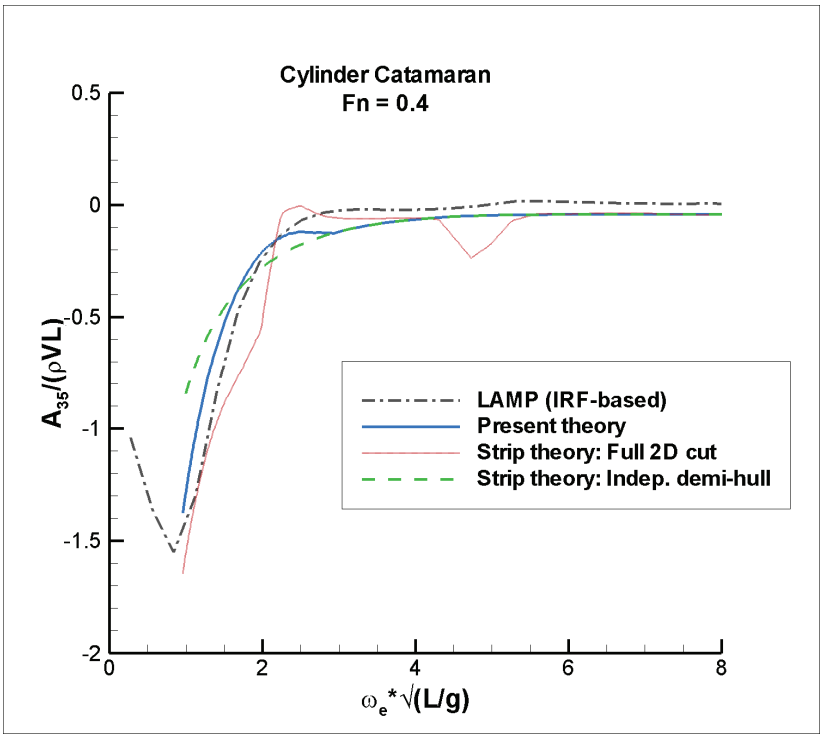

Figure 4.25 Cylinder Catamaran A_{35} at Fn=0.4

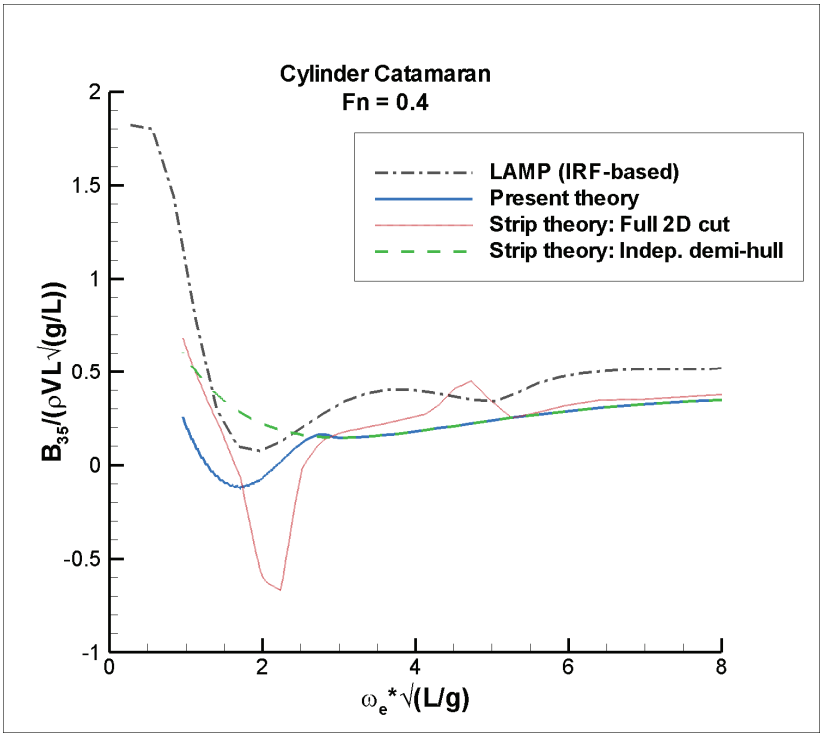

Figure 4.26 Cylinder Catamaran B_{35} at Fn=0.4

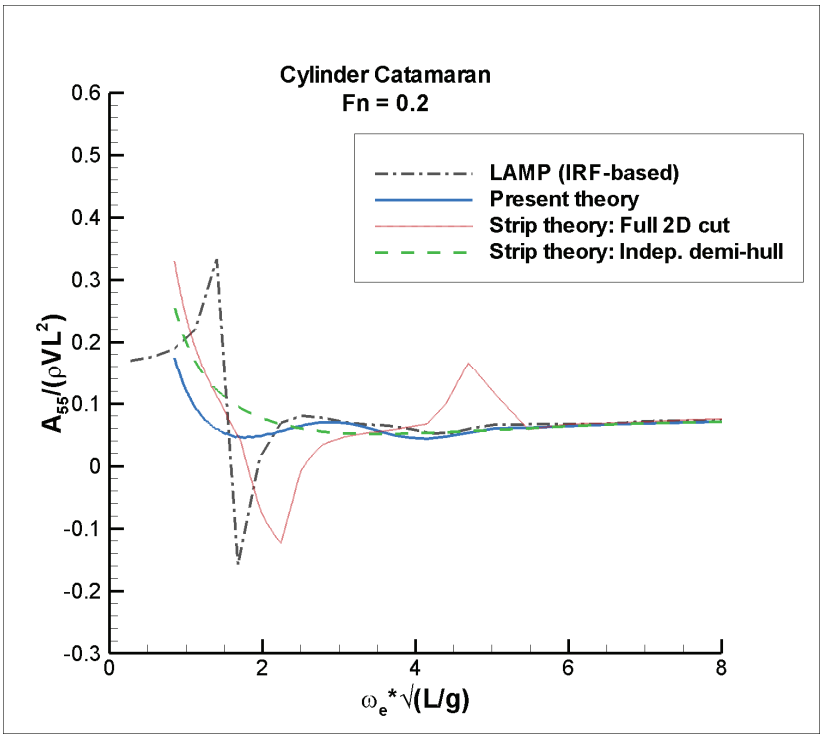

Figure 4.27 Cylinder Catamaran A_{55} at Fn=0.2

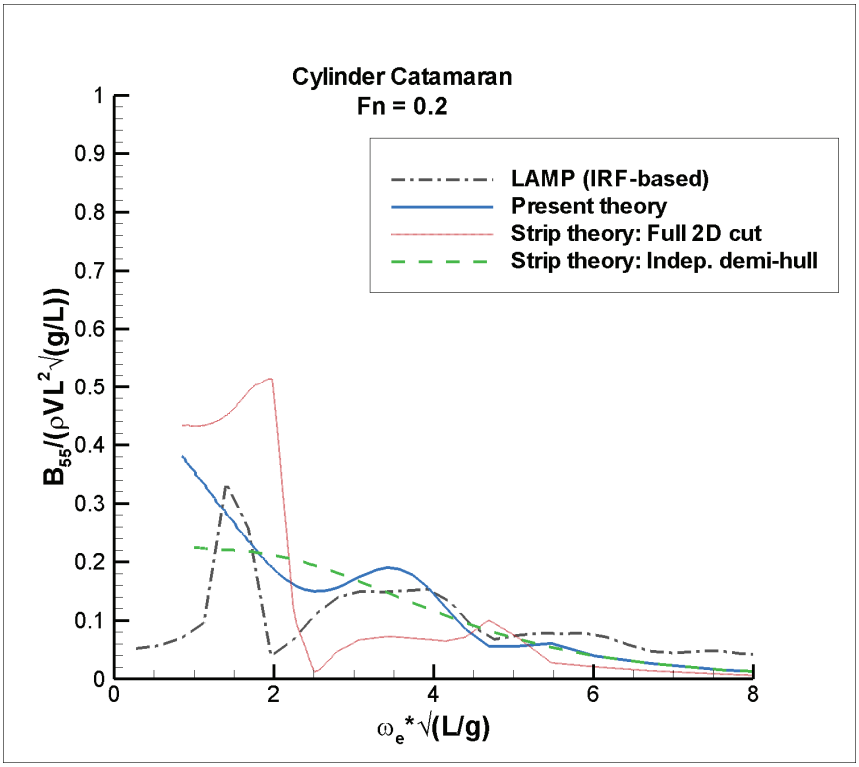

Figure 4.28 Cylinder Catamaran B_{55} at Fn=0.2

4.2.1.2 Motion Transfer Functions

Motion transfer functions were developed with the Cylinder Catamaran operating over a range of speeds in head seas. LAMP-1, which is body-linear in its boundary value problem solution, was run in the time-domain in regular waves. A harmonic analysis was performed on the motion time histories to find the amplitude of the first harmonic.

For zero speed, the present interaction theory leads to a significant over-prediction of the pitch response at $L/\lambda=2$, as seen in Figure 4.29, as well as an under-prediction in pitch for a wide range of wavelengths. The significant over-prediction near $L/\lambda=2$ can be traced to the near-zero damping coefficient for B_{33} at the corresponding non-dimensional encounter frequency of approximately 3.5, as seen in Figure 4.30, occurring near the pitch natural frequency. The zero-valued damping coefficient in this case is due to the interaction force contribution being equal in magnitude but opposite in sign to the independent demi-hull damping coefficient. This can occur when the phasing of the

interaction force is such that it is completely imaginary. The proof that the magnitude of the zero-speed interaction force is equal to the imaginary part of the independent radiation potential is given in Appendix E.

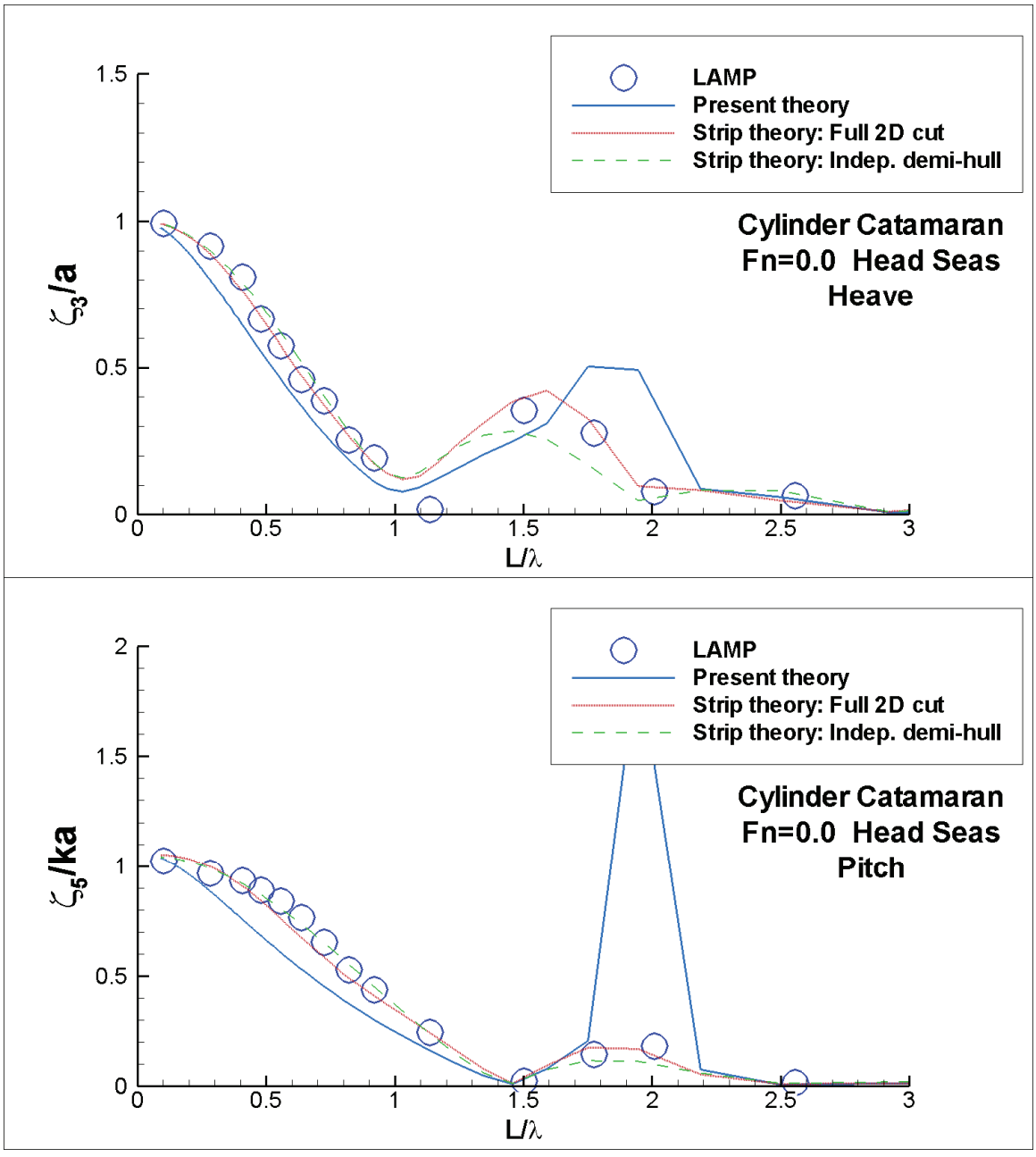

Figure 4.29 Cylinder Catamaran heave and pitch transfer functions at Fn=0.0 in head seas

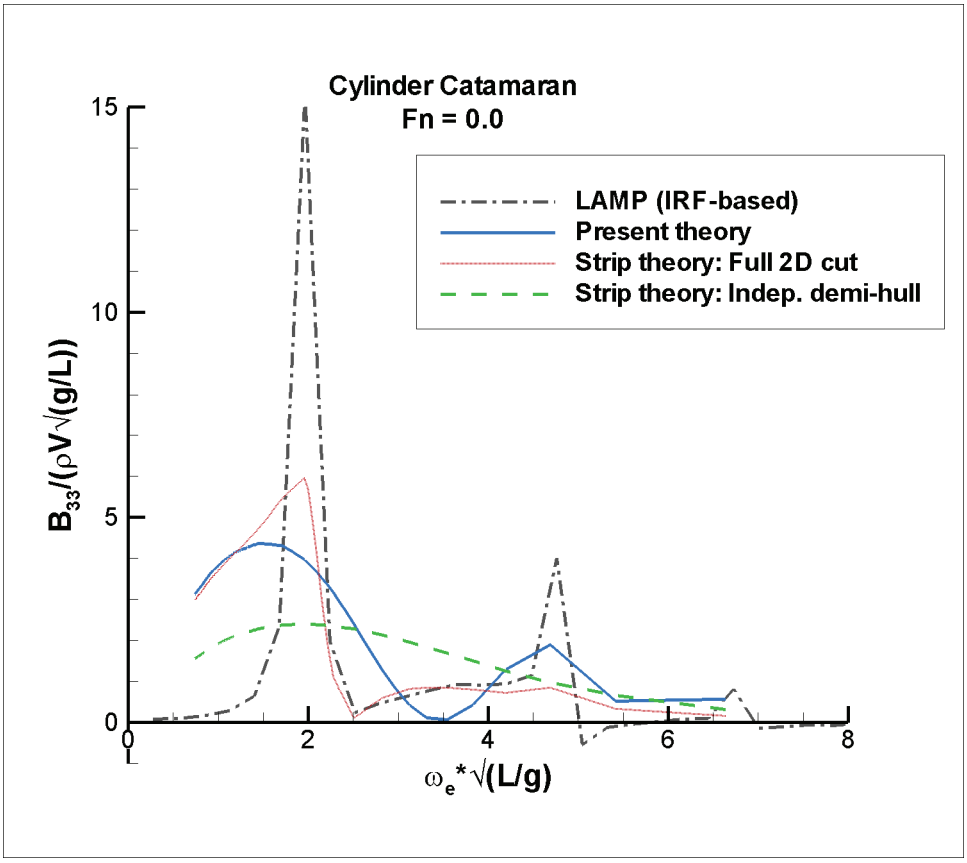

Figure 4.30 B_{33} damping coefficient at Fn=0.0 for Cylinder Catamaran

The other modes of motion are reasonably predicted in the cases with forward speed, with the interaction theory providing a benefit in some conditions. In other conditions, such as shown in Figure 4.31, the interaction theory seems to capture the correct trend in the motion response, but the overall effect appears to be too strong. The complete set of motion transfer function comparisons is given in Appendix A.

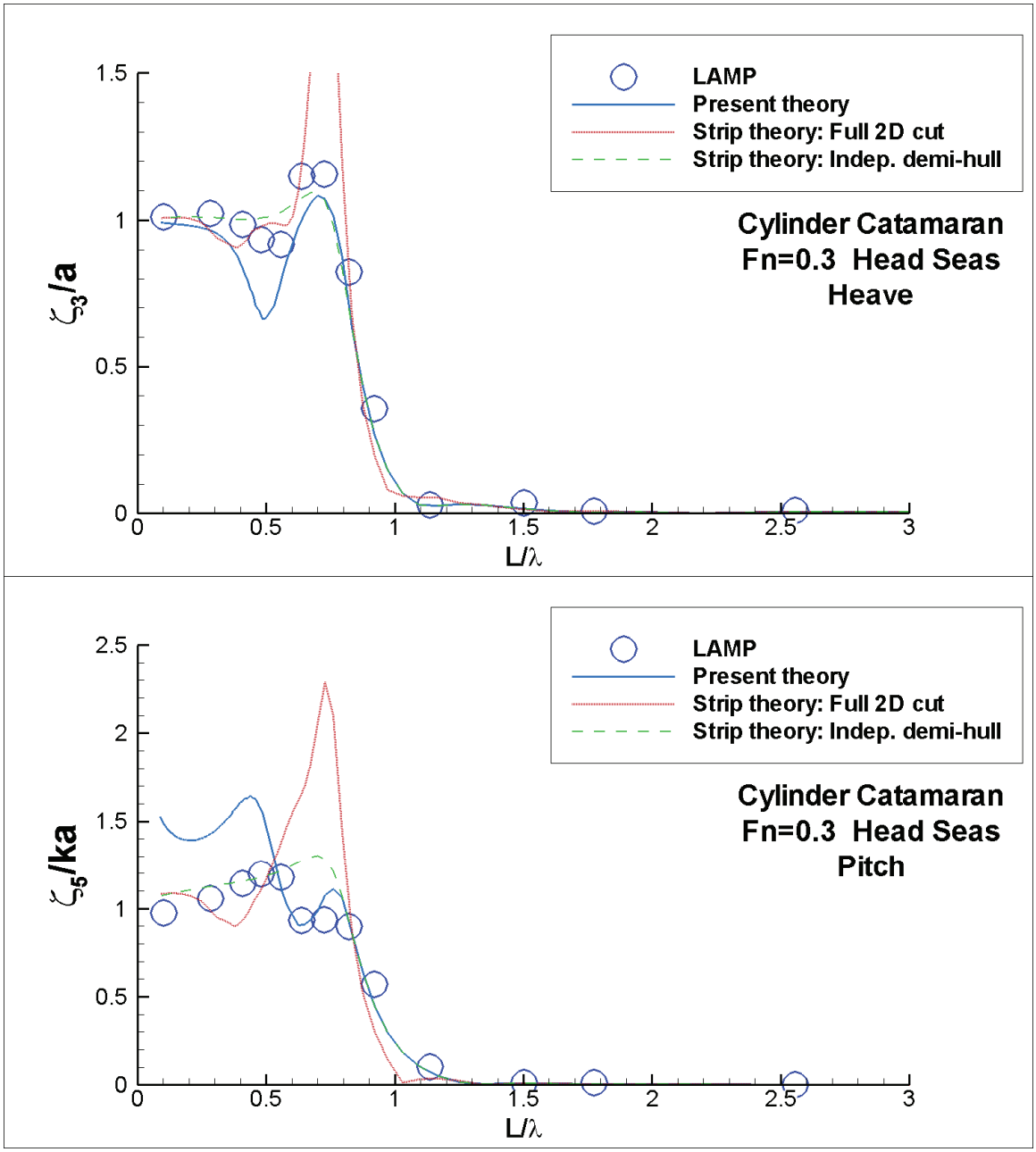

Figure 4.31 Cylinder Catamaran heave and pitch transfer functions at Fn=0.3 in head seas

4.2.2 Delft Catamaran

The Delft Catamaran validation case is a catamaran of conventional design that was model-tested at Delft University of Technology and MARIN (see van't Veer, 1998a,b). The overall test program included forced oscillations in calm water at Fn=0.3, wave excitation measurements for head seas at Fn=0.3, and regular wave motion transfer

functions at speeds of Fn=0.3 to Fn=0.75. The regular wave motion tests were primarily focused on head seas, with the tests conducted at MARIN providing motions for wave headings of β=195° and β=225°. Figure 4.32 and Figure 4.33 show the sections and relative spacing of the Delft Catamaran demi-hulls.

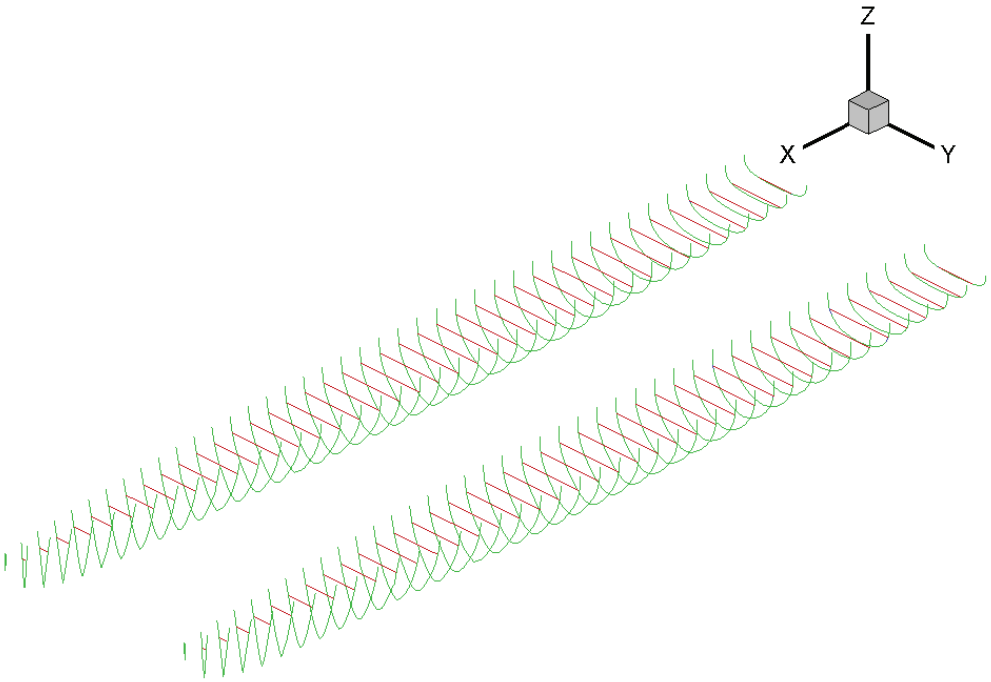

Figure 4.32 Isometric view of Delft Catamaran sections

Figure 4.33 Body plan view of Delft Catamaran sections

4.2.2.1 Added Mass and Damping Coefficients

Added mass and damping coefficients were developed from forced heave and pitch oscillation tests in calm water at a speed of Fn=0.3. The full set of comparisons to the model data are presented in Appendix B. In general, the model data trends were

generally captured well by the present interaction theory, whereas the full-2D-cut strip theory and the independent demi-hull strip theory appear to miss the trends. Two example comparisons are shown in Figure 4.34 and Figure 4.35.

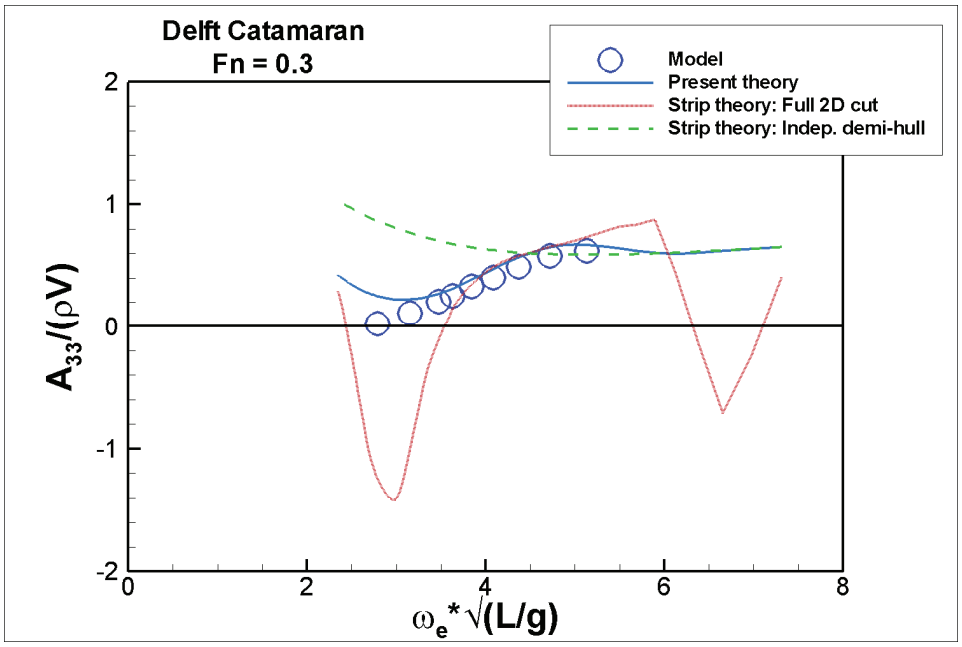

Figure 4.34 Delft Catamaran A_{33} at Fn=0.3

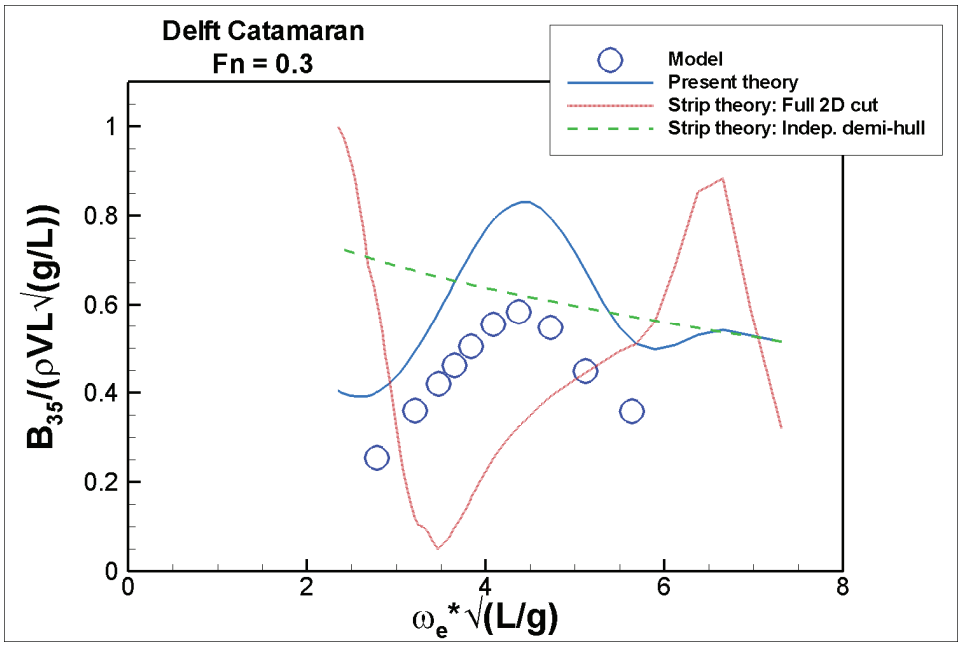

Figure 4.35 Delft Catamaran B_{35} at Fn=0.3

4.2.2.2 Wave Excitation

Ambient wave excitation data was obtained for head waves at Fn=0.3. The present theory does not include interactions, and therefore, excitation force predictions are identical to the independent demi-hull strip theory prediction. Because the radiation potentials are used in the solution of the diffraction force, the full-2D-cut strip theory retains in the excitation force the strong two-dimensional standing wave effects at certain frequencies. From the data presented in Figure 4.36 and Figure 4.37, there is no indication that such an effect is present in head seas. Given the fairly close agreement of model data and predictions using the independent demi-hulls, the assumption of no interaction effects seems reasonable, at least for head seas.

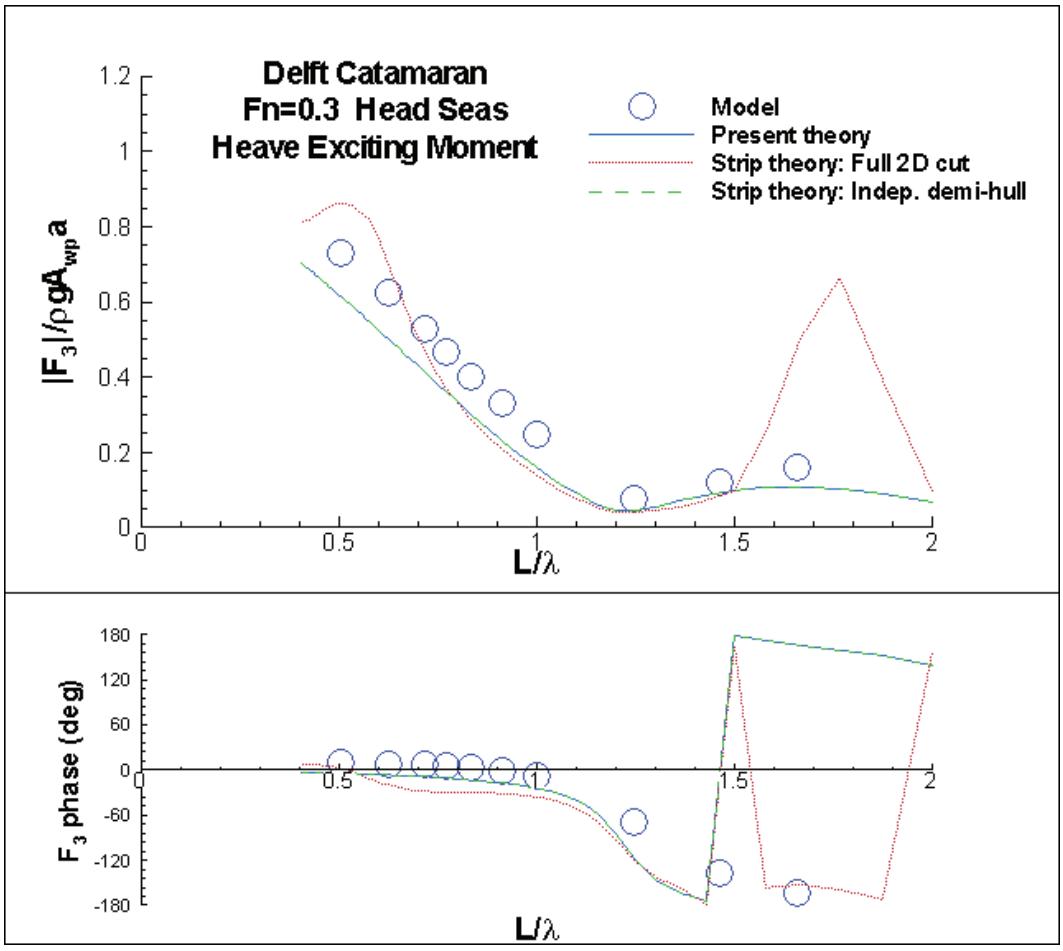

Figure 4.36 Wave excitation heave force for Delft Catamaran at Fn=0.3 in head seas

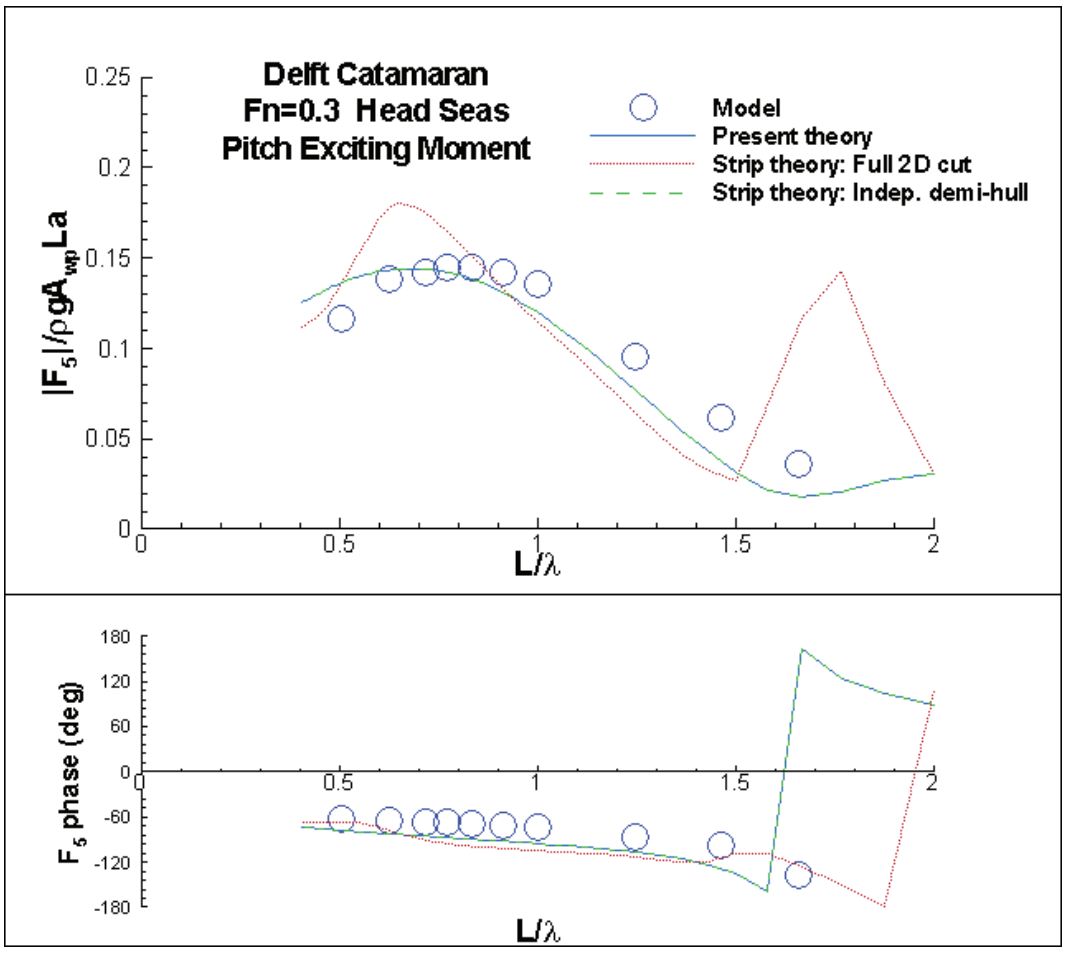

Figure 4.37 Wave excitation pitch moment for Delft Catamaran at Fn=0.3 in head seas

4.2.2.3 Motion Transfer Functions

Motion transfer function comparisons are given in Figure 4.38 through Figure 4.41. Additional oblique sea heading transfer functions are provided in Appendix B. At the lowest Froude number tested, Fn=0.3, the interaction theory performed well in capturing the motion trends in head seas. As forward speed increased beyond the assumed range of applicability for strip theory, results were slightly poorer. At these speeds (in this data set, Fn $\geq$ 0.6), the radiated waves have been swept downstream before they can interact with the opposite demi-hull, so there is no difference between the present theory and the independent demi-hull strip theory.

In oblique wave headings, lateral plane motions are not as well predicted as heave and pitch. In roll, as seen in Figure 4.41, response exists at frequencies higher than for which the model responds. The full-2D-cut strip theory captures this suppression of motion, which may indicate that the diffraction force at oblique headings contains interaction effects for which the full-2D-cut radiation solution provides a good approximation. Measurements of oblique heading wave excitation would be beneficial in understanding this result.

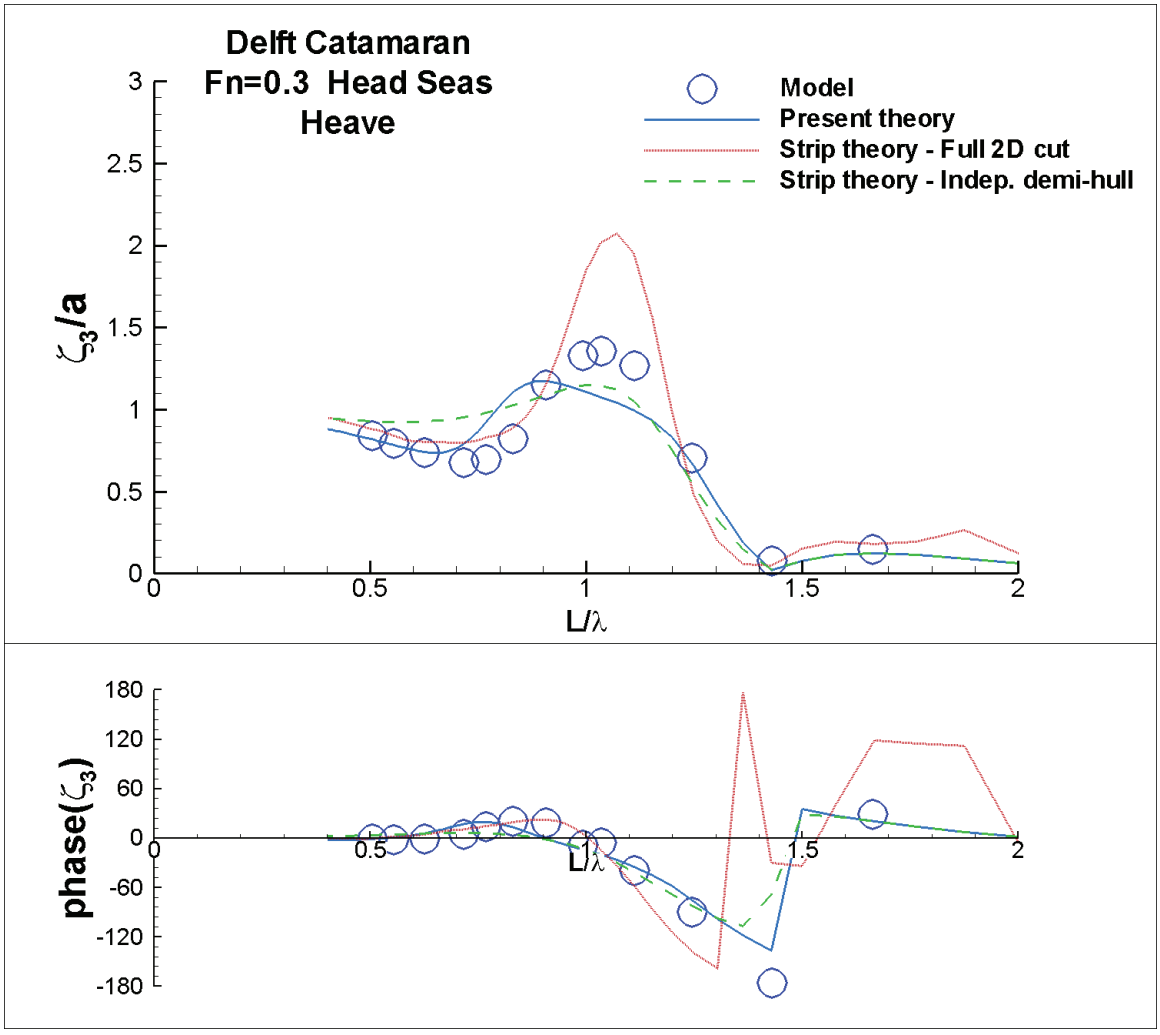

Figure 4.38 Heave transfer function amplitude and phase for Delft Catamaran at Fn=0.3 in head seas

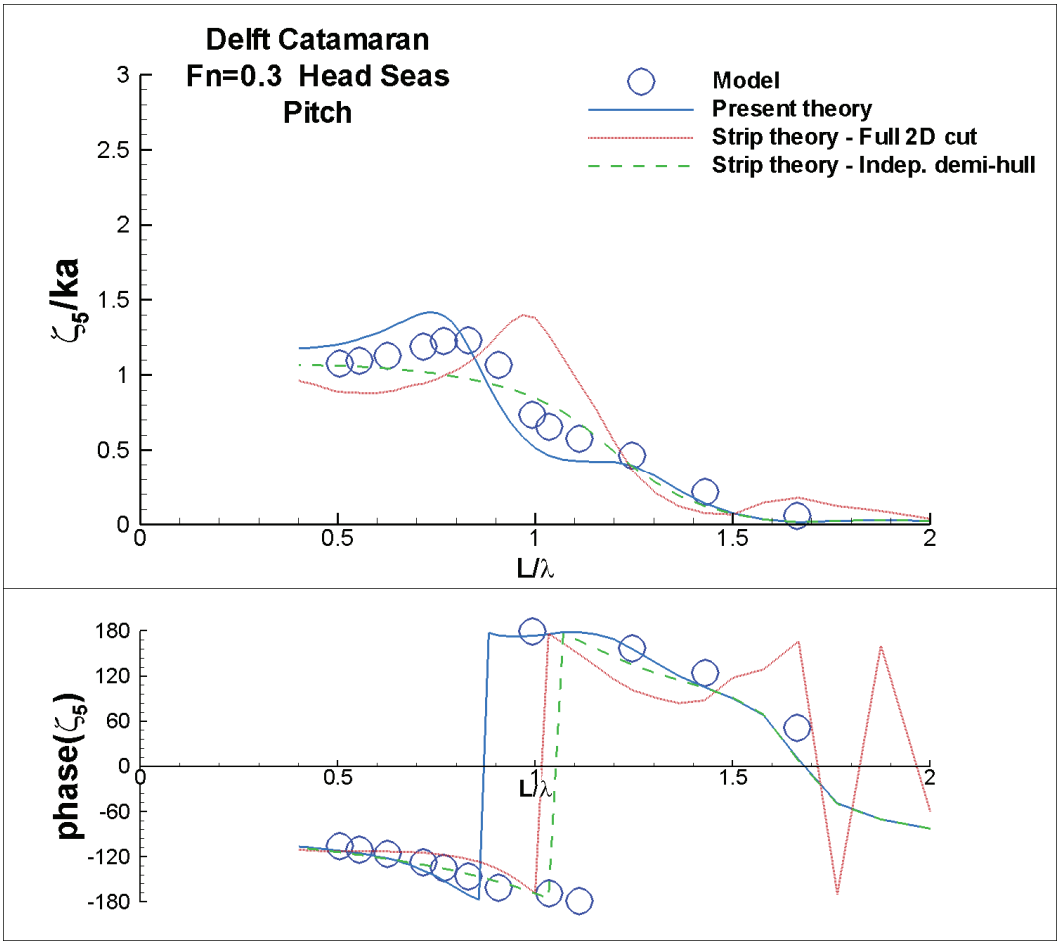

Figure 4.39 Pitch transfer function amplitude and phase for Delft Catamaran at Fn=0.3 in head seas

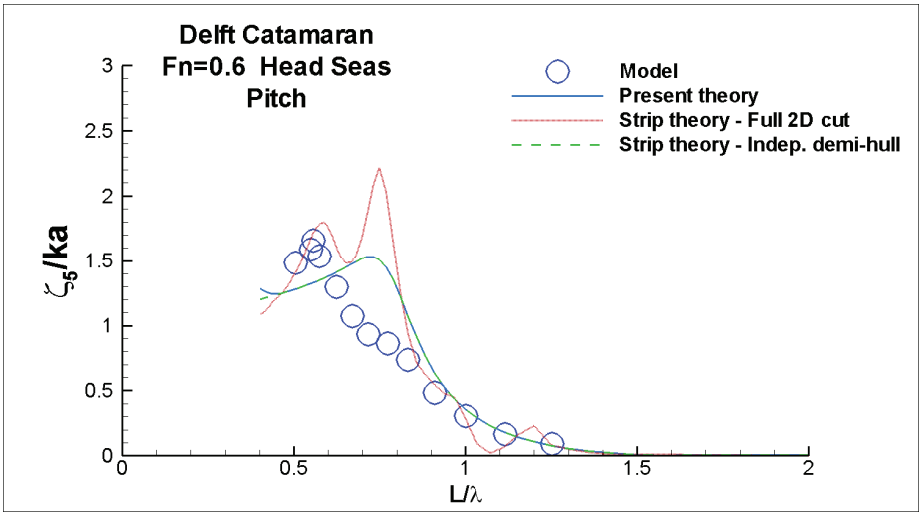

Figure 4.40 Pitch transfer function amplitude for Delft Catamaran at Fn=0.6 in head seas

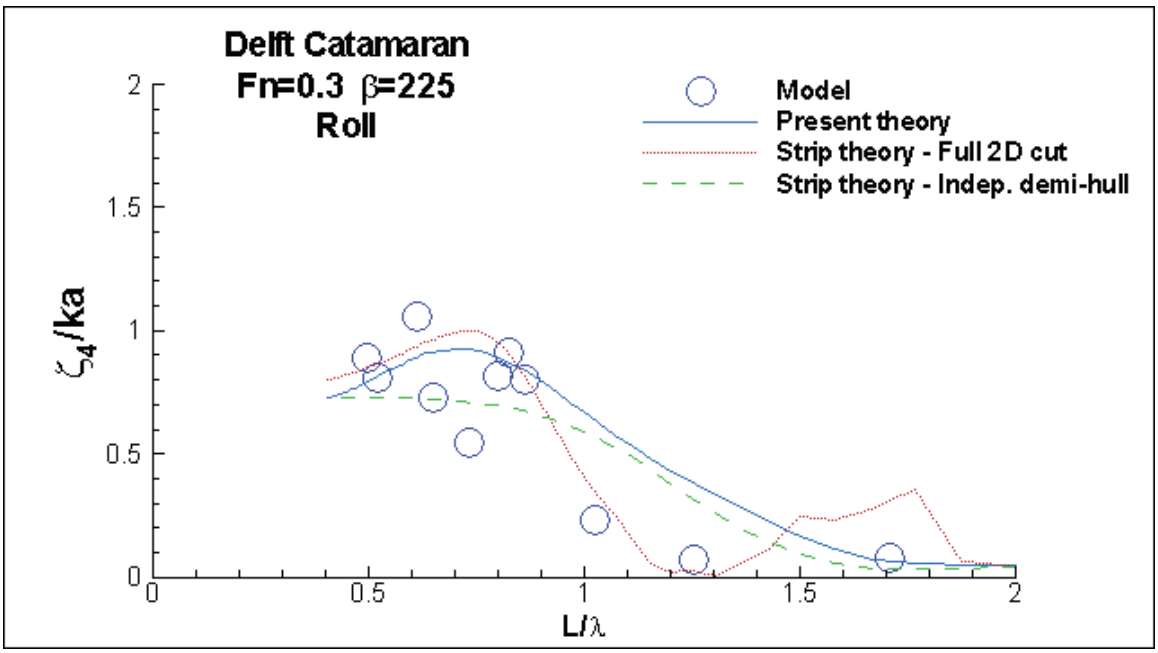

Figure 4.41 Roll transfer function amplitude for Delft Catamaran at Fn=0.3, β=225°

4.2.3 Kashiwagi Lewis-Form Catamaran

Kashiwagi (1993) presents experiments on a 1.5-m Lewis-form catamaran that is fore-aft symmetric. Isometric and body views of the sections are given in Figure 4.42 and Figure 4.43. The sections are generally fuller than a typical multihull design and, with L/B=6, the hulls are not as slender as many demi-hulls. Furthermore, while separation between the transverse centers of buoyancy of the demi-hulls is reasonable (=2*B), the separation distance between the hulls at the waterline is equal to the waterline beam of the demi-hulls. Given the far-field assumptions made in the derivation of the present theory and strip theory in general, this data set would appear to push the limits of applicability.

Model data is available for oscillations in calm water, wave excitation in head seas, and motion transfer functions in head seas. The data are available at two forward speeds: Fn=0.15 and Fn=0.30.

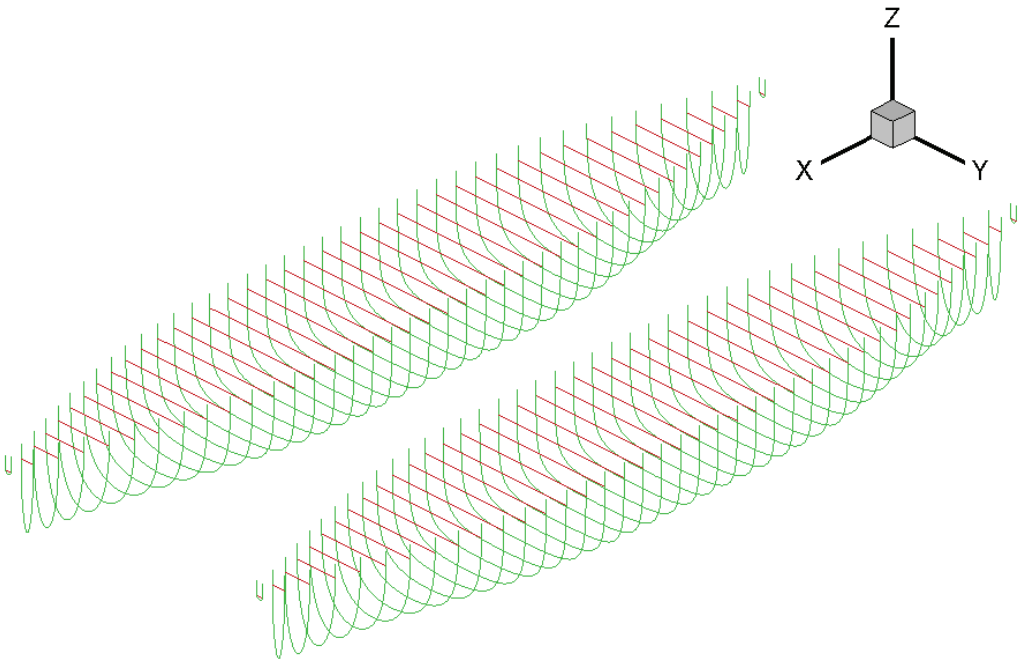

Figure 4.42 Isometric view of Kashiwagi Lewis-Form Catamaran sections

Figure 4.43 Body-plan view of Kashiwagi Lewis-Form Catamaran sections

4.2.3.1 Added Mass and Damping Coefficients

Forced heave and pitch oscillation experiments in calm water provide added mass and damping coefficients for Fn=0.15 and Fn=0.30. In general, predictions failed to properly capture the correct behavior of the coefficients. The full set of comparisons is available in Appendix C. Example comparisons are given in Figure 4.44 through Figure 4.47.

To test the effect of having neglected the wave-free terms due to the opposite demi-hull in the radiation solution of the independent demi-hull, an alternate implementation of the present theory including this influence was produced. Results

were only marginally affected, as shown in Figure 4.48. More likely, three-dimensionality and a need for modeling reflections could be required.

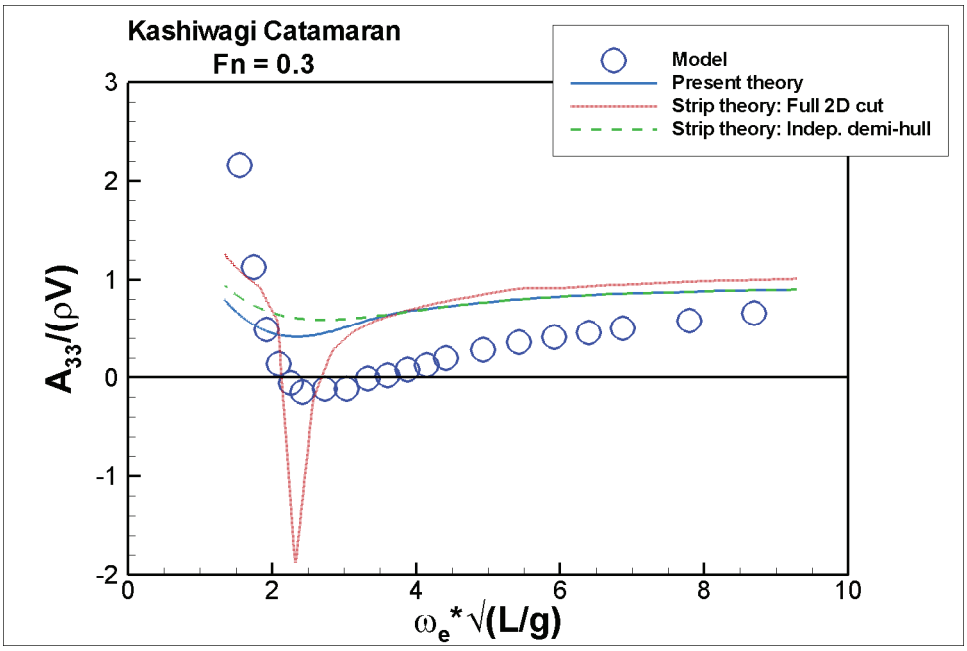

Figure 4.44 Kashiwagi Lewis-Form Catamaran A_{33} at Fn=0.3

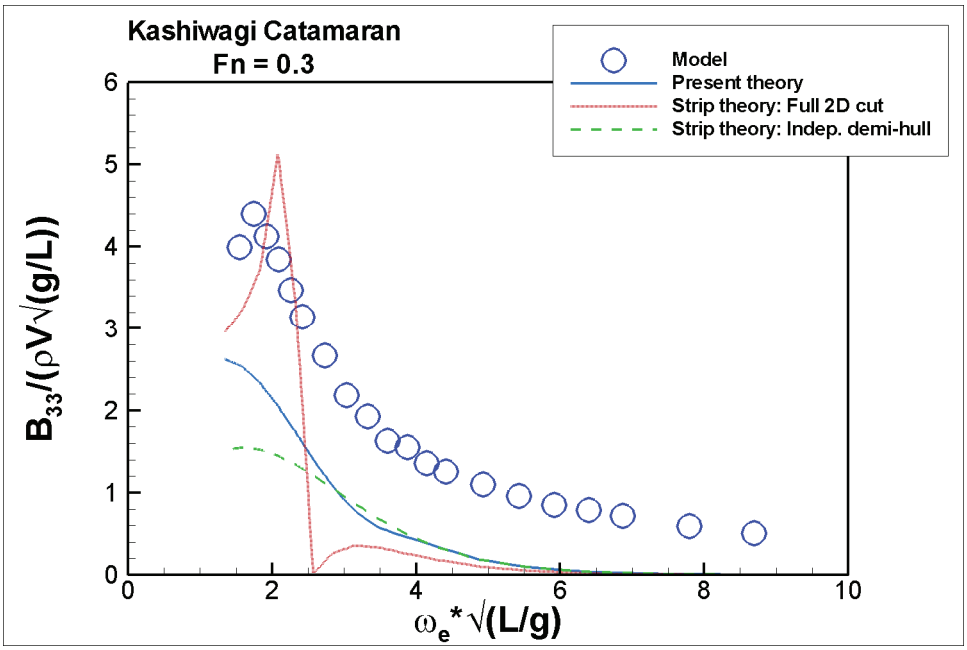

Figure 4.45 Kashiwagi Lewis-Form Catamaran B_{33} at Fn=0.3

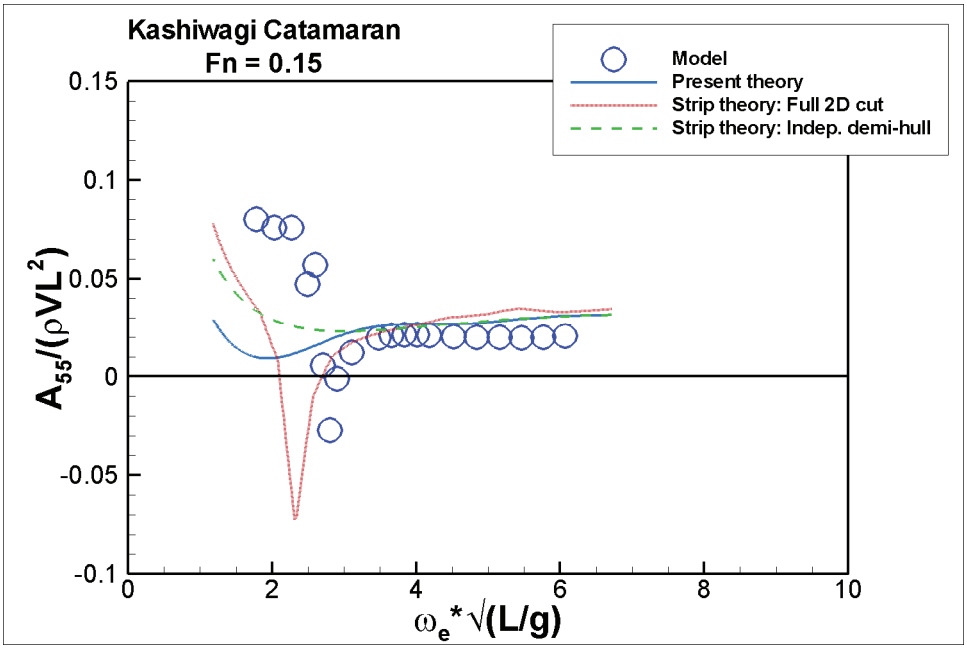

Figure 4.46 Kashiwagi Lewis-Form Catamaran A_{55} at Fn=0.15

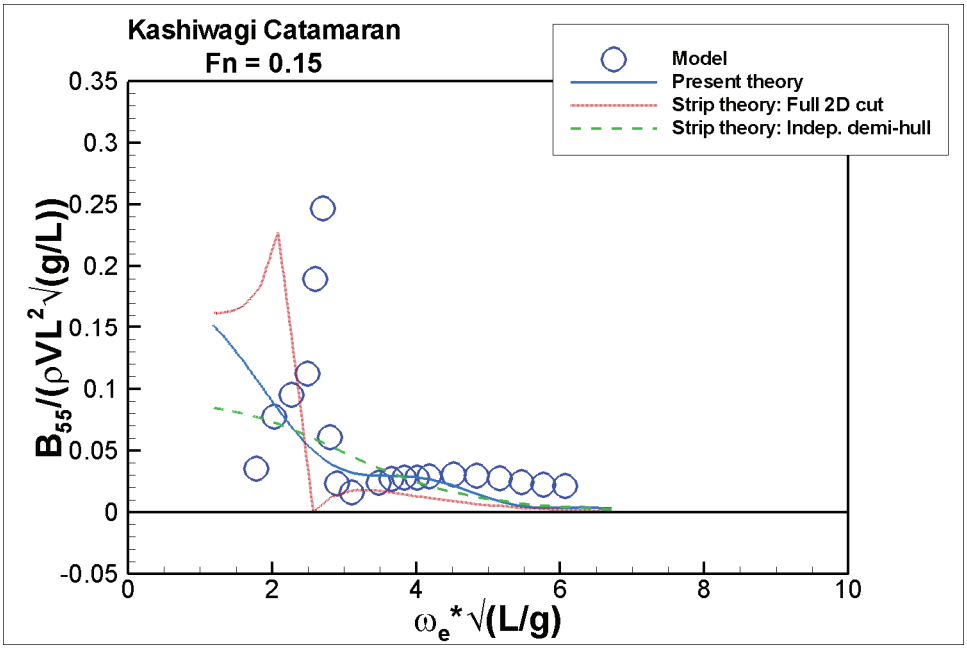

Figure 4.47 Kashiwagi Lewis-Form Catamaran B_{55} at Fn=0.15

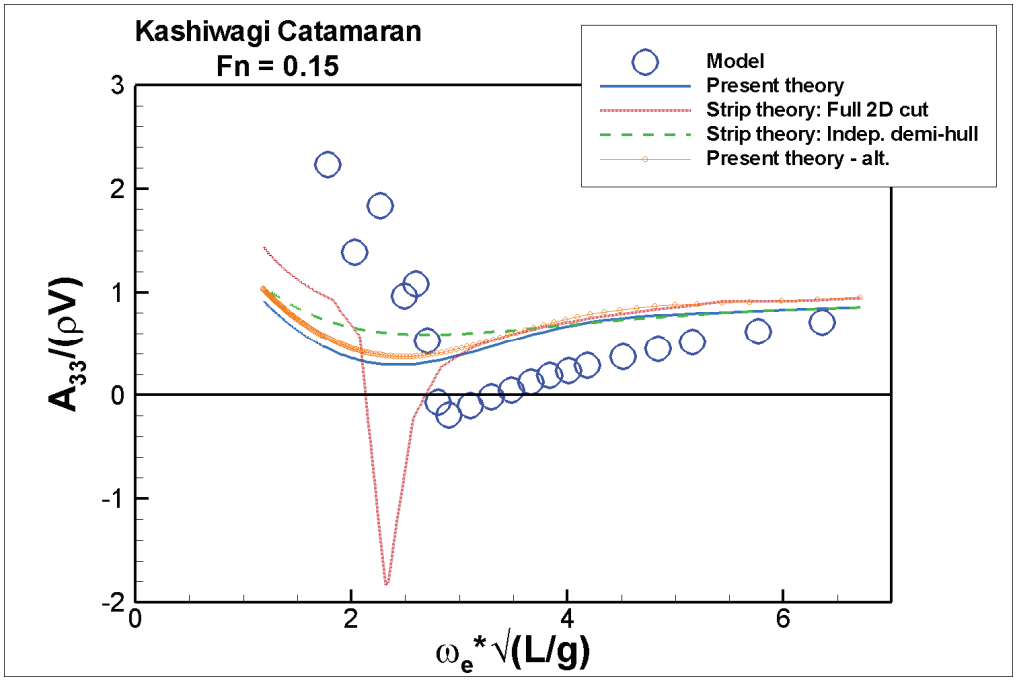

Figure 4.48 Kashiwagi Catamaran A_{33} with alternative independent demi-hull solution

4.2.3.2 Wave Excitation

Wave excitation comparisons for head seas waves at Fn=0.15 and Fn=0.3 are given in Figure 4.49 through Figure 4.52. Differences between model data and predictions are not significant, though the deviation of the full-2D-cut strip theory toward the model data heave force may signify that there is internal wave reflection occurring. Even though the data are for head seas, the three-dimensionality of the hull form could lead to such a phenomenon.

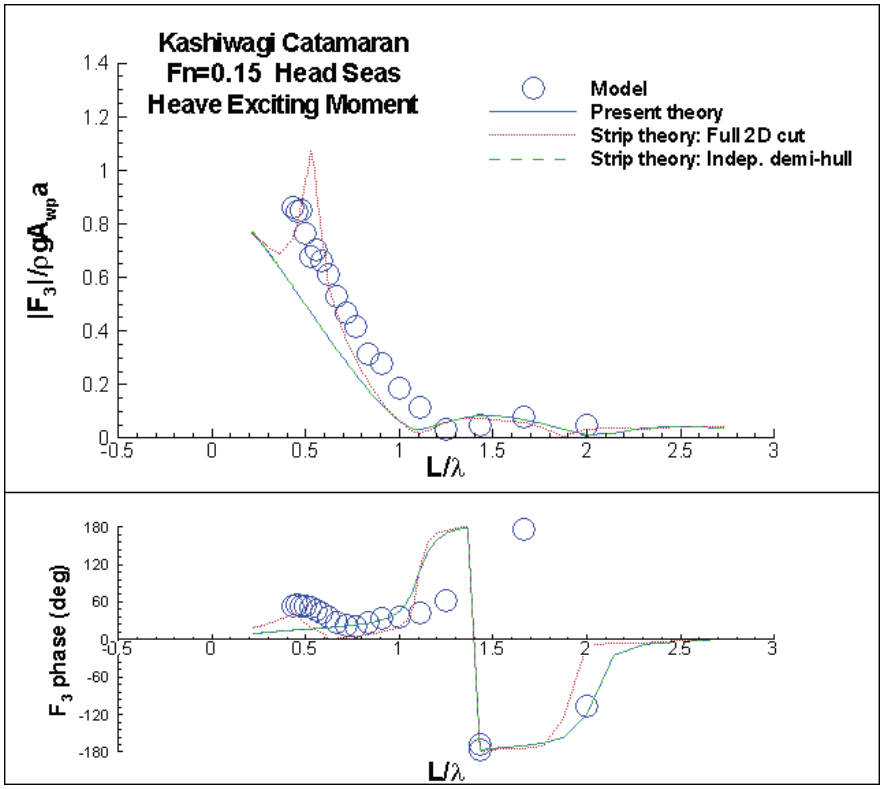

Figure 4.49 Head seas wave excitation heave force for Kashiwagi Cat. at Fn=0.15

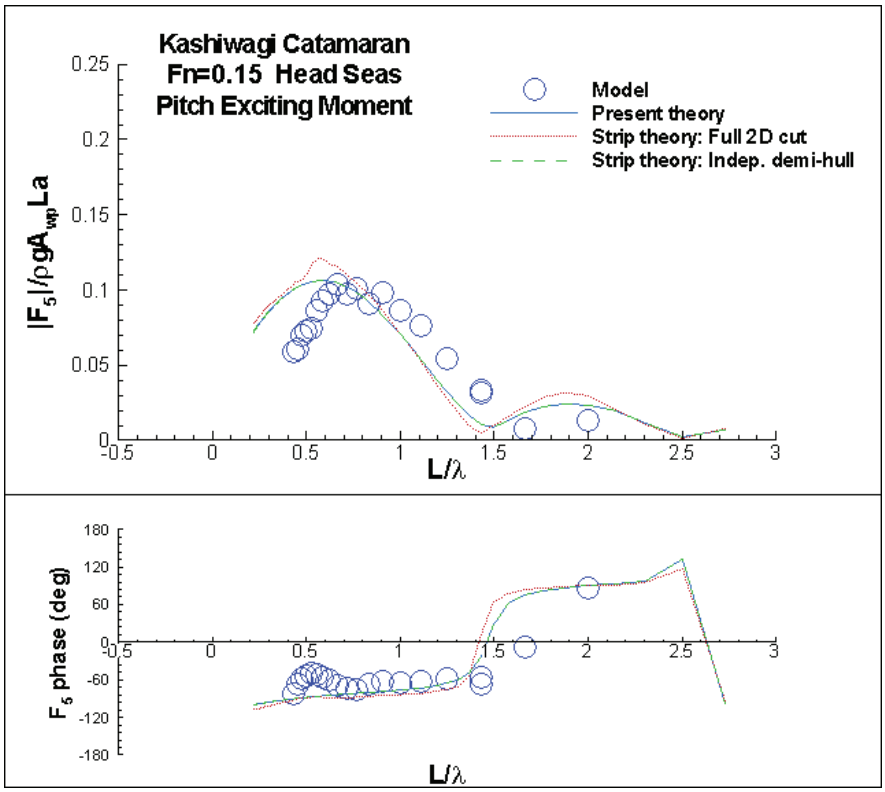

Figure 4.50 Head seas wave excitation pitch moment for Kashiwagi Cat. at Fn=0.15

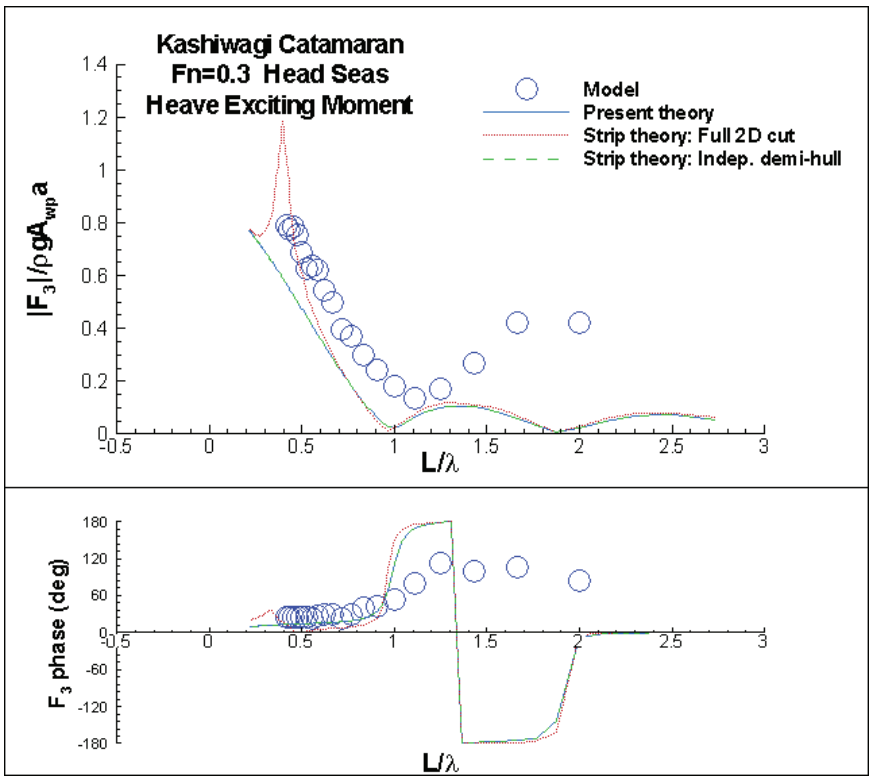

Figure 4.51 Head seas wave excitation heave force for Kashiwagi Cat. at Fn=0.3

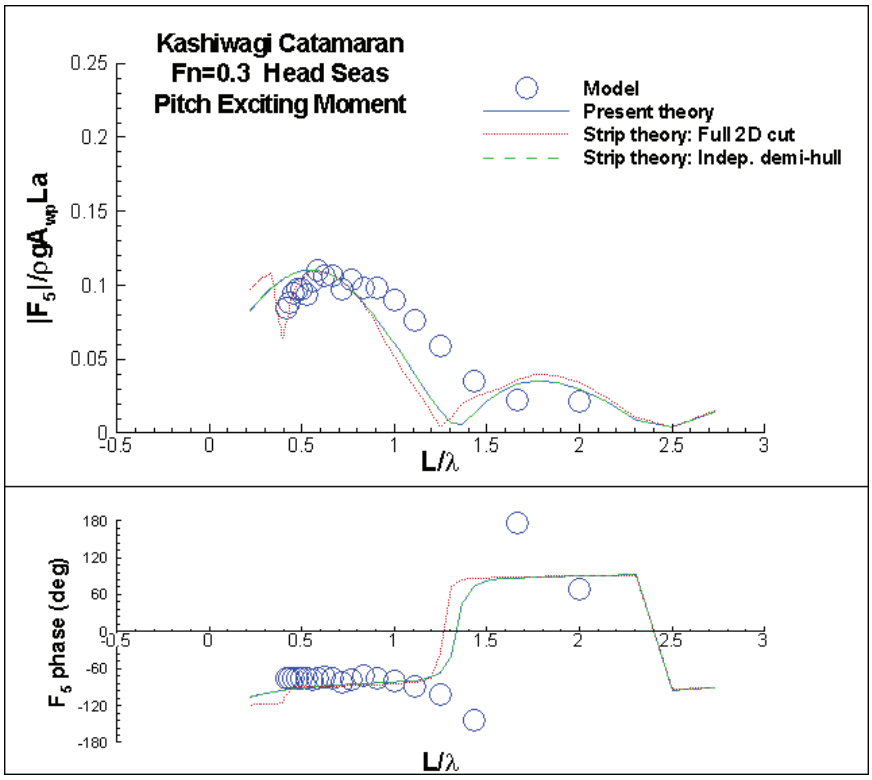

Figure 4.52 Head seas wave excitation pitch moment for Kashiwagi Cat. at Fn=0.3

4.2.3.3 Motion Transfer Functions

Heave and pitch motion transfer functions are compared for head seas runs at Fn=0.15 and 0.3, as shown in Figure 4.53 through Figure 4.56. Given the poor comparisons with the added mass and damping coefficients, it is perhaps surprising that the present theory correlates as well as it does. As in the Cylinder Catamaran test case, the motion trends seem to be well captured, though the interaction effects appear to be too strong in some cases. For example, at Fn=0.3, the suppressed heave peak is properly captured by the present interaction theory, but the pitch motions magnify the trend seen in the pitch model data.

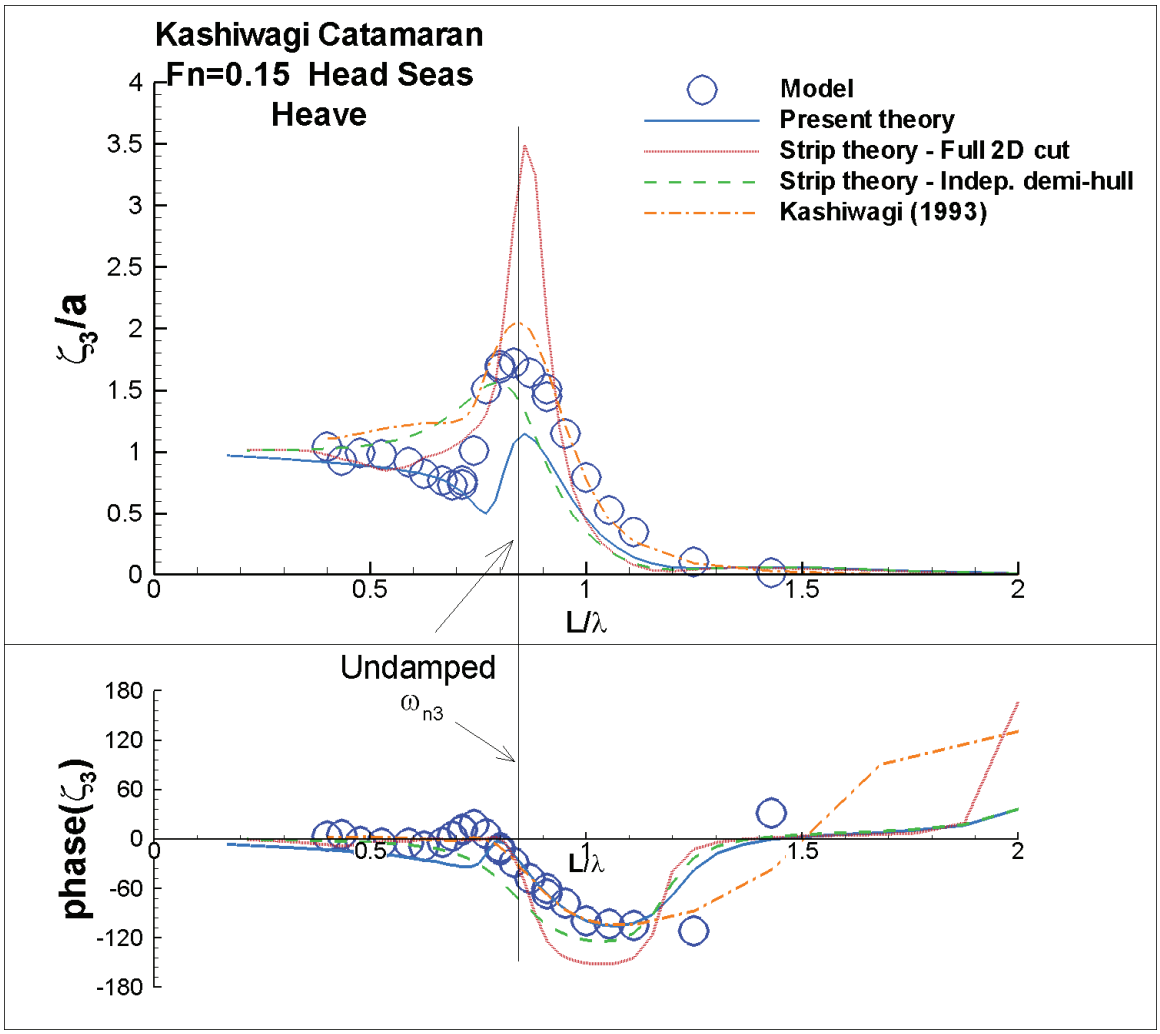

Figure 4.53 Heave transfer function amplitude and phase for Kashiwagi Catamaran at Fn=0.15 in head seas

For additional comparison, the results from Kashiwagi (1993) are included in the figures. The theory employed for Kashiwagi's calculations uses Newman's unified slender-ship theory with a far-field interaction model. In general, the present theory compares favorably to Kashiwagi's calculations, and in some cases matches the data more closely.

To provide insight to the results, the undamped coupled natural frequencies were calculated using the added mass values predicted by the present theory. These are presented in each of the figures. In the case of imaginary eigenvalues, which occurred for the Fn=0.15 results where the total mass (M+A) and inertia (I+A) are negative, the uncoupled natural frequencies are presented as calculated following equation 4.1.

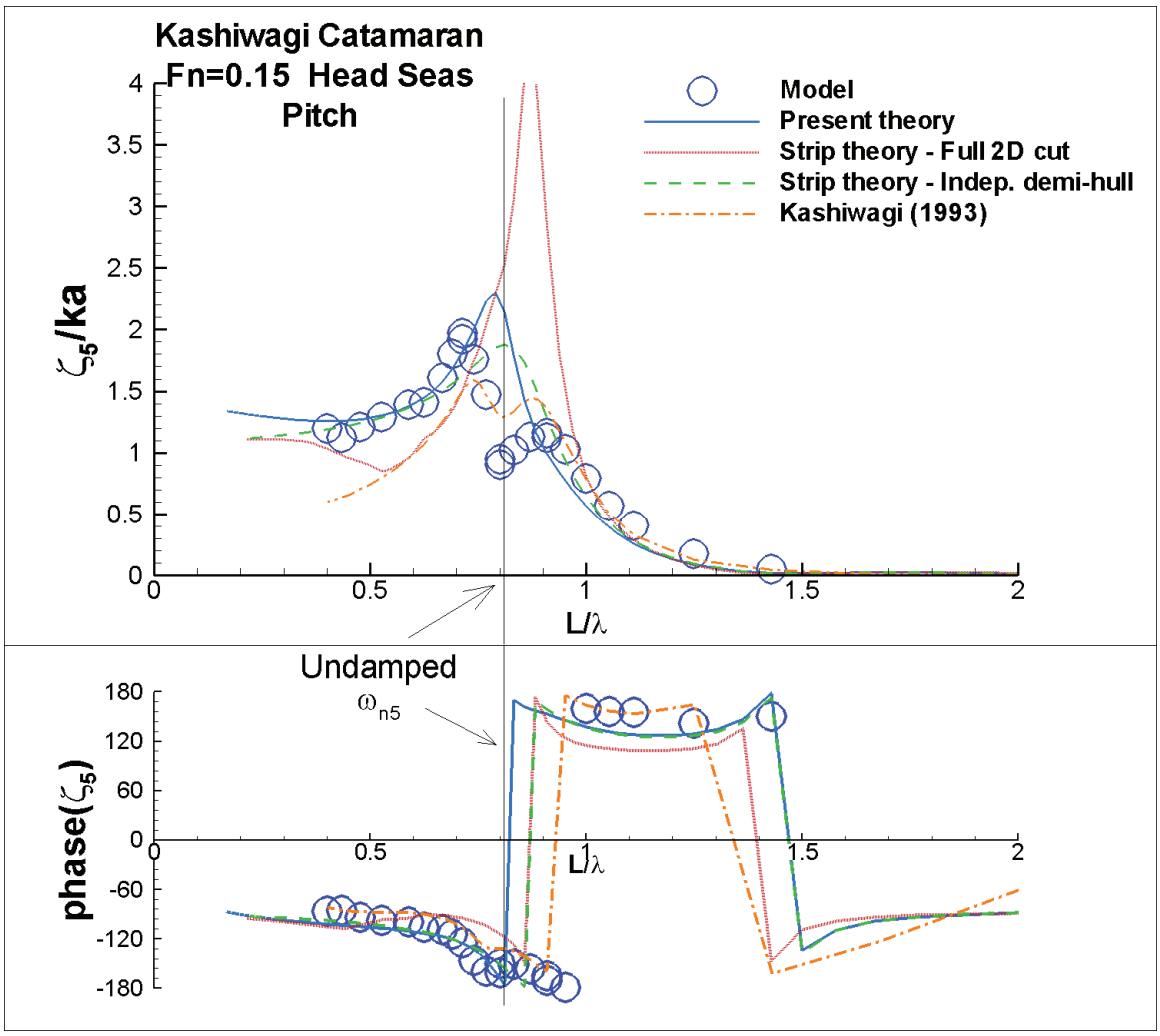

Figure 4.54 Pitch transfer function for Kashiwagi Cat. at Fn=0.15 in head seas

$$\omega_{n,k} = \sqrt{\frac{\left(C_{kk} - A_{kk} \cdot \omega_e^2\right)}{M_{kk}}} \quad \text{, when } (M_{kk} + A_{kk}) < 0 \tag{4.1}$$

As can be seen in the Fn=0.3 pitch transfer function plot in Figure 4.56, the present theory is predicting the pitch natural frequency, with accompanying large response, at a frequency where no other presented theory demonstrates significant pitch response. Interestingly, the model does show a noticeably increased response near this frequency, though not as significant as predicted by the present theory.

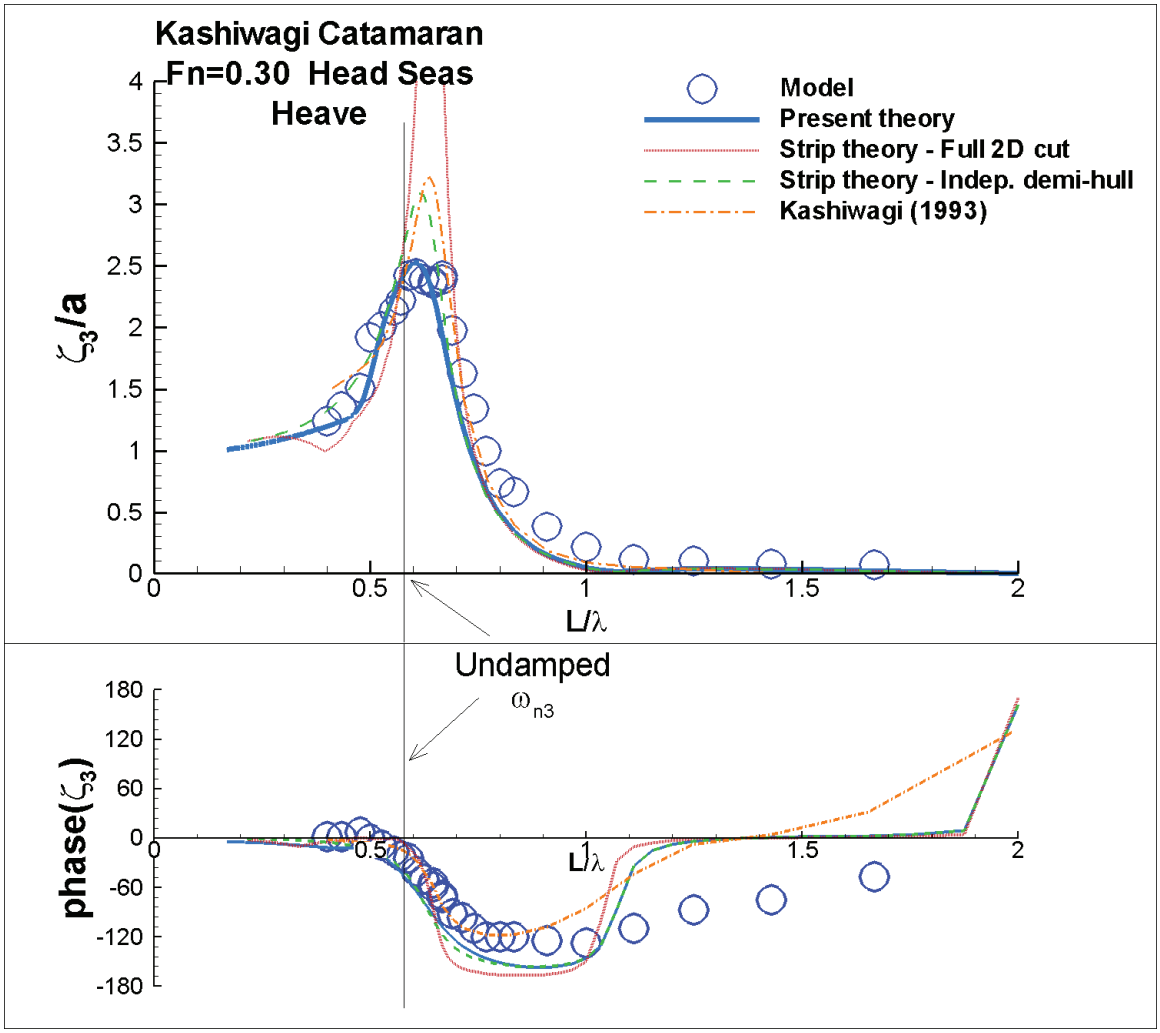

Figure 4.55 Heave transfer function for Kashiwagi Cat. at Fn=0.3 in head seas

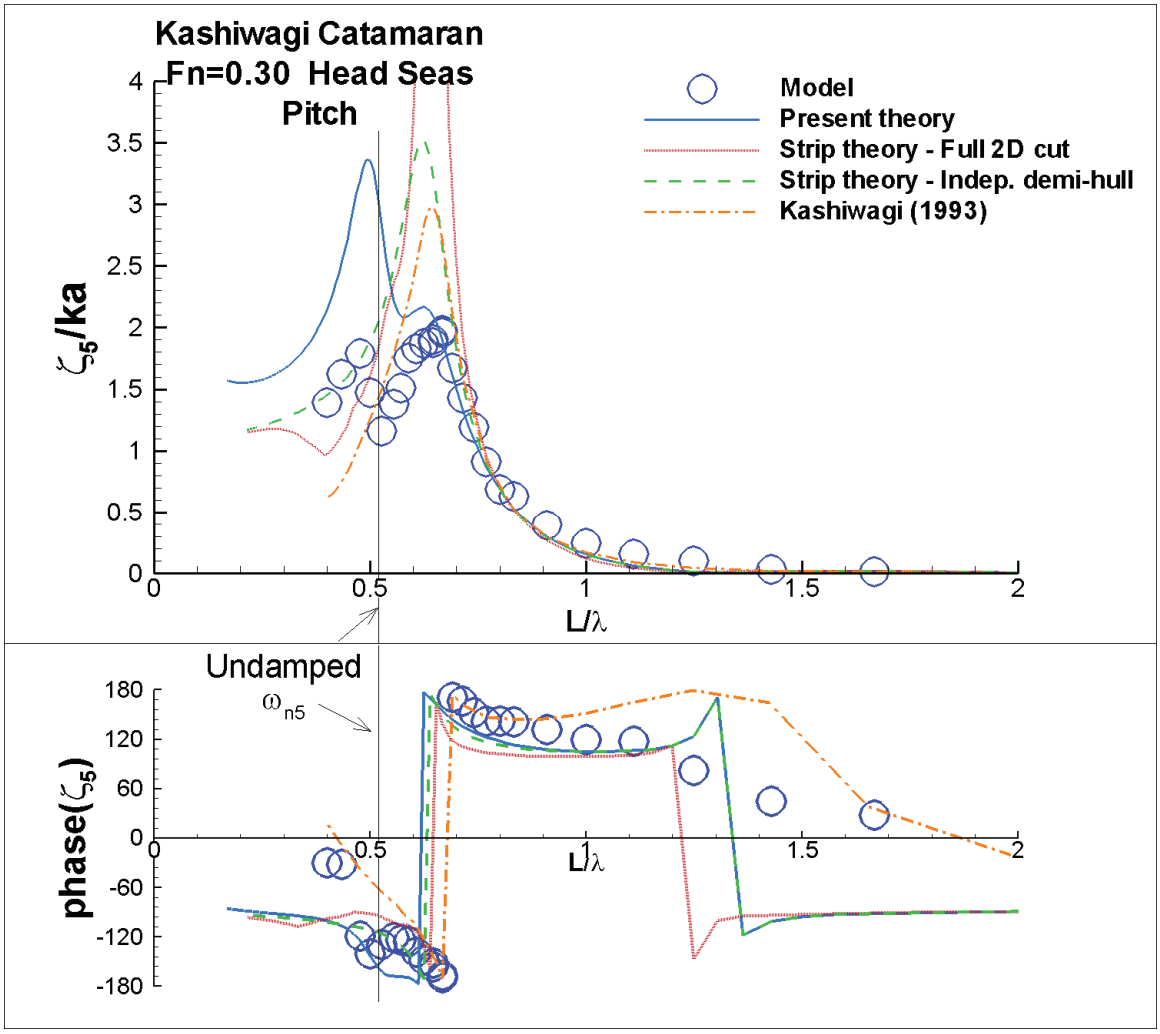

Figure 4.56 Pitch transfer function for Kashiwagi Cat. at Fn=0.3 in head seas

4.2.4 HSSL Trimaran

The HSSL (High Speed Sea-Lift) Trimaran was designed as part of an ONR project investigating novel designs for high-speed transport and the computational tools to support their development. Seakeeping model tests were performed at MARIN on one of the designs, referred to here as the HSSL trimaran. As opposed to many trimaran designs that primarily use the sub-hulls for reserve hydrostatic stability, the sub-hulls on the HSSL trimaran are comparable in length and displacement to the main hull. The design features three demi-hulls of the same length, with the main hull extending considerably forward of the sub-hulls. An isometric view of the HSSL trimaran sections

is given in Figure 4.57. As can be seen from the body plan view in Figure 4.58, the spacing of the hulls is fairly close for the region of main hull and sub-hull overlap.

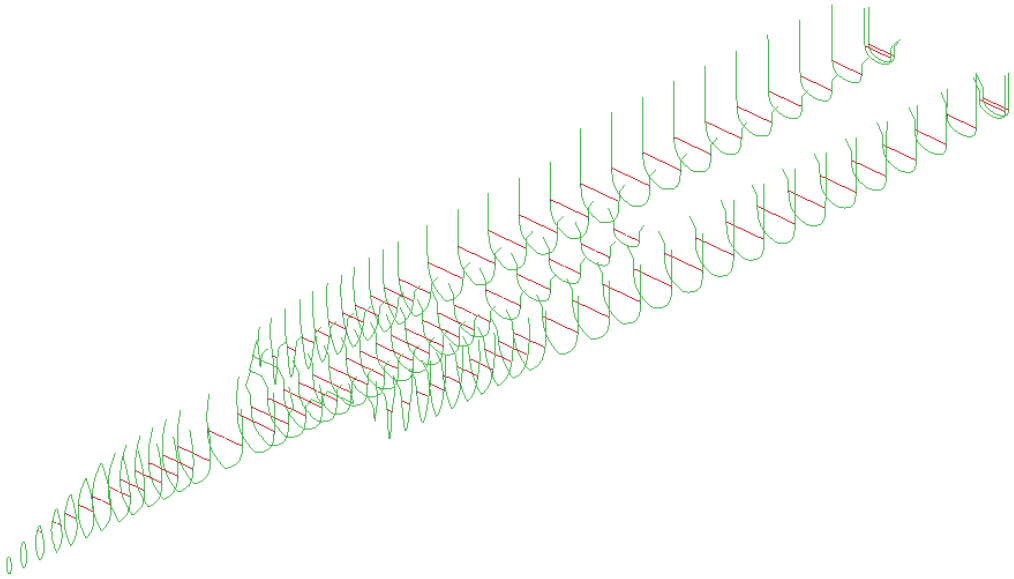

Figure 4.57 Isometric view of HSSL Trimaran sections

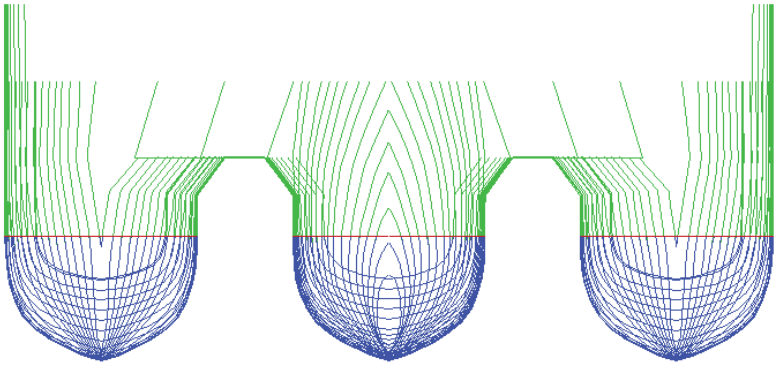

Figure 4.58 Body plan view of HSSL Trimaran sections

Motion transfer functions comparisons are made for Fn=0.44 (based on overall length) at headings of 180°, 150°, and 90°. A full set of comparisons is available in Appendix D. Example comparisons are given in Figure 4.59 through Figure 4.62. As in the case of the Lewis-form catamaran comparisons, the quality of the predictions by the present theory is mixed.

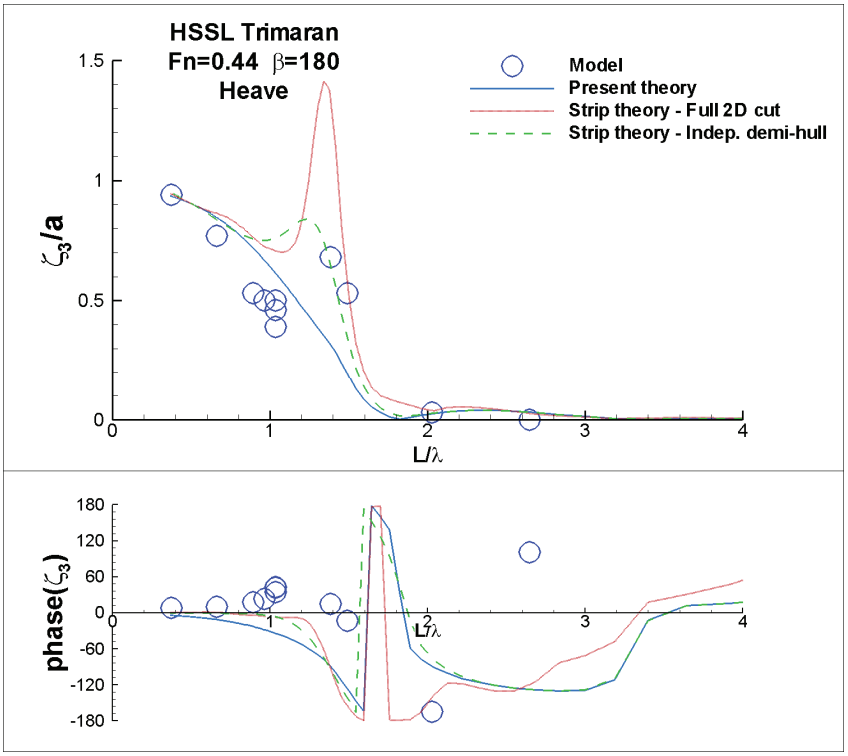

Figure 4.59 Heave transfer function for HSSL Trimaran at Fn=0.44 in head seas

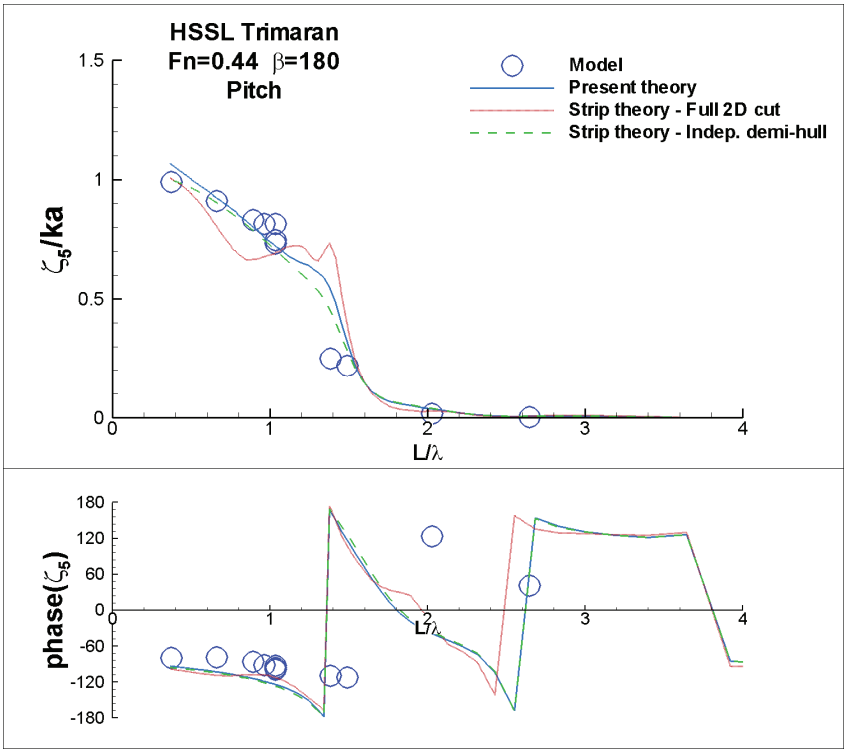

Figure 4.60 Pitch transfer function for HSSL Trimaran at Fn=0.44 in head seas

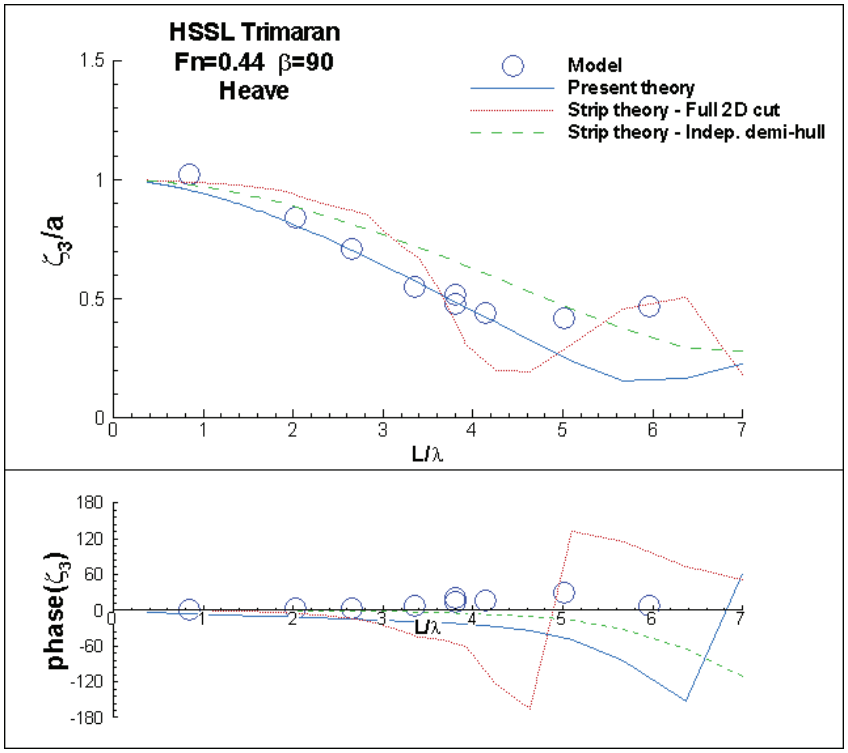

Figure 4.61 Heave transfer function for HSSL Trimaran at Fn=0.44 in beam seas

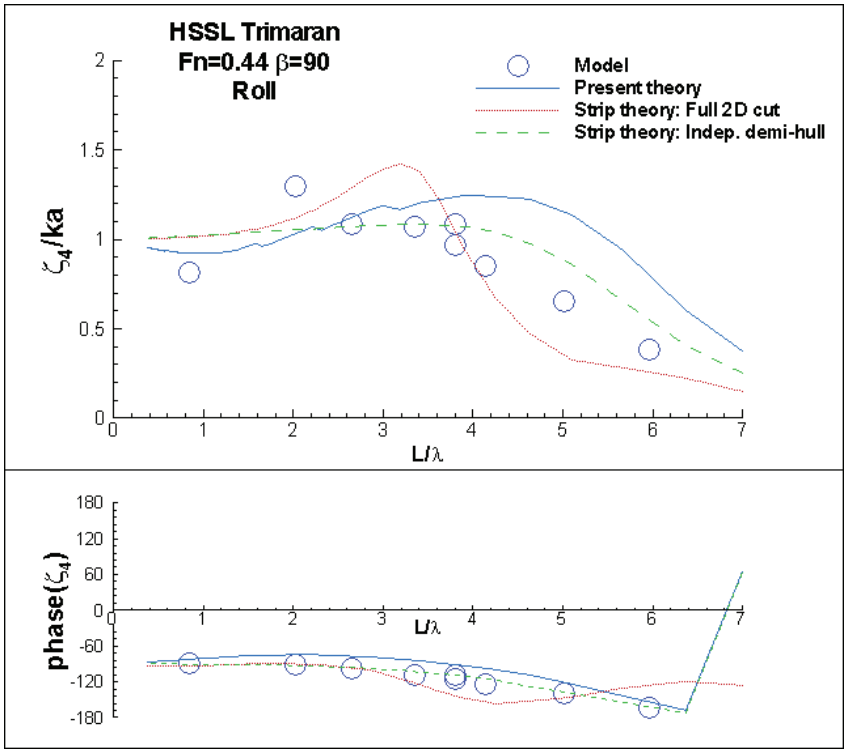

Figure 4.62 Roll transfer function for HSSL Trimaran at Fn=0.44 in beam seas

4.3 Nonlinear Time-Domain Validation

In order to examine the validity of the nonlinear time-domain theory, the LAMP program was used to produce motion time history data using its body-exact hydrostatic and Froude-Krylov force formulation. This version of LAMP is referred to as LAMP-2 and can be considered the 3D panel method equivalent of the blended-method theory implemented in the present code.

The Delft Catamaran was chosen as the test case hull form. A screen capture of a sample large amplitude wave run with this hull is shown in Figure 4.63. The shallow aft sections and proximity of the wet-deck to the free surface allow for rapidly changing wetted area.

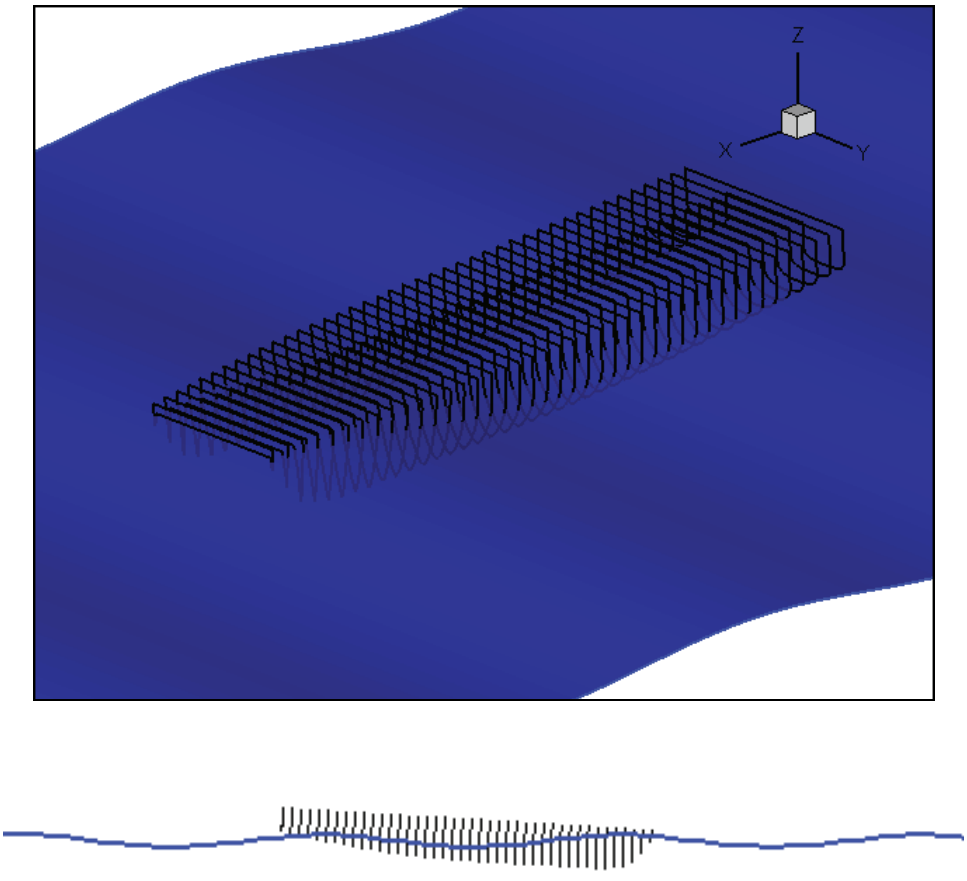

Figure 4.63 Screen captures of Delft Catamaran from time-domain simulation

The validation test cases use a wave condition that was selected based on where interactions are deemed to matter: Fn=0.3, L/λ=0.7, head seas. As seen in Figure 4.38, the heave transfer function is significantly reduced from the independent demi-hull solution.

To demonstrate the introduction of nonlinear forces, the present theory was run in cases of increasing wave amplitude, a. The wave amplitude ranged from 10% of the draft, T, to 100% of the draft. A time history of the heave divided by wave amplitude is given in Figure 4.64, showing a significant change to the heave response. The corresponding plot for pitch is given in Figure 4.65.

The present theory is then compared to the LAMP and the independent demi-hull strip theory predictions for small and large amplitude waves. Figure 4.66 and Figure 4.67 show the heave time histories for small and large amplitude waves, respectively. At small amplitude, both the present theory and LAMP appear to collapse to the linear solution. At large amplitude, the nonlinear forces have driven the heave response to a proportional value larger than the linear solution, an effect that has been captured by LAMP and the present theory alike. In pitch, the effect is similarly captured, as seen in Figure 4.68 and Figure 4.69, though proportional pitch motion decreases with larger amplitude waves. The phase shift in the pitch response predicted by the present theory (see Figure 4.65) is similarly predicted by LAMP.

While the ability to predict similar results with the present theory to results predicted by a much higher fidelity and computationally expensive code, it does not constitute a pure validation of the theory. As such, large amplitude motion model data should be sought for future validation work.

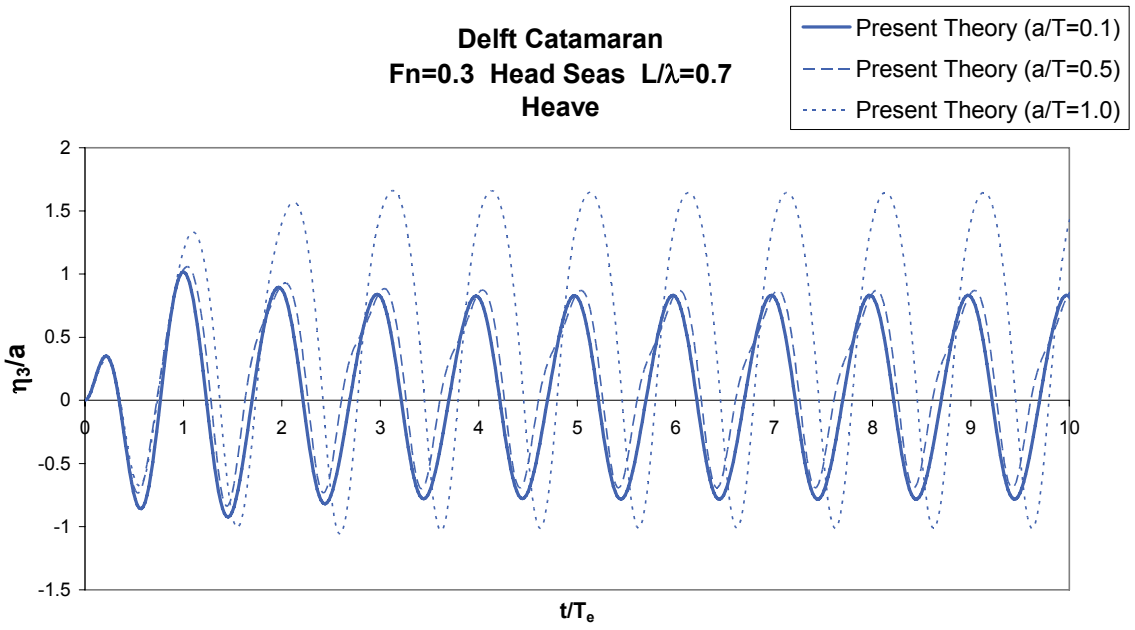

Figure 4.64 Time history of non-dimensional heave for 3 wave amplitudes

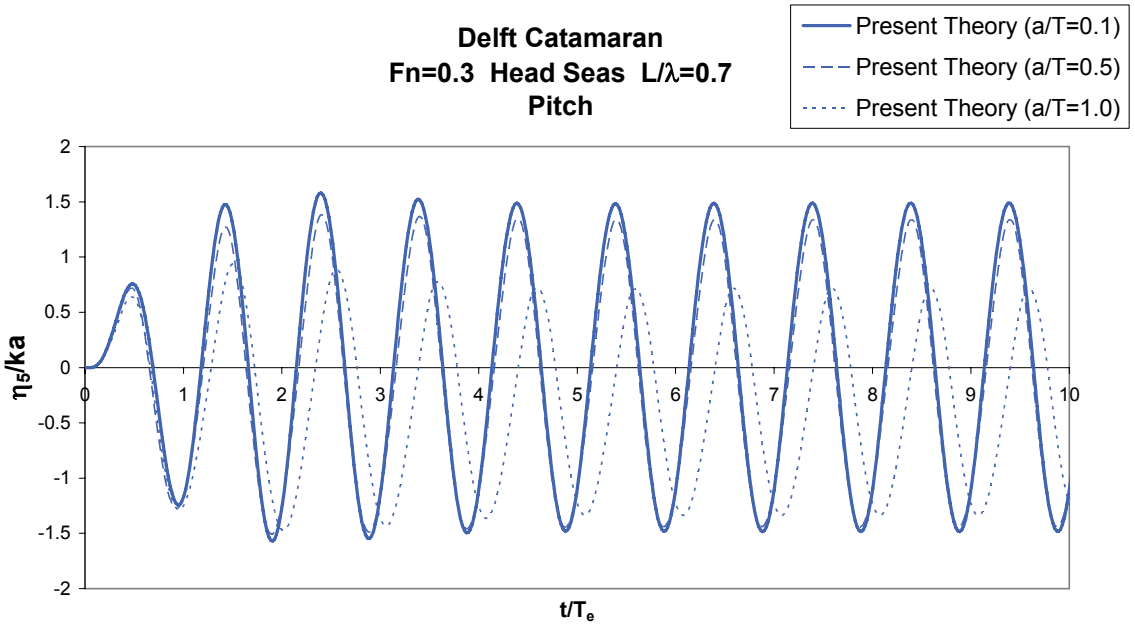

Figure 4.65 Time history of non-dimensional pitch for 3 wave amplitudes

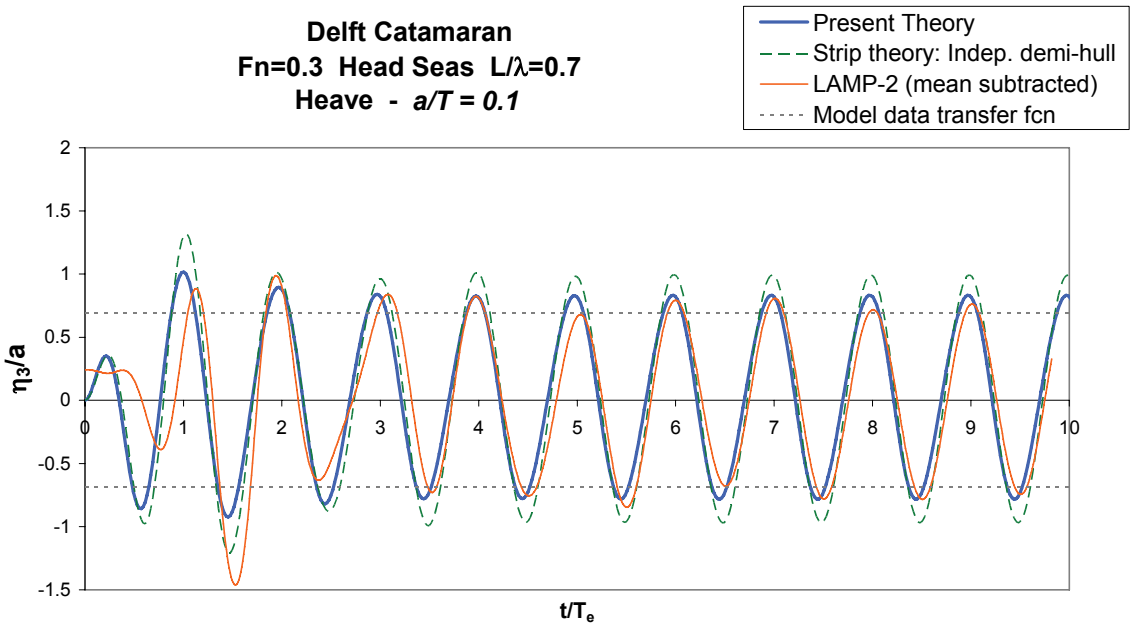

Figure 4.66 Time histories of non-dimensional heave at small wave amplitude

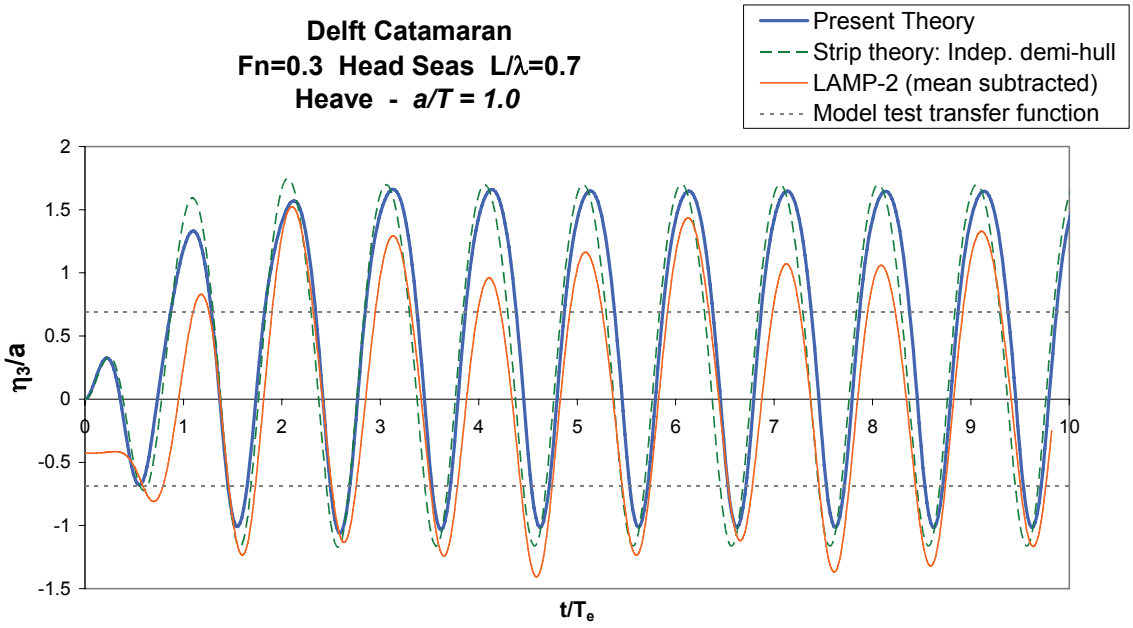

Figure 4.67 Time histories of non-dimensional heave at large wave amplitude

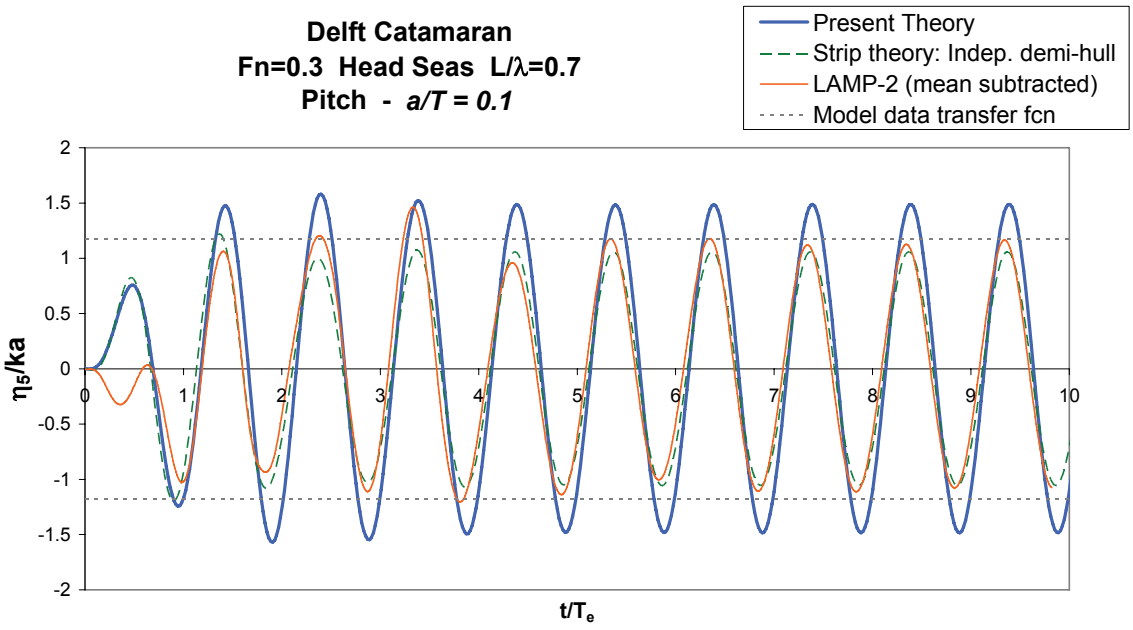

Figure 4.68 Time histories of non-dimensional pitch at small wave amplitude

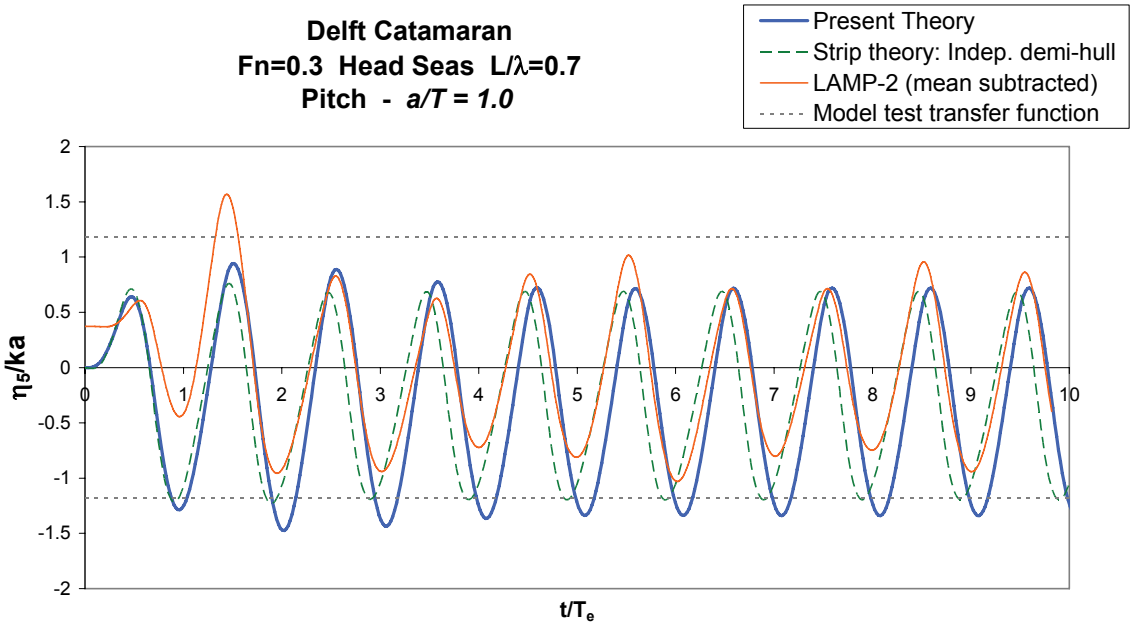

Figure 4.69 Time histories of non-dimensional pitch at large wave amplitude

4.4 Computational Speed

One of the primary aims of the present theory was to develop a theory that would be extremely computationally efficient. Therefore, assessment of the present theory's computation speed should be considered a part of the theory's validation.

The aspect of the present theory that provides an advantage in computational effort over other theories is that the hydrodynamic forces can be developed solely from 2D potentials that are independent of ship speed and relative wave heading. That is, the 2D independent demi-hull radiation potentials at a given frequency of encounter are used in the determination of 3D total radiation (including interaction forces) and diffraction forces. The 2D radiation potentials on each section can be computed and stored for a set of "basis" encounter frequencies that cover an appropriate range with an appropriate resolution. For a "run" in the frequency domain at a particular ship speed, relative wave heading, and wave frequency, the radiation potentials on each 2D panel at the resulting encounter frequency can be interpolated from the stored potentials at the basis frequencies. This avoids significant computational expense if the number of frequency-domain runs exceeds the number of basis frequencies. Given that experience has shown 25 basis frequencies to be adequate, providing seakeeping predictions at multiple ship speeds and wave headings will almost certainly benefit from this approach.

One measure of validation of the present theory's computational efficiency is to compare the expense to calculate a single frequency domain run to ordinary strip theory. As a test case, the Delft Catamaran geometry was used, consisting of 41 sections and 20-24 2D panels per demi-hull section. Running on a laptop with a 1.2GHz Intel Core™2 Duo processor (using a single core), the independent demi-hull basis radiation potentials are computed in approximately 3 seconds and the frequency domain "runs" require:

- ~0.003s per speed-heading-frequency for regular strip theory
- ~0.005s per speed-heading-frequency for present theory

This time comparison is made for the Fn=0.0 condition, where every section will have an interaction force in the present theory. With increasing forward speed, the present theory's computation time will reduce due to the reduced number of interacting sections. The difference in memory requirements between regular strip theory and the present

theory is very small, with both methods using approximately 14MB of memory in the NSHIPMO_multihull program.

For additional comparison, a 3D forward speed panel code requires anywhere from 1-30 minutes per frequency-domain run. Also, while generally not applicable for Froude numbers less than 0.4, the 2½-D strip theory with multihull interactions as described by Hermundstad et al. (1999) runs at about 10-20 seconds per frequency-domain run. From this perspective, the increase in computational cost for the present theory over regular strip theory is negligible.

For the nonlinear time-domain (blended method) calculations, the computation time of the present theory is compared to the LAMP-2 calculations presented in Figure 4.66 through Figure 4.69. Making a direct comparison of the present theory to a 3D time-domain panel code is not necessarily an objective measurement, because, for the 3D panel code, the panel density on the ship body and free surface can be optimized for computational stability and accuracy. For the comparisons made here, the panel density and domain extent followed past experience with LAMP, and, therefore, may not have been fully optimized. Nevertheless, a comparison of computation times demonstrates a rough order of magnitude measure of relative computational efficiency. For the Delft Catamaran time-domain runs presented in the figures cited above, the present theory required about 3 seconds of "start-up" time to calculate the frequency-domain hydrodynamic coefficients and 0.017 seconds per time step. In comparison, the LAMP-2 run required about 2 minutes of "start-up" time to solve for the source strengths on each panel and 0.66 seconds per time step during the simulation.

Chapter 5

Conclusion

5.1 Overview

A computationally efficient theory has been developed to quickly characterize the motions of a multihull with hull interactions, both in the frequency-domain and the time-domain. The nonlinear time-domain capability provides an accessible simulation capability that captures the significant nonlinearities due to body-exact Froude-Krylov and hydrostatic forces, while including a higher fidelity radiation force.

The developed interaction theory is not universally valid, though it appears to capture the correct trends in many cases. Of the validation cases tested, the hull form with the most slender proportions and one of the largest demi-hull separations showed the best correlation. Other validation cases that pushed the limits of the theory's assumptions with respect to slenderness, far-field separation, and other 3D effects tended to have poorer correlation. While it is clear that a multihull at zero to moderately high speed must contend with hull interactions, attempting to capture the interaction forces in the predictions can lead to large errors in motions if the developed forces are too strong. In many cases, the independent demi-hull strip theory performed the best among the strip theory approaches, because it was approximately correct.

5.2 Physical Insights

The extensive comparisons to model data and the work involved in developing the present theory and code have led to some physical insights to the multihull seakeeping problem.

Capturing the "sweep-down" effect of the radiated waves is essential. At high speeds, if the full-2D-cut strip theory were to be used, the motion responses are over-predicted. The Cylinder Catamaran validation case has provided data to support the argument that the radiation problem converges to the independent demi-hull solution as forward speed increases.

The radiated wave "sweep down" mechanism means that multihull interactions are sensitive in pitch with forward speed. Pitch motion creates the largest waves at bow (and stern, but those are swept away from hull), which can hit the stern of the ship, where the moment arm is greatest.

At zero-speed, using the traditional strip theory with a full 2D cut may be the best option. In this case, the waves are not swept downstream and can get trapped between the hulls. The validation cases seem to support such a modeling decision. This leads to the hypothesis that the inclusion of reflections in the present theory may improve results. Future developments in this area would need to address the difficulty of solving for the diffraction potential.

The nonlinear time-domain validation case showed that capturing hull interactions in the linear radiation solution is important. That is, the magnitude difference between the present theory and the independent demi-hull strip theory was not diminished at large amplitude motion. While the nonlinear change to the hydrostatic and Froude-Krylov force can be significant, it may not be enough to over-power any difference in the radiation forces.

5.3 Future Efforts

There are several possible future improvements to the frequency-domain solution. If available through an alternate analysis, the steady potential could be utilized to enable a more exact "mean wetted surface" to be used in the calculations, as well as to adjust the hulls for sinkage and trim. It would also facilitate the implementation of a 2 ½-D method for high-speed predictions.

Another possible improvement to the theory is the inclusion of interaction effects in the wave excitation forces. At oblique headings, this may prove to be necessary. If a

reflection capability were developed for the radiation problem, it could be applied in the diffraction interaction problem as well.

In the time-domain solution, nonlinear radiation forces could be implemented in the simplified manner outlined in 3.3.1. Extending the proposed method to include memory effects would be very difficult, due to the changing dependence of the source radiating section on frequency of encounter.

Appendices

Appendix A

Cylinder Catamaran Validation Figures

Appendix A contains the full set of hydrodynamic coefficient and motion transfer function comparisons for the Cylinder Catamaran. The added mass and damping plots are given in Figure A 1 through Figure A 12. The motion transfer functions are shown in Figure A 13 through Figure A 20.

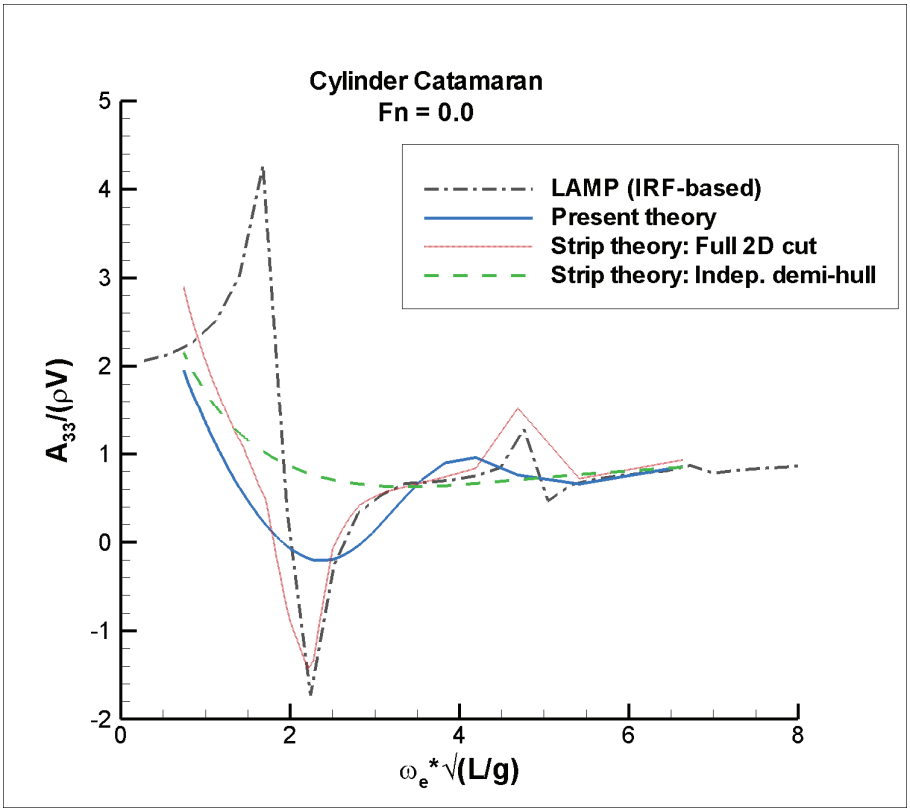

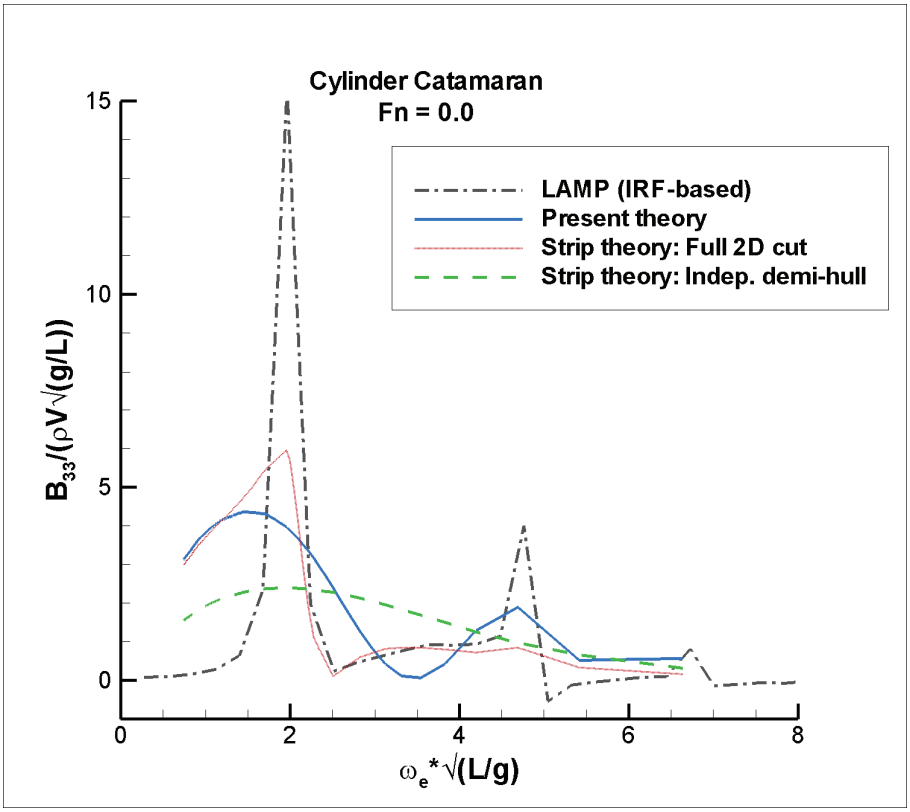

Figure A 1 Cylinder Catamaran – A_{33} and B_{33} at Fn=0.0

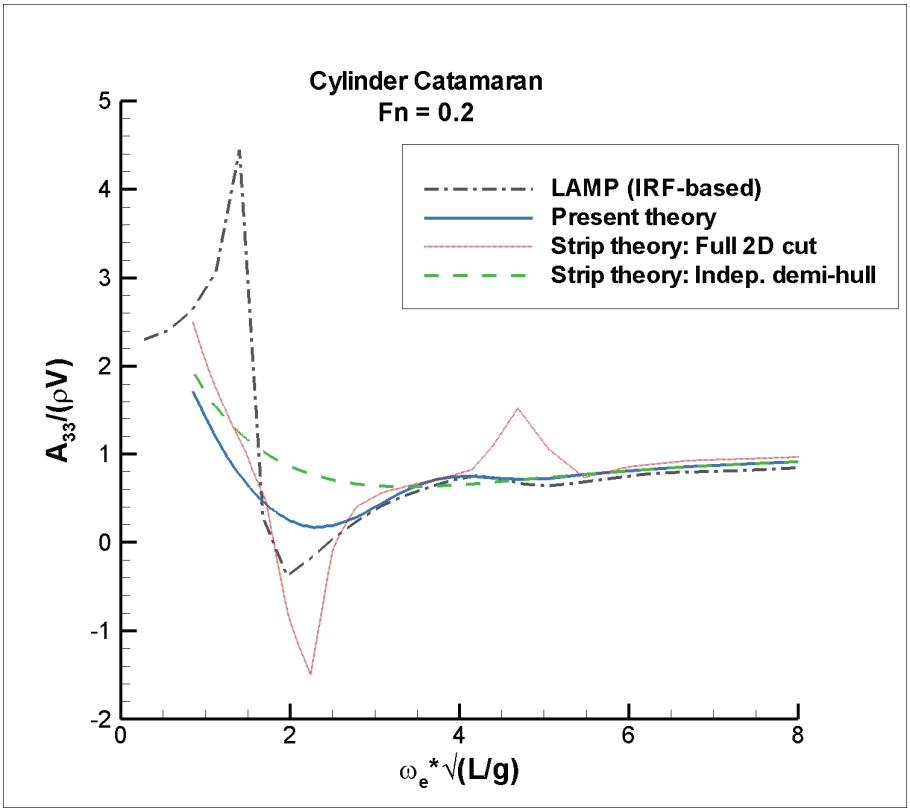

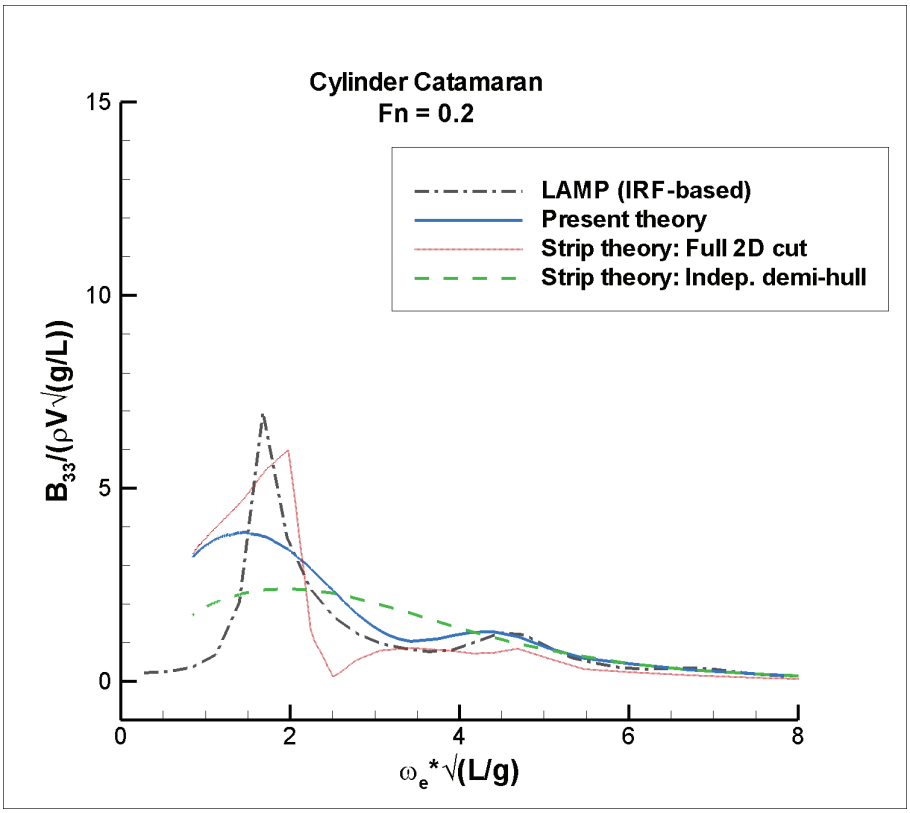

Figure A 2 Cylinder Catamaran – A_{33} and B_{33} at Fn=0.2

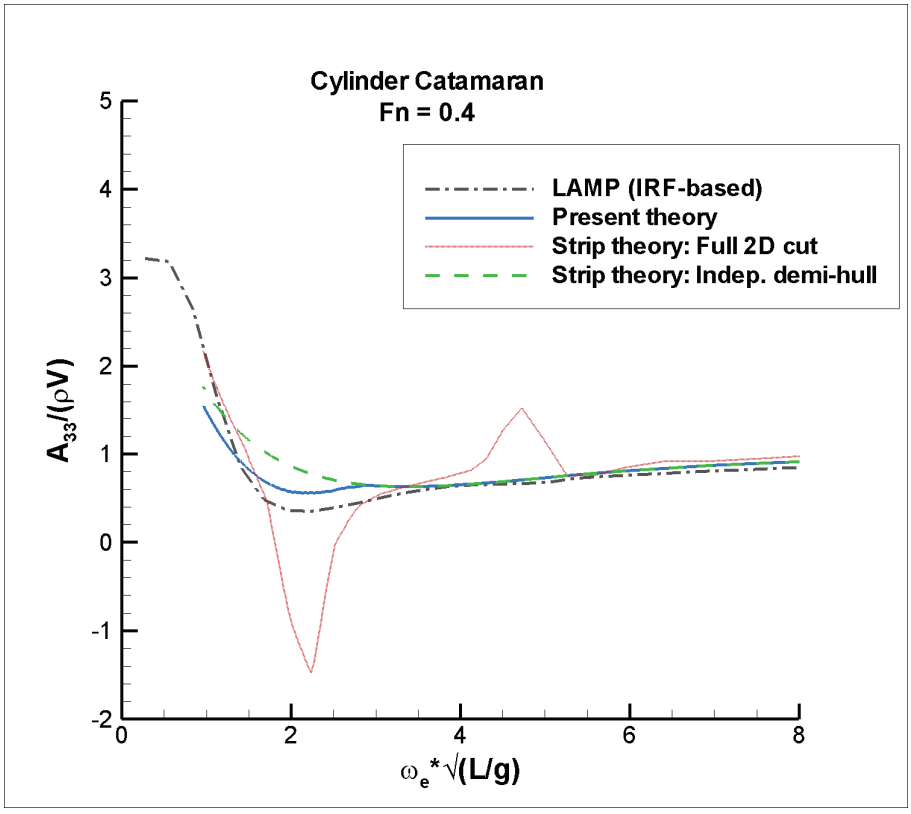

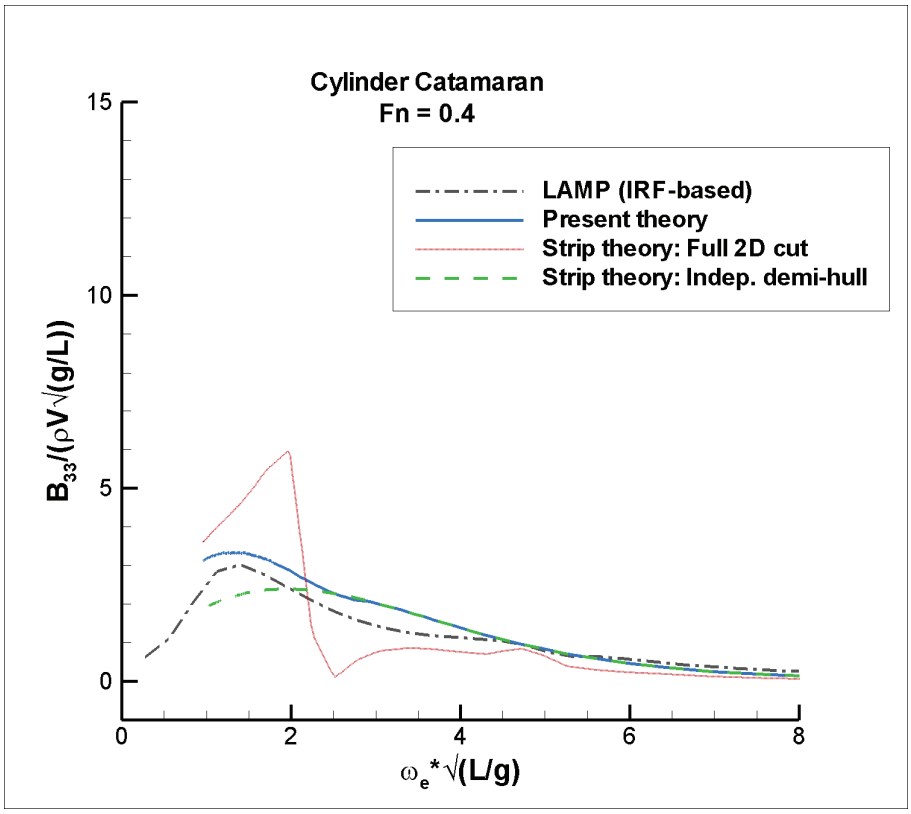

Figure A 3 Cylinder Catamaran – A_{33} and B_{33} at Fn=0.4

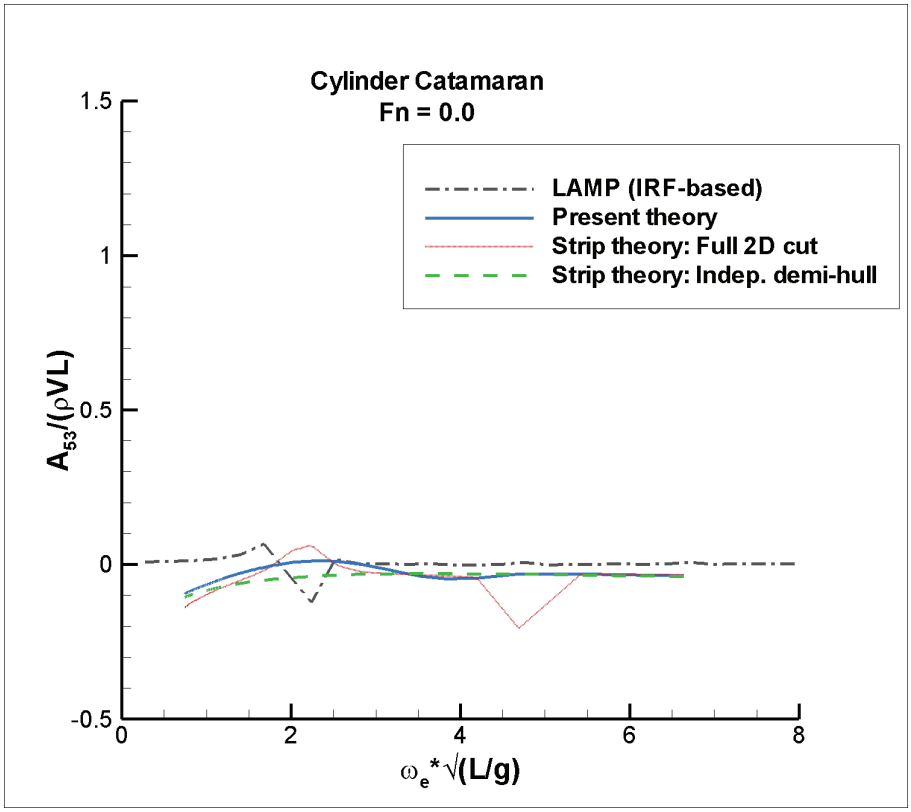

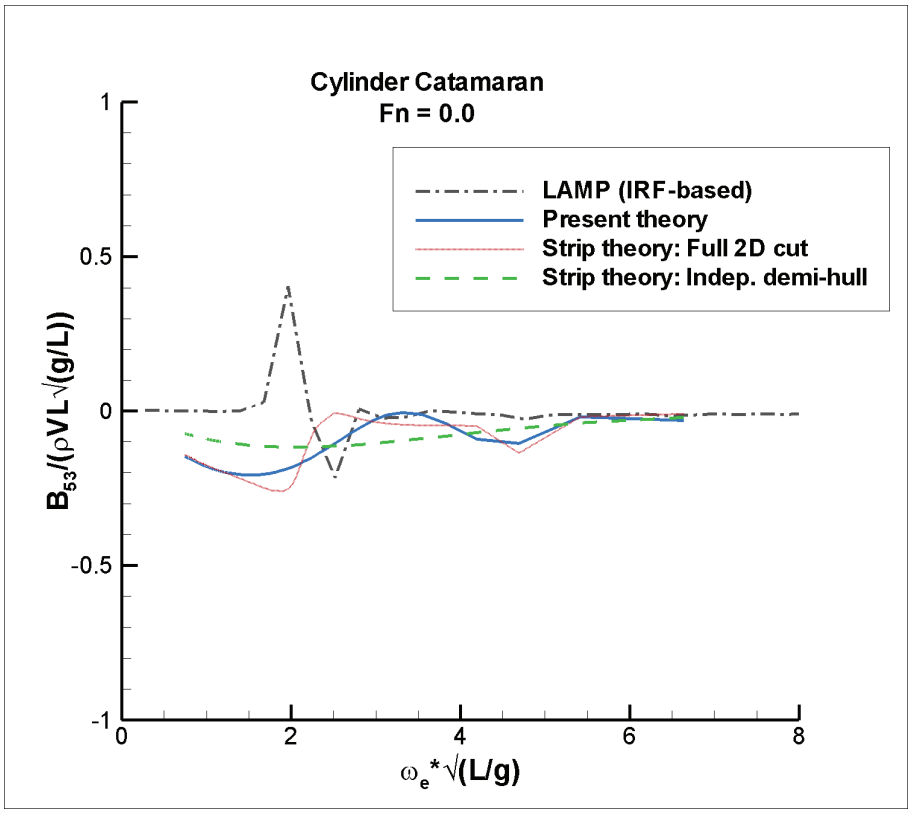

Figure A 4 Cylinder Catamaran – A_{53} and B_{53} at Fn=0.0

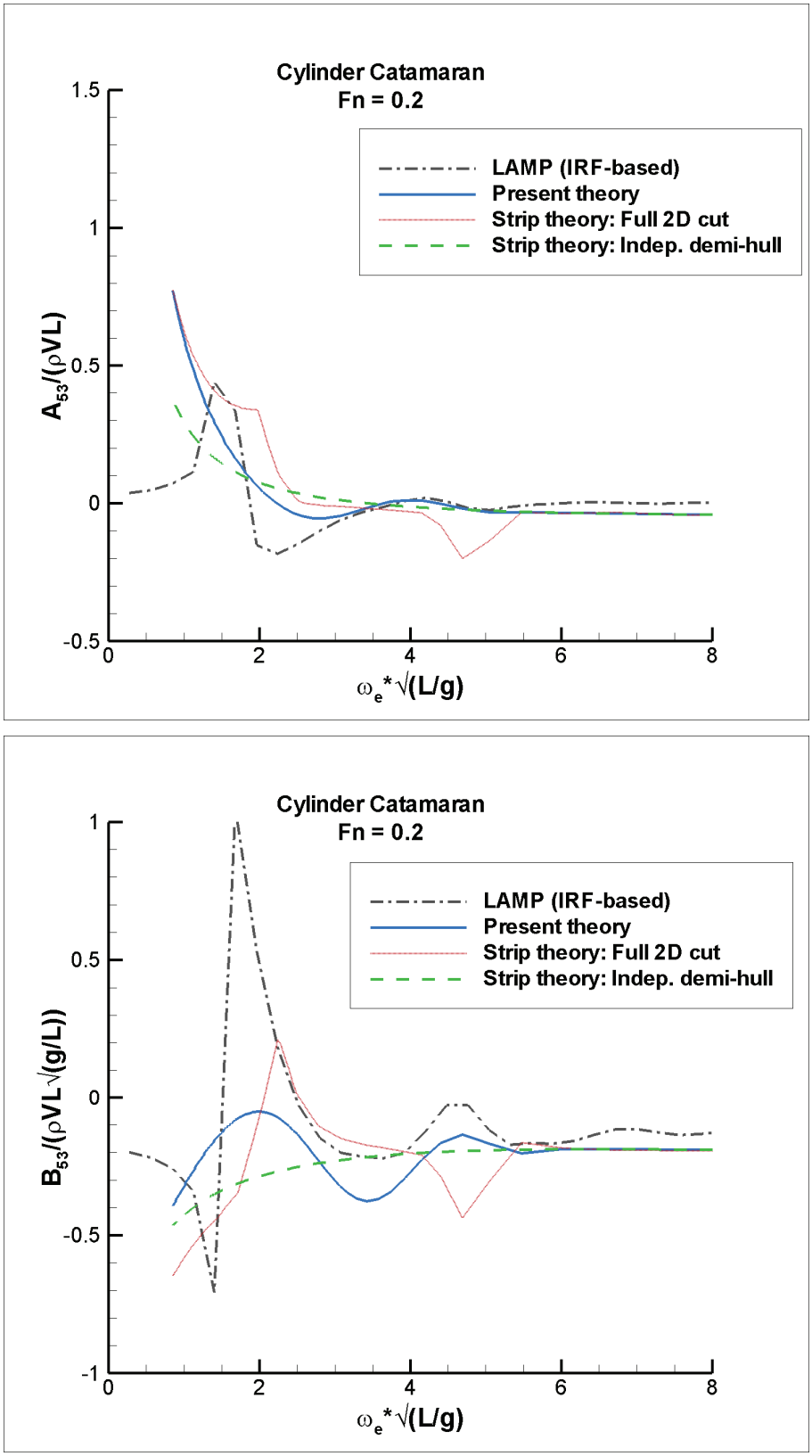

Figure A 5 Cylinder Catamaran – A_{53} and B_{53} at Fn=0.2

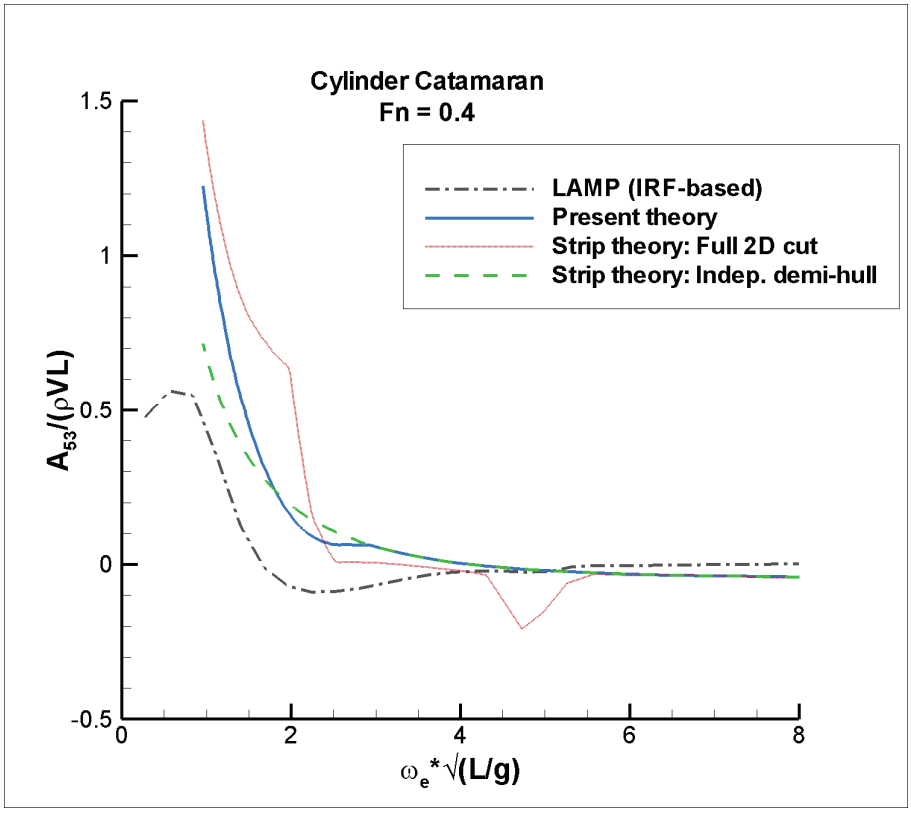

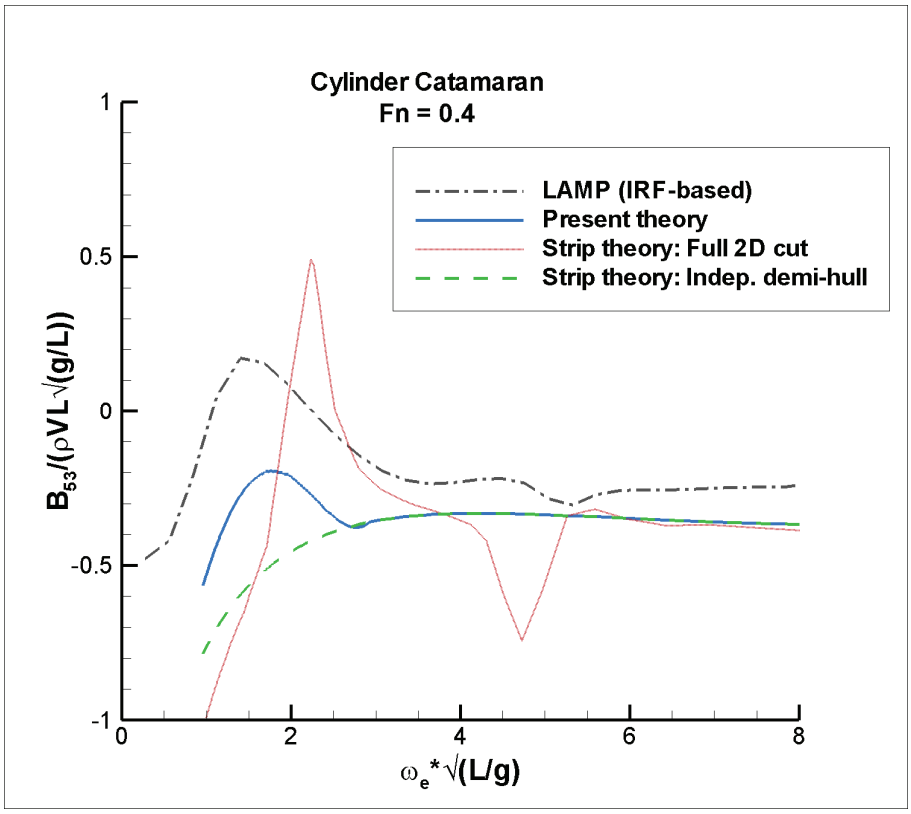

Figure A 6 Cylinder Catamaran – A_{53} and B_{53} at Fn=0.4

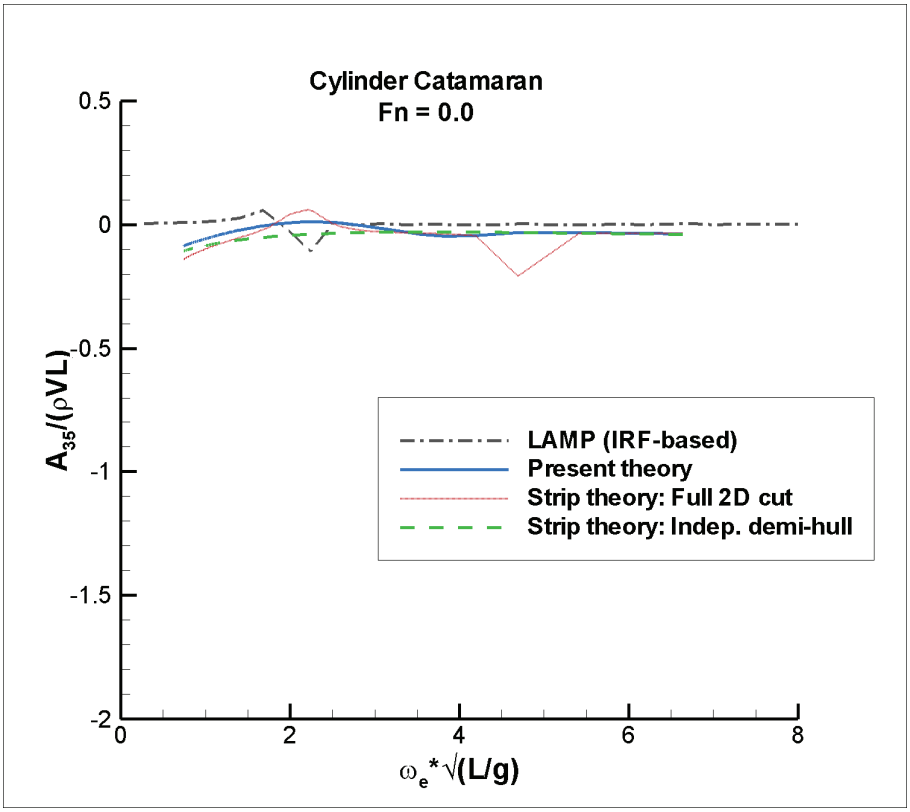

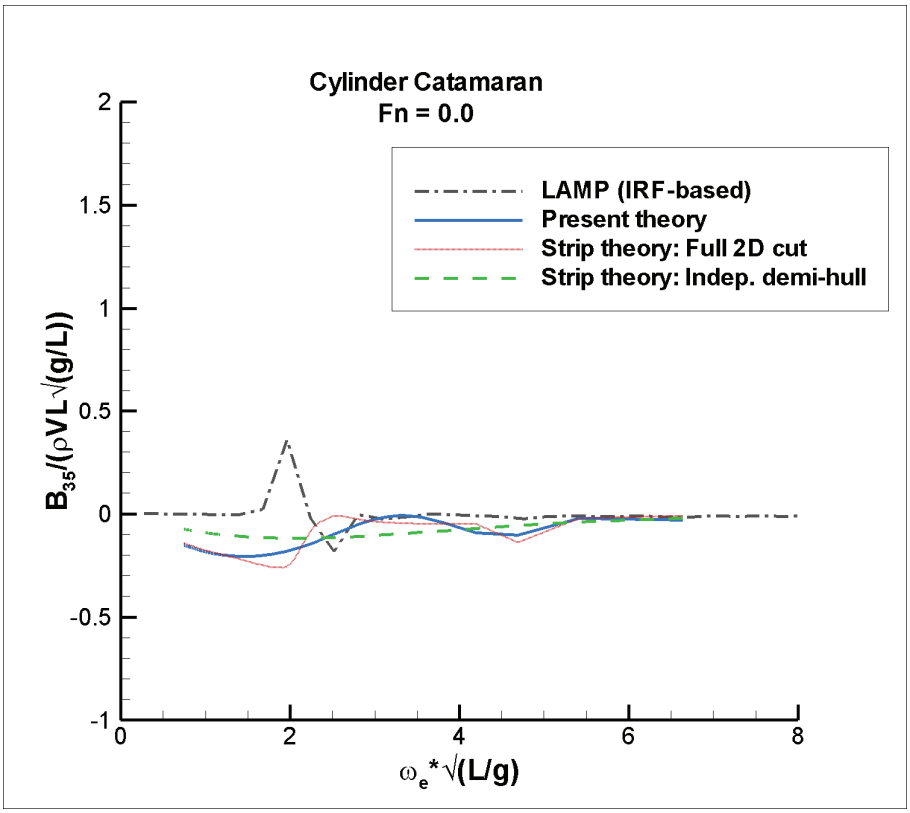

Figure A 7 Cylinder Catamaran – A_{35} and B_{35} at Fn=0.0

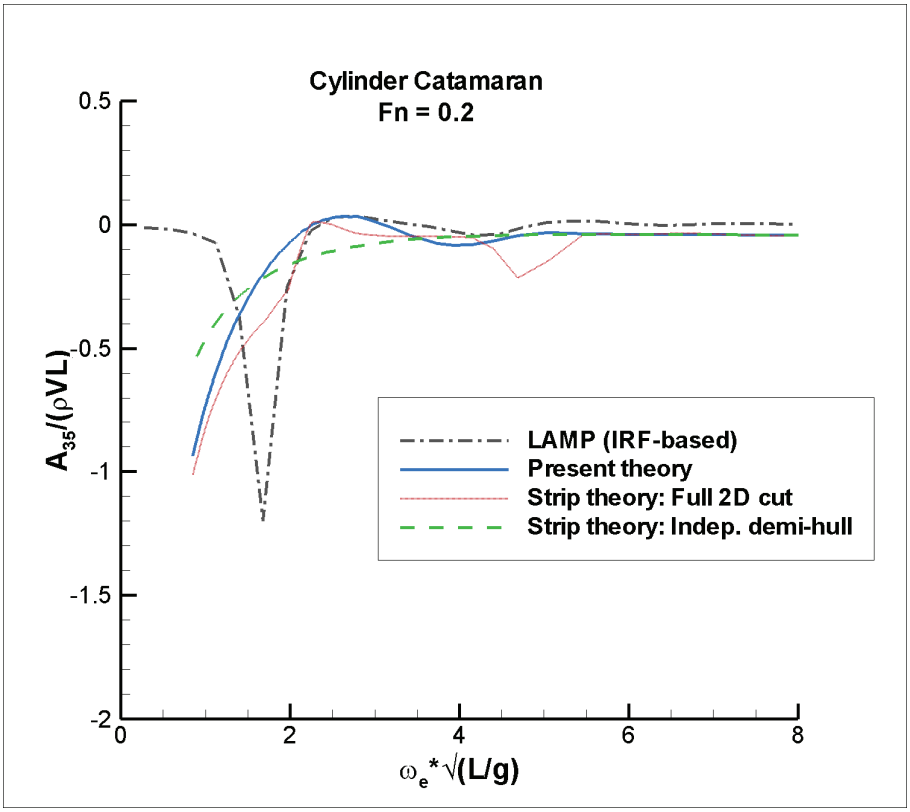

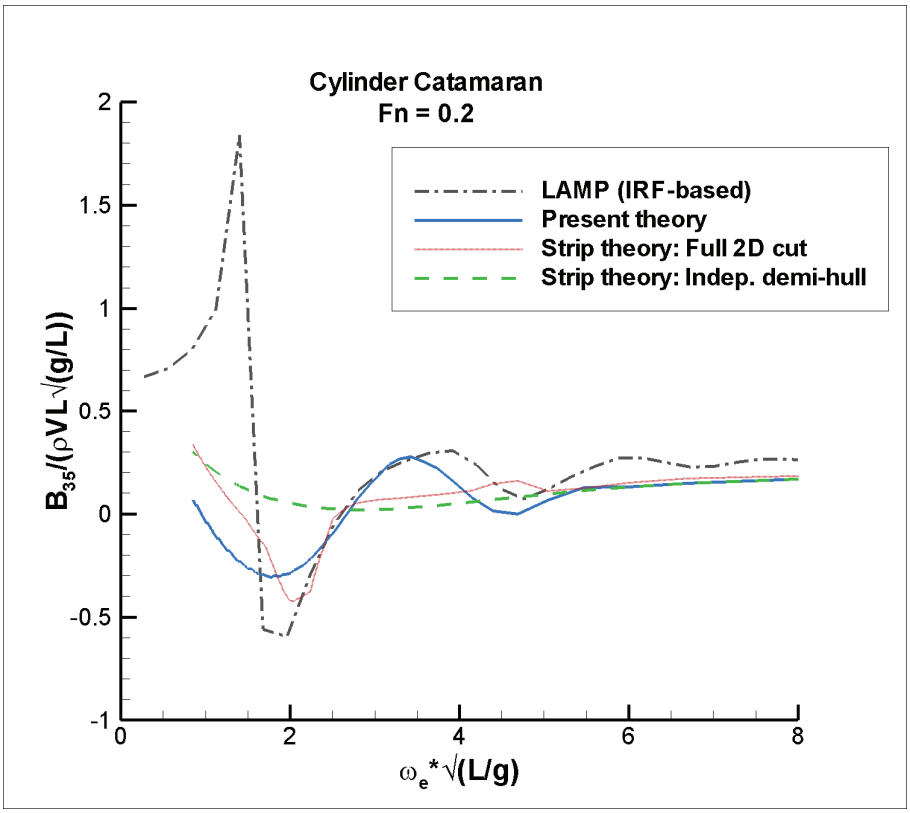

Figure A 8 Cylinder Catamaran – A_{35} and B_{35} at Fn=0.2

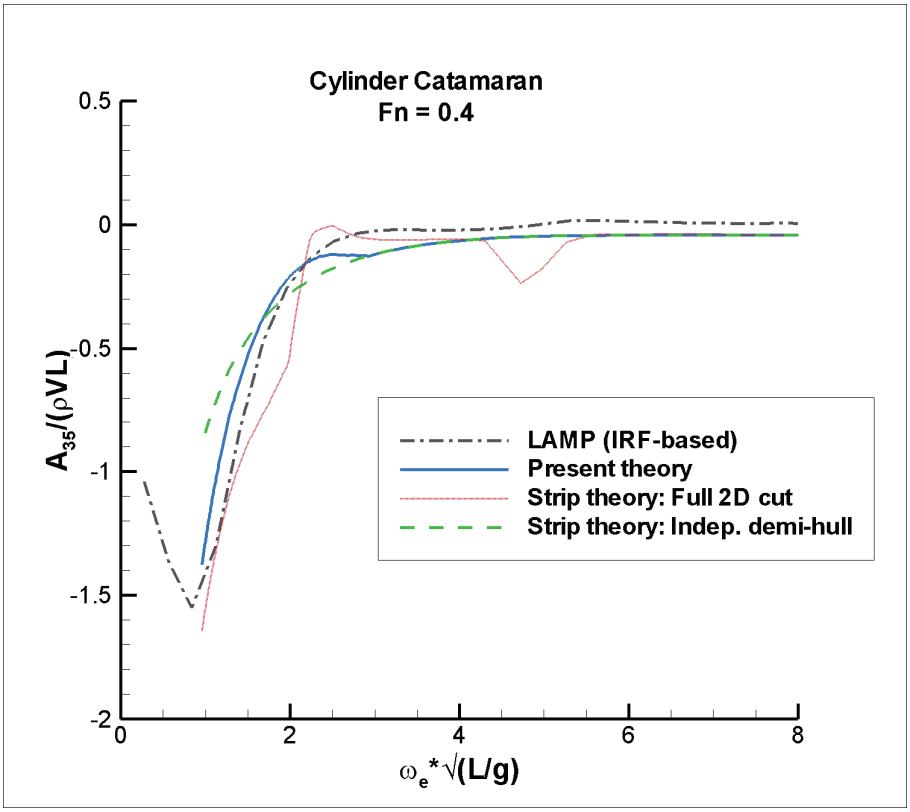

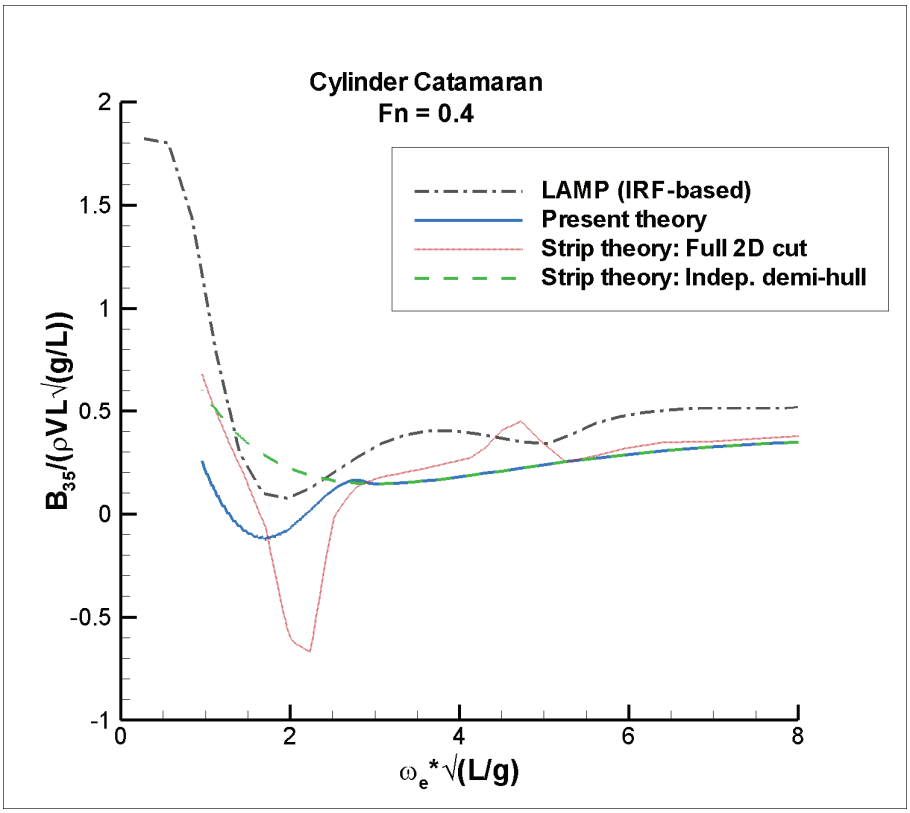

Figure A 9 Cylinder Catamaran – A_{35} and B_{35} at Fn=0.4

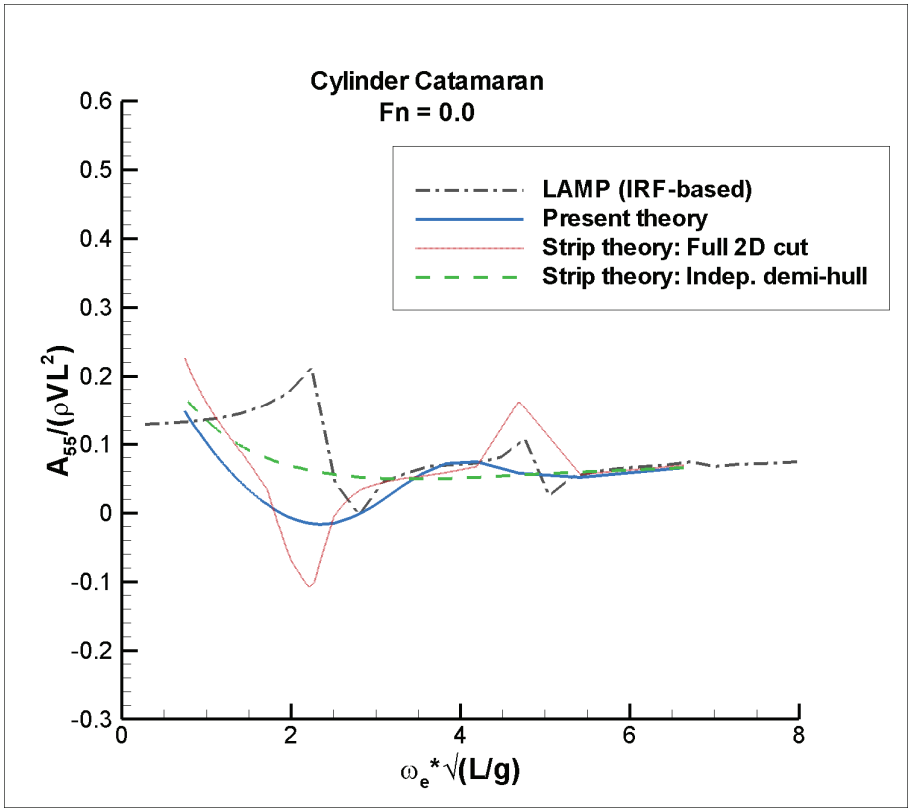

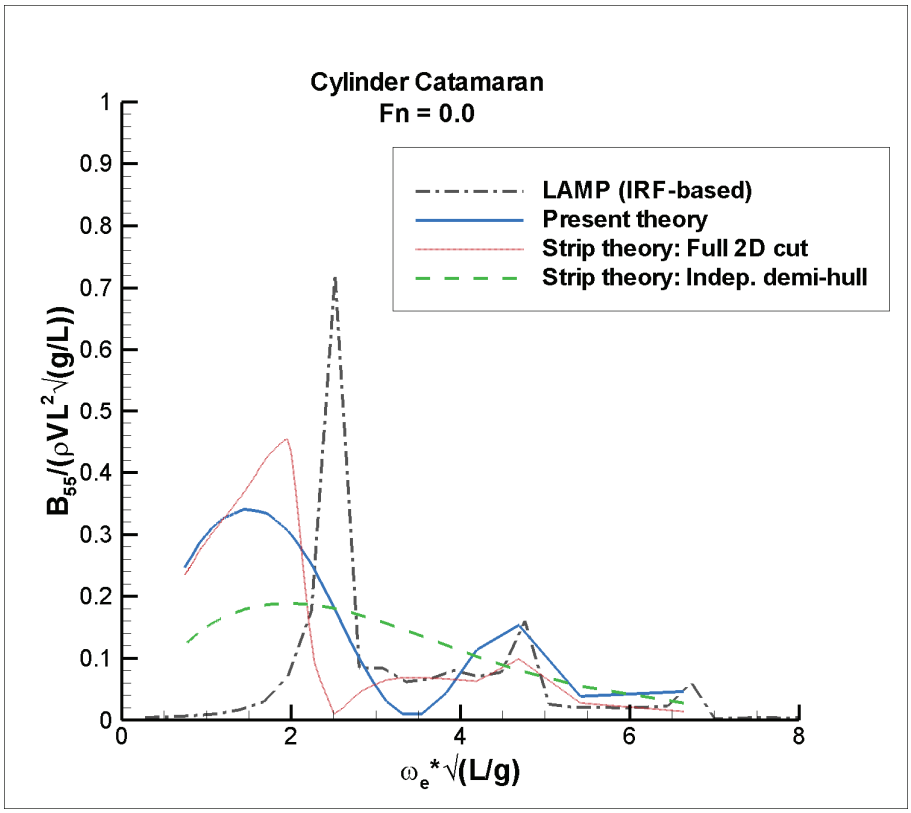

Figure A 10 Cylinder Catamaran – A_{55} and B_{55} at Fn=0.0

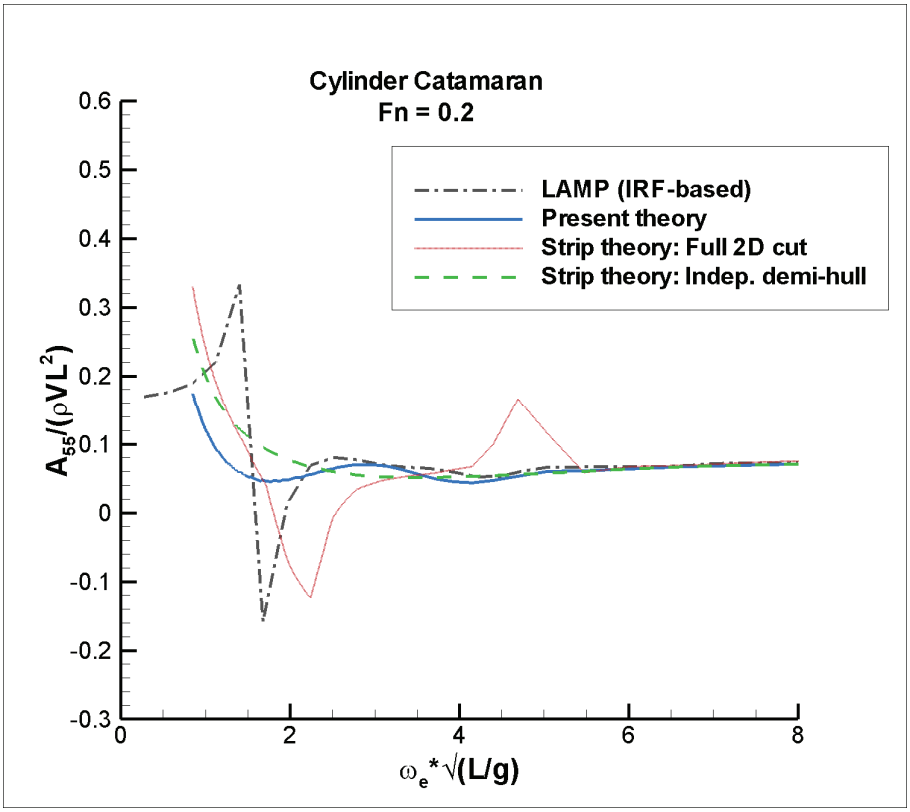

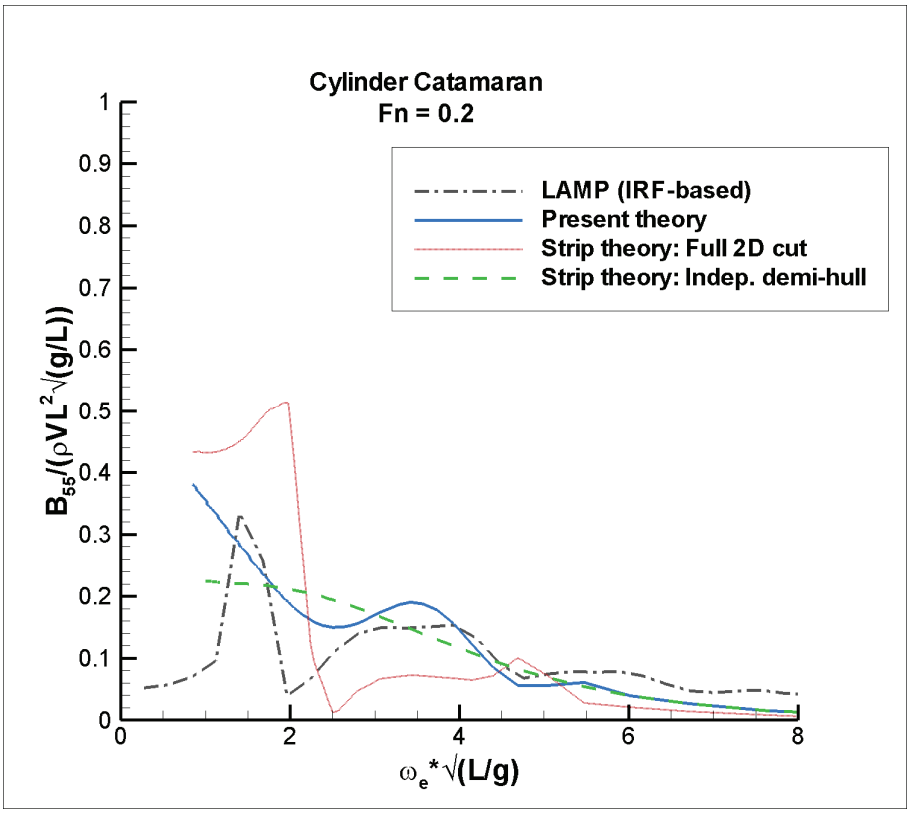

Figure A 11 Cylinder Catamaran – A_{55} and B_{55} at Fn=0.2

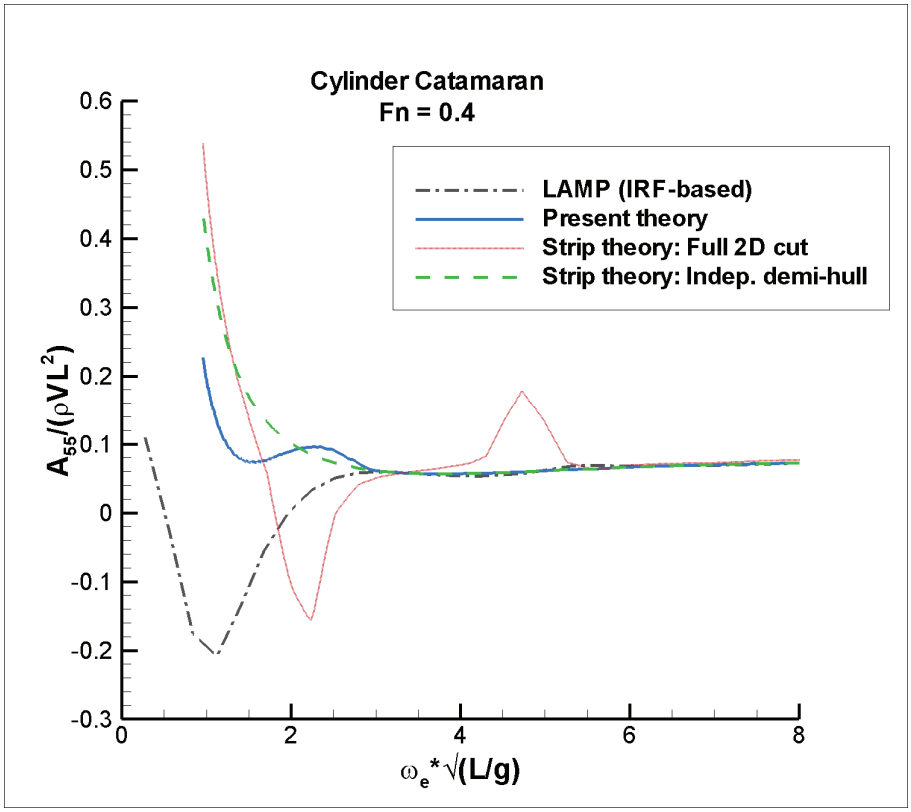

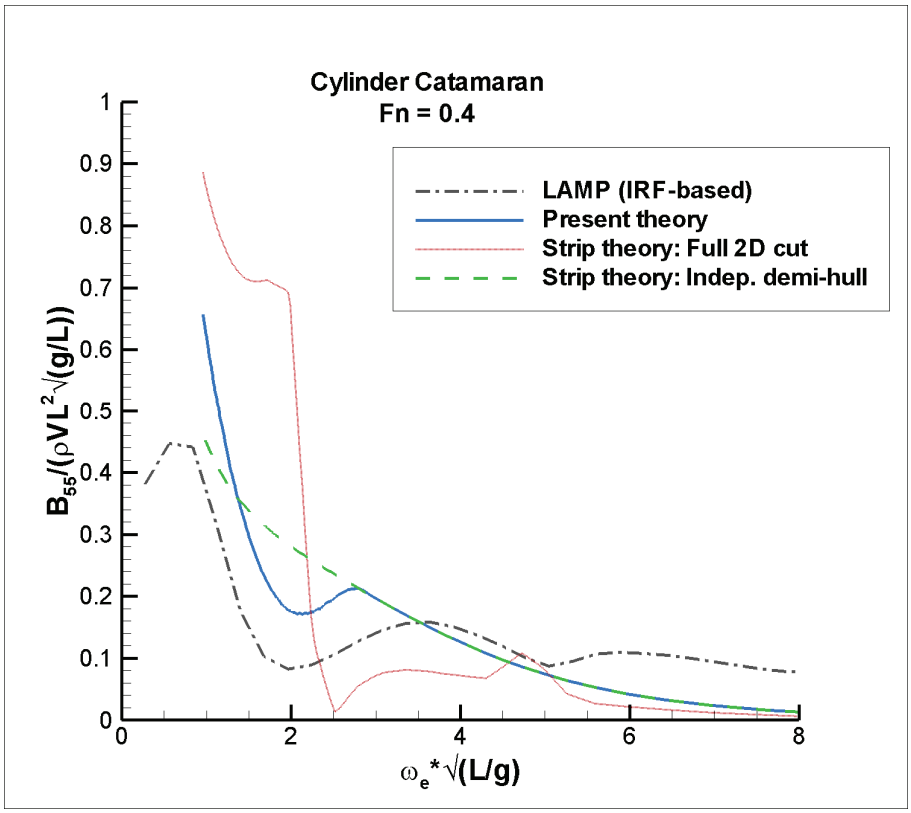

Figure A 12 Cylinder Catamaran – A_{55} and B_{55} at Fn=0.4

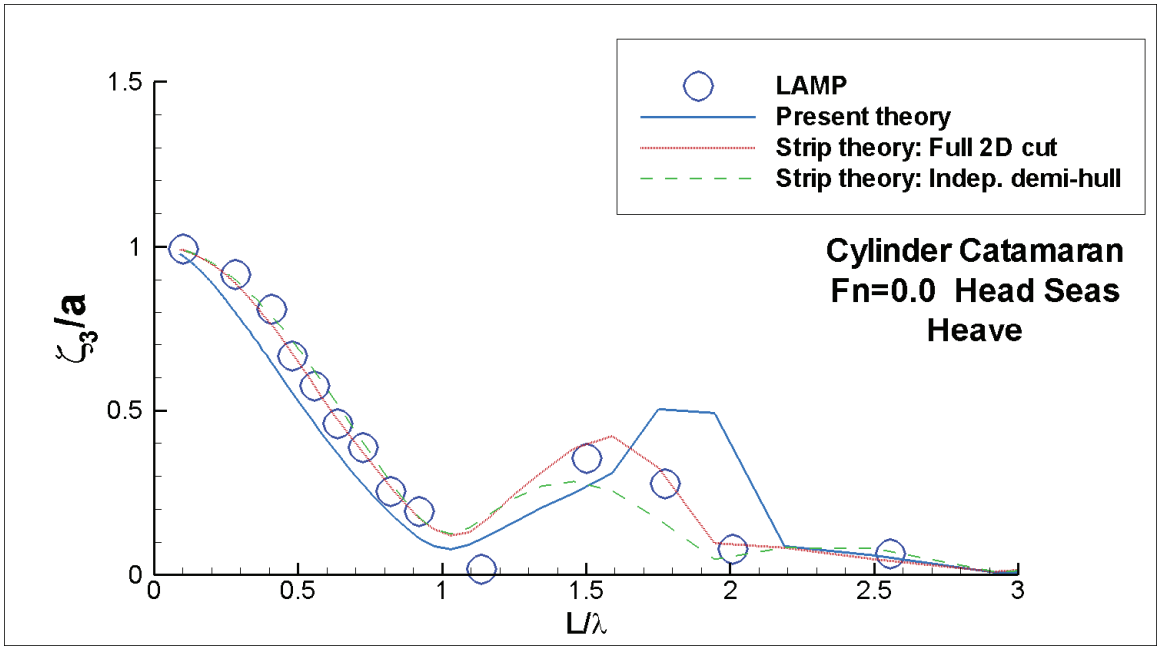

Figure A 13 Cylinder Catamaran heave transfer function at Fn=0.0 in head seas

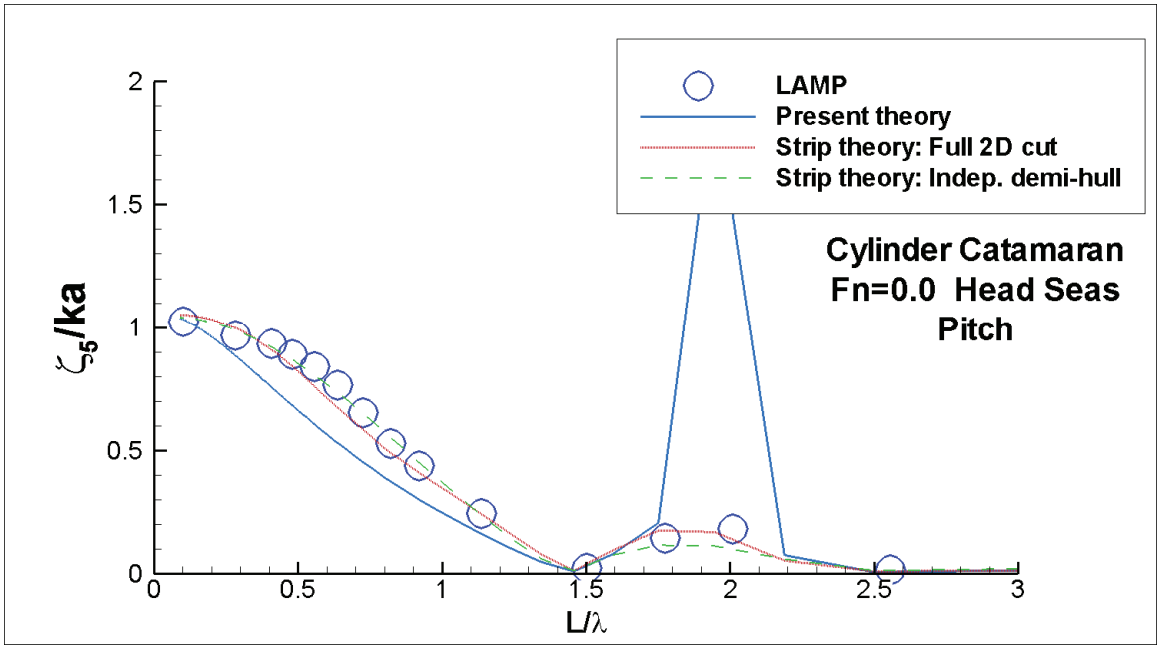

Figure A 14 Cylinder Catamaran pitch transfer function at Fn=0.0 in head seas

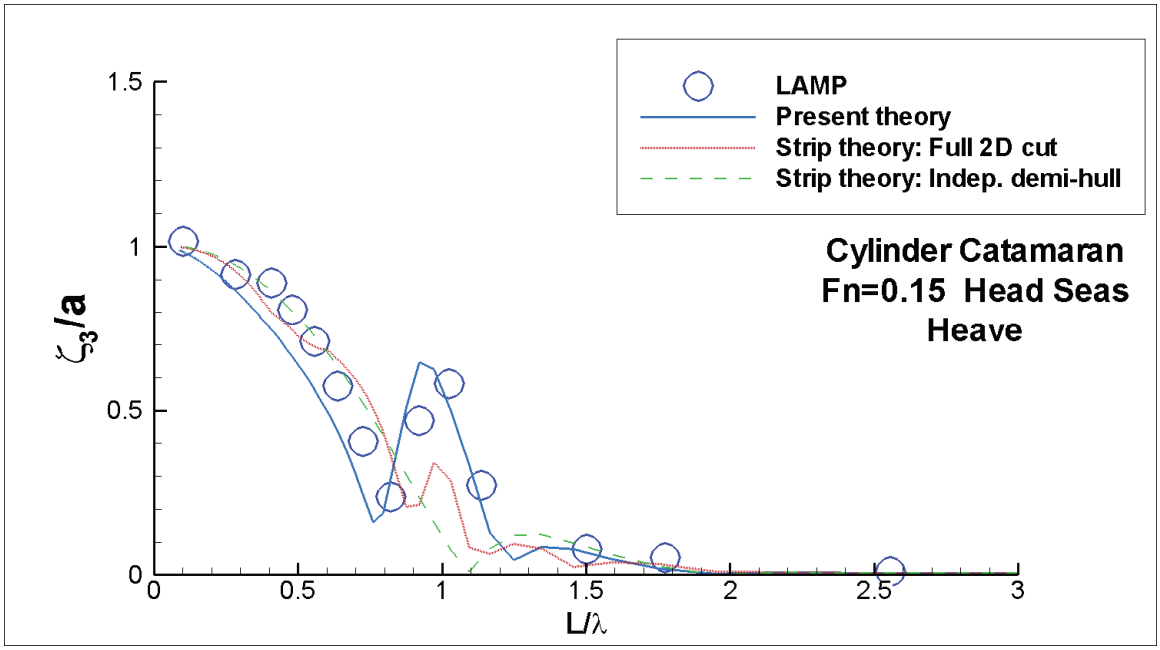

Figure A 15 Cylinder Catamaran heave transfer function at Fn=0.15 in head seas

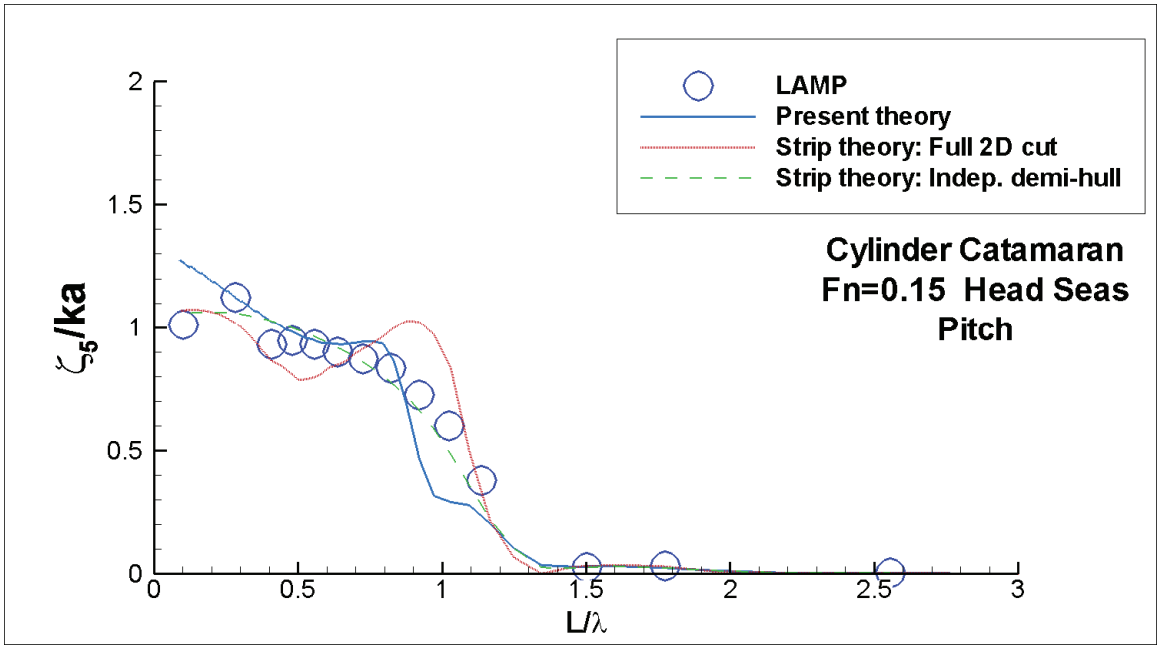

Figure A 16 Cylinder Catamaran pitch transfer function at Fn=0.15 in head seas

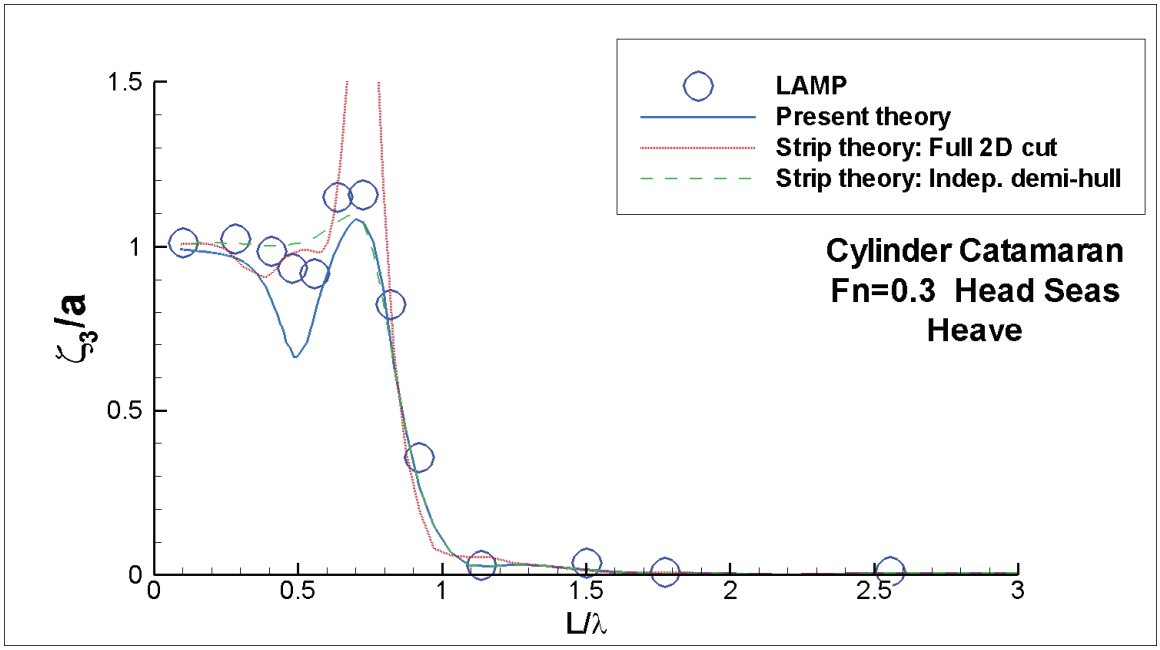

Figure A 17 Cylinder Catamaran heave transfer function at Fn=0.3 in head seas

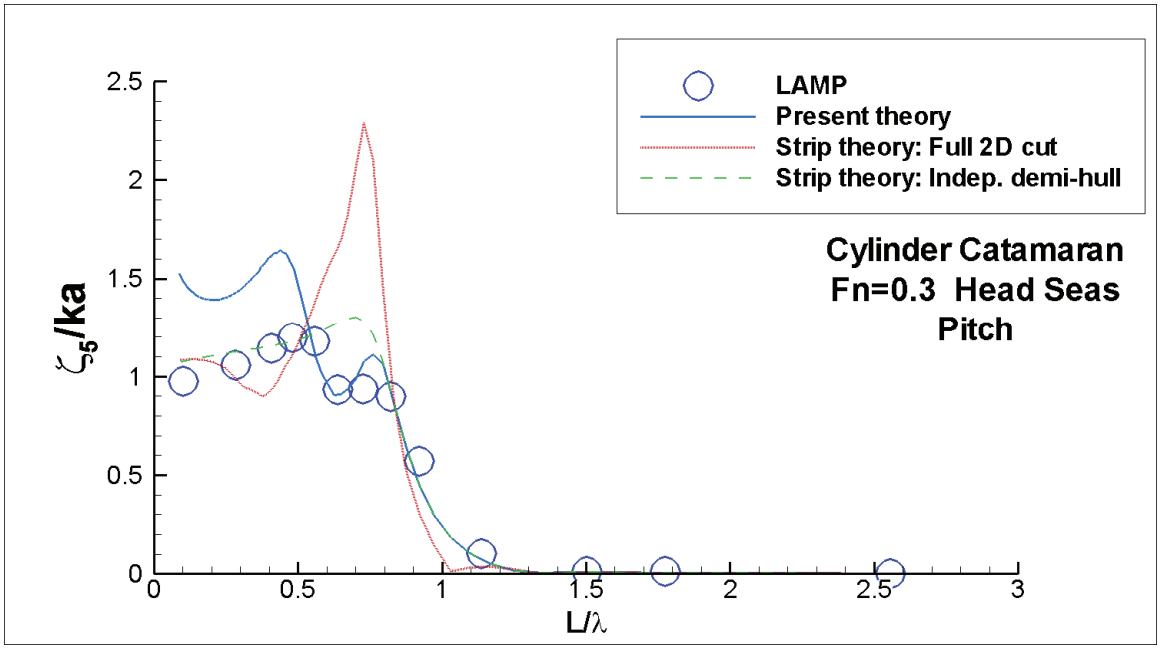

Figure A 18 Cylinder Catamaran pitch transfer function at Fn=0.3 in head seas

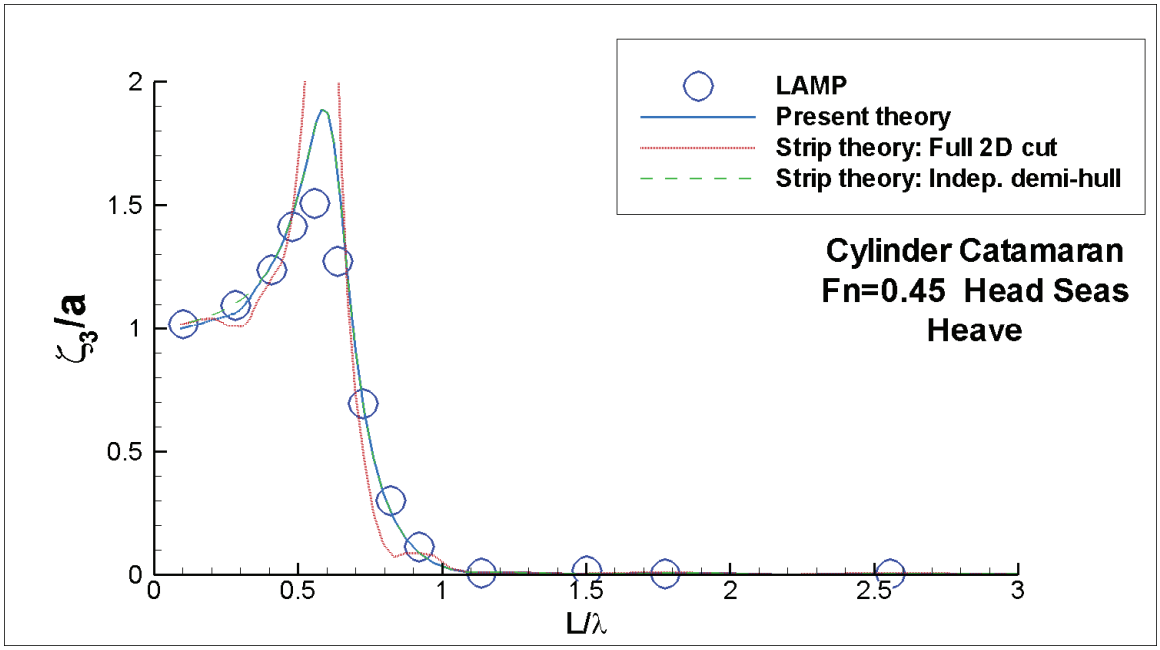

Figure A 19 Cylinder Catamaran heave transfer function at Fn=0.45 in head seas

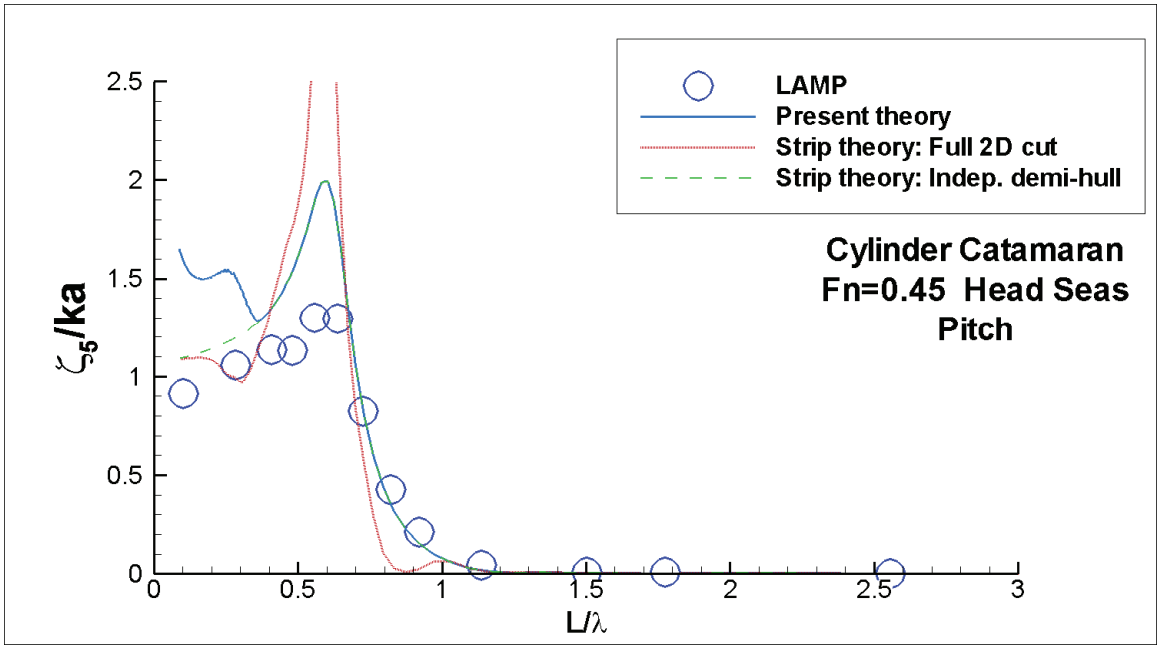

Figure A 20 Cylinder Catamaran pitch transfer function at Fn=0.45 in head seas

Appendix B

Delft Catamaran Validation Figures

Appendix B contains the full set of hydrodynamic coefficient and motion transfer function comparisons for the Delft Catamaran. The added mass and damping plots are given in Figure B 1 through Figure B 4. The motion transfer functions are given in Figure B 5 through Figure B 18.

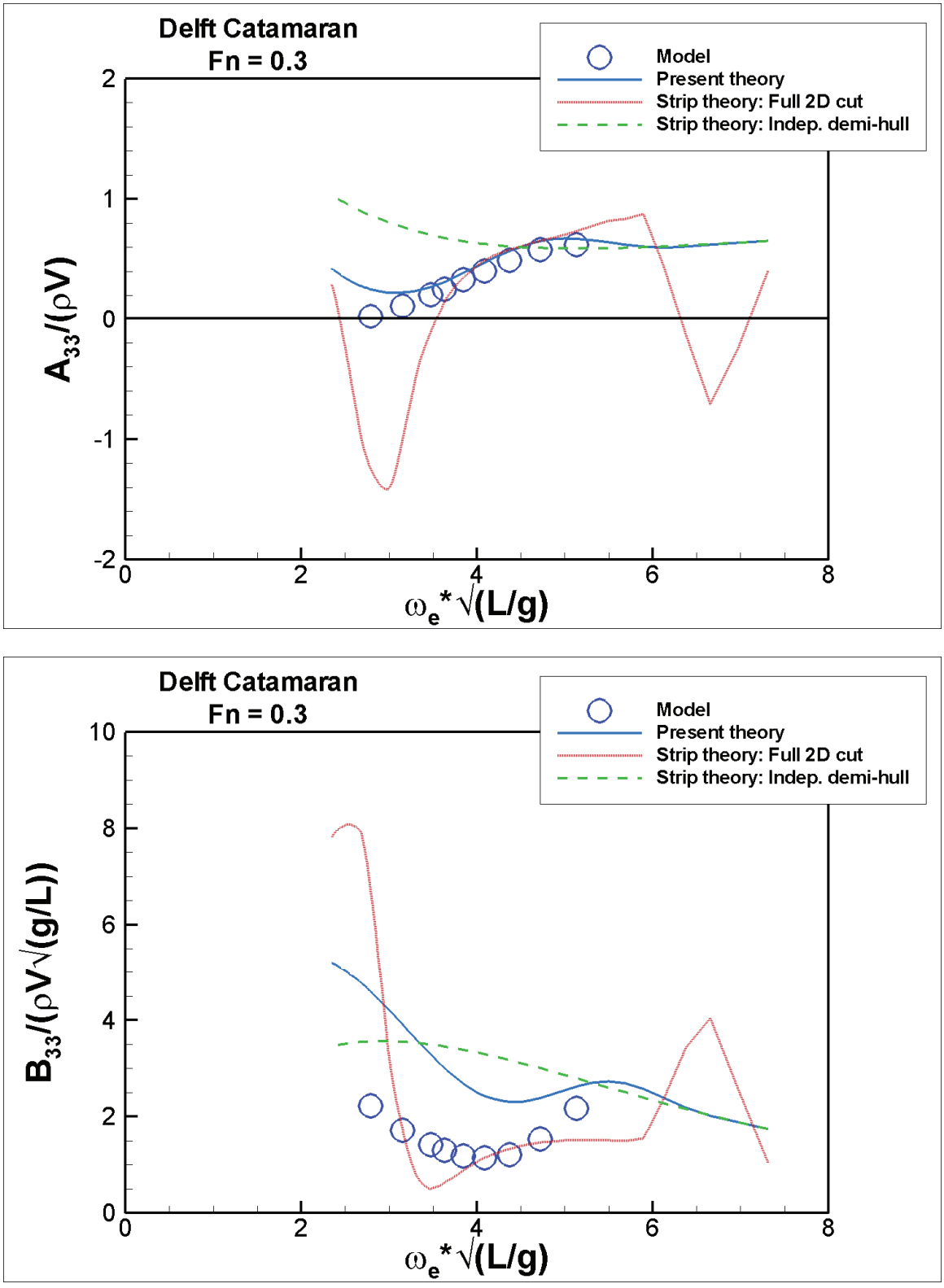

Figure B 1 Delft Catamaran A_{33} and B_{33} at Fn=0.3

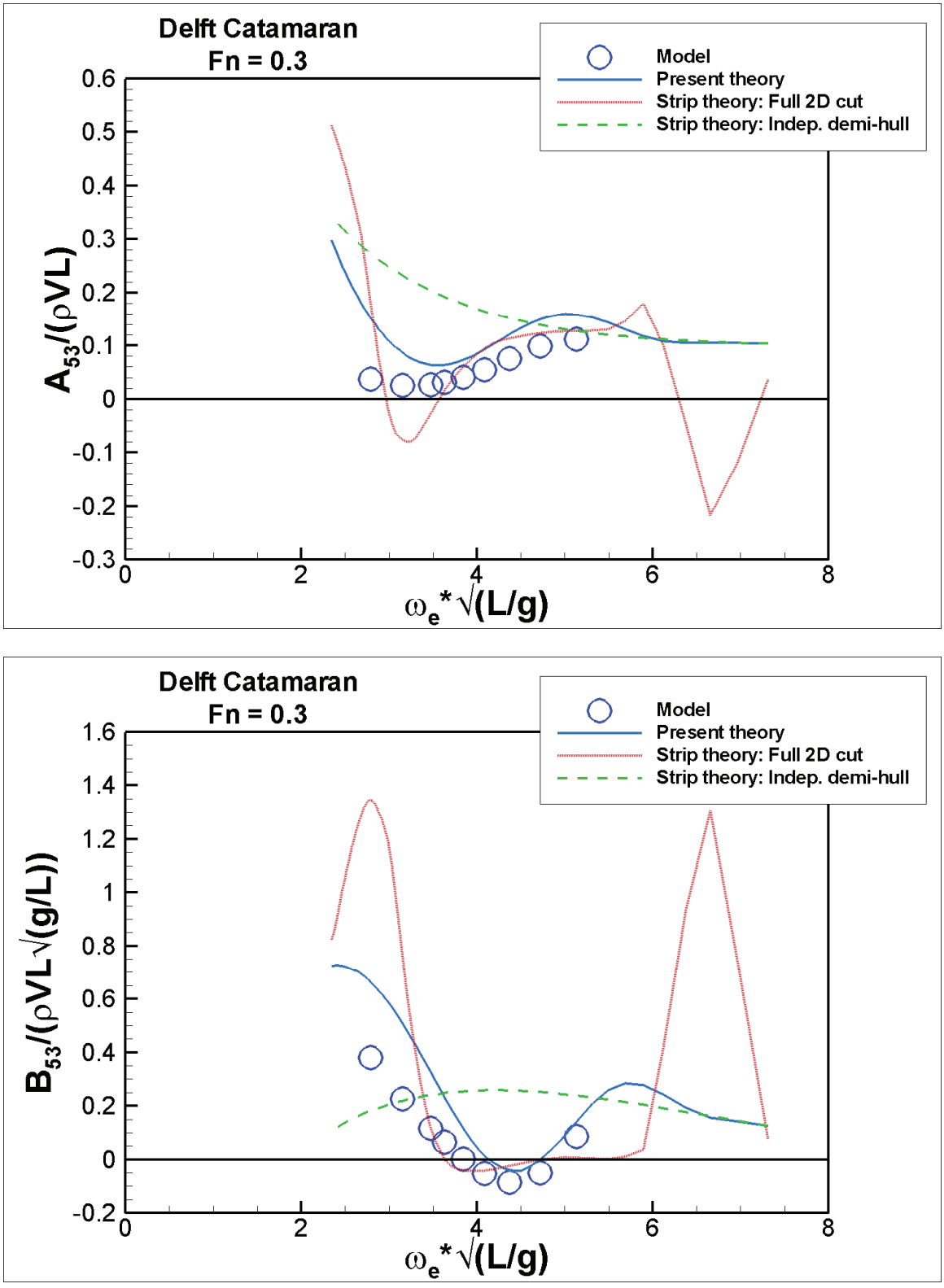

Figure B 2 Delft Catamaran A_{53} and B_{53} at Fn=0.3

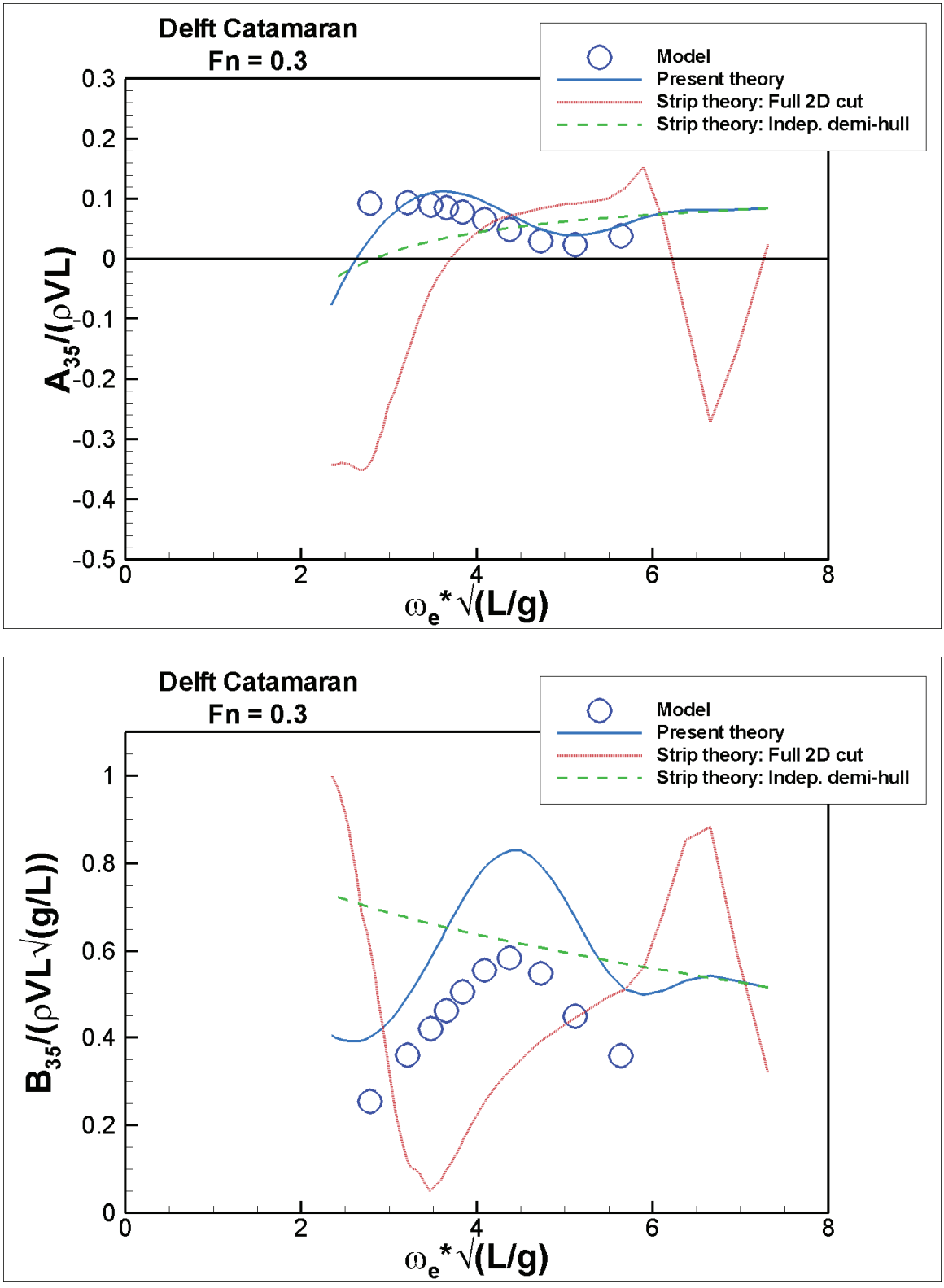

Figure B 3 Delft Catamaran A_{35} and B_{35} at Fn=0.3

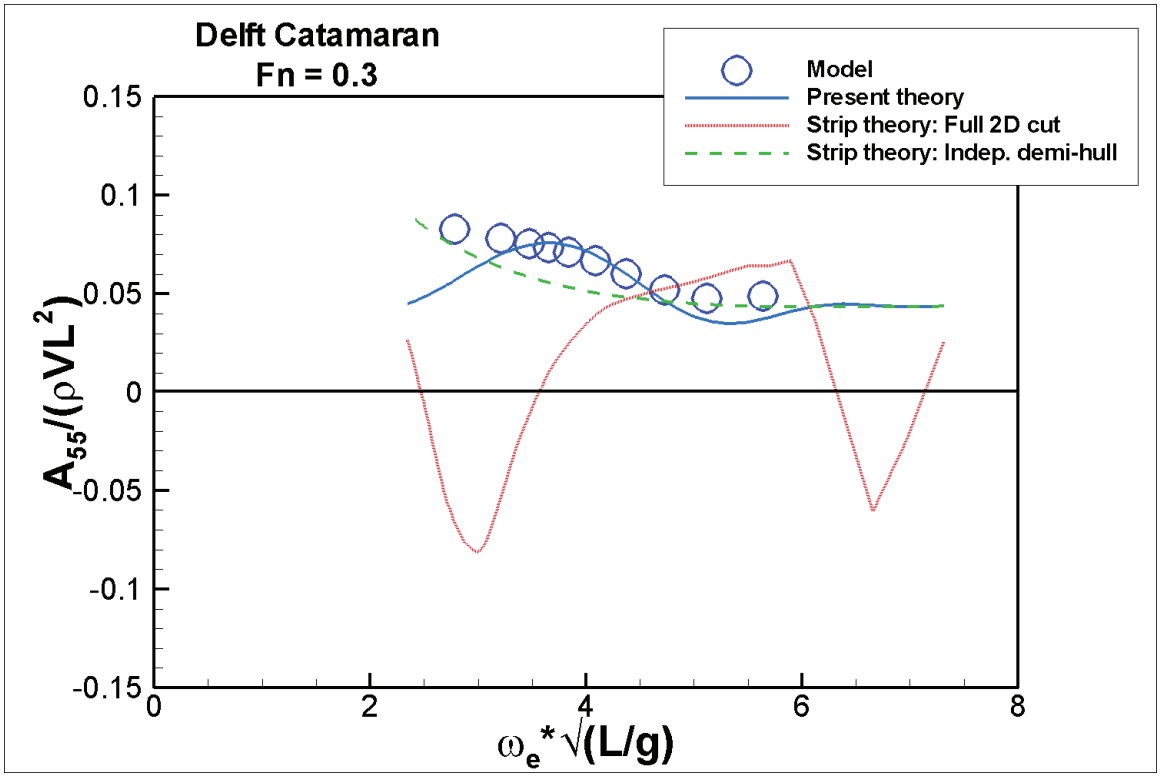

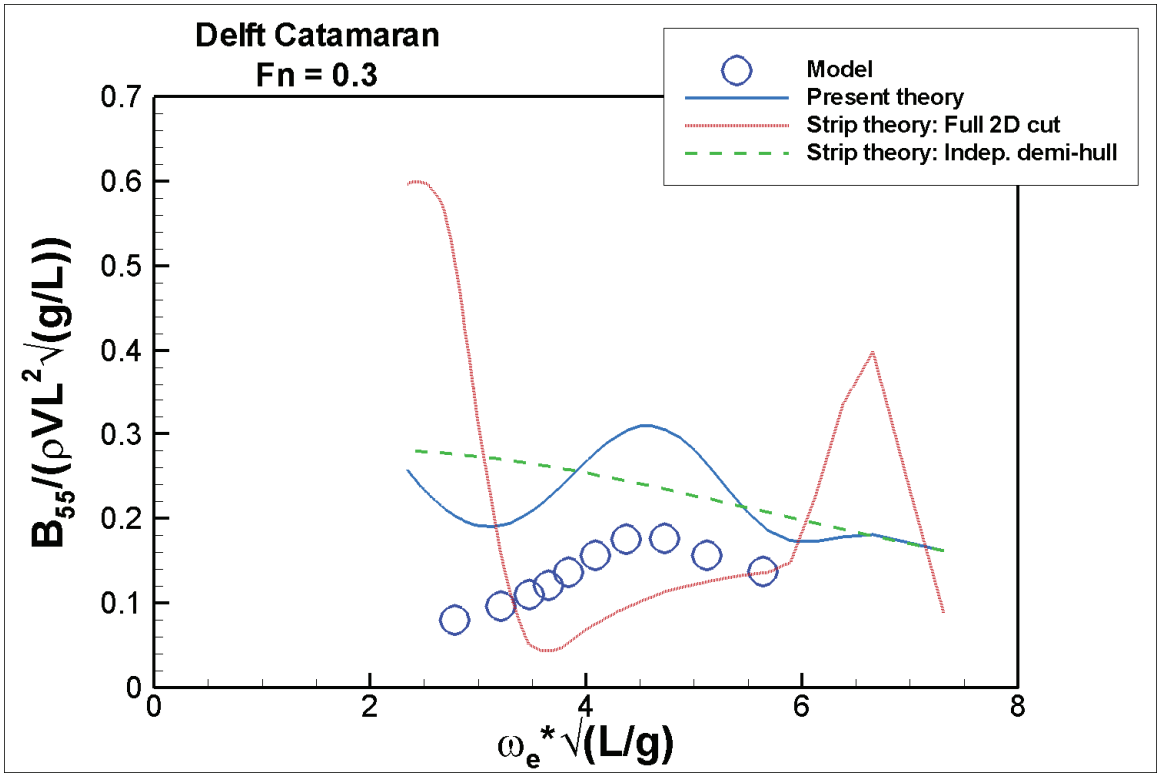

Figure B 4 Delft Catamaran A_{55} and B_{55} at Fn=0.3

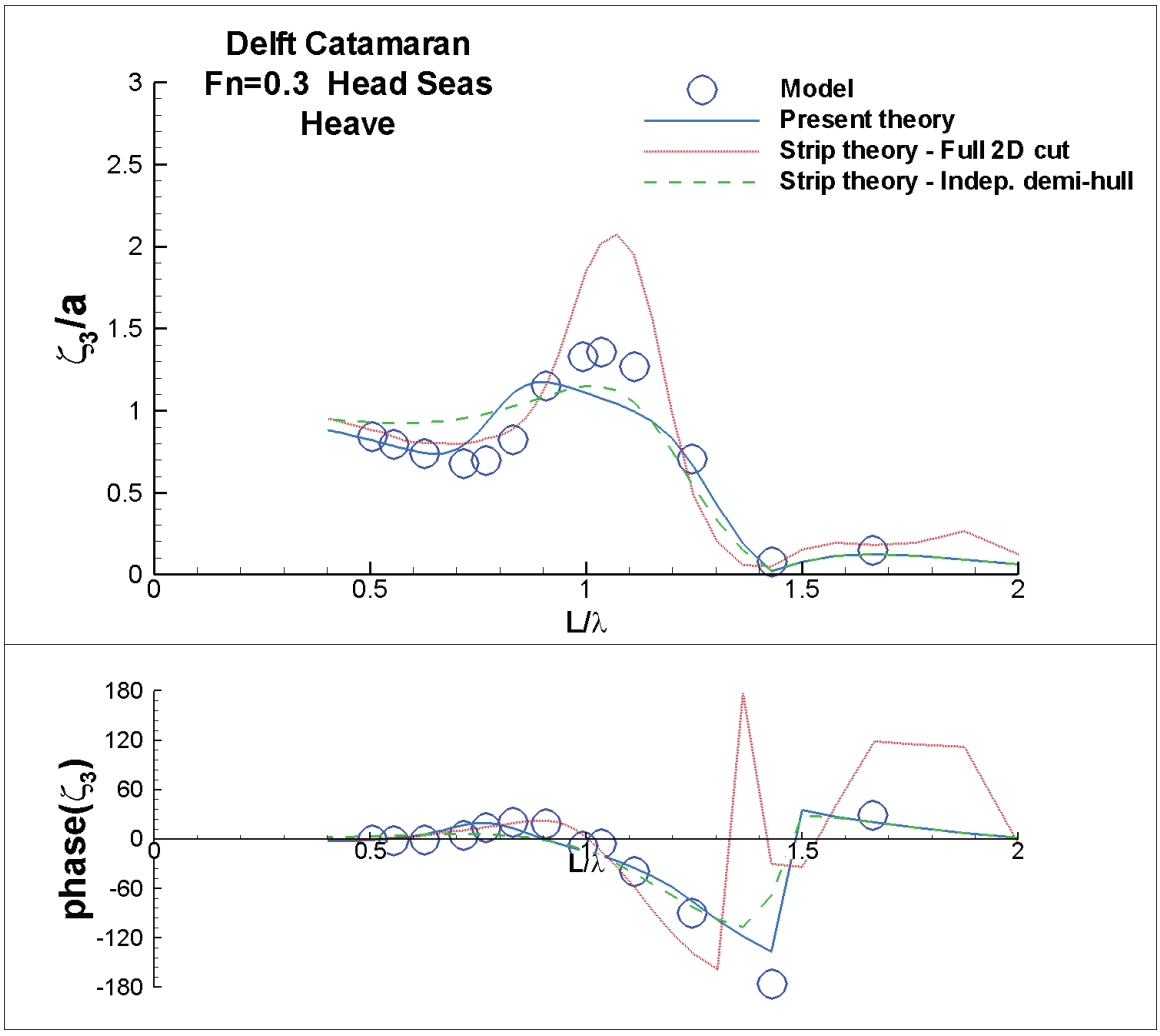

Figure B 5 Delft Catamaran heave transfer function at Fn=0.3 in head seas

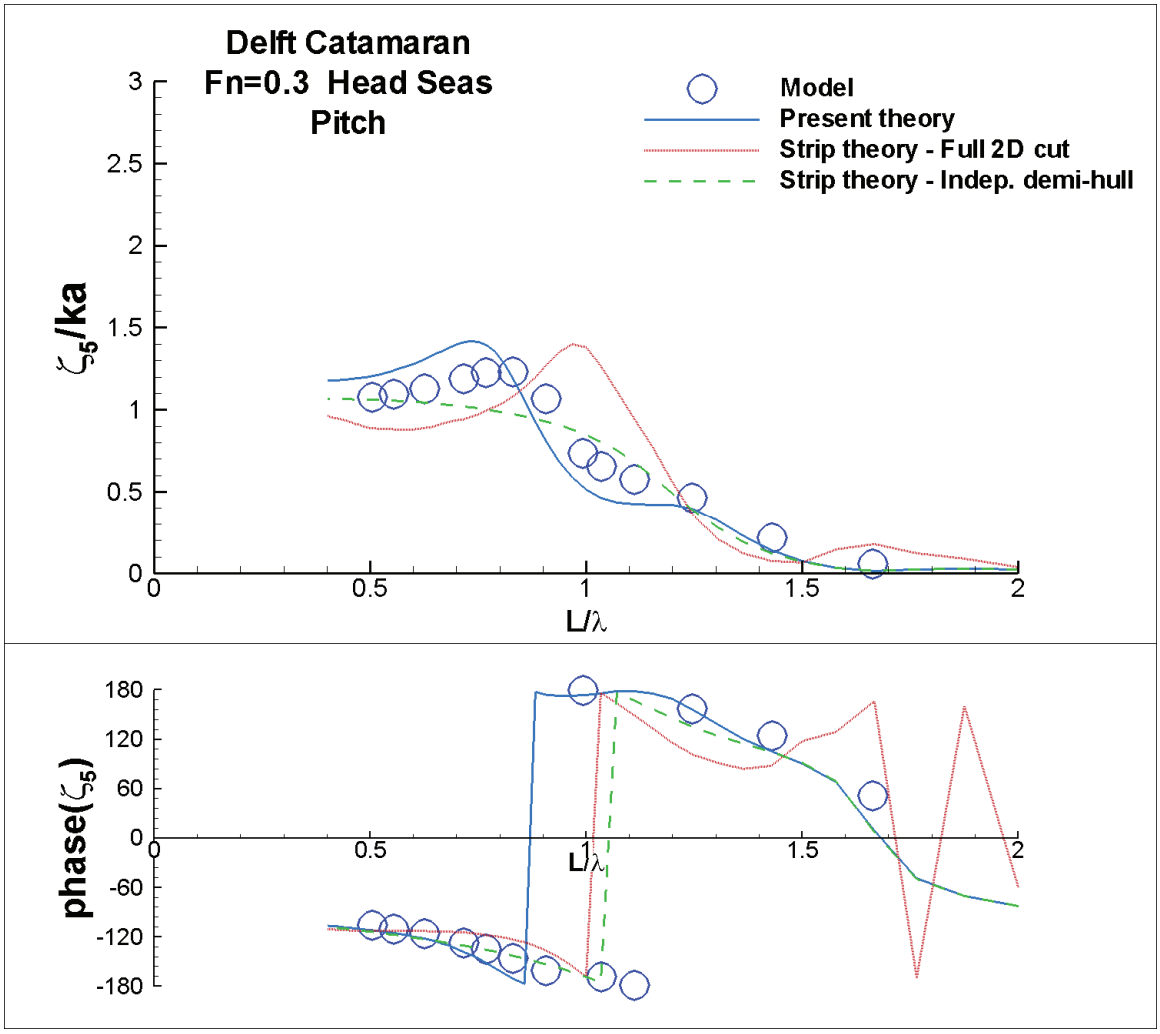

Figure B 6 Delft Catamaran pitch transfer function at Fn=0.3 in head seas

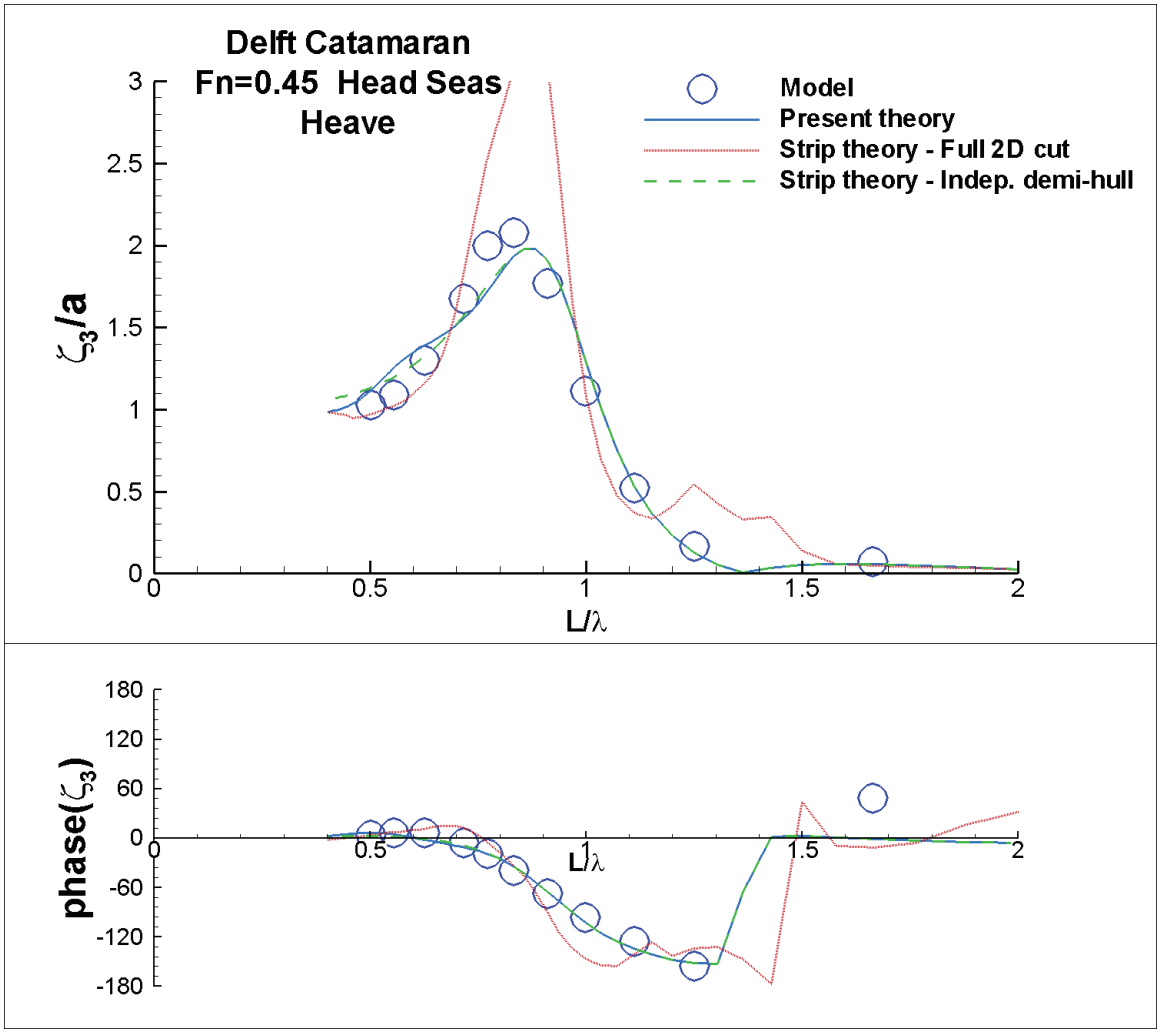

Figure B 7 Delft Catamaran heave transfer function at Fn=0.45 in head seas

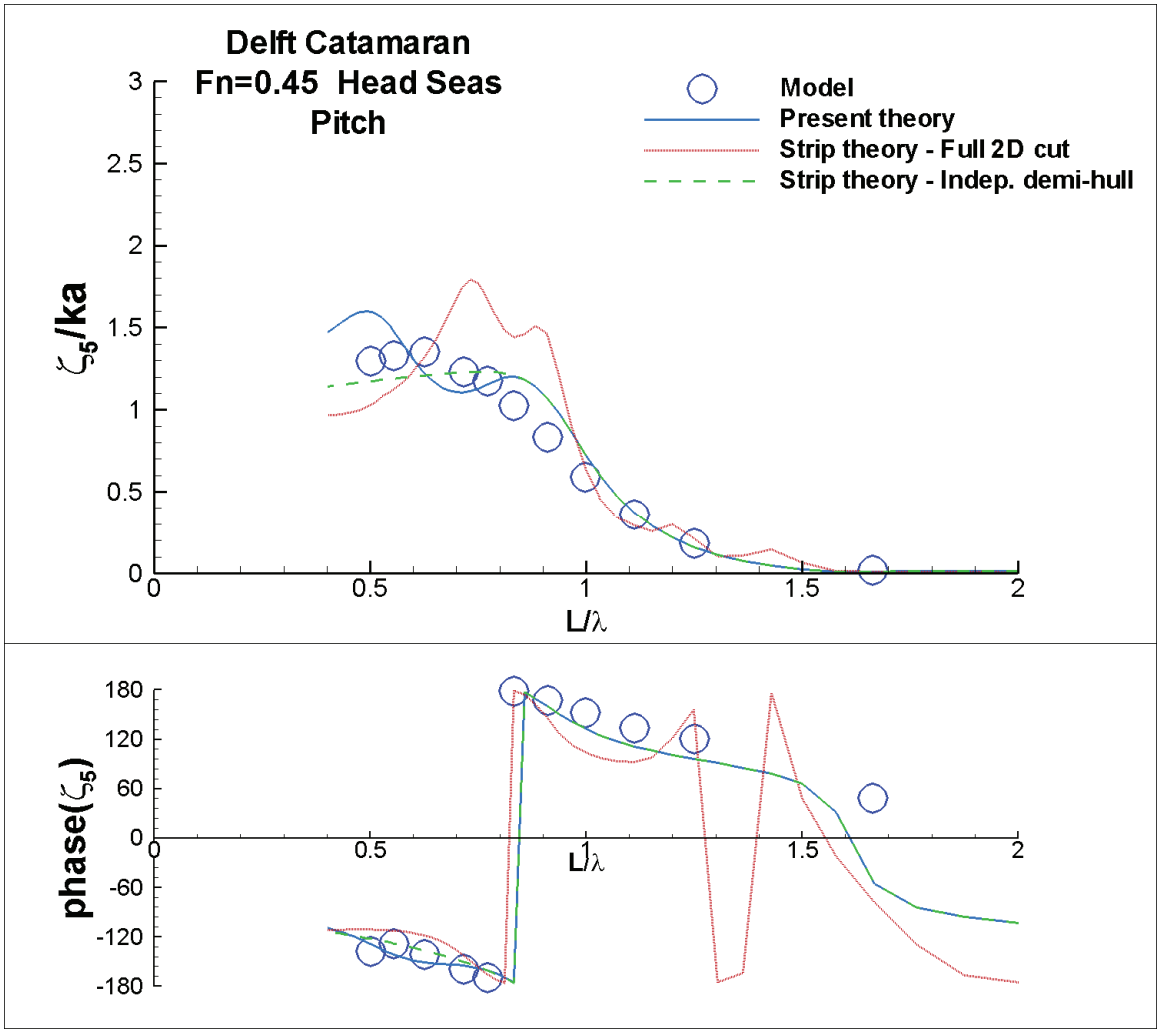

Figure B 8 Delft Catamaran pitch transfer function at Fn=0.45 in head seas

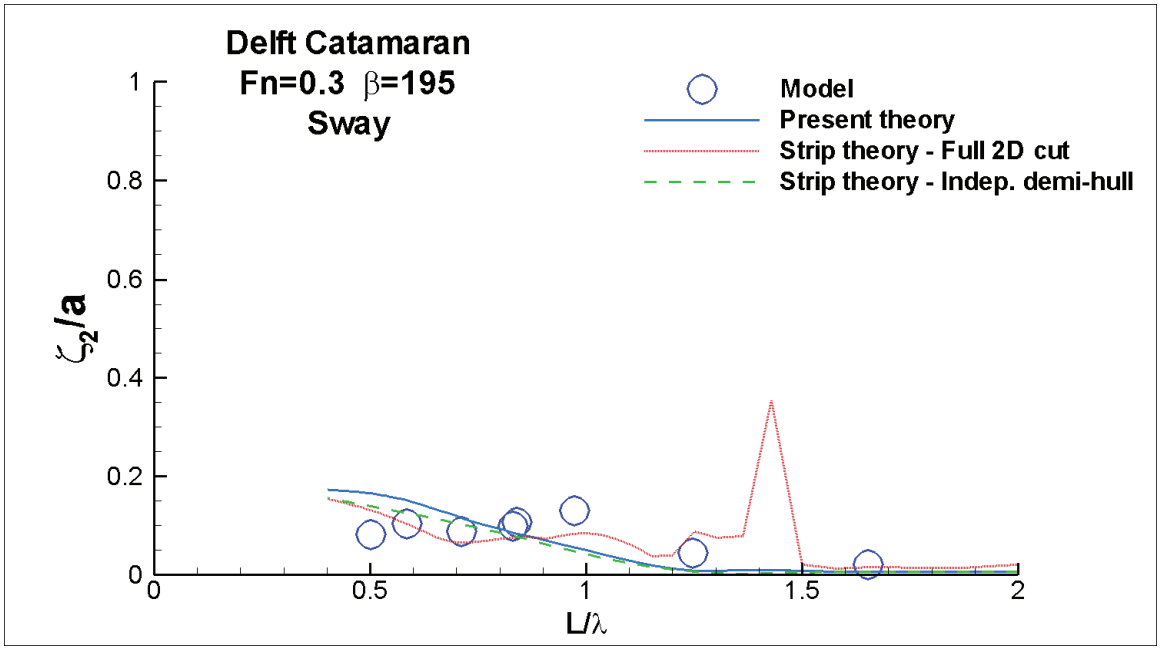

Figure B 9 Delft Catamaran sway transfer function at Fn=0.3, β=195°

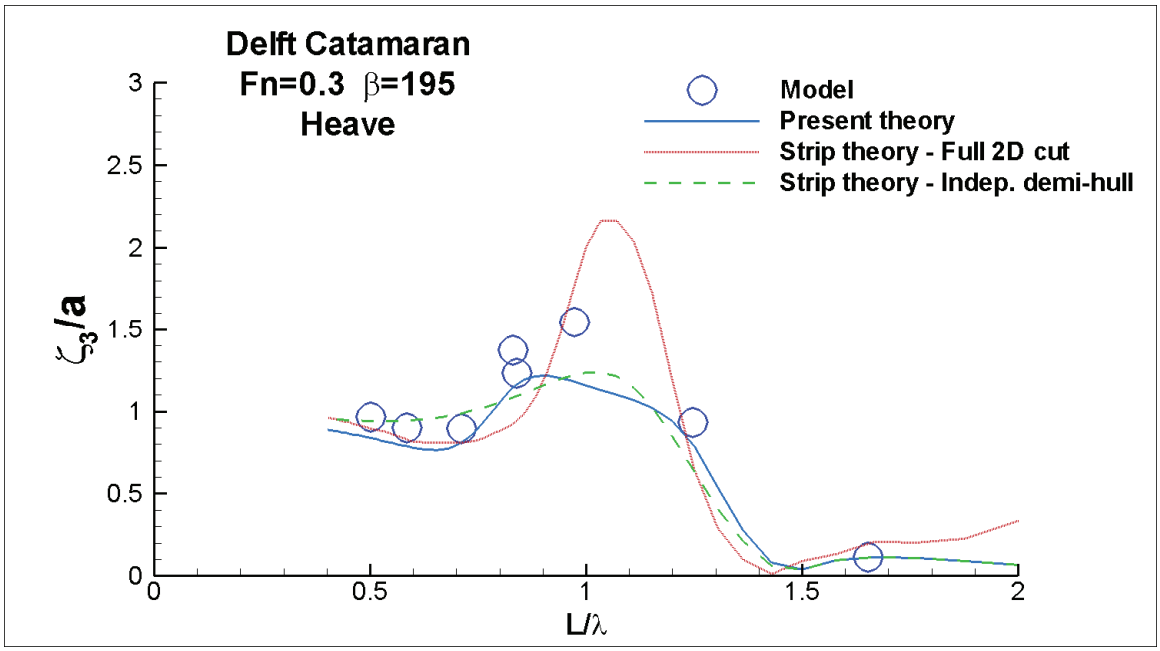

Figure B 10 Delft Catamaran heave transfer function at Fn=0.3, β=195°

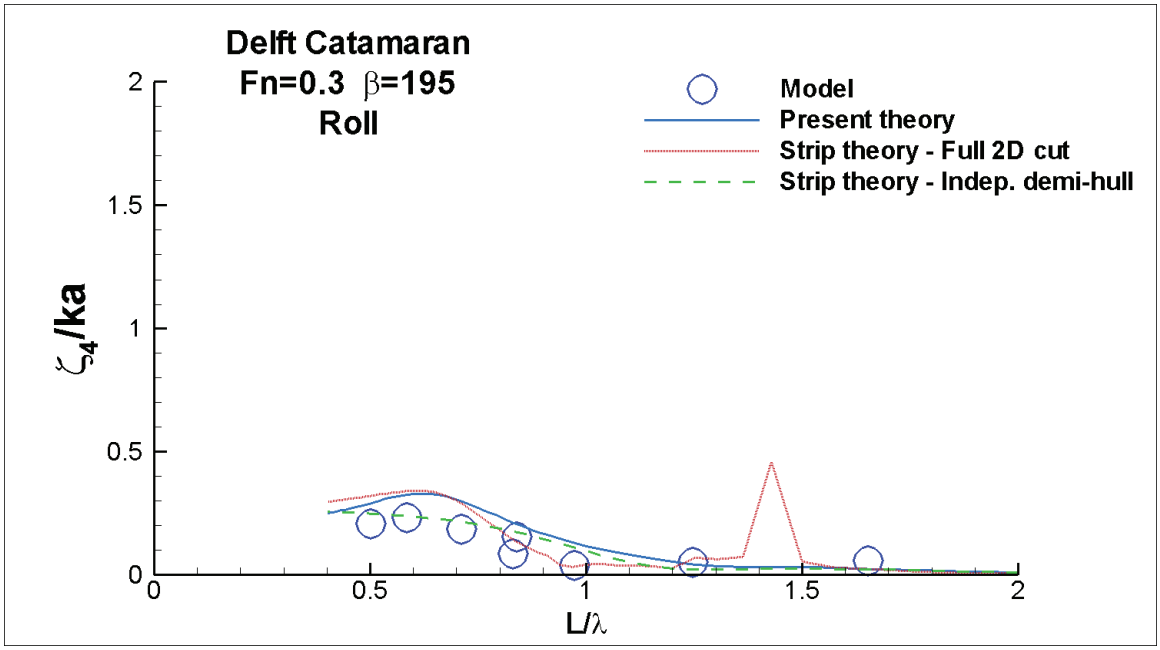

Figure B 11 Delft Catamaran roll transfer function at Fn=0.3, β=195°

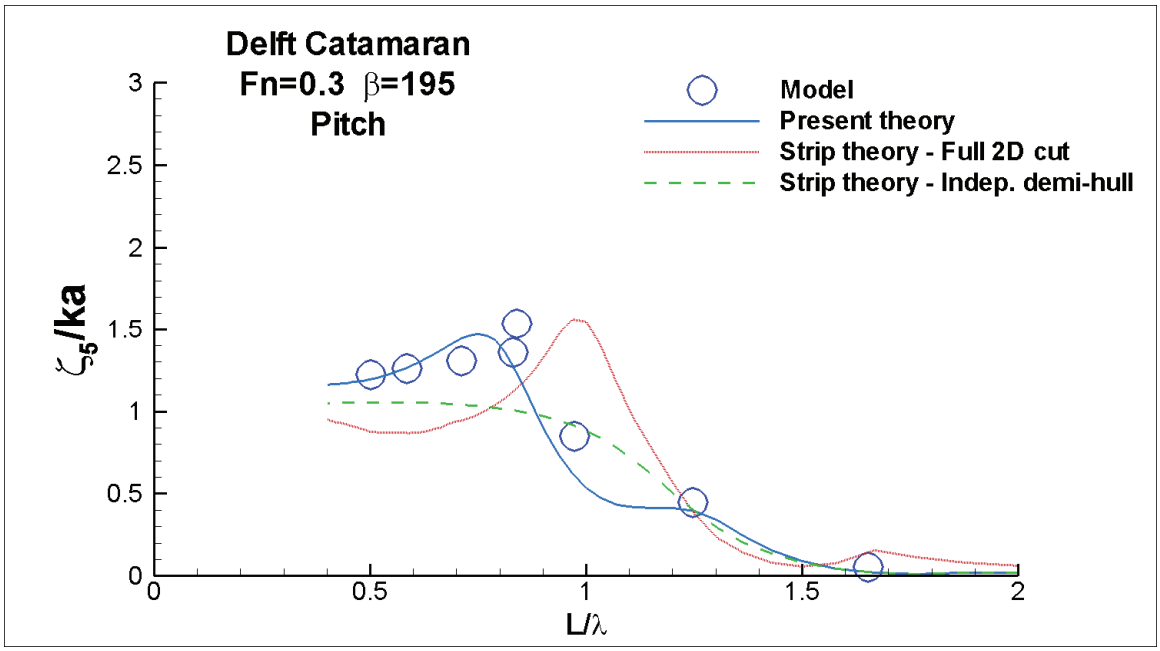

Figure B 12 Delft Catamaran pitch transfer function at Fn=0.3, β=195°

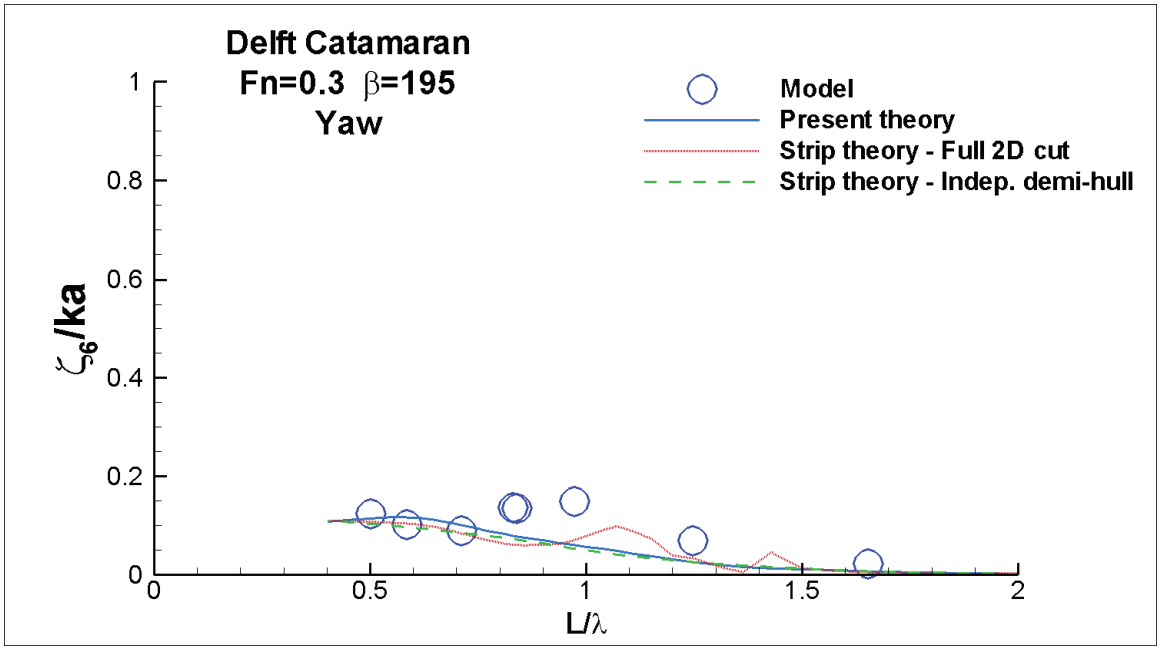

Figure B 13 Delft Catamaran yaw transfer function at Fn=0.3, β=195°

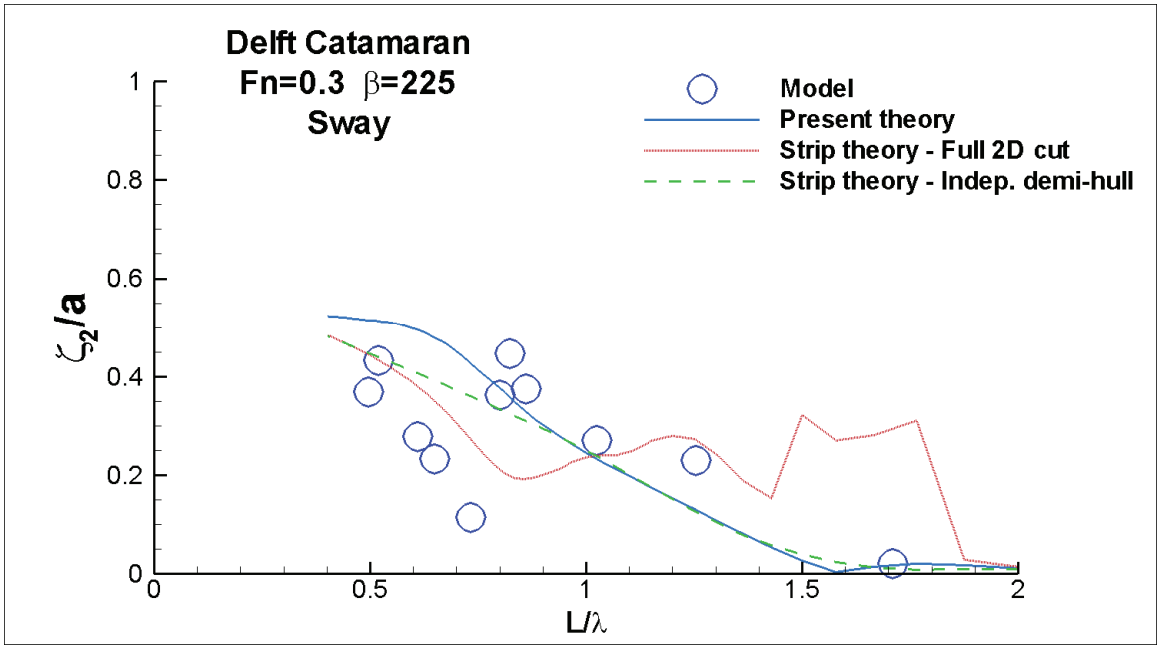

Figure B 14 Delft Catamaran sway transfer function at Fn=0.3, β=225°

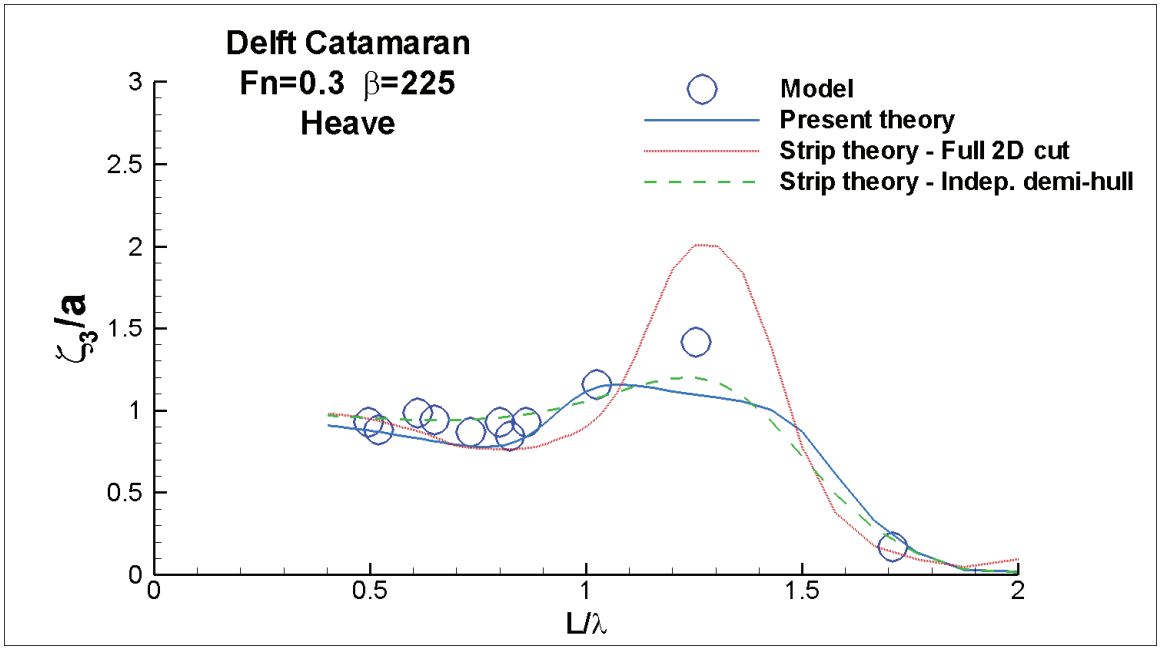

Figure B 15 Delft Catamaran heave transfer function at Fn=0.3, β=225°

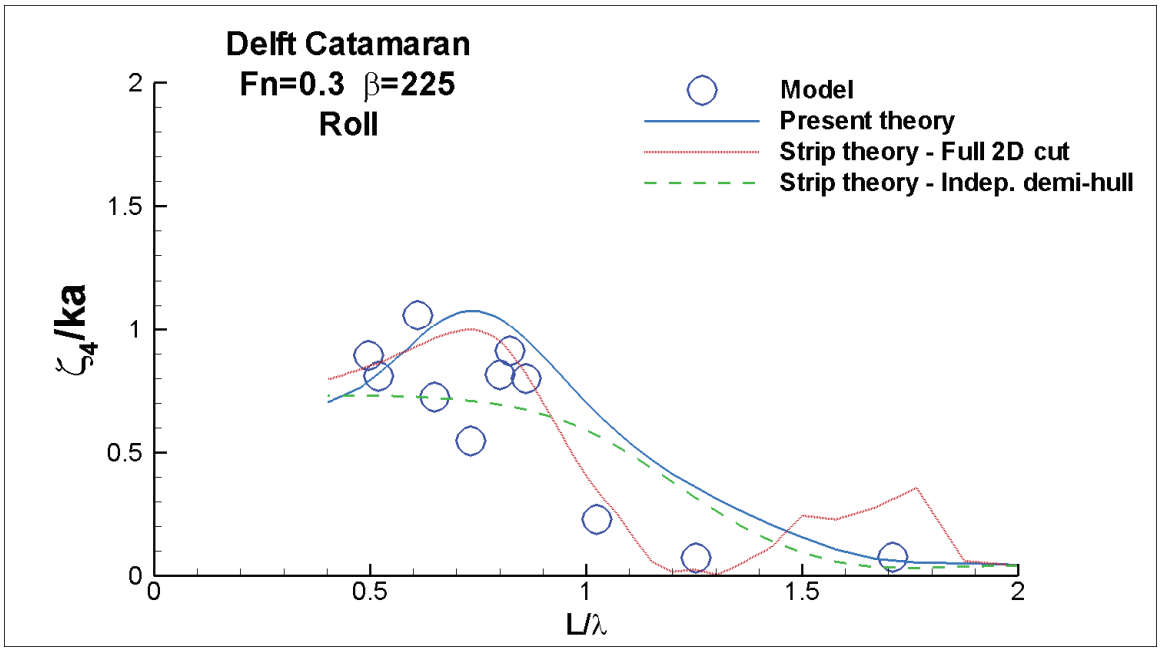

Figure B 16 Delft Catamaran roll transfer function at Fn=0.3, β=225°

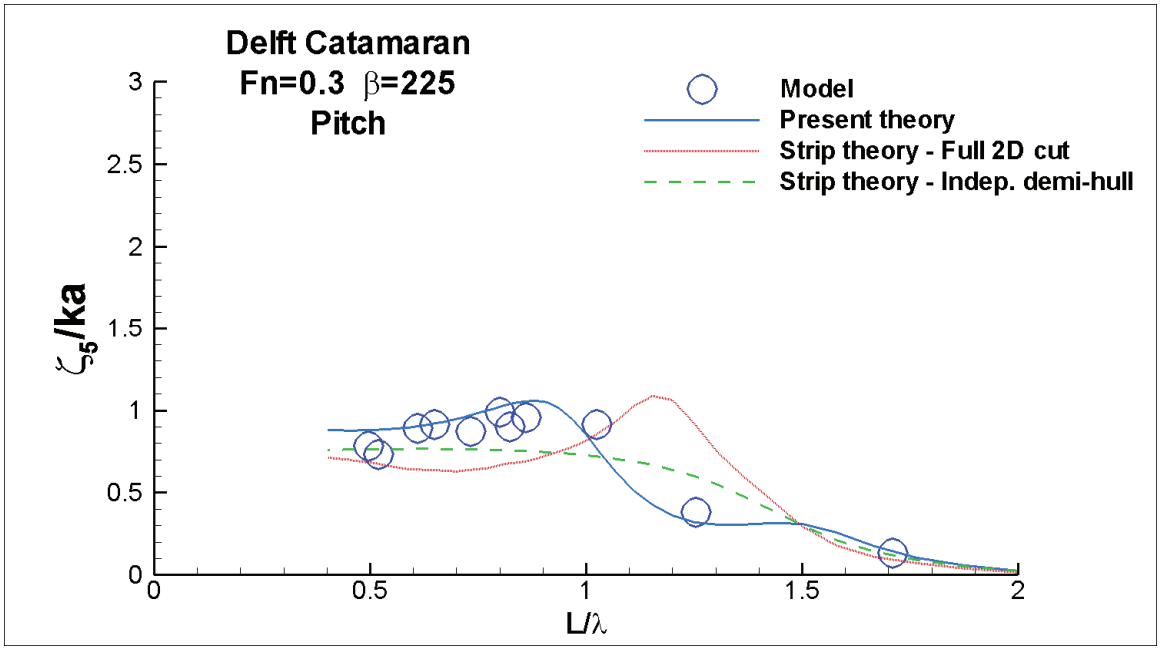

Figure B 17 Delft Catamaran pitch transfer function at Fn=0.3, β=225°

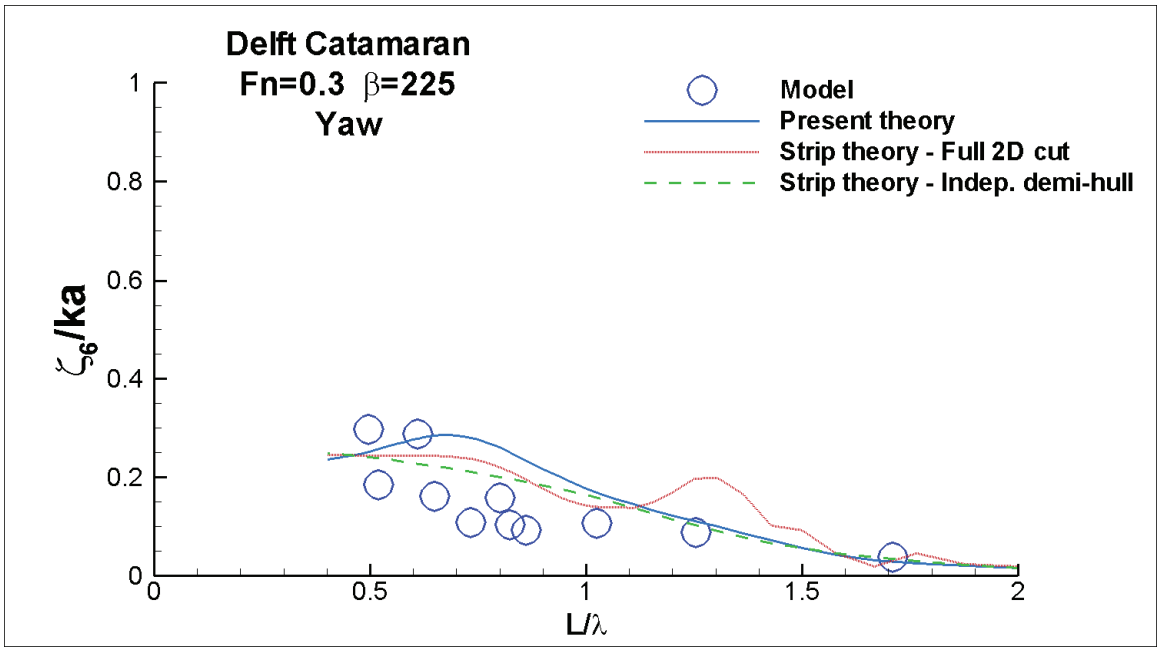

Figure B 18 Delft Catamaran yaw transfer function at Fn=0.3, β=225°

Appendix C

Kashiwagi Catamaran Hydrodynamic Coefficients

Appendix C contains the full set of hydrodynamic coefficient comparisons for the Kashiwagi Catamaran. The added mass and damping plots are given in Figure C 1 through Figure C 8.

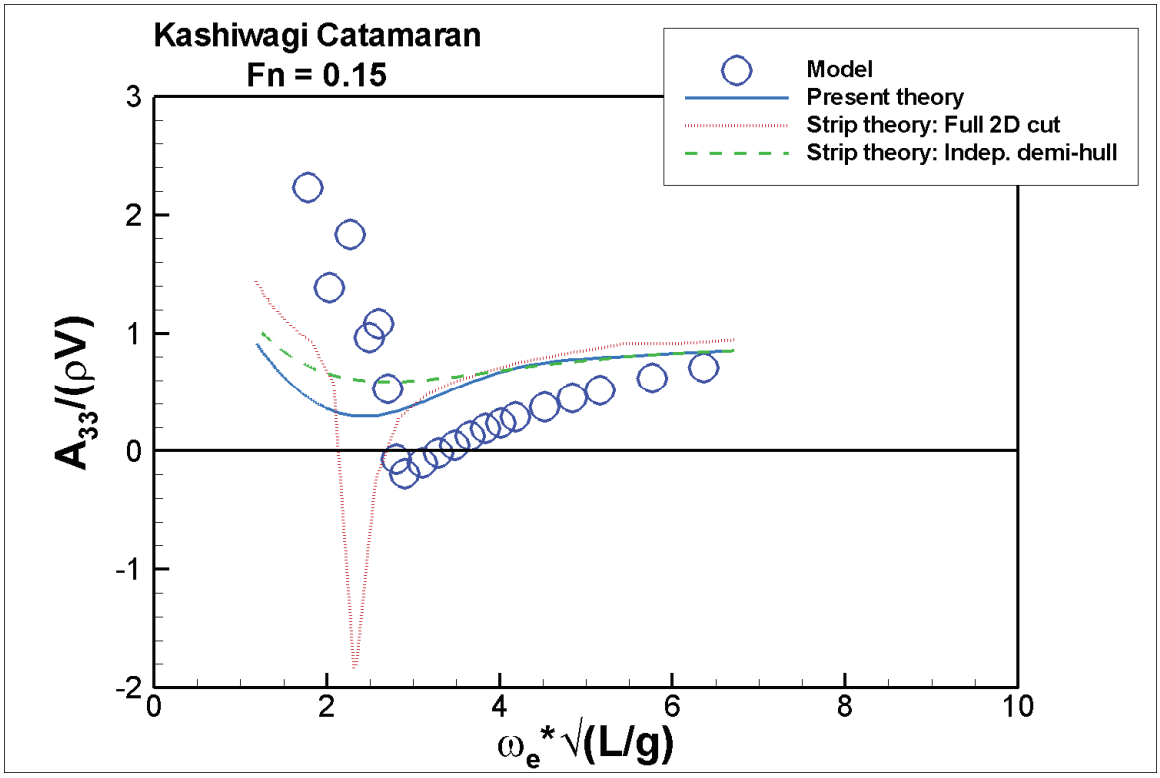

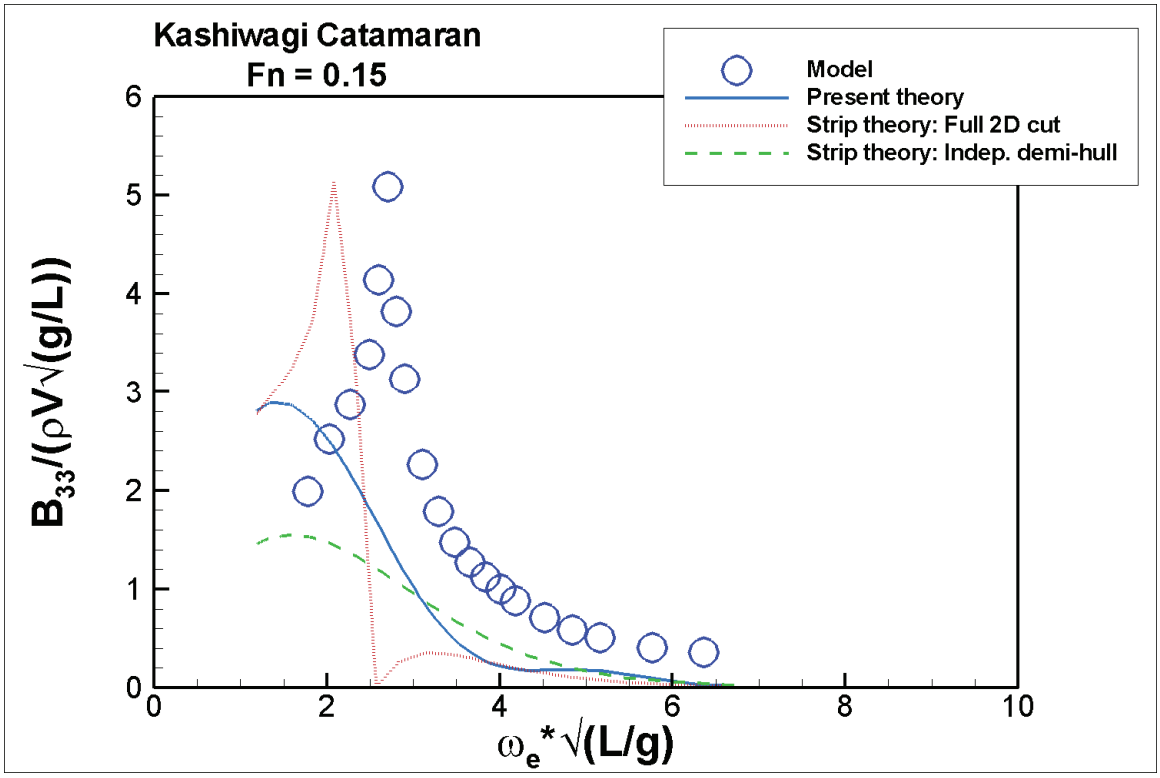

Figure C 1 Kashiwagi Catamaran – A_{33} and B_{33} at Fn=0.15

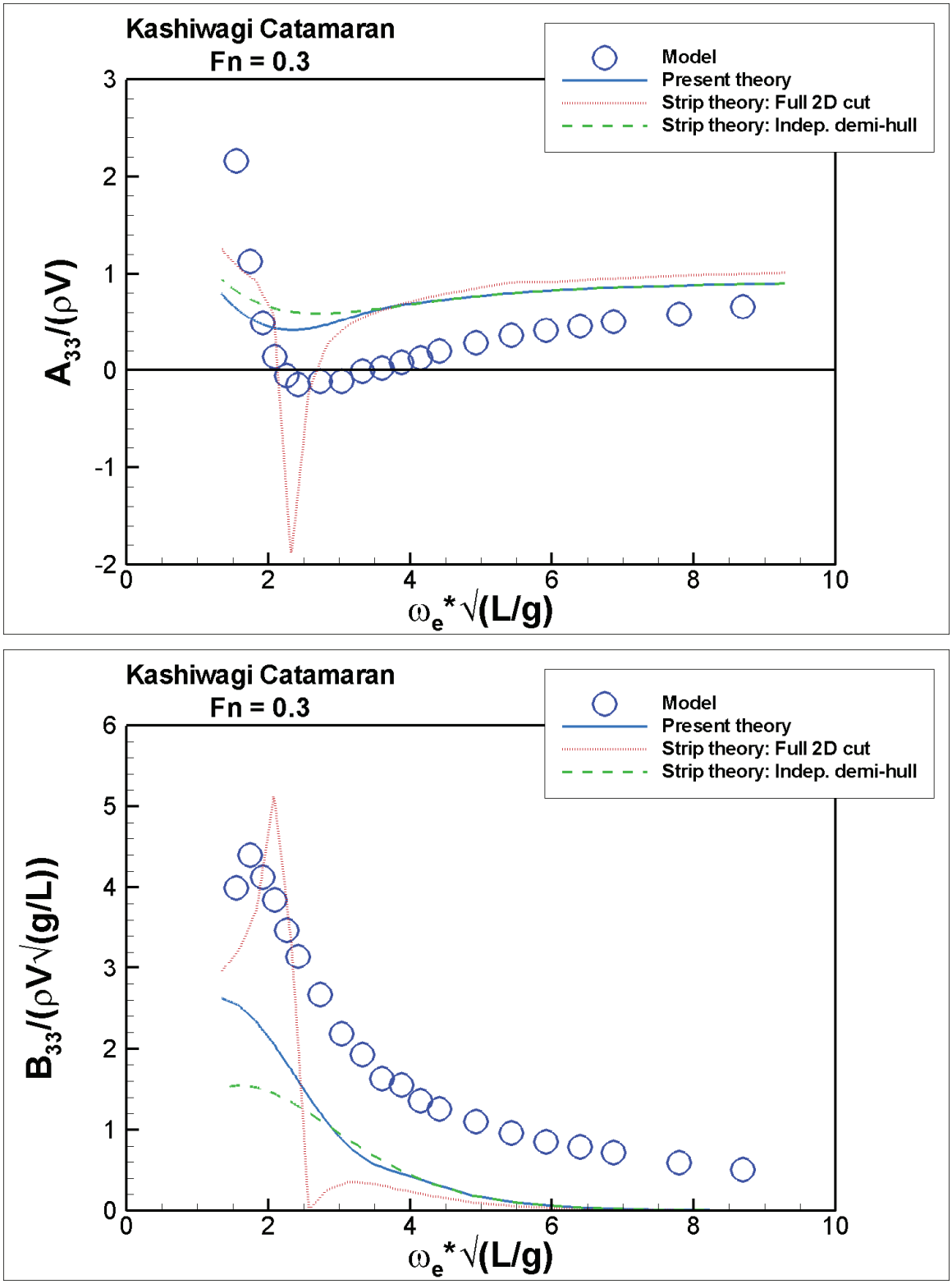

Figure C 2 Kashiwagi Catamaran – A_{33} and B_{33} at Fn=0.3

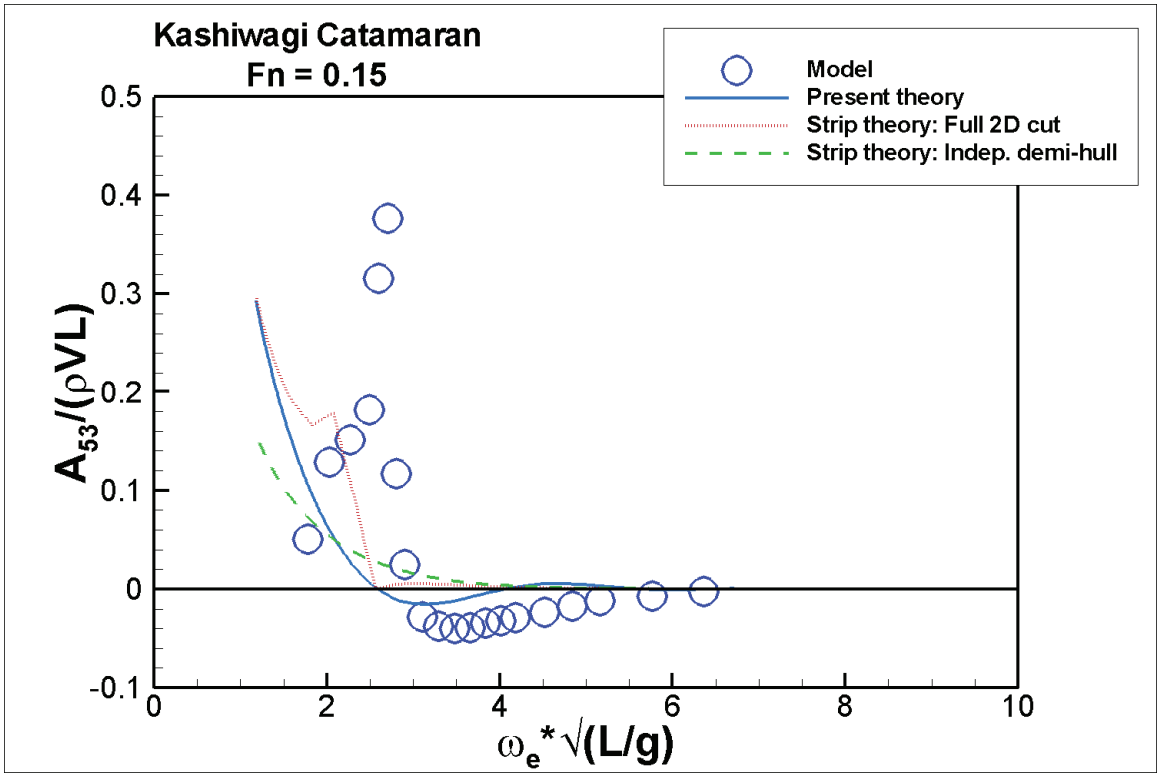

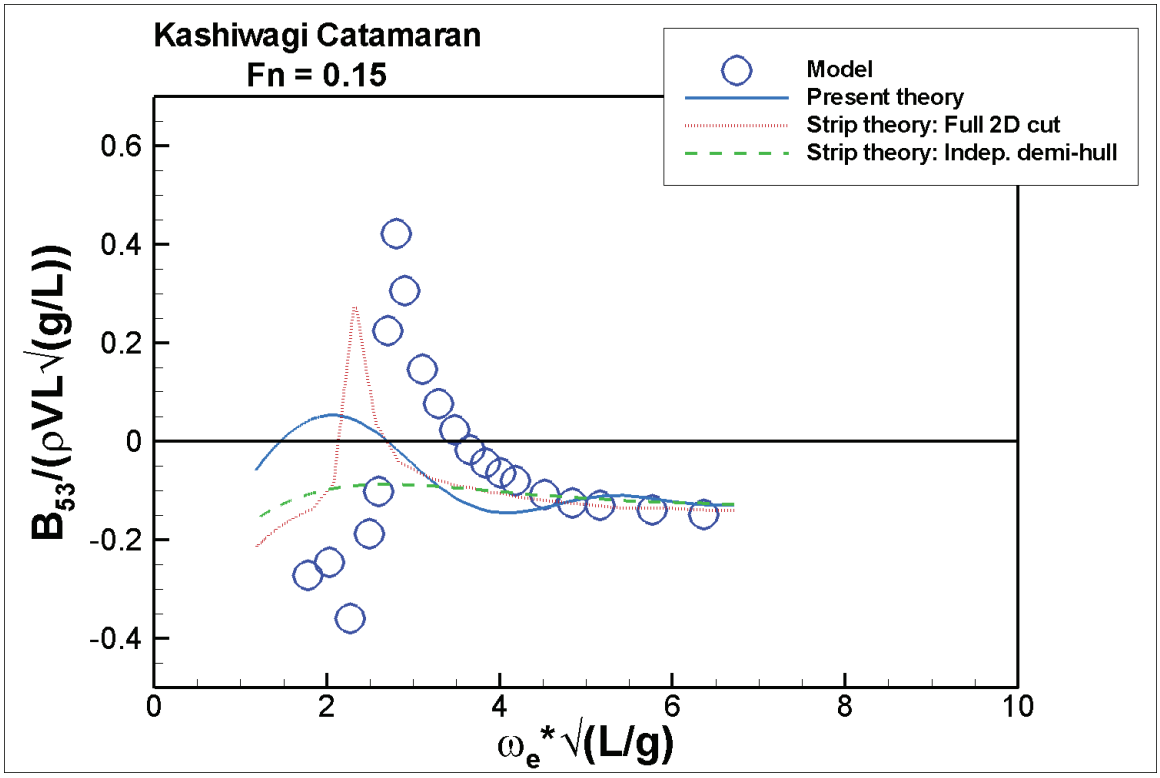

Figure C 3 Kashiwagi Catamaran – A_{53} and B_{53} at Fn=0.15

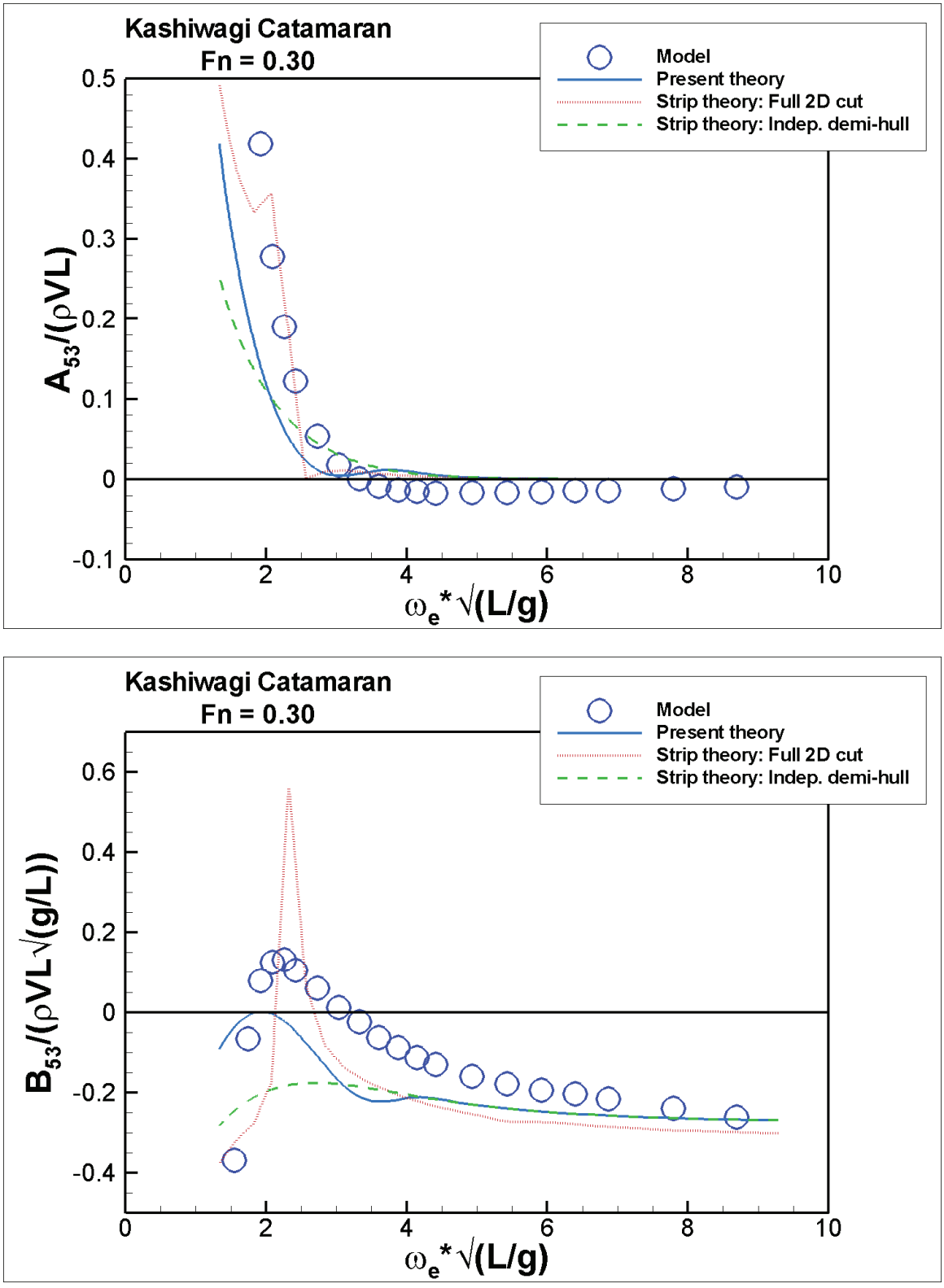

Figure C 4 Kashiwagi Catamaran – A_{53} and B_{53} at Fn=0.3

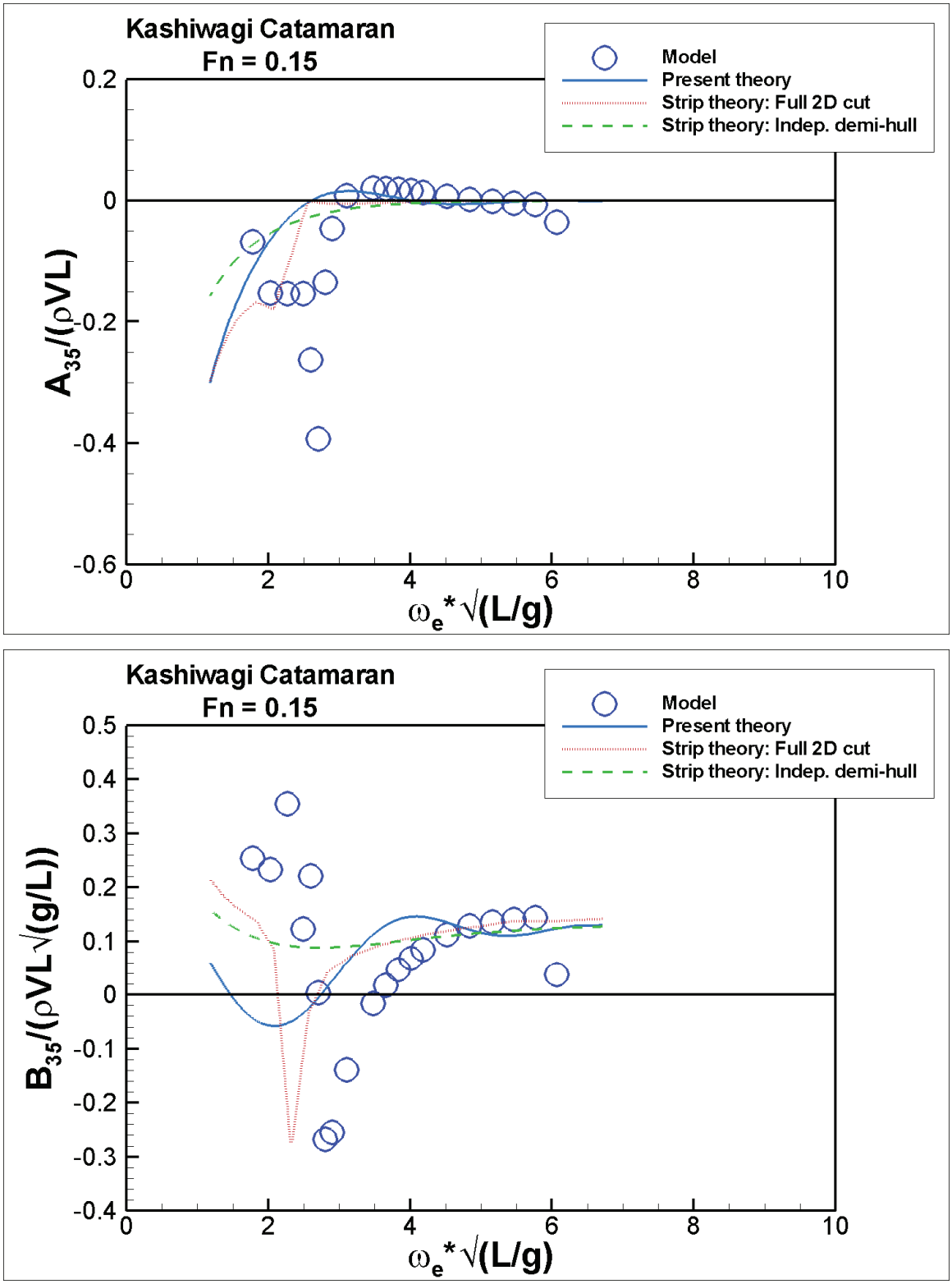

Figure C 5 Kashiwagi Catamaran – A_{35} and B_{35} at Fn=0.15

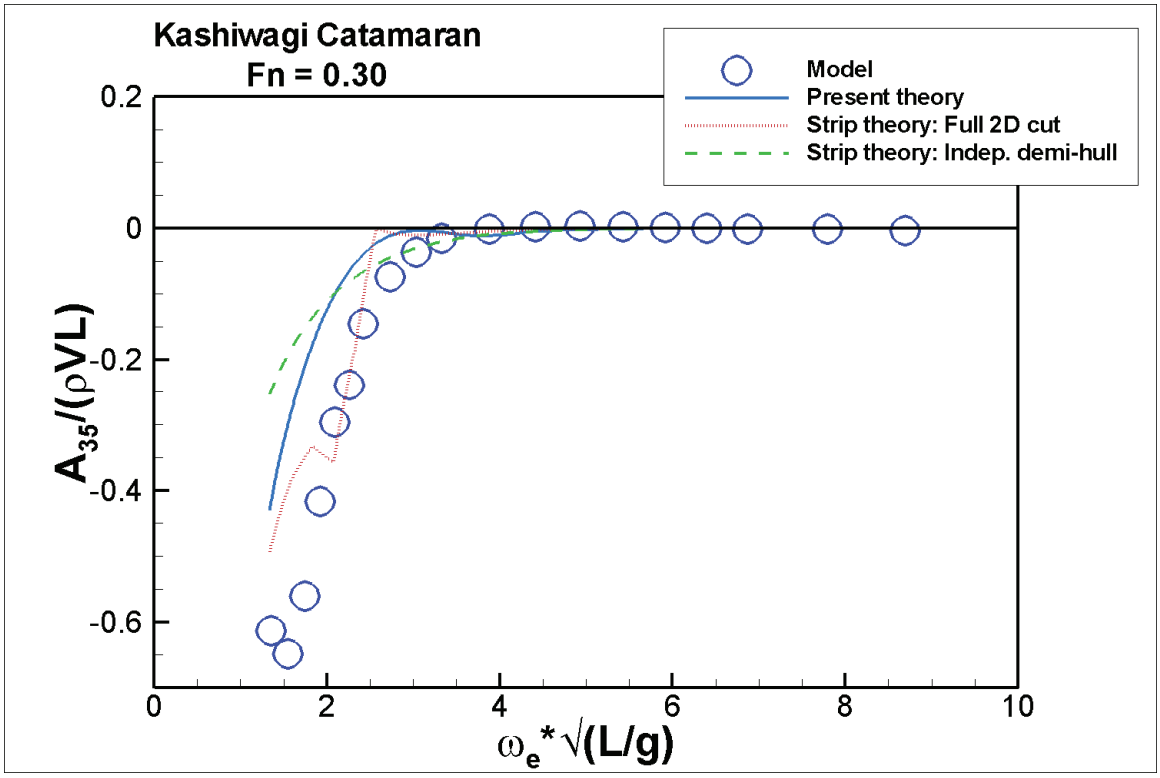

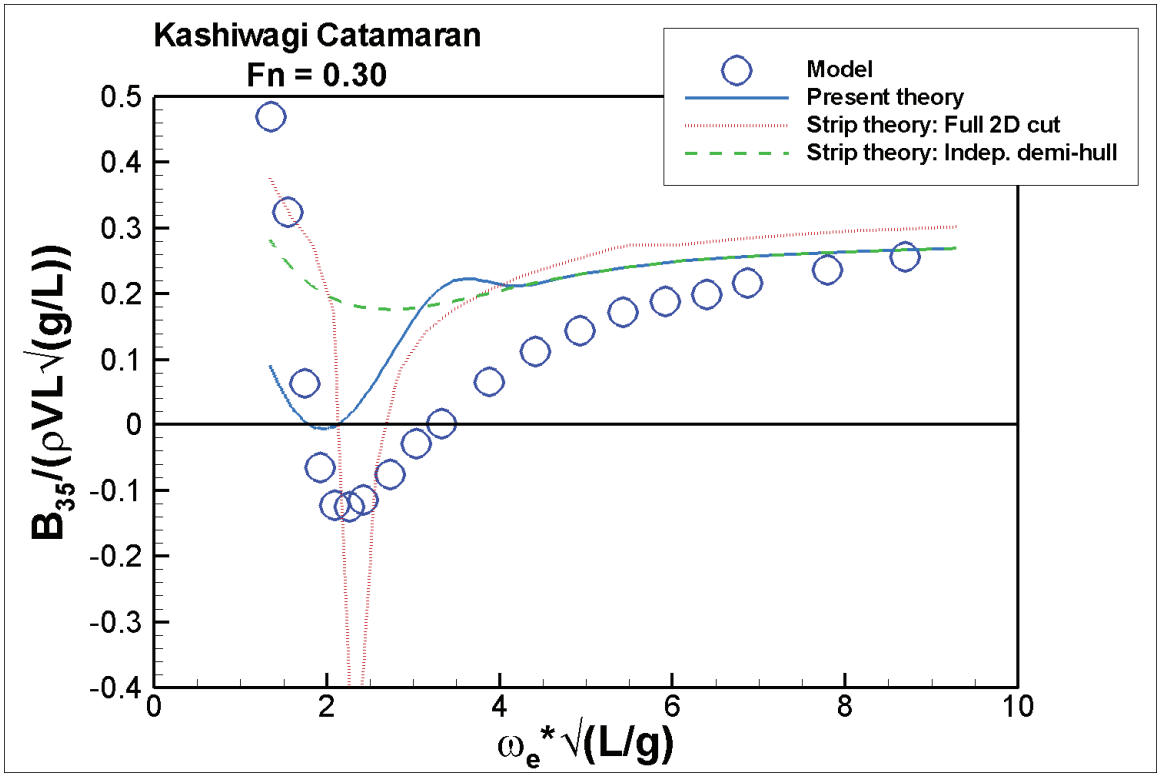

Figure C 6 Kashiwagi Catamaran – A_{35} and B_{35} at Fn=0.3

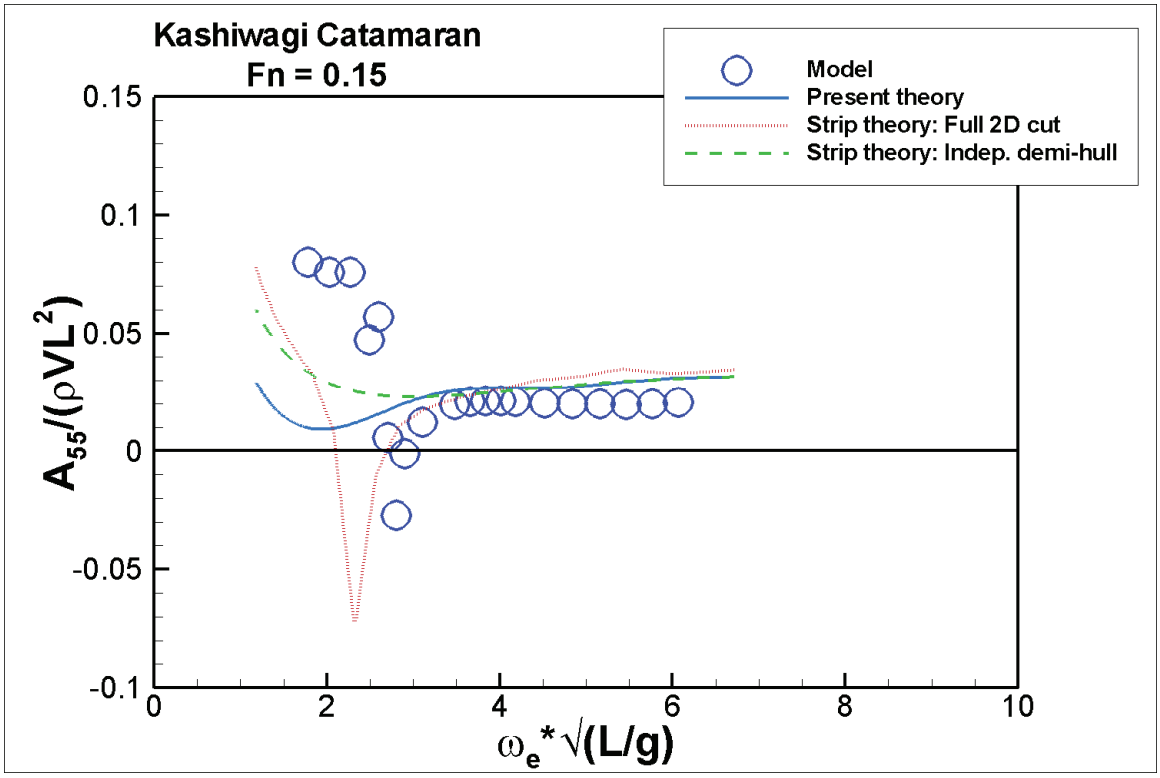

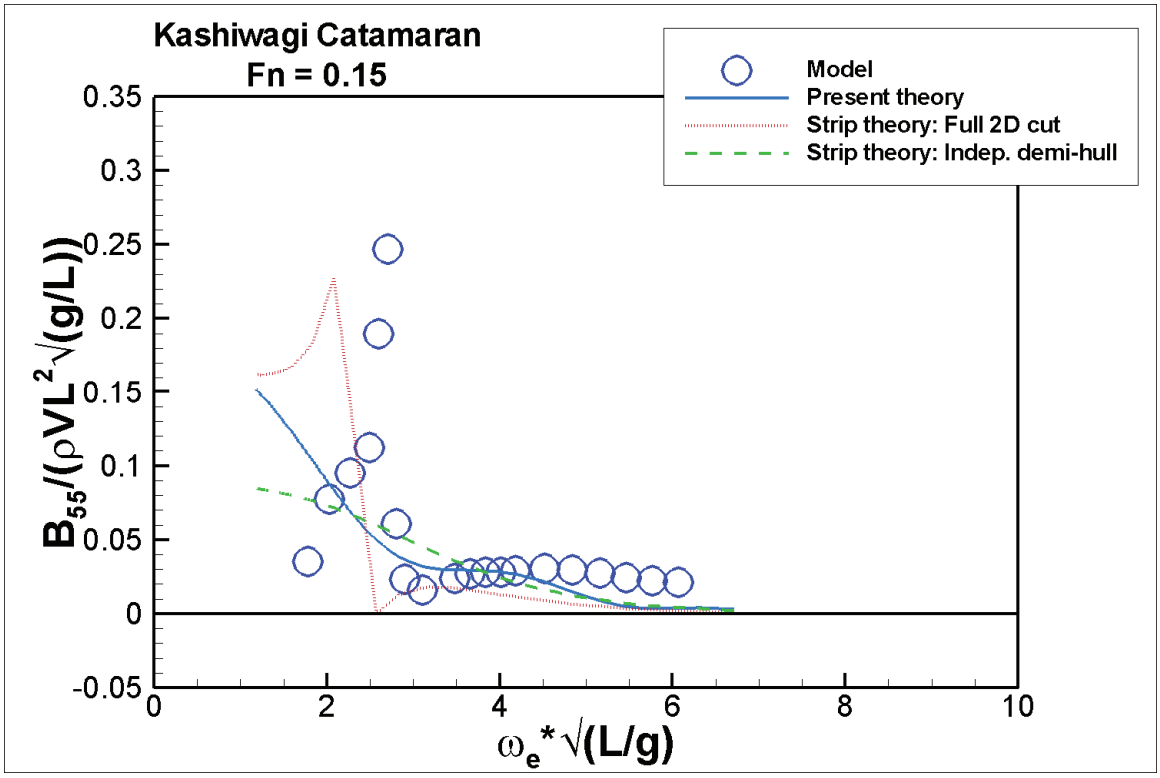

Figure C 7 Kashiwagi Catamaran – A_{55} and B_{55} at Fn=0.15

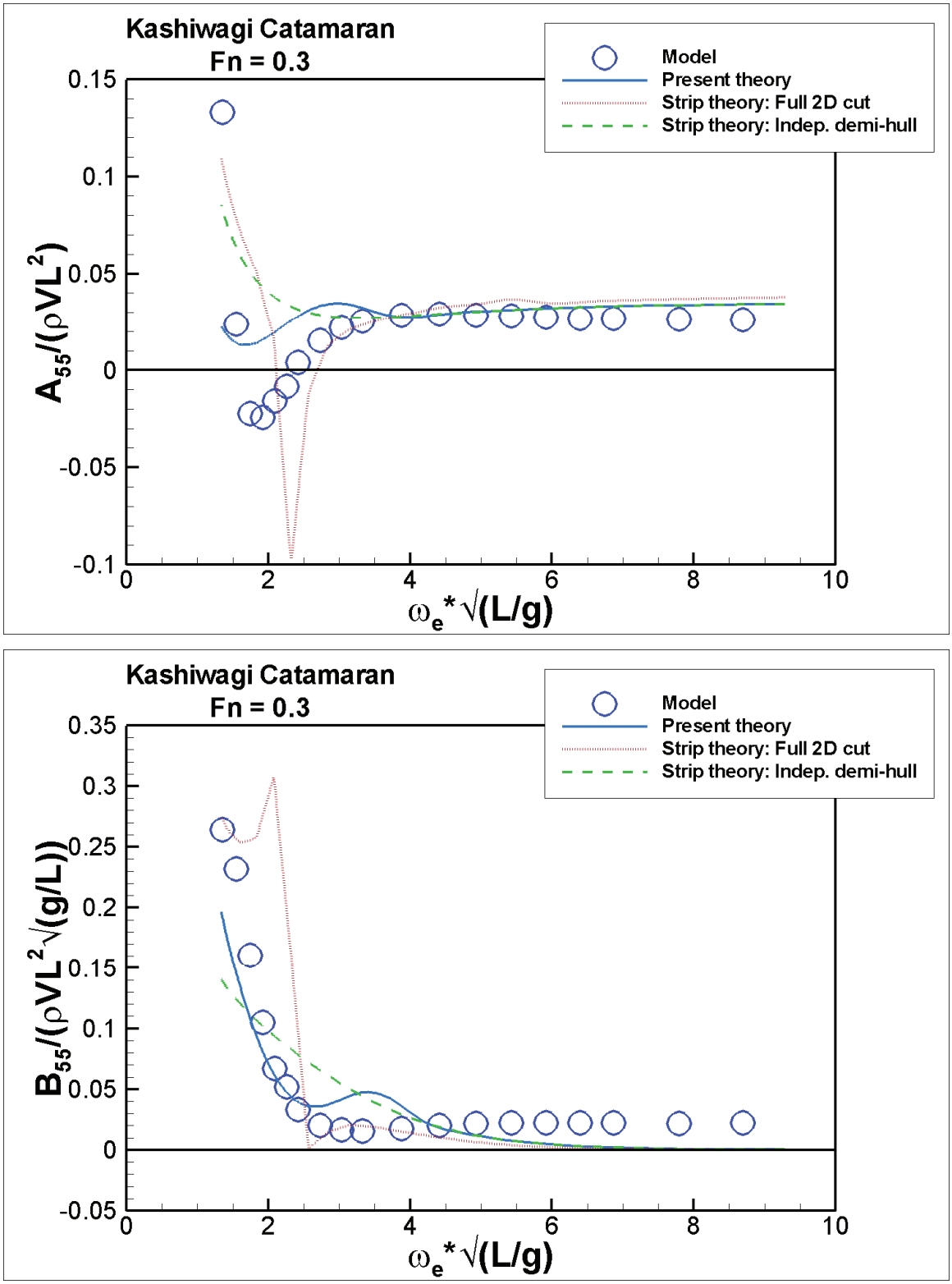

Figure C 8 Kashiwagi Catamaran – A_{55} and B_{55} at Fn=0.3

Appendix D

HSSL Trimaran Motion Transfer Functions

Appendix D contains the full set of motion transfer function comparisons for the HSSL Trimaran. The transfer function plots are given in Figure D 1 through Figure D 12.

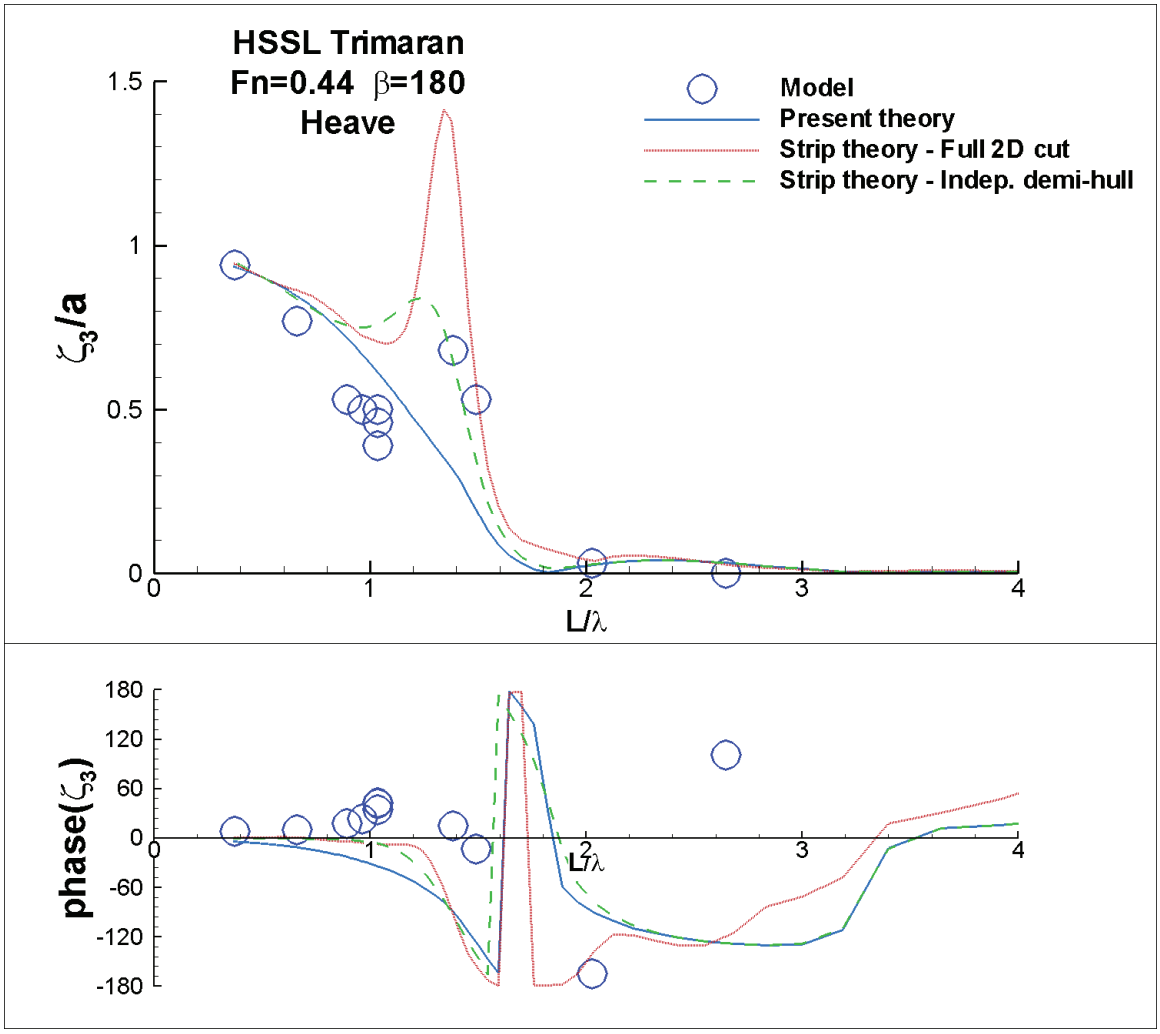

Figure D 1 HSSL Trimaran heave transfer function at Fn=0.44 in head seas

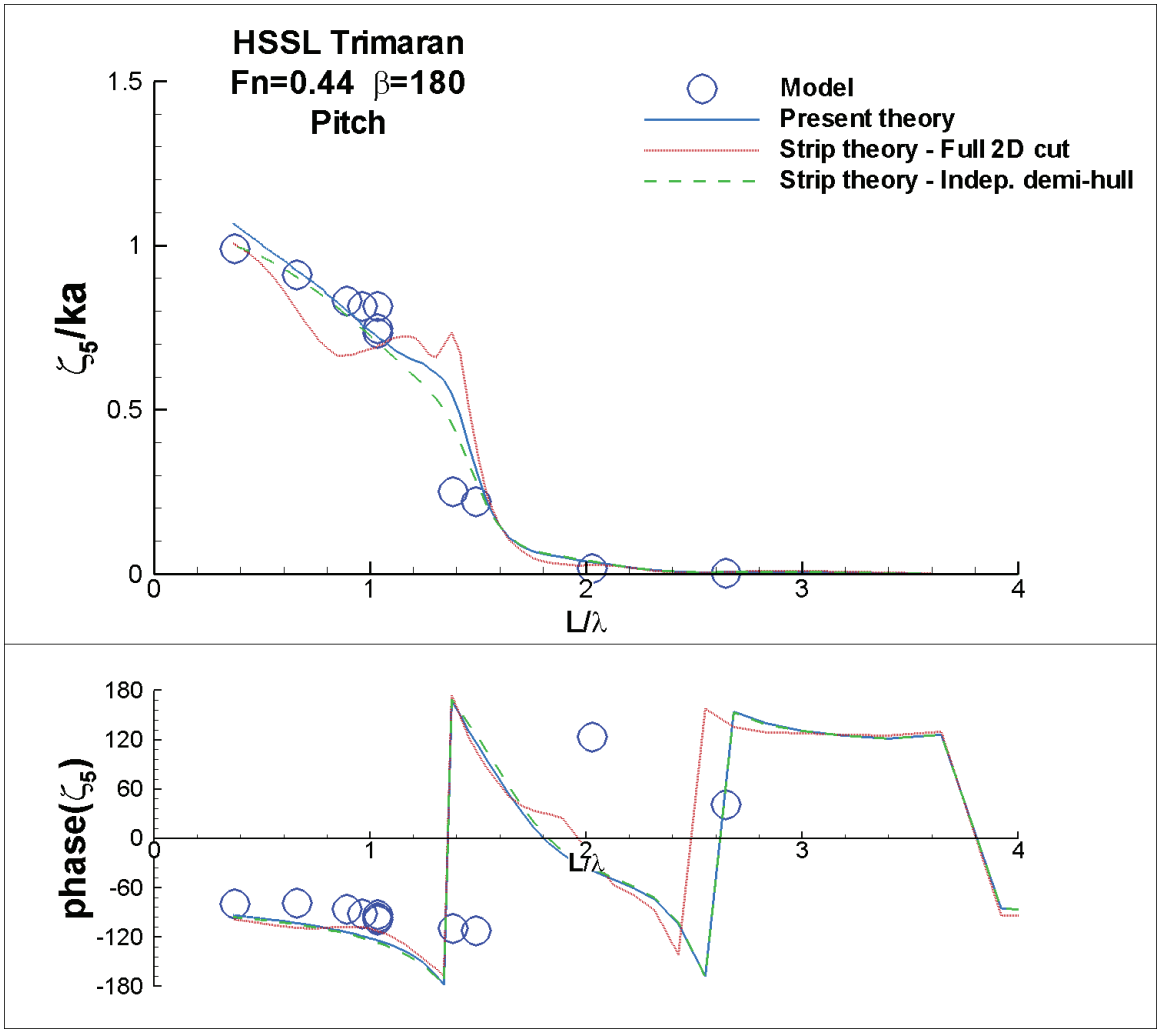

Figure D 2 HSSL Trimaran pitch transfer function at Fn=0.44 in head seas

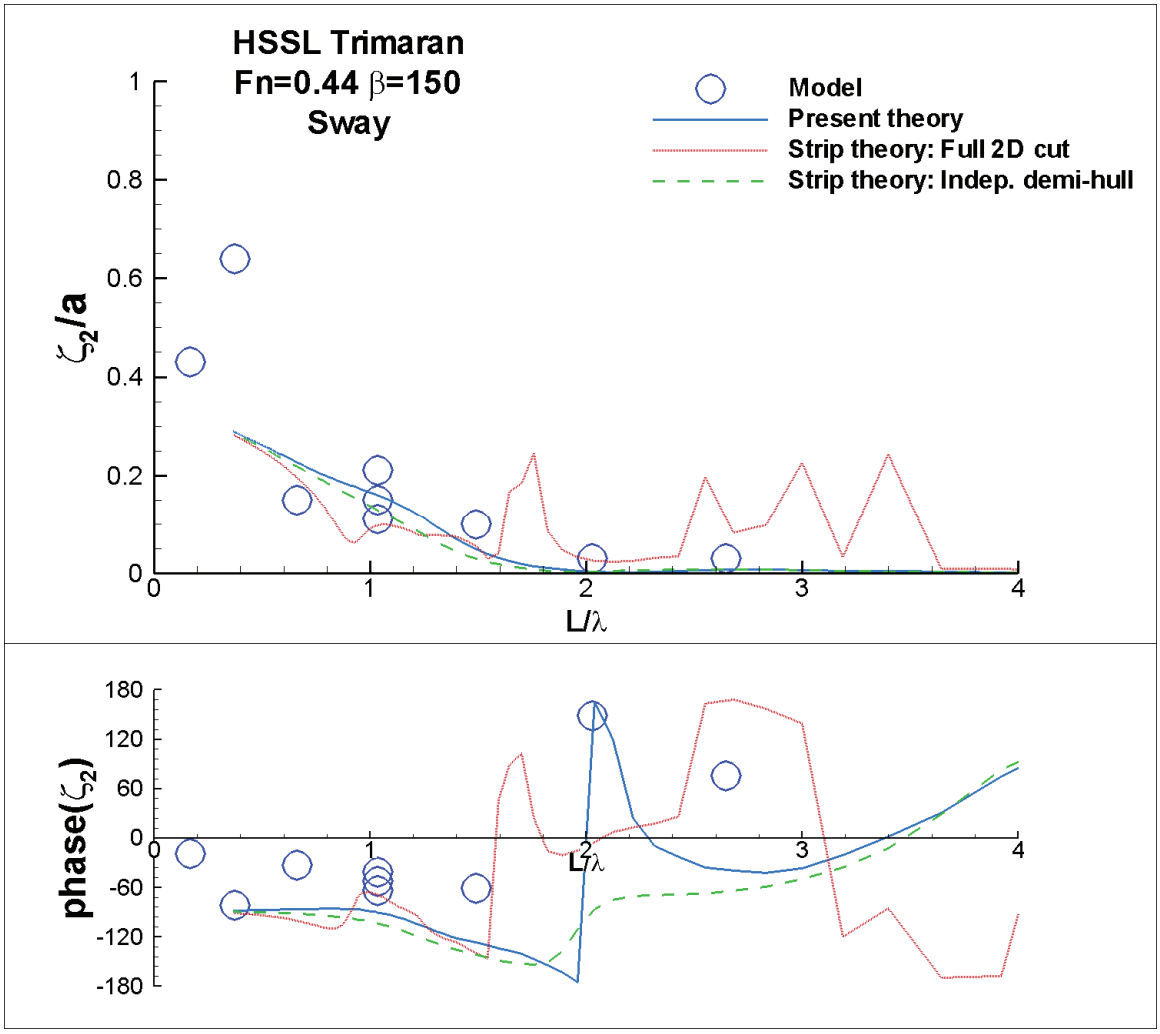

Figure D 3 HSSL Trimaran sway transfer function at Fn=0.44, β=150°

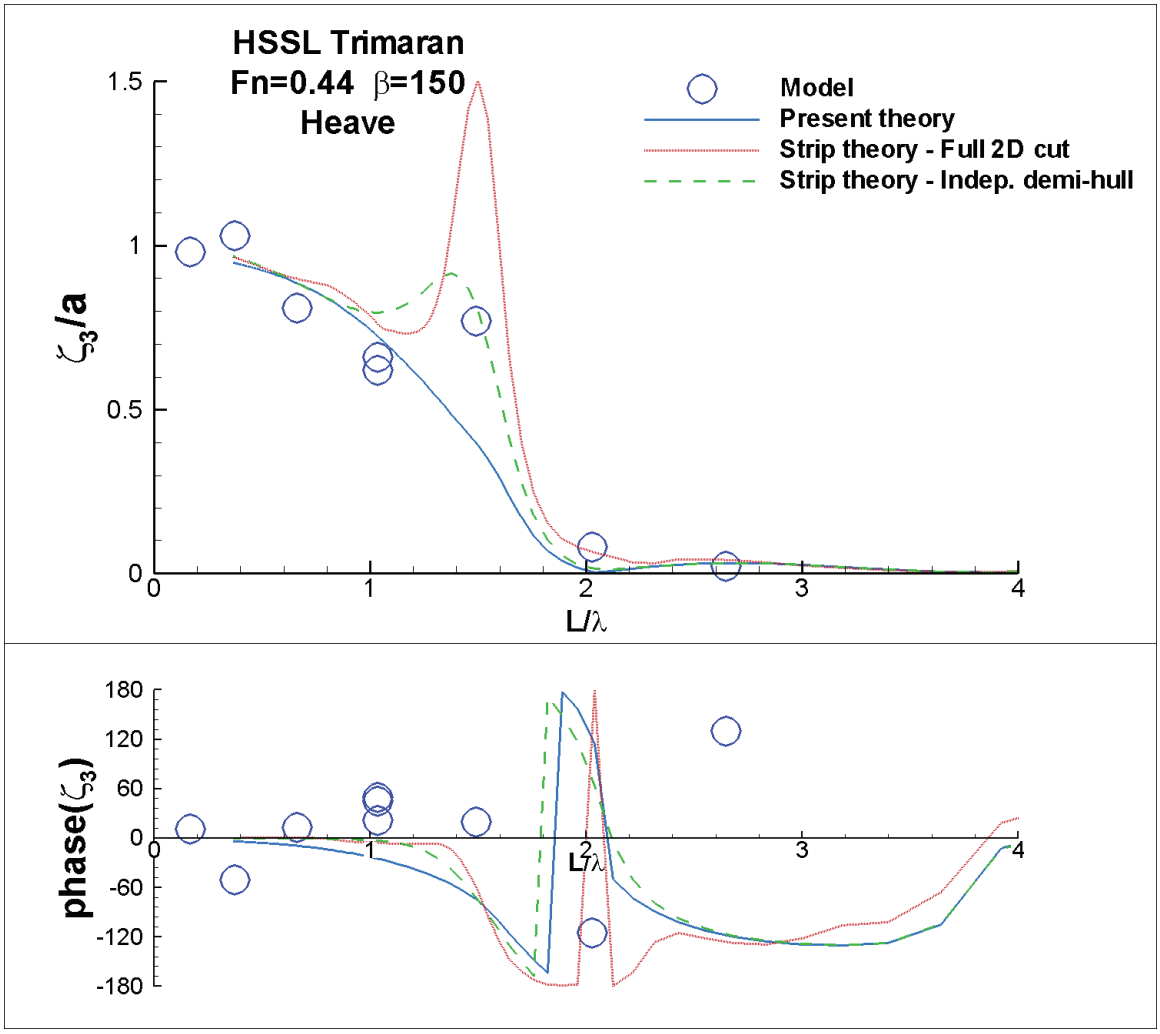

Figure D 4 HSSL Trimaran heave transfer function at Fn=0.44, β=150°

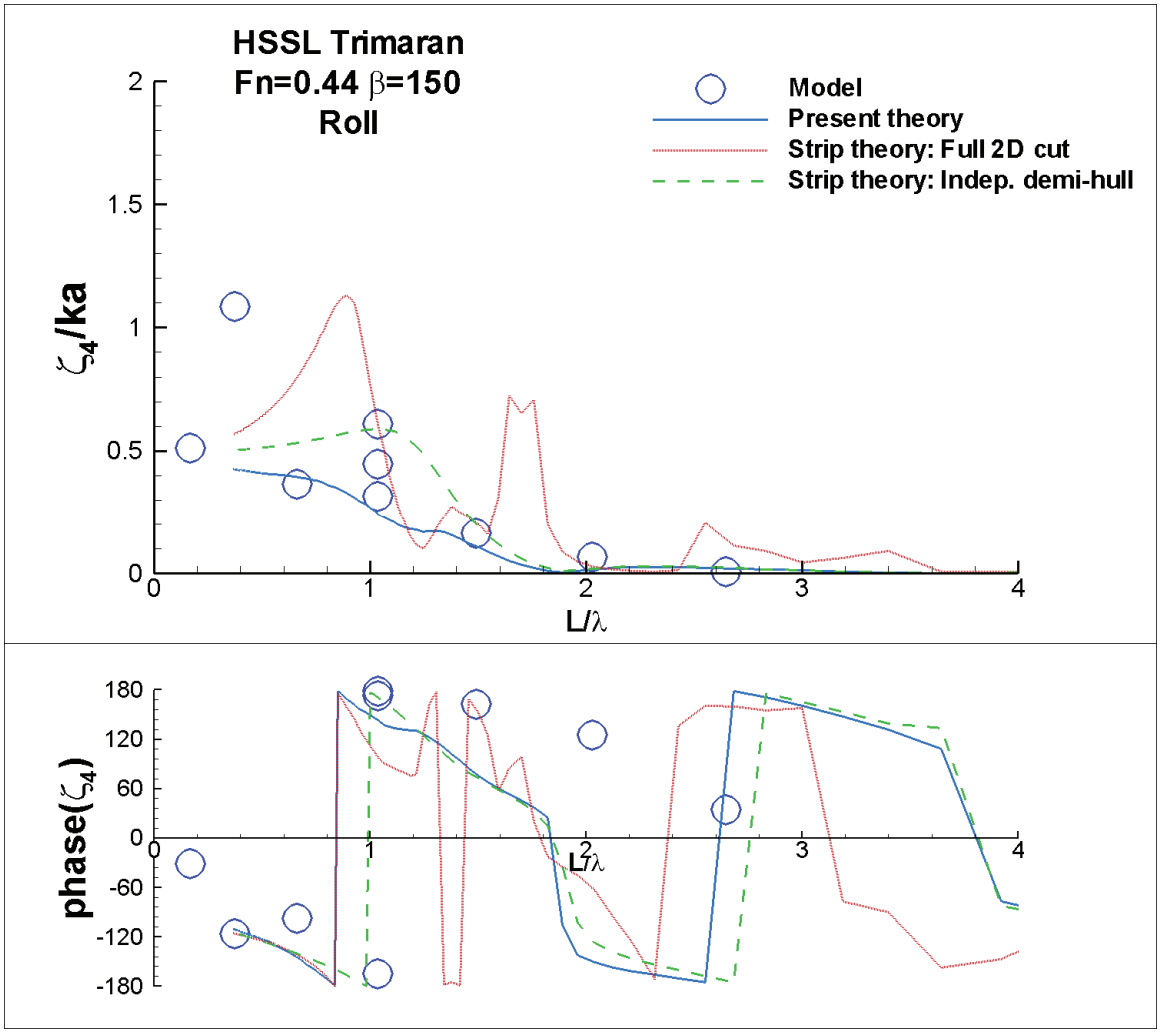

Figure D 5 HSSL Trimaran roll transfer function at Fn=0.44, β=150°

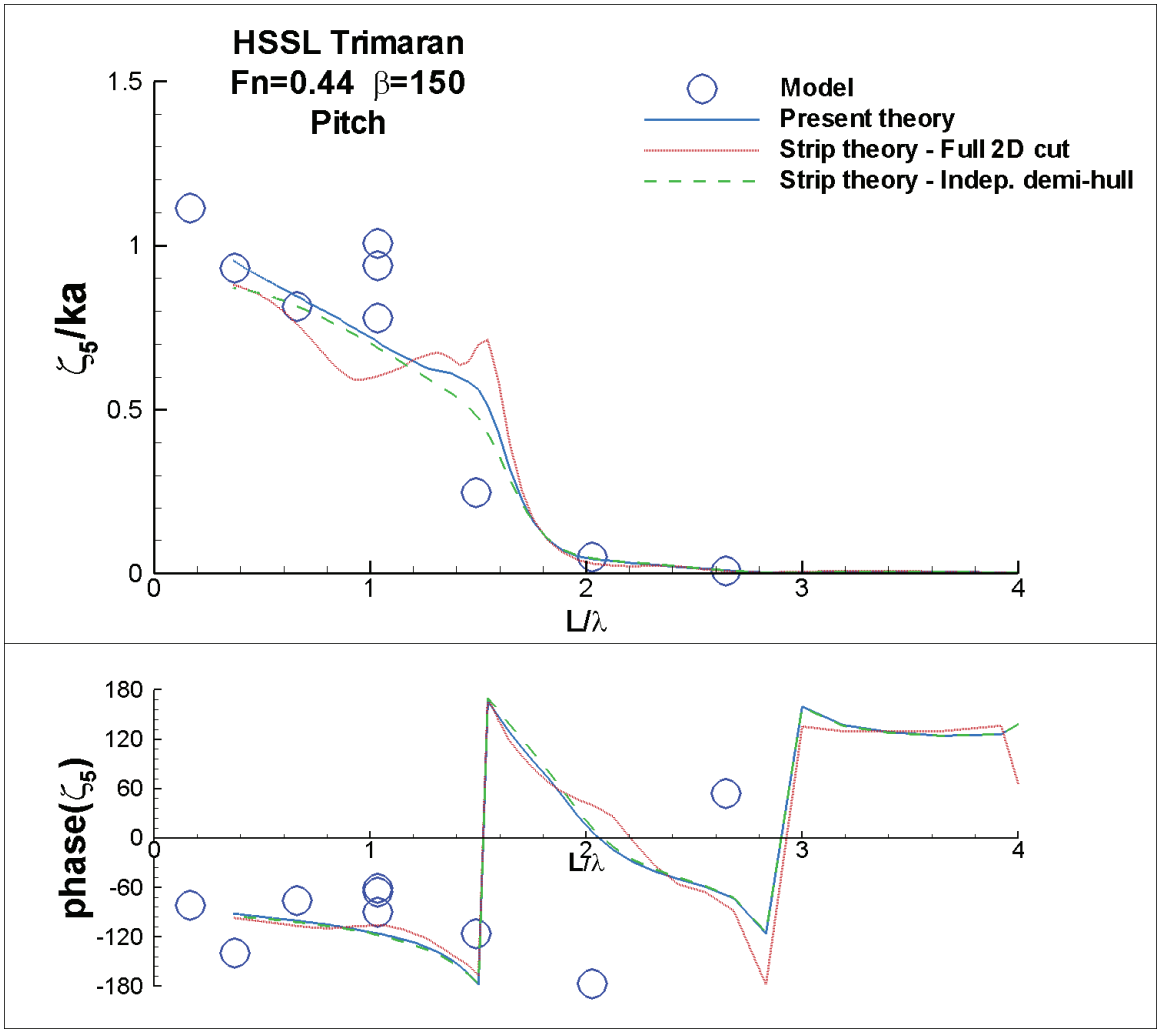

Figure D 6 HSSL Trimaran pitch transfer function at Fn=0.44, β=150°

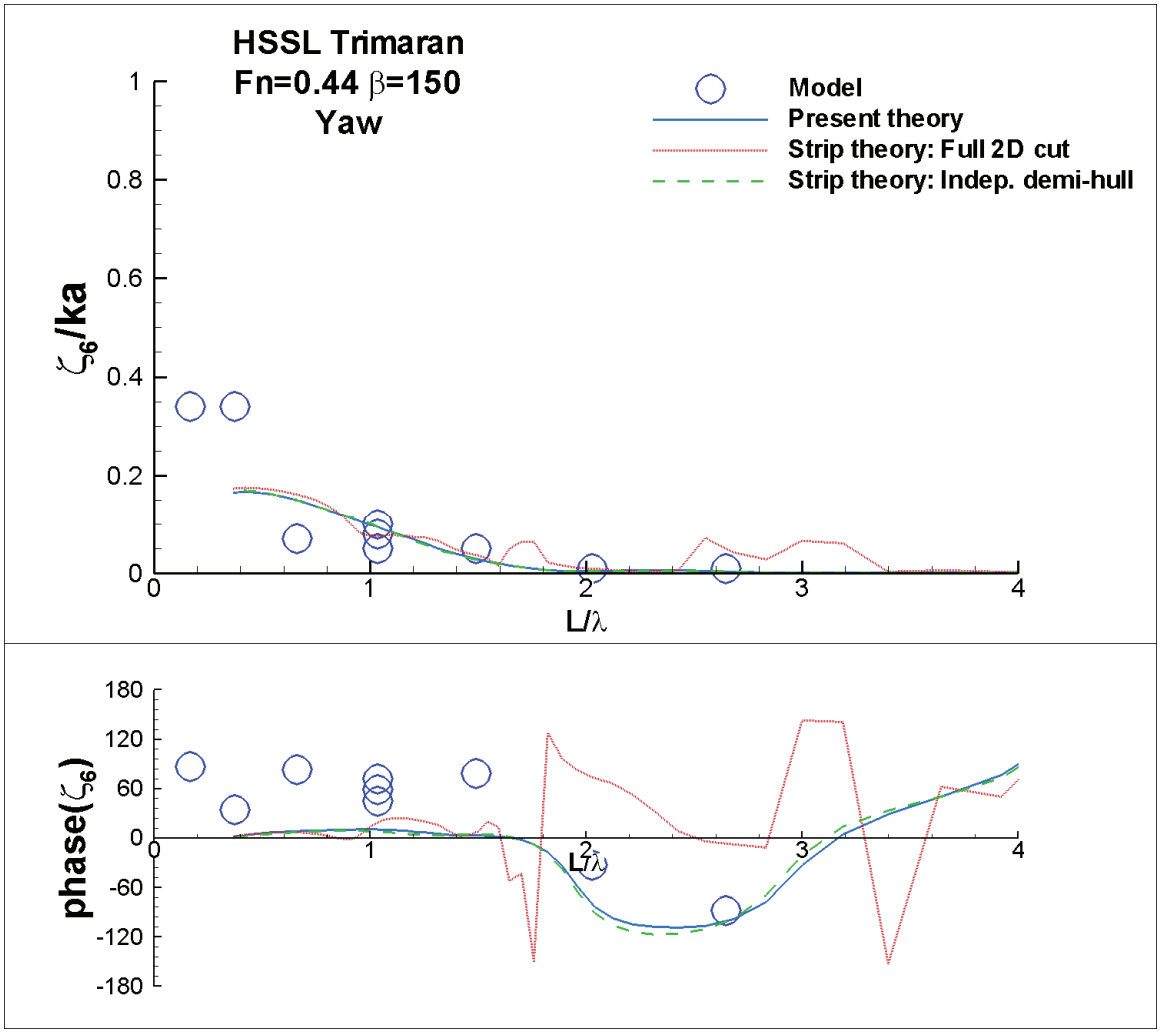

Figure D 7 HSSL Trimaran yaw transfer function at Fn=0.44, β=150°

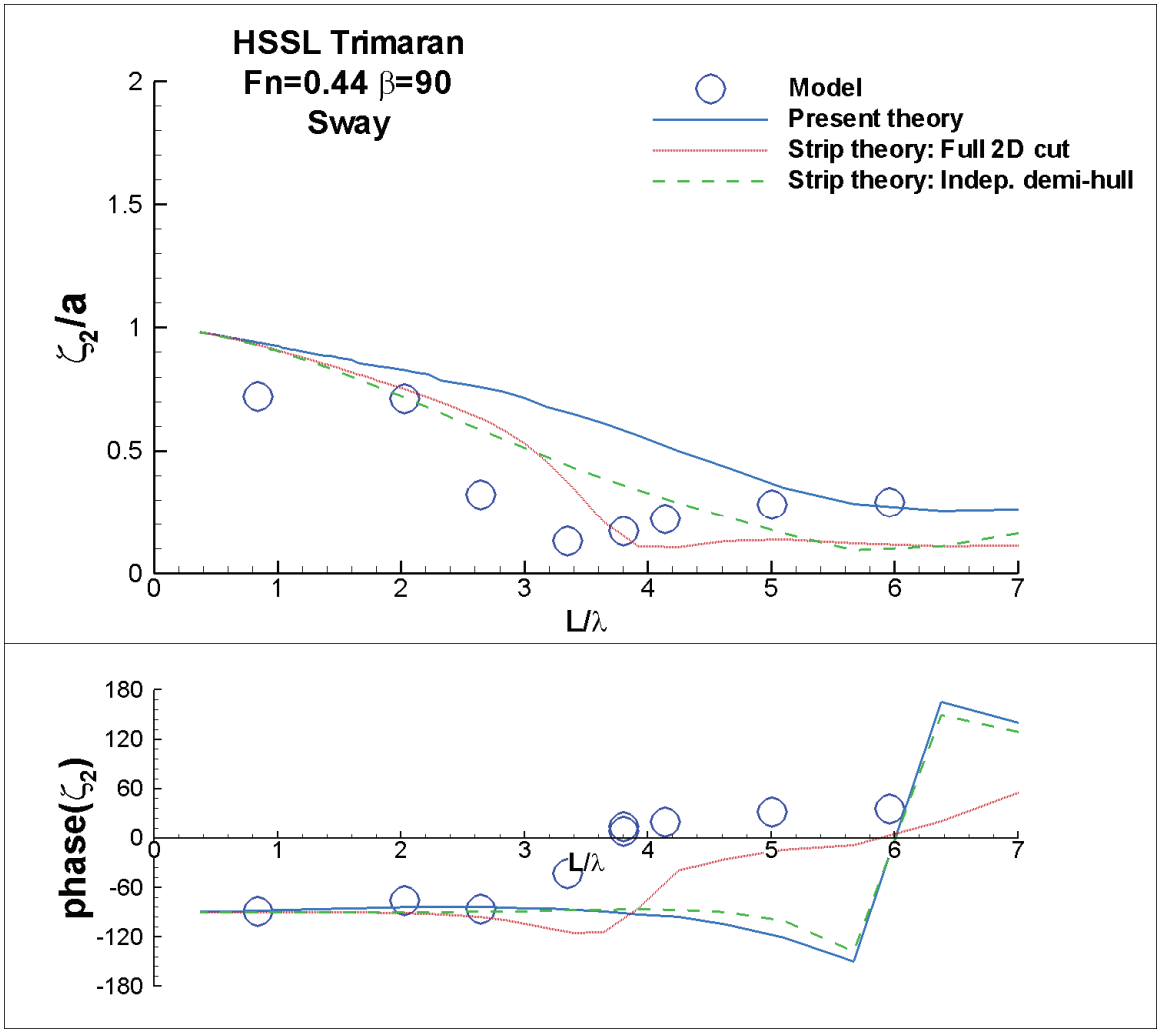

Figure D 8 HSSL Trimaran sway transfer function at Fn=0.44, β=90°

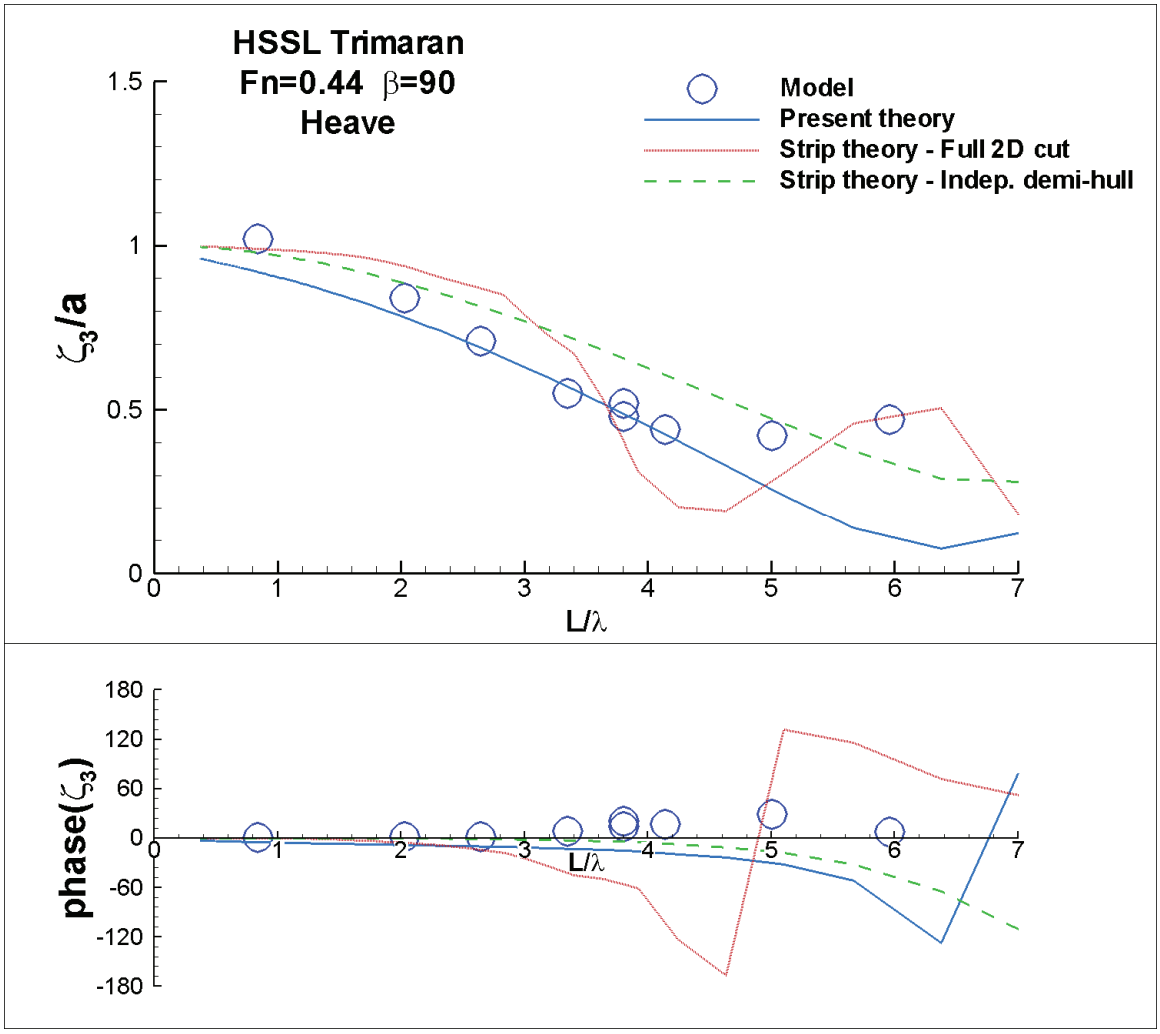

Figure D 9 HSSL Trimaran heave transfer function at Fn=0.44, β=90°

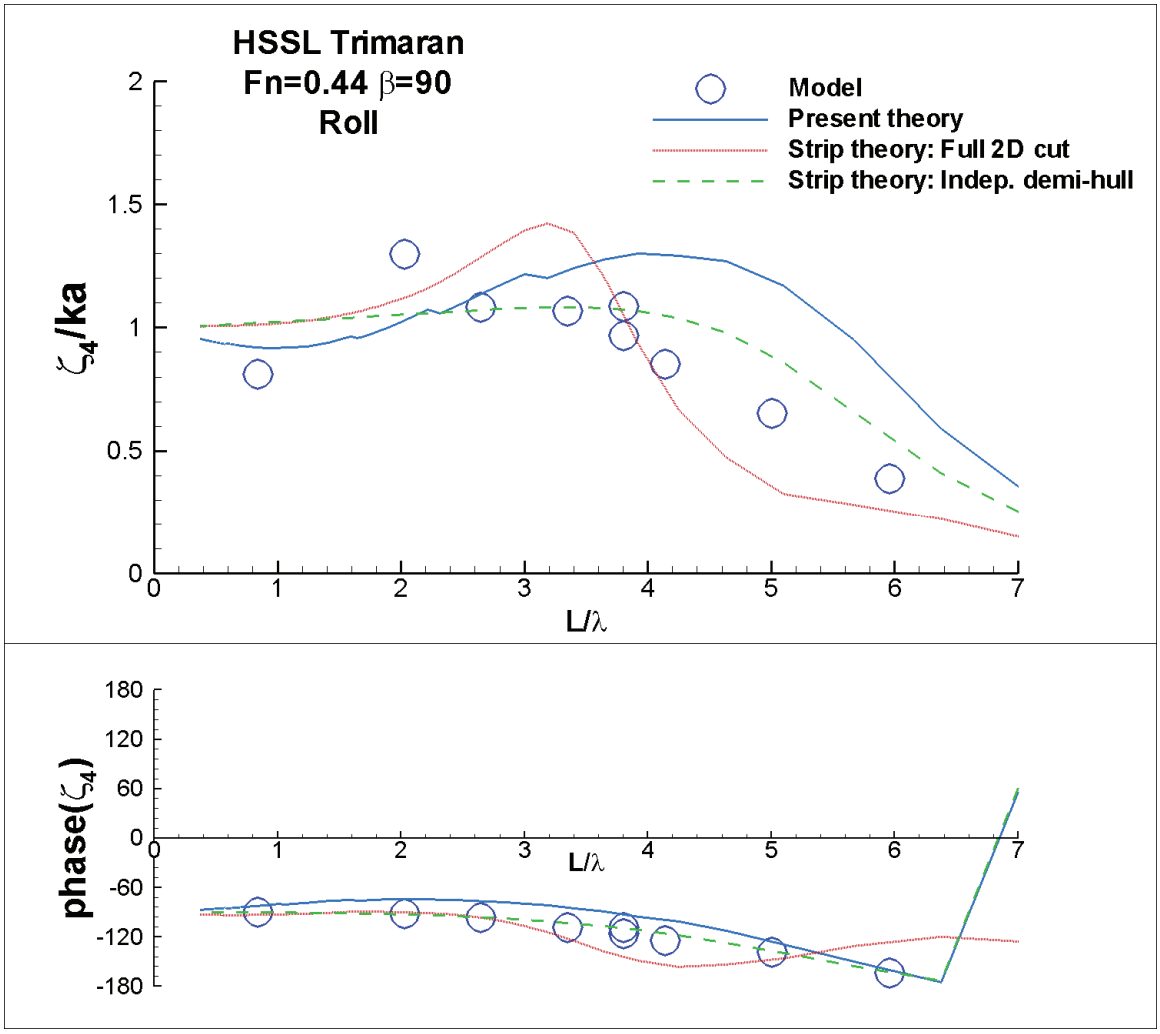

Figure D 10 HSSL Trimaran roll transfer function at Fn=0.44, β=90°

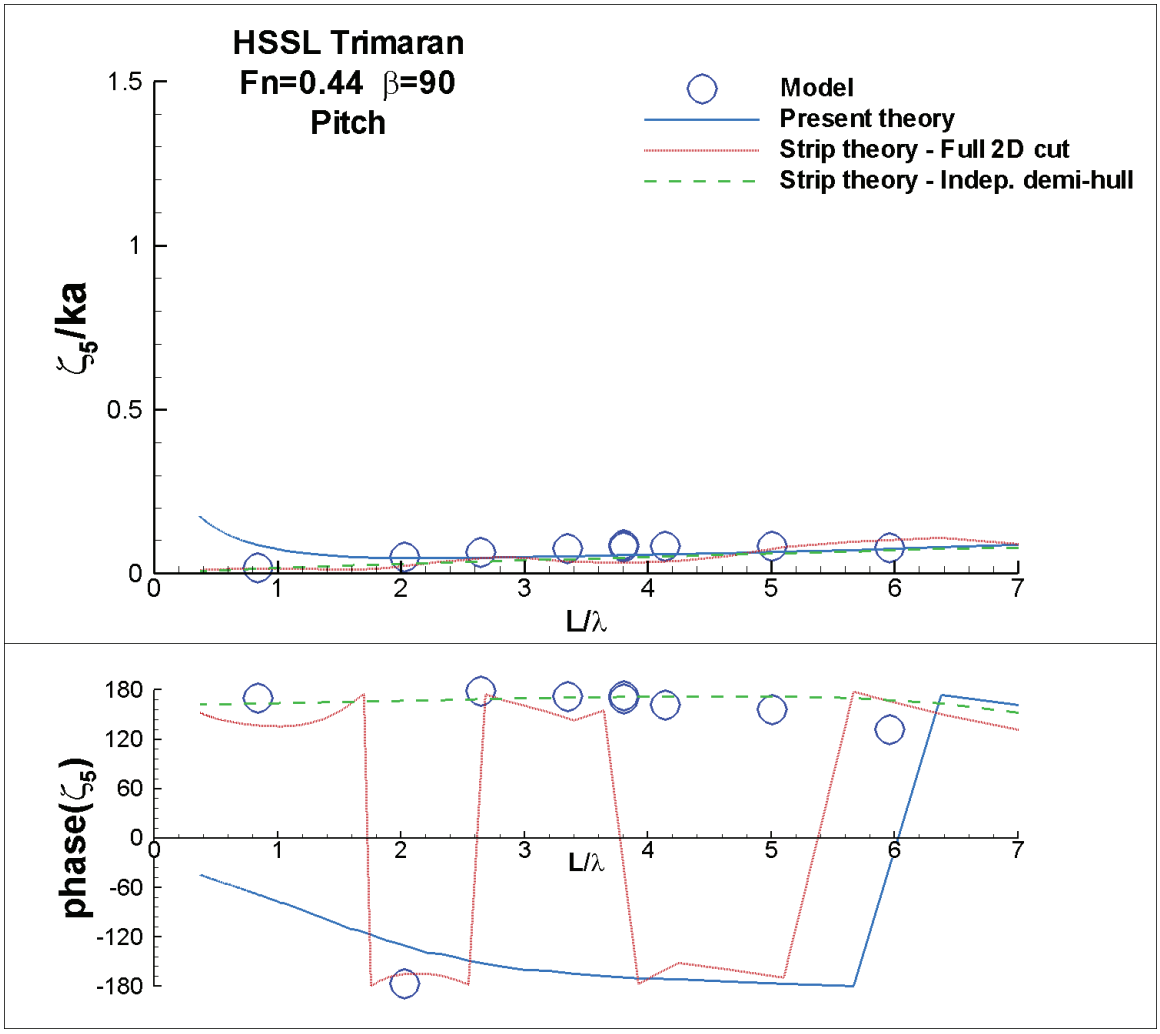

Figure D 11 HSSL Trimaran pitch transfer function at Fn=0.44, β=90°

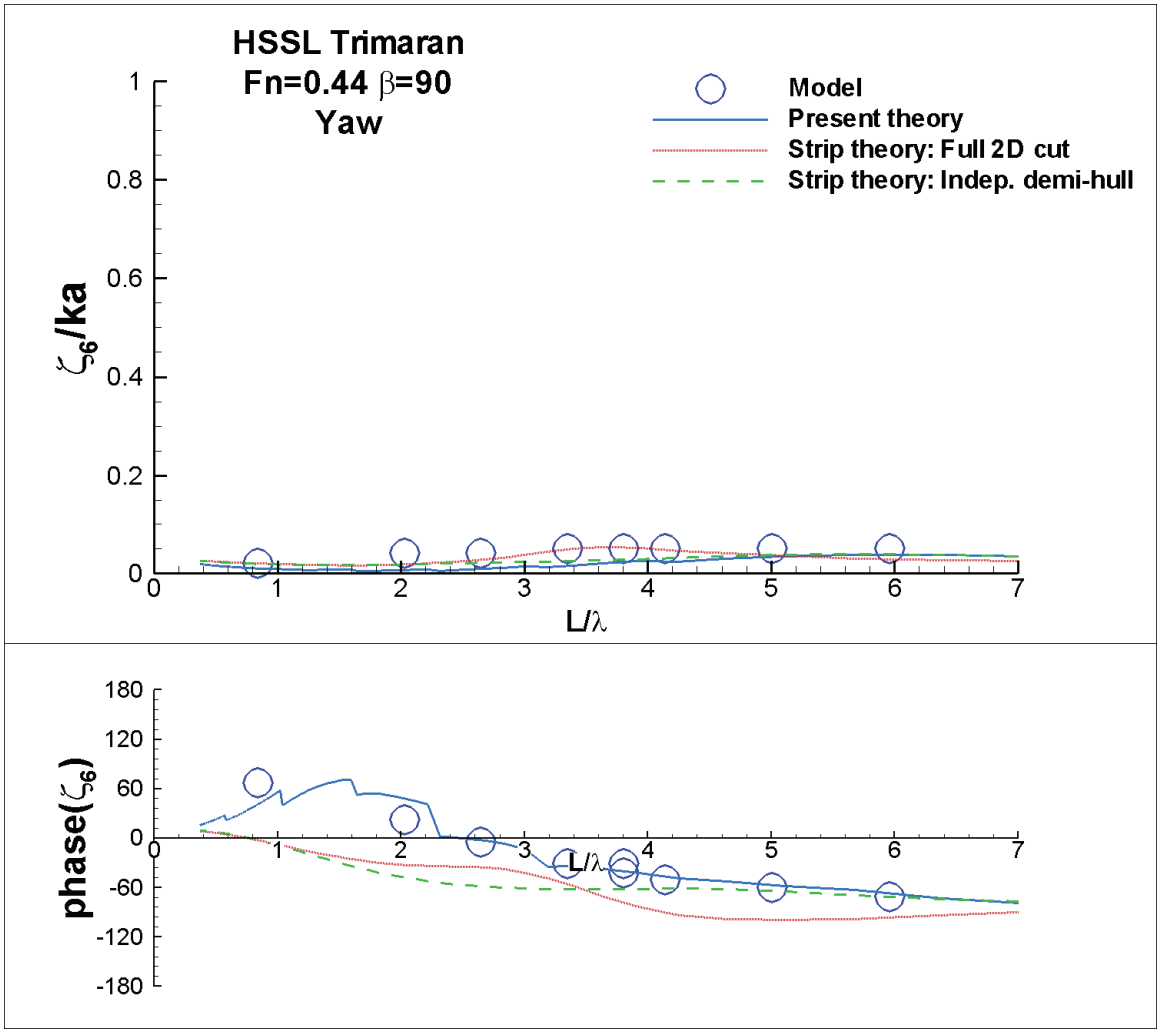

Figure D 12 HSSL Trimaran yaw transfer function at Fn=0.44, β=90°

Appendix E

Magnitude of 2D Interaction Force at Zero Speed

To show that it is possible for the total damping coefficient in mode, ii, to go to zero (at zero ship speed) with the present interaction theory, it must be shown that $b_{ii}^{\sim}$ (the sectional interaction force damping coefficient) can equal minus b_{ii} (the sectional independent demi-hull damping coefficient). In other words, the amplitude of the interaction force is equal to the imaginary part of the independent demi-hull radiation force.

The interaction force, which is the wave excitation force due to the far-field radiated wave, is a complex phaser whose phase depends on the hull separation and frequency. When the interaction force is stated in terms of 2D added mass and damping coefficients, the interaction damping coefficient is equal to

$$b_{ii}^{\sim} = -\mathrm{Im}(F_{ii}^{\sim}) / \omega_e \qquad \textbf{(E1)}$$

If the phase is such that the entire interaction force is imaginary,

$$|b_{ii}^{\sim}| = |F_{ii}^{\sim}| / \omega_e \qquad \textbf{(E2)}$$

Newman (1977) shows that the magnitude of the total 2D excitation force, X_i, for unit wave amplitude on a symmetric body is related to the section's own damping coefficient, b_{ii}, by

$$b_{ii} = \frac{|X_i|^2}{2\rho g V_g} \qquad \textbf{(E3)}$$

In the case of the radiation interaction force, the incident wave is the radiated wave which has frequency equal to the encounter frequency. Using the deep-water group velocity, $V_g=(1/2)*g/\omega_e$, equation E3 is restated as:

$$X_i = \sqrt{\frac{\rho g^2 b_{ii}}{\omega_e}} \qquad \textbf{(E4)}$$

The amplitude of the far-field radiated wave is known from the damping coefficient of the radiating section, which in the case of a zero-speed catamaran, is the same section shape. This amplitude is

$$\tilde{a} = \sqrt{\frac{b_{ii}\omega_e^3}{\rho g^2}} \qquad \textbf{(E5)}$$

Therefore, the magnitude of the exciting force due to a wave of amplitude, $\tilde{a}$, is equal to $\tilde{a} * X_i$, which leads to

$$\tilde{a} \cdot |X_i| = \sqrt{\frac{\rho g^2 b_{ii}}{\omega_e}} \cdot \sqrt{\frac{b_{ii}\omega_e^3}{\rho g^2}} \qquad \textbf{(E6)}$$

$$\tilde{a} \cdot |X_i| = \sqrt{b_{ii}^2 \omega_e^2} = b_{ii}\omega_e$$

The damping coefficient due to the interaction force is then found from equation E2 as

$$\left|\tilde{b_{ii}}\right| = \frac{\tilde{a} \cdot |X_i|}{\omega_e} = b_{ii} \qquad \textbf{(E7)}$$

By this argument, using equation E1, it is shown that the interaction damping coefficient can be equal and opposite to the demi-hull damping coefficient, leading to a total sectional damping coefficient equal to zero.

Bibliography

Bibliography

Bailey, P.A., Hudson, D.A.., Price, W.G., and Temarel, P., 1999, "Theoretical and Experimental Validation of the Seakeeping Characteristics of High Speed Mono- and Multi-hulled Vessels," *Proc. 5th Intl. Conf. on Fast Sea Trans*., Seattle, USA, pp. 429-441.

Beck, R.F., and Reed, A.M., 2001, "Modern Computational Methods for Ships in a Seaway," *SNAME Transactions*, Vol. 109, pp. 1-51.

Beck, R.F., and Troesch, A.W., 1989, "Student Manual for the Computer Program SHIPMO.BM," Department of Naval Architecture & Marine Engineering, Univ. of Michigan, Ann Arbor, Michigan.

Breit, S., and Sclavounos, P., 1986, "Wave Interaction Between Adjacent Slender Bodies," *J. Fluid Mech*., vol. 165, pp. 273-296.

Davis, M.R., and Holloway, D.S., 2003, "Motion and Passenger Discomfort on High Speed Catamarans in Oblique Seas," *Int. Shipbuild. Progr*., 50, no. 4, pp. 333-370.

Doctors, L.J., and Scrace, R.J., 2004, "Hydrodynamic Interactions between the Subhulls of a Trimaran during Rolling Motion," *RINA Proc. of the International Conf. on Design and Operation of Trimaran Ships*, London, England, pp. 31-39.

Faltinsen, O.M., 1990, "Sea Loads on Ships and Offshore Structures," Cambridge University Press, pp. 45-47.

Faltinsen, O.M., 2005, "Hydrodynamics of High-Speed Marine Vehicles," Cambridge University Press.

Faltinsen, O.M., Landrini, M., and Lugni, C., 2003, "Hydrodynamic Aspects of High-Speed Vessels," *Proc. 7th Intl. Conf. on Fast Sea Trans*., Ischia, Italy, Vol. 1, pp. 13-22.

Faltinsen, O.M., and Zhao, R., 1991, "Numerical Predictions of Ship Motions at High Forward Speed," *Phil. Trans. R. Soc. London*, Vol. 334, pp. 241-252.

Frank, W., 1967, "Oscillation of Cylinders In or Below the Free Surface of Deep Fluids," Report 2375, Naval Ship Research and Development Center, Bethesda, MD.

Hermundstad, O.A., Aarsnes, J.V., and Moan, T., 1999, "Linear Hydroelastic Analysis of High-Speed Catamarans and Monohulls," *Journal of Ship Research*, Vol. 43, No. 1, pp 48-63.

Holloway, D.S., 1998, "A High Froude Number Time Domain Strip Theory Applied to the Seakeeping of Semi-SWATHs," PhD. thesis, University of Tasmania.

Holloway, D., Davis, M., Giles, T., 2003, "Rigid Body Dynamic Hull Bending Moments, Shear Forces and PCM in Fast Catamarans*," Proc. 7th Intl. Conf. on Fast Sea Transportation*, Ischia, Italy, Session B1, pp. 57-64.

Jones, H.D., 1972, "Catamaran Motion Predictions in Regular Waves," Report No. 3700, Naval Ship Research and Development Center, Bethesda, MD.

Journée, J.M.J., 1992, "Quick Strip Theory Calculations in Ship Design," PRADS '92 *Conf. on Practical Design of Ships and Mobile Structures*, Newcastle upon Tyne, U.K., Vol. 1, pp 1-11.

Kashiwagi, M., 1993, "Heave and Pitch Motions of a Catamaran Advancing in Waves," *Proc. 2nd Intl. Conf. on Fast Sea Trans*., Yokohama, Japan, Vol. 1, pp. 643-655.

de Kat, J.O., 1994, "Irregular Waves and their Influence on Extreme Ship Motions," *Proc. 20th Symposium on Naval Hydrodynamics*, Santa Barbara, CA, pp. 48-67.

Kring, D., Sclavounos, P., 1991, "A New Method for Analyzing the Seakeeping of Multi-Hull Ships," *Proc. 1st Intl. Conf. on Fast Sea Trans*., Trondheim, Norway, Vol. 1, pp. 429-444.

Lee, C.M., 1976, "Theoretical Prediction of Motion of Small-Waterplane-Area, Twin-Hull (SWATH) Ships in Waves," Report No. 76-0046, David W. Taylor Naval Ship Research and Development Center, Bethesda, MD.

Lee, C.M., 1978, "Approximate Evaluation of Added Mass and Damping Coefficients of Two-Dimensional SWATH Sections," Report No. DTNSRDC-78/084, David W. Taylor Naval Ship Research and Development Center, Bethesda, MD.

Lin, W.M., Zhang, S., Weems, K., Yue, D.K.P.,1999, "A Mixed Source Formulation for Nonlinear Ship-Motion and Wave-Load Simulations," *Proc. of the Seventh Intl. Conf. on Numerical Ship Hydrodynamics*, Nantes, France.

Min, K.S., Yum, D.J., and Song, K.J., 1993, "A Study on the Prediction Method of Motion Characteristics for the High-Speed Catamaran Ship," *Proc. 2nd Intl. Conf. on Fast Sea Trans.*, Yokohama, Japan, Vol. 1, pp. 127-137.

Newman, J.N., 1977, "Marine Hydrodynamics," The MIT Press, p 296, p 304.

Ogilvie, T.F., and Tuck, E.O., 1969, "A Rational Strip Theory of Ship Motions: Part 1," Report No. 013, Dept. of Naval Architecture and Marine Engineering, University of Michigan, p. 69.

Ohkusu, M., and Wen, G.-C., 1993, "Prediction of Relative Motion of a High Speed Catamaran in Oblique Seas," *Proc. 2nd Intl. Conf. on Fast Sea Trans*., Yokohama, Japan, Vol. 1, pp. 657-670.

Ronæss, M., 2002, "Wave Induced Motions of Two Ships Advancing on Parallel Course," PhD. thesis, Norwegian University of Science and Technology, Trondheim.

Salvesen, N., Tuck, E.O., and Faltinsen, O., 1970, "Ship Motions and Sea Loads*," Trans. Society of Naval Architects and Marine Engineers*, Vol. 78, pp. 250-287.

Simon, M.J., 1982, "Multiple Scattering in Arrays of Axisymmetric Wave-Energy Devices. Part 1. A Matrix Method Using a Plane-Wave Approximation," *J. Fluid Mech.*, Vol. 120, pp. 1-25.

Sun, F., 1982, "Analysis of Motions of a Catamaran in Arbitary Heading Waves," *Proc. Offshore Mechanics / Arctic Engineering / Deepsea Systems Symp*., New Orleans, USA, Vol. 1, pp.11-22.

Timman, R., and Newman, J.N., 1962, "The Coupled Damping Coefficients of Symmetric Ships," *Journal of Ship Research*, Vol. 5, No. 4, pp. 34-55.

Tønnessen, R., Vada, T., and Nestegård, A., 1993, "A Comparison of an Extended Strip Theory with a Three-Dimensional Theory for Computation of Response and Loads," *Proc. 2nd Intl. Conf. on Fast Sea Trans*., Yokohama, Japan, Vol. 1, pp. 671-680.

van't Veer, R., 1998a, "Experimental Results of Motions, Hydrodynamic Coefficients and Wave Loads on the 372 Catamaran Model," Delft University of Technology Report 1129, February.

van't Veer, R., 1998b, "Experimental Results of Motions and Structural Loads on the 372 Catamaran in Head and Oblique Waves," Delft University of Technology Report 1130, December.

Wahab, R., and Hubble, E.N., 1972, "Simplified Theoretical Methods of Predicting the Motions of a Catamaran in Waves," Report No. 3736, Naval Ship Research and Development Center, Bethesda, MD.

Watanabe, I., 1992, "A New Method of Calculating Unsteady Hydrodynamic Forces Acting Upon High-Speed Catamaran Ships," *Proc. 19th Symp. on Naval Hydrodynamics*, Seoul, Korea, pp. 447-459.

Wehausen, J.V., Laitone, E.V., 1960, "Surface Waves," In Encyclopaedia of Physics, vol. IX, pp. 446-778.

Wheeler, J. D., 1969, "Method for Calculating Forces Produced by Irregular Waves," *First Annual Offshore Technology Conference*, Volume I.

Zhao, R., and Aarsnes, 1995, "Numerical and Experimental Studies of Nonlinear Motions and Loads of a High-Speed Catamaran," *Proc. 3rd Intl. Conf. of Fast Sea Transportation*, Lubeck-Travemunde, Germany., pp. 1017-1030.

Zhao, R., and Faltinsen, O.M., 1992, "Slamming Loads on High-Speed Vessels," *Proc. 19th Symp. on Naval Hydrodynamics*, Seoul, Korea.

Zhao, R., 1997, "A Complete Linear Time-Domain Analysis for Predicting Ship Motions at High Froude Number," *Intl. Shipbuilding Progress*, Vol. 44, No. 440, pp. 341-361.

Zhao, R., 2003, "A Nonlinear Time Domain Simulation for Predicting Wet-Deck Slamming of Catamaran," *Proc. 7th Intl. Conf. on Fast Sea Transportation*, Ischia, Italy, Vol. 2, pp. 95-102.